# NUMERICAL MODELLING OF UNSATURATED FLOW IN VERTICAL AND INCLINED WASTE ROCK LAYERS USING THE SEEP/W MODEL

A Thesis Submitted to the College of
Graduate Studies and Research
in Partial Fulfillment of the Requirements
for the Degree of Master of Science
in the Department of Civil Engineering
University of Saskatchewan
Saskatoon

By

Jaime Alexis Wilson

## Permission To Use

In presenting this thesis in partial fulfilment of the requirements for a Postgraduate degree from the University of Saskatchewan, I agree that the Libraries of this University may make it freely available for inspection. I further agree that permission for copying of this thesis in any manner, in whole or in part, for scholarly purposes may be granted by the professor or professors who supervised my thesis work or, in their absence, by the Head of the Department or the Dean of the College in which my thesis work was done. It is understood that any copying, publication, or use of this thesis or parts thereof for financial gain shall not be allowed without my written permission. It is also understood that due recognition shall be given to me and to the University of Saskatchewan in any scholarly use which may be made of any material in my thesis.

Requests for permission to copy or to make other use of material in this thesis in whole or part should be addressed to:

Head of the Department of Civil Engineering
University of Saskatchewan
Saskatoon, Saskatchewan
S7N 5A9

## Abstract

Conventional disposal of waste rock results in the construction of benches with interbedded fine and coarse layers dipping at the angle of repose. The waste rock benches are typically 20-meters in height and are constructed in a vertical sequence to form waste rock dumps commonly greater than 100-meters high. The interbedded structure influences the flow pathways for infiltration water within the waste rock profile. Preferential flow pathways develop when one material becomes more conductive than the surrounding material. The flow of meteoric waters through the interbedded waste rock structure is difficult to describe since the dumps are constructed above natural topography and are generally unsaturated.

Two previous research studies were undertaken at the University of Saskatchewan to study end dumped waste rock piles and the relationship to preferential flow for unsaturated conditions. The first study was conducted during the excavation of a large waste rock pile at Golden Sunlight Mine in Montana (Herasymuik, 1996). Field observations showed that the waste rock pile consisted of steeply dipping fine and coarse-grained layers. The results of further laboratory analysis indicated the potential for preferential flow through the fine-grained material under conditions with negative pore-water pressures and unsaturated flow.

The second study investigated the mechanism for preferential flow in vertically layered, unsaturated soil systems (Newman, 1999). The investigation included a vertical two-layer column study and a subsequent numerical modelling program showing that water prefers to flow in the finer-grained material. The preferential flow path was determined to be a function of the applied surface flux rates and the unsaturated hydraulic conductivity of the fine-grained material layer.

A numerical modelling program to evaluate preferential flow was conducted for the present study in an inclined four-layer system consisting of alternating fine and coarse-grained waste rock. The numerical modelling program was undertaken using the commercial seepage software package, Seep/W, that is commonly used by geotechnical engineers. The result obtained using Seep/W showed preferential flow to occur in the fine-grained layer. However, difficulties with respect to convergence under low flow conditions with steep hydraulic conductivity functions were encountered.

A comprehensive sensitivity analysis was completed to investigate the factors that influence convergence in the Seep/W model including: convergence criteria, mesh design and material properties. It was found that the hydraulic conductivity function used for the coarse-grained material was the most important factor. The problem of the steep slope for the hydraulic conductivity function specified for the coarse-grained material was solved by progressively decreasing the slope of the hydraulic conductivity function at $10^{-8}$ m/s (for applied fluxes of $10^{-7}$ m/s or less). The sensitivity analysis showed that the manipulation of the hydraulic conductivity function had insignificant changes in the flux distribution between the waste rock layers and great significance for achieving convergence. Based on the discoveries of the sensitivity analysis, a 20-meter high multi-layer waste rock profile inclined at 50º with an applied flux of $7.7e10^{-9}$ m/s equal to the annual precipitation at the Golden Sunlight Mine was successfully simulated. A parametric study was subsequently conducted for an applied flux rate of $10^{-5}$ m/s for slope heights of 1-meter to 20 meters with slope angles varying between 45º and 90º. The parametric study demonstrated that flow in a multi-layered waste rock dump is a function of inclination, contact length between the layers, and the coarse and fine-grained hydraulic properties for the waste rock. An alternative numerical modelling technique based on a modified Kisch solution was also used to investigate preferential flow. The

Kisch method helped to verify and simplify the numerical problem as well as to illustrate the mechanics of preferential flow in a two-layered system.

In general, commercial seepage modeling packages are powerful and useful tools that are designed to adequately accommodate a wide range of geotechnical problems. The results of this research study indicate that Seep/W may not be the best-suited tool to analyze unsaturated seepage through sloped waste rock layers. However, numerical modelling is a process and working through the process helps to enhance engineering judgment. The Seep/W model provided an adequate solution for a simplified simulation of unsaturated seepage through waste rock layers. The modified Kisch solution independently verified the solution and provided additional confidence for the results of Seep/W model.

## Acknowledgements

I would like to thank and acknowledge the support of my supervisors Dr. Ward Wilson, and the late Dr. Bill Stolte. Dr. Wilson's enthusiastic support proved to be critical over the course of the research. I would like to thank Dr. Jim Kells and Mike O'Kane for the solid advice and kind words of encouragement they gave me, and Dr. Dennis Pufahl and Dr. Bruce Sparling for their approval and support needed to extend and complete my masters program.

I would like to give special thanks to Dr. Del Fredlund, Dr. Lee Barbour, and Dr. Malcom Reeves. Dr. Fredlund provided the insight and funding that revived my masters program that lead to the eventual conclusion. Dr. Barbour, officially not a member of my thesis program, provided the critical technical expertise in the field of numerical modelling and the thought process necessary for successful analysis of the problem. Dr. Barbour's door was always open; an empty chair readily available, and his limited time was freely given. Dr. Reeves provided the critical review and comments necessary for the acceptance of this research study.

I would like to thank Greg Herasymuik and Lori Newman for their pioneering work that led to this thesis. I wish to thank Alex Kozlow, Björn Weeks, and my fellow researchers for their assistance and support. A grateful thanks goes to my friends and parents for all that they did throughout the years.

The thesis is a result of several years of work that was completed in stages as my life changed from 'student' to 'husband' to 'father'. I foremost owe a special debt of gratitude to my wife Ranee, whose unfailing support saw us successfully through several difficult times. A thanks is owed to my daughter Jadra, for being the motivating force behind the final push to complete this research.

## Table of Contents

## LIST OF TABLES

## LIST OF FIGURES

# CHAPTER 1

# INTRODUCTION

## 1.1 Background

The mining industry has a significant impact on both the economy and the environment. Environmental regulations specify the standard for protecting the environment, and an economically viable mining industry is one that can protect the environment and produce a profit. Research has contributed significantly to the minimization of environmental impact from mining operations. Through continuing research, improvements to current mining practice can lead to newer and less expensive construction and decommissioning technologies for new mine sites.

Computers play an important role in the rapidly developing field of design and decommissioning for waste rock dumps, with respect to their hydrologic behavior. Increases in computing power have made numerical modelling an active part of engineering in the mining industry. One of the most relevant roles of predictive modelling is to ensure that a reclaimed waste rock dump will not have long-term negative impacts associated with the infiltration of precipitation and subsequent discharge to the environment. The design of cost efficient control measures during mining and decommissioning depends heavily on the ability to model and predict the potential for acid generation and drainage from a waste rock dump.

Herasymuik (1996) described several models for waste rock hydrology and geochemistry, and for the prediction of acid generation and drainage. Herasymuik noted that the models were weak in predicting secondary mineral

production, water flow, and solute transport in unsaturated heterogeneous waste rock. Herasymuik also noted that there appeared to be a lack of understanding with respect to the interactions between hydrogeology and geochemical processes active in waste rock piles.

Current predictive models generally treat waste rock hydrology as a “black box.” However, the “black box” is known to interact with the atmosphere and drain acid water into the environment. In cases, which involve tailings impoundments, there are models available that accommodate saturated and unsaturated flow in homogenous media and calculate the geochemical reactions together with environmental loadings. However, the lack of a comparable understanding regarding the properties of waste rock may result in the incorrect application of control measures for acid drainage. In order to achieve an acceptable level of confidence in the design of a waste rock pile overly conservative approaches are often implemented. Herasymuik (1996) acknowledged the lack of understanding of waste rock properties and conducted research focused on determining the internal structure and characteristics of the hydrogeologic properties of a waste rock pile.

Waste rock dumps frequently contain significant quantities of reactive sulphide minerals. The piles also have a high coefficient of permeability, and rapid drainage through the pile produces an unsaturated rock structure when the pile is constructed above the water table. The sulphide bearing minerals are exposed to oxidizing conditions and react with water and atmospheric oxygen to produce acid rock drainage (ARD). Herasymuik (1996) documented detailed observations made while excavating a waste rock pile at the Golden Sunlight Mine (GSM) in Montana, USA. GSM is situated in a semi-arid climate where the potential evapotranspiration is two to three times greater than the average annual precipitation of 243 mm/year (Swanson, 1995). From these observations, Herasymuik developed a conceptual model for the hydrogeology of the waste rock pile. In general, Herasymuik’s conceptual model predicts that

water due to surface infiltration will tend to flow in the finer materials within the waste rock profile. The broad objective of the present study is to evaluate the conceptual model presented by Herasymuik (1996) using numerical modelling techniques for unsaturated flow.

## 1.2 Research Objective and Scope

Protection of the environment in a more economical manner can be achieved through use of a superior predictive model. The development of a superior predictive model requires an understanding of the hydrogeologic properties of a waste rock dump. The conceptual model developed by Herasymuik (1996) provided such an understanding. Further development required that a mathematical model be developed based on the conceptual model. However, the translation of the conceptual model to a mathematical model proved to be difficult.

Several studies related to waste rock piles and the production of ARD have been undertaken by other researchers. These studies mainly emphasized the importance of infiltrating water. One such study conducted by Newman (1999) determined the mechanism for preferential flow in a vertically layered, unsaturated system. Further study was required to link the work of Newman (1999) with the conceptual model for a waste dump proposed by Herasymuik (1996) since field observations showed the layers to be inclined at the angle of repose (i.e., 38º). A new numerical modelling program was undertaken in this thesis to evaluate the flow of water in both vertical and inclined layers of waste rock. However, the difficulties associated with modelling inclined waste rock layers were extensive. It was also difficult to accurately characterize the layered structure in a waste dump. Furthermore, texture, geochemical and mineral properties of the rock affect the weathering and oxidation. In many cases, these parameters that are unknown and site specific conditions significantly influence the flow of water.

The objective of this thesis is to evaluate the conceptual model for the hydrogeology of an unsaturated end dumped waste rock pile using the numerical software called Seep/W (Geo-Slope, 1995) for saturated/unsaturated flow. Seep/W is a computer model routinely used by geotechnical engineers for the design of earth structures. The specific objectives are as follows:

1) To conduct a literature review of existing numerical techniques for modelling the flow of water through waste rock dumps;
2) To develop finite element domains and material properties that represent waste rock systems;
3) To conduct a parametric study to establish the influences of slope angle and contact length between layers with respect to flow and numerical convergence;
4) To develop criteria for achieving convergence for nonlinear seepage problems associated with waste rock;
5) To develop a simple pseudo two dimensional finite difference numerical method to independently analyze the seepage solutions based on first principles; and
6) To provide recommendations for future research.

The modelling work presented in this thesis considered the steady-state saturated/unsaturated flow of water through a waste rock pile, but did not consider chemical reactions or gas transport. The scope of this thesis is considered to be an initial step towards the numerical modelling of an entire waste rock pile.

Herasymuik (1996) showed that end dumped waste rock segregates into layers of waste rock at residual slope angles with a water content of 6%. The layers consisted of waste rocks that had been stratified due to segregation during down slope ravelling upon dumping. The stratified layers were also formed as a result of variations in rock type. Oxidation and weathering to finer-textured material at different rates induced greater variations with respect to texture. These layers were often relatively uniform in grain size but were not always continuous along the length of the slope. The adjacent layers were also uniform but were either coarser or finer than one another. Observations showed that there was

moisture in the fine-grained layers while the coarse-grained layers remained dry. The different textures between the sloping layers appeared to be sufficient to result in preferential unsaturated flow of precipitation that infiltrated the surface of the waste rock. It is possible that there is need for further study on induced preferential flow pathways to create an environmentally benign design of waste rock piles to avoid ARD (Mehling et al., 1997). This possibility is assumed to be outside the scope of the present thesis.

## 1.3 Research Methodology

The research program followed a standard modelling methodology. A physical problem was examined and a conceptual model developed. The conceptual problem was then described using a mathematical model and a solution was sought. The solution was then evaluated.

Only a few researchers have set out to study the hydrogeology internal to a waste rock dump. The field study and conceptual model developed by Herasymuik (1996) provided the important first steps towards the development of a predictive model. Newman (1999) continued the work by providing an understanding of the mechanism for preferential flow. The study by Newman (1999) for vertical waste rock layers was conducted in the laboratory followed by numerical modelling. The numerical modelling program developed for this study began by considering these previous studies. Various slope angles were investigated and heights typical of benches from end dumped waste rock piles were considered. A sensitivity analysis presented in Appendix B, studied the effects of the input parameters (i.e., convergence criteria, material properties, and geometry) on the finite element numerical model. The analysis concluded by examining an alternative numerical solution using a finite difference method and then revisiting the finite element solution.

## 1.4 Thesis Outline

This research study provides the background required for the development of a numerical model for waste dumps. Chapter 2 describes the modelling

methodology used together with a literature review. The literature review summarizes the related research conducted previously, and describes the physical problem.

Chapter 3 presents the theoretical background required to understand the main processes involved in the movement of water in unsaturated systems. The mathematical methods used for the numerical models are also presented. Chapter 4 presents the detailed parametric study that was undertaken using the Seep/W finite element model. The independent finite difference numerical method developed is presented at the end of Chapter 4. The results obtained from both modelling programs are presented, analyzed, and discussed in Chapter 5. A summary and conclusion are provided in Chapter 6, as well as recommendations for continuing research.

The outputs from the modelling programs are presented in three appendices. The output of the parametric study is located in Appendix A. An outline of an extensive sensitivity analysis along with a discussion of the results, and the tables summarizing the results are presented in Appendix B. Appendix C provides the spreadsheet results of the finite difference numerical method developed.

# CHAPTER 2

# LITERATURE REVIEW AND BACKGROUND

## 2.1 Introduction

The development of a numerical model should adhere to the scientific method of problem solving. When a problem is identified and a need to solve the problem arises, a certain methodology is followed. The first section of this chapter demonstrates the evolution of a numerical model from a conceptual problem to a feasible solution. The following sections provide background for the physical problem under consideration, and a review of related research.

## 2.2 Modelling Methodology

The purpose of a modelling exercise is to define the performance of a physical model prior to the construction of the full-scale system. Models may encompass large-scale field-testing, scaled models, analogue models, or numerical models. However, the greatest benefit of numerical modelling is seldom realized except during the final prediction of performance. Modelling can be beneficial to design, interpretation of data, and generic numerical experiments. The advantage of modelling lies in the ability of a model to enhance judgment. Modelling is primarily about the processes involved more than about prediction (Barbour, 1998).

The National Research Council (NRC, 1990) defines a mathematical model as a replica of some real-world object or system. The model is an attempt to take the current understanding of the processes involved (i.e., conceptual model) and translate these processes into mathematical terms.

There are several steps in the development of a model as noted by NRC (1990), Mercer and Faust (1981), and Freeze and Cherry (1979). Common to the conceptual frameworks for modelling are the following components:

1. Conceptualization: Definition of the site and scope of the physical phenomenon;
2. Definition: Description of physical processes;
3. Formulation: Representation of the physical phenomena with mathematical descriptions;
4. Solution: Obtaining a numerical solution; and
5. Interpretation: Validation and calibration of the numerical model with respects to the physical system.

Spitz and Moreno, 1996, identified modelling components in detail, as presented in Table 2.1 below.

**Table 2.1 Modelling Components (after Spitz and Moreno, 1996)**

| Component | Key Elements | Examples |
|---|---|---|
| Natural System | Geometry<br><br>Dimensionality<br>State<br>Hydrogeology<br><br><br>Observed responses<br>Groundwater problem | • Lateral extent, thickness, source volume<br>• One-, two-, three-dimensional<br>• Transient, steady<br>• Porosity, hydraulic conductivity, dispersivity, storativity, chemical properties<br>• Water level, concentration<br>• Extraction, contamination |
| Conceptual Model | Idealized system<br>Relevant units<br>Boundary and initial conditions<br>Controlling processes | • Aquifer, aquitard, aquiclude<br><br>• Initial condition<br><br>• Flow, capillarity, gravity, transport, chemical reactions |
| Mathematical Model | Physical laws<br><br>Differential equations<br>Boundary conditions<br><br>Initial conditions | • Conservation of mass<br>• Conservation of energy<br>• Equilibrium of forces<br>• Constitutive relationships<br>• Material relationships<br>• Laplace equation<br>• First-, second-, third-kind conditions<br>• Specified head or concentration |
| Solution | Analytical model<br>Porous media (bench-scale) model<br>Analog model<br><br><br>Empirical model<br>Mass balance (single-cell) model<br>Numerical model | • Viscous fluid model<br>• Membrane model<br>• Electrical analog model<br><br><br>• Finite-difference model<br>• Finite-element model<br>• Random walk model<br>• Method of characteristics<br>• Boundary element method |
| Calibration | Solution versus observation<br>Adjustment of model input data | |
| Validation | Testing of model prediction versus observations not used in calibration | |
| Simulations | Parameter sensitivity<br>Predictive simulations<br>Analysis of uncertainty | |

Barbour, (1998) outlined the modelling process in the following steps:

Step 1 – The physical problem and the pertinent processes taking place are monitored and the actual objective of the model is defined. The hypothesis for the expected model outcome is determined and a definition of the conceptual model that describes the relevant area, and effect of outside influences and the outcome is provided.

Step 2 – The relevant area is measured or defined. A brief discussion of the important processes occurring is provided, accompanied by the most relevant equations and theories (i.e., the relevant fundamental laws). A statement of the essential assumptions and approximations used in definitions is included with a data set of all known information. The area of interest is defined, as are any influencing conditions. The responses of the system are noted and a mathematical model is developed using the provided information.

Step 3 – An analytical or numerical method of solving the problem is chosen and an accurate solution and explanation of results is obtained. The solution obtained is compared with known solutions and published field studies in order to establish its accuracy. The limitations of the solution obtained and possible error sources are also defined.

Step 4 – The solution is verified and interpreted with respect to the pertinent physical problem and a modelling experiment or laboratory study is designed with proper calibration and adjustment so that the model parameters are in agreement with field responses. The range of reasonable and acceptable responses to the solutions is decided upon and a sensitivity analysis is carried out through a selection of a range of relevant parameters (properties, boundary conditions, etcetera). The parameters are varied individually and the simulation is repeated. The responses of the key systems are discussed and the model is

confirmed by applying the calibrated model to the new set of responses. The model is audited and submitted for independent review and the results are presented.

Swanson (1995) provided an example that illustrated how the methods described above can be adapted to solve a problem. Swanson (1995) conducted a predictive modelling program of moisture movement through engineered soil covers. The modelling methodology was divided into six stages:

1. Site Familiarization;
2. Introductory Modelling;
3. Preliminary Modelling;
4. Field Response Modelling;
5. Predictive Modelling; and
6. Methodology Summary and Analysis.

The general methodology and approaches outlined above are those most commonly found in the literature.

## 2.3 Modelling Issues

There are several key characteristics and limitations associated with numerical models. Numerical models are simple representations of a "greater reality." Therefore, the model is subject to the accuracy of the interpreted data collected (for example, soil sampling and associated laboratory analysis). The development of the model should start from a simple representation and move to a more complex representation.

It should to be noted that the numerical modelling is not a solution to a problem but is rather a tool for solving the governing equations. The numerical model is an incorporation of the site-specific geometry, boundary conditions, and relevant parameters, which include calibrating and verifying the model (Spitz and Moreno, 1996). The modelling exercise relies heavily on the engineer/ researchers' judgment. Sensitivity studies are helpful in the evaluation of the significance of 'uncertainties' in the input parameters.

Potential errors in model development can be reviewed in terms of the modelling steps described in the previous section. The conceptual model is a simplified, but a realistic representation of a real physical system. Misinterpretation of the physical system or a poor definition of the boundary conditions or material properties are not compensated for by sophisticated numerical modelling. The adage, “garbage in results in garbage out” is of significance to the case at hand. However, it is not a requirement that the physical model be fully defined prior to the application of a numerical model. An iterative approach can be used. An initial conceptual model can be simulated based on estimated conditions. A further definition of the physical system can be pursued until an acceptable agreement between the model and reality is developed. The critical aspect is to keep the accuracy of the model in perspective, in light of the initial definition of the physical system. It often happens that complex models are used too early in a study (Barbour, 1998).

Sophisticated numerical models do not compensate for limitations in the basic definition of the physical system. In many areas of geotechnical engineering, there are fundamental processes that are still not well understood. Secondly, all of these theoretical descriptions are based on a series of assumptions. The significance of these assumptions in light of the physical system being modelled must be kept in mind (Barbour, 1998).

Errors can often develop in mathematical solutions due to difficulties with numerical oscillation or dispersion, or round-off and truncation errors. When large systems of equations are being solved, repeated round-off error can become problematic. The significance of these error can usually be detected by studying the effect of machine precision. Errors of this type are dangerous when working with small numbers and steep soil property functions (Barbour, 1998).

Barbour (1998) states, “The greatest danger of model misuse is blind faith. This occurs when the model user is not familiar with the physical system,

assumptions, and theoretical foundations, and limitations of the numerical solution described previously, yet accepts the results of the model simulation without question. This is potentially a greater problem with the increasing use of general modelling packages. In every case, an interpretation of the numerical model results that would contradict engineering intuition should be considered suspect. The basic question still is are the results reasonable?"

## 2.4 The Physical Problem

The physical problem to be studied is the hydrogeology of waste rock dumps as it relates to acid rock drainage (ARD). MEND, 1995 noted that many researchers have studied waste pile hydrology with regards to ARD; however, the internal seepage behavior of mine waste rock dumps is poorly understood. The literature shows that observations indicate that waste rock pile stratigraphy may be a determining factor in internal seepage behavior. From the literature review undertaken for the purposes of this thesis, it can be deduced that the amount of information available is seriously limited. No single site provides a complete data record of important parameters required for the characterization of the hydrologic behavior of a waste rock pile

MEND (1995) characterized the generation of acidic water within a waste rock pile as being quite "complicated." The process involves an intricate interaction amongst hydraulic, chemical, and thermal processes, including variably saturated fluid flow and air circulation in the rock mass above the water table. In addition, ARD involves heat generation and heat transfer in both the aqueous and gaseous phases, oxygen consumption and re-supply, reaction kinetics. Furthermore, solutes are transported in an exceptionally heterogeneous medium containing both a porous matrix and open voids. It should be noted that other processes are also relevant to the flow of water through waste rock piles. Examples of such factors are weathering, fines migration, and deposition, sealing of channels, settlement of the rock pile, and temporal changes in the spatial distribution of permeable pathways.

MEND (1995) proposed four hydrostratigraphic types to characterize waste rock piles. The types differ depending upon the material and construction methods, and the characteristics of flow. The flow of water is porous in finer sandy gravel materials whereas it is channelized in coarser materials. The types are outlined as follows:

1. Non-segregated coarse-grained rock piles that transmit water rapidly to the base of the pile;
2. Non-segregated fine-grained rock piles that are likely to contain a basal saturated zone;
3. Segregated rock piles that contain a fine-grained crest zone that may not permit the passage of significant quantities of water; and
4. Layered, segregated dumps that contain a finer-grained crest and sandy gravel layers parallel to the face of the rock pile.

The current study will look at the fourth type. Figure 2.1 shows a typical example of segregated waste rock piles. Segregated waste rock dumps exhibit a dominant vertically graded stratigraphy. This is caused by the segregation that occurs as materials roll down the pile at the angle-of-repose. Finer sandy gravels are present at the crest, while coarser materials accumulate further down-slope. The vertical thickness of the finer segregated crest zone depends on the source rock textural composition and the dump height. According to the studies reviewed, most end dumped fills exhibit areas of finer material in the crest that are about one-third of the total dump height (MEND, 1995).

**Figure 2.1a Segregated End Dump Waste Rock Pile at Golden Sunlight Mine (after Herasymuik, 1996)**

**Figure 2.1b Excavated Profile of a Waste Rock Pile at Golden Sunlight Mine (after Herasymuik, 1996)**

MEND (1995) indicated that the segregated fine-grained material in the top third of these dumps exhibited infiltration capacities several orders of magnitude lower than that of the material in the lower slope area. Thus, it is anticipated that flow through these dumps should be largely dominated by infiltration into the coarser rock-like material.

Several investigations have revealed that in addition to the vertically graded stratigraphy, a distinct layering parallel to a dump face formed as different materials were placed. Dawson and Morgenstern (1995) have shown that when materials consisting mostly of finer sandy gravel are end-dumped, little segregation occurs and a finer grained layer is formed in the dump. These finer layers could develop a perched water table as saturation approaches 100 percent due to infiltration or compression. A perched water table might continue to develop until the hydrostatic head exceeds the capillary barrier formed at the fine/coarse interface. The excess pore-water pressure developed in the fine layer may have implication with respect to slope stability and may also result in higher ARD.

In 1994, a unique occurrence provided a rare opportunity for the study of the hydraulic properties and flow pathways in an end-dumped waste rock pile at the Golden Sunlight Mine (GSM) located in Montana, USA. End-dumping at this site produced a layered, segregated dump as identified in MEND 1995.

GSM was subject to a large earth movement underneath a 100 million-ton waste rock pile. To stabilize the movement, 15 million tons of waste rock were relocated. A research program began in 1994 to study this event involving Placer Dome Canada Inc. and the Unsaturated Soil Group (USG) at the University of Saskatchewan (Newman et al, 1997).

The research program consisted of several phases, in which an extensive field investigation was conducted. The waste rock at the site was removed in a

series of 18-meter high benches. Twenty-nine test pits were excavated on the benches, with the pits ranging in depth from 3- to 4-meters. The test pits exposed layers of waste rock, which resulted from the end-dumping process. The layers were extensive but not continuous down the slope and ranged in thickness of 10 cm to several meters. The layers were visually logged with respect to minerological components, grain sizes, texture, structure, matrix quantity and quality, state of oxidation and weathering, color, strike, dip and any other notable features. In situ measurements of water content, matric suction, temperature, and relative humidity were also taken (Herasymuik, 1996).

The field logging and sampling program documented a highly structured waste rock material, defined by color and/or grain size differences. The layers were found to dip at approximately the angle of repose for the material and strike at an angle consistent with the edge of the dump-top surface from which the material was end dumped. Changes in grain size were observed to occur horizontally and vertically within the pile. These observations agreed with the MEND (1995) observations.

A typical cross section of the excavated waste rock pile is presented in Figure 2.2. Note the distinctive dipping layers produced by end-dumping waste rock. The contrasting colors of the layers are indicative of different mineralogy as well as of different oxidation rates of and degrees of weathering between layers. The gray layers were observed as coarse-grained waste rock, while the reddish layers were fine-grained waste rock. The reddish colour is an indication of advanced oxidation and weathering in the fine-grained layers, and is a direct result of higher volumetric water contents. This observation was contrary to the MEND (1995) findings, which indicated that flow through the waste rock dumps should be largely dominated by infiltration into the coarse-grained rock-like layers.

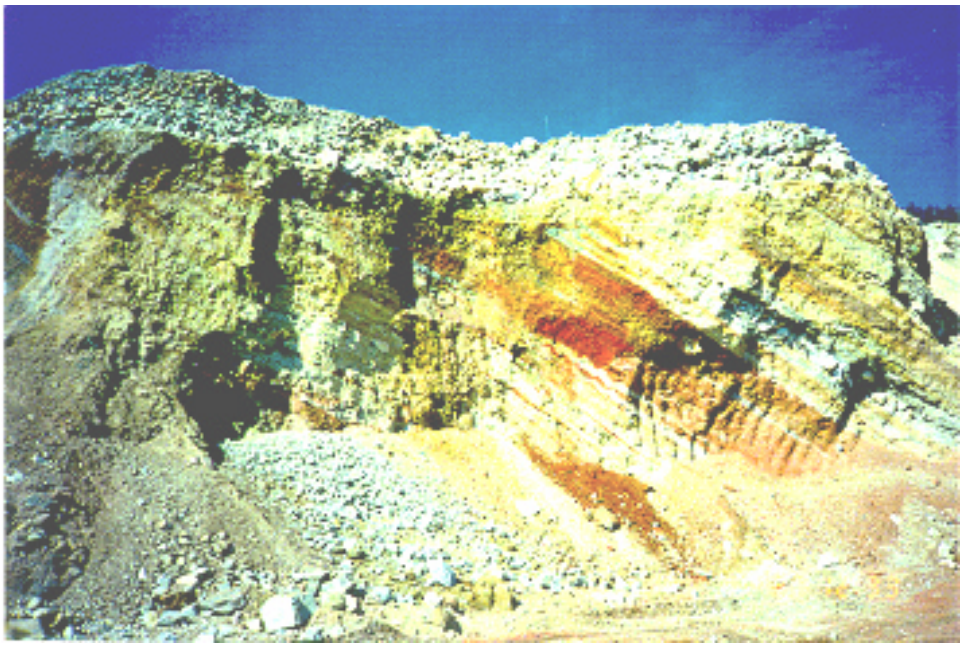

**Figure 2.2 Cross-Section of a Typical End-Dumped Waste Rock Pile (after Herasymuik, 1996)**

The second phase of the GSM research program involved data reduction and laboratory analysis. The wide ranges of grain-size found were classified based on grain-size distribution. Waste rock with a large amount of coarse material (less than 40% passing the 4.75-mm sieve) drains rapidly under small values of matric suction and also shows a corresponding rapid decrease in unsaturated hydraulic conductivity. In contrast, fine waste rock (containing more than 40% passing 4.75-mm sieve) is capable of retaining water under a larger matric suction and therefore retains a relatively higher unsaturated hydraulic conductivity than the coarse material (Herasymuik, 1996).

The grain size distribution, soil-water characteristic curves and the hydraulic conductivity function curves were determined for each sample. The material property curves are shown in Figures 2.3 to 2.5, respectively. The material properties show that the fine-grained waste rock layers have a higher air entry value (AEV), which indicates that the material can have a higher water content under a specific matric suction. Therefore, the fine-grained waste rock will be the preferential layers for the storage of water and will provide pathways for the

liquid water flow in the waste rock pile under unsaturated conditions (Herasymuik, 1996).

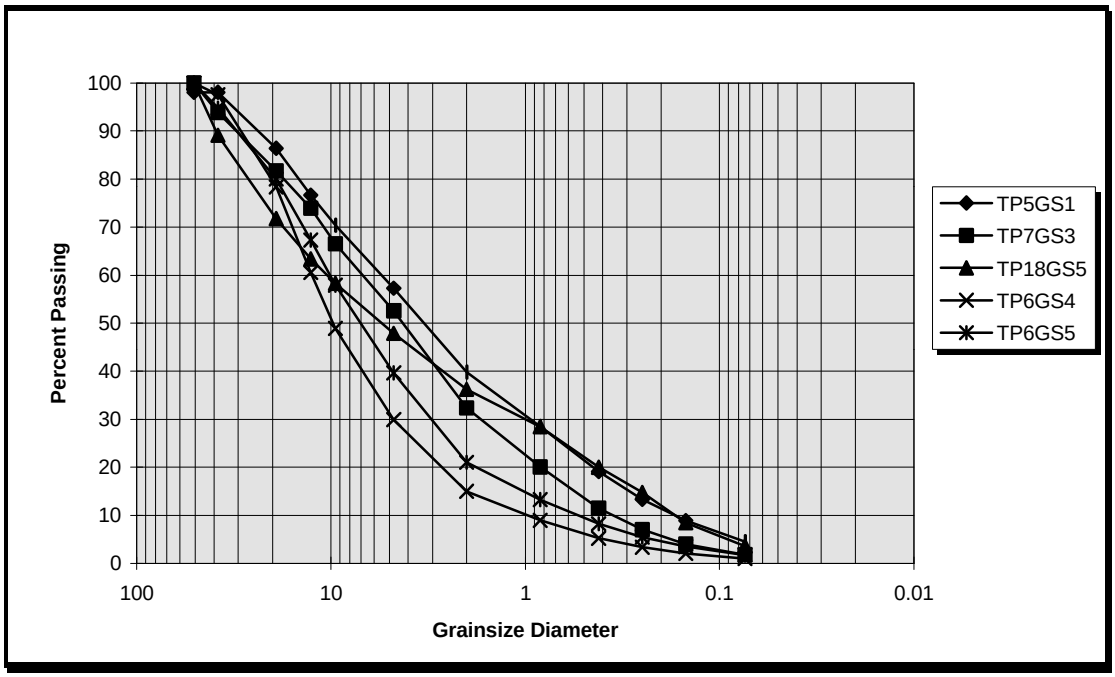


**Figure 2.3 Grain Size Distribution Curves for Field Samples Chosen for Large Diameter Pressure Plate Testing (after Herasymuik, 1996)**

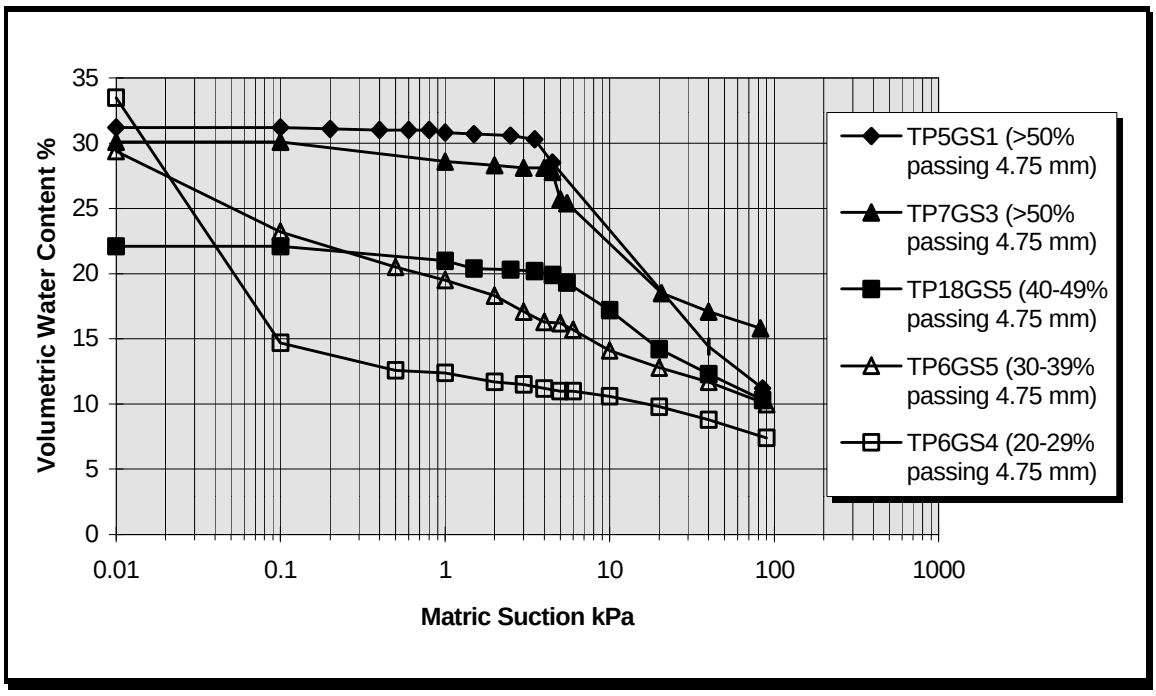


**Figure 2.4 Soil-Water Characteristic Curve for Sampled Waste Rock (after Herasymuik, 1996)**

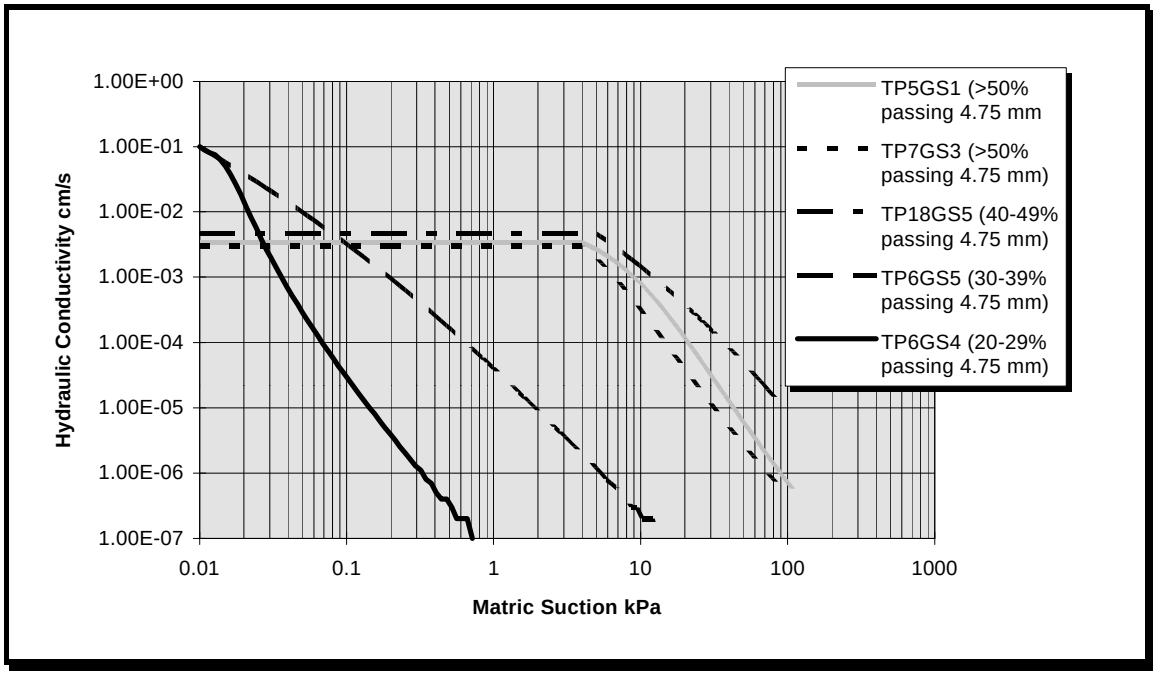


**Figure 2.5 Hydraulic Conductivity Function for Sampled Waste Rock (after Herasymuik, 1996)**

## 2.5 Conceptual Model

Herasymuik (1996) developed a detailed conceptual model describing the internal workings of an end-dumped waste pile. The model showed that end-dumped waste rock would result in stratified layers of waste rock at approximately the angle of repose, and the layers would be at residual water content. The stratified layers consisted of waste rock that had segregated after dumping during down-slope raveling. The stratified layers also formed due to variations in rock type. These layers were often relatively uniform in grain size but were not continuous down the slope. The adjacent layers were also uniform but were either coarser-grained or finer-grained. The hydraulic conductivity of adjacent layers may vary by several orders of magnitude. The difference in texture between the layers may be sufficient to result in preferential flow. A diagram showing a 2-dimensional simplification of the observations at GSM is presented in Figure 2.6.

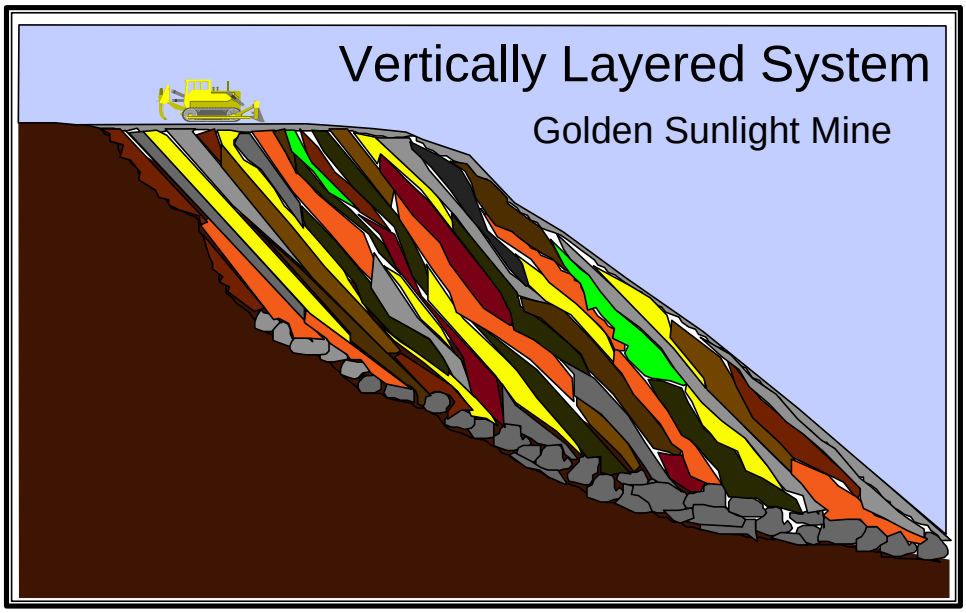


**Figure 2.6 Diagram of Layered System at GSM (after Herasymuik, 1996)**

Herasymuik (1996) described a conceptual model for the hydrogeology of an end-dumped waste rock pile. The conceptual model begins with the infiltration of water due to precipitation. Water that infiltrates into the coarse-grained

material at the top of the waste rock pile, or into the material on the slope, cannot be retained. The water will form into a film or droplets, and drain vertically from the coarse-grained layers due to gravity. It was suggested that Darcy's flow law does not describe the flow of water on the particle surfaces. The film of water on the coarse material enters the fine-grained layers, where it is then stored and transported under saturated/ unsaturated conditions (i.e., Darcy's law applies). Sulphide-bearing minerals present in the fine-grained layers interact with the infiltrating water and oxygen in a biochemical reaction. The biochemical reaction results in oxidation and weathering, and produces sulphuric acid. The contaminated infiltrated water can eventually drain from the waste rock pile. The increased heat and lowered pH caused by the initial reaction accelerates the oxidation process. The heat also increases the evaporation of water, with water vapor transported upwards in the waste rock pile. Coarse-grained waste rock layers with open interpartical voids provide a preferential pathway for the movement of water vapor and other escaping gases. The upward movement of water vapor may redistribute water within the wetting front where the vapor condenses to liquid or exits the pile. This process is active in the upper portion of the waste rock pile associated with the wetting front.

## 2.6 Aspects of the Physical Problem and Related Studies

An important part of developing a numerical model is the study and review of related research. Unfortunately, little research has been published on the prediction and analysis of seepage through waste rock dumps. Newman (1999) conducted a closely related study and the present study is largely an extension of this initial work. The study of the capillary barrier effect in engineered soil covers is also somewhat related to the present study and has received considerable attention in the research literature.

### 2.6.1 Mechanism for Preferential Flow

Newman (1999) studied the mechanism for preferential flow. The study was based on the conceptual model developed by Herasymuik (1996) and

observations made by Horton and Hawkins (1965). The research methodology followed by Newman (1999) included a column study and a numerical modelling program.

A laboratory test was conducted with a column that measured 15 by 30 by 140 cm and was constructed of clear plastic (Figure 2.7). The column was designed to allow two different materials to be placed side by side in a series of lifts, separated by a thin adjustable metal sheet. The materials used in the experiment had contrasting grain sizes (i.e., a coarse-grained material in contact with a fine-grained material). The first column experiment used a fine-grained Beaver Creek sand separated from a coarse-grained medium silica sand. The second column test consisted of a coarse-grained waste rock from GSM next to a fine-grained waste rock.

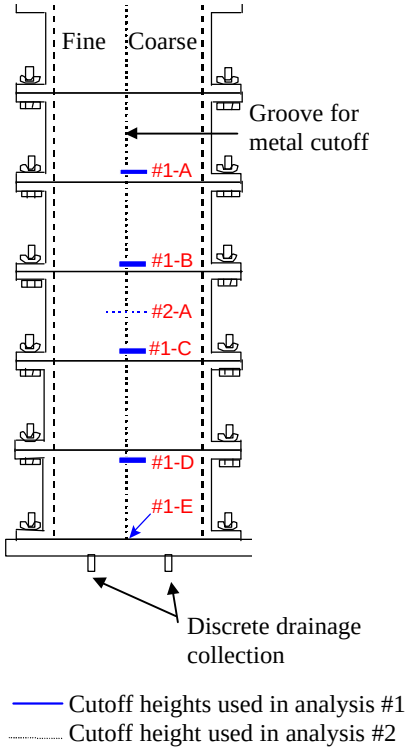


**Figure 2.7 Column Design (after Newman et al, 1997)**

The laboratory analysis consisted of four steady-state fluxes applied evenly over the surface of the column for different cutoff heights. Two of the applied flux rates exceeded the saturated hydraulic conductivity ($K_{sat}$) of the fine-grained layer, while two other applied flux rates were less than the $K_{sat}$ of the fine-grained material. At the end of the experiments, the resulting discharge was collected from each vertical layer and the percentage of flow transported through the coarse-grained material was compared to that transported by the fine-grained material. For each different contact length, the procedure was repeated. The different contact lengths controlled the length over which water could flow between the two materials. The larger contact length resulted in an increase in horizontal transport of liquid water between the materials. Once the laboratory experiment was completed, numerical modelling was performed using the finite element-modelling package Seep/W by Geo-Slope International (Newman et al, 1997).

Newman et al, (1997) presented the results from the column experiment and numerical modelling program and stated, "…that when the applied flux is greater than $K_{sat}$ of the fine-grained material, water flows preferentially through the coarse-grained material…" as shown in Figure 2.8. In addition, "Under steady-state conditions, pore-water pressures at the surface are reduced in the fine-grained material, as the material pores become water filled. The coarse material also experiences negative pore-water pressure under the applied flux. Between the suctions of 0 kPa to the suction where the hydraulic conductivity of the coarse and fine-grained materials intersect, the coarse-grained material is more conductive and waters that enters the fine-grained material flows preferentially towards the coarser material."

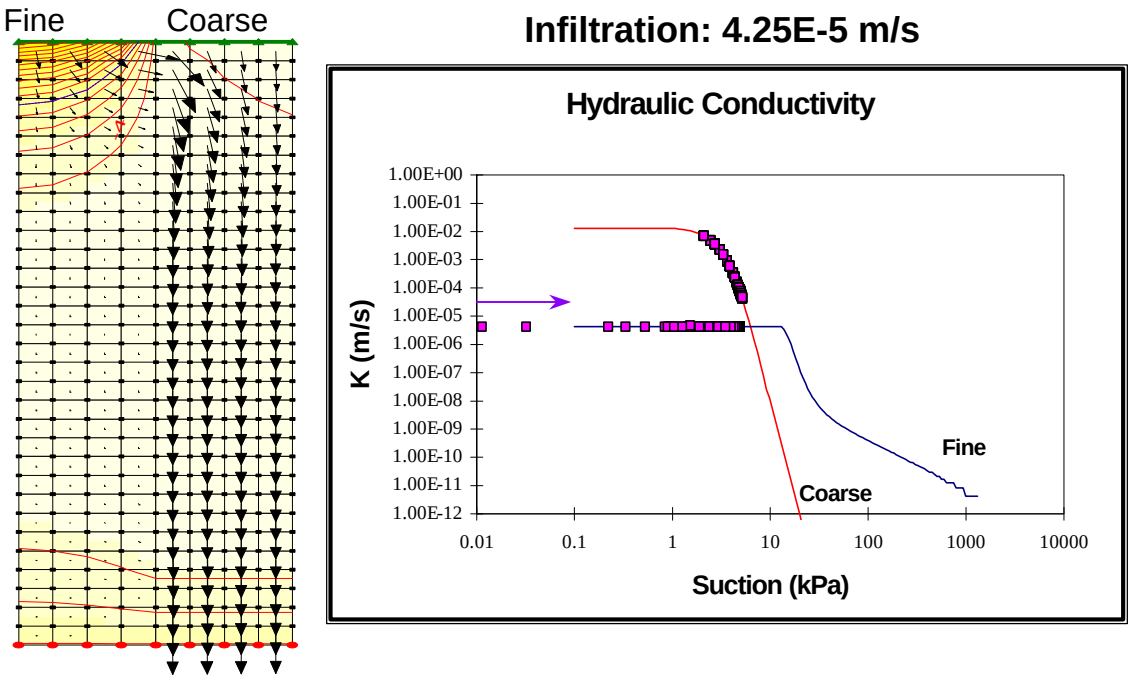


**Figure 2.8 Numerical Modelling Result When the Applied Flux was Greater than the $K_{sat}$ of the Fine-Grained Material (after Newman et al, 1997)**

Newman et al, (1997) also stated that, "When the applied flux is less than $K_{sat}$ of the fine-grained material, water flows preferentially through the fine material…" (Figure 2.9). "Under an applied flux of 4.25E-7 m/s, the suction in the layers is greater than the intersection suction and fine-grained material will exhibit the greater conductivity. In both the laboratory experiment and the numerical simulations, a pressure equal to zero boundary condition was placed at the bottom of the column. The pressure contours show that as the water flows towards the bottom, suction must reduce in order to satisfy this condition. The point of re-crossover occurs at a point where the matric suction in that the coarse and fine-grained materials correspond to the same value hydraulic conductivity."

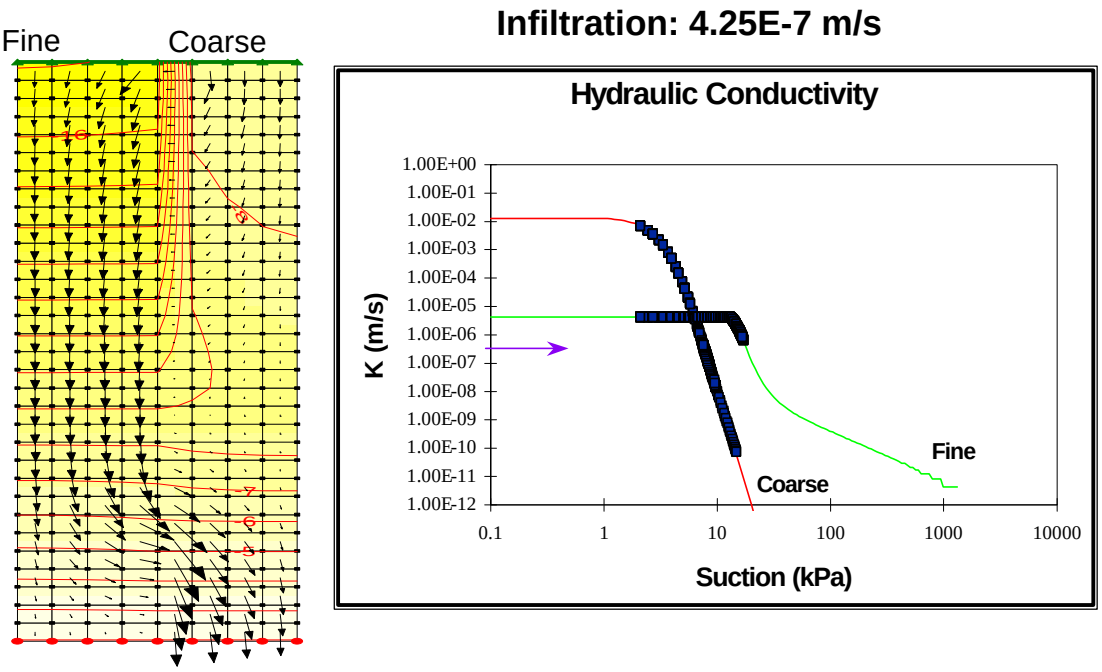


**Figure 2.9 Numerical Modelling Result when the Applied Flux was Less than the $K_{sat}$ of The Fine-Grained Material (after Newman et al, 1997)**

The major finding the work of Newman (1999) was that water would flow preferentially in the fine-grained layer for infiltration fluxes less than the saturated hydraulic conductivity of the fine material. This contradicts the conventional theory of flow explained in the waste rock dumps that was described in MEND (1995). The primary significance of the preferential flow is the ability of a waste rock pile to store water, which is one of the constituents required to produce ARD.

### 2.6.2 Studies on sloping layered system

The study of the capillary barrier effect in engineered soil covers is somewhat related to the problem at hand. Capillary barriers have received considerable attention in the research literature. Several laboratory and numerical modelling studies have been conducted by various researchers, (e.g., Frind et al., 1976; Zaslavsky and Sinai, 1981; Selim, 1987; Miyazaki, 1988; Larson et al., 1988; Ross, 1990; Wallach and Zaslavsky, 1991; Steenhuis et al., 1991; Tsai and Chen, 1993; Oldenburg and Pruess, 1993; Yeh et al., 1994; Stormont, 1995; Kumar et al., 1995). A detailed review of experimental, analytical, and numerical

works in this area has been presented by Bussière et al. (1997) who investigated capillary barriers on slopes.

The main difference between previous studies of capillary barrier and the current study is the slope angle. Capillary barrier covers installed on a tailings pond are typically constructed between 2° to 4° from the horizontal, while end-dumped waste rock dumps are constructed at the angle of repose (Aubertin et al, 1997). However, the similarities are that research has been conducted with regards to flow within each layer and across the interface of adjacent layers. The layers are constructed of sharply contrasting materials with the top layer being a fine-grained material and the lower layer being a coarse-grained material. Both systems are also subjected to unsaturated flow regimes (Bussière et al., 1997).

Miyazaki (1988) measured the water flow in unsaturated soil slopes where a fine soil was sandwiched between coarse materials. The objective of the study was to observe the effects of the coarse materials on down-slope water flow, and to extend the refraction law of water flow in saturated soils into unsaturated soils.

Miyazaki (1988) showed that the wetting front does not stop at the interface of the fine and coarse-grained soil layers. Water moves down along the inclined interface and the amount of lateral flow increases with distance down slope. Accumulation of the unsaturated flow along the interface may lead to a saturated condition at the lower end of the sloping interface when the interface is sufficiently long.

The incidence angle of the water flux between layers at the point where the wetting front reaches the interface is determined by combining the pressure head gradient and gravity. The direction of the pressure head gradient is practically perpendicular to the wetting front, while the direction of gravity is vertical. Figure 2.10 presents the difference in the refraction of flow between a

saturated and unsaturated layered system for different values of hydraulic conductivities.

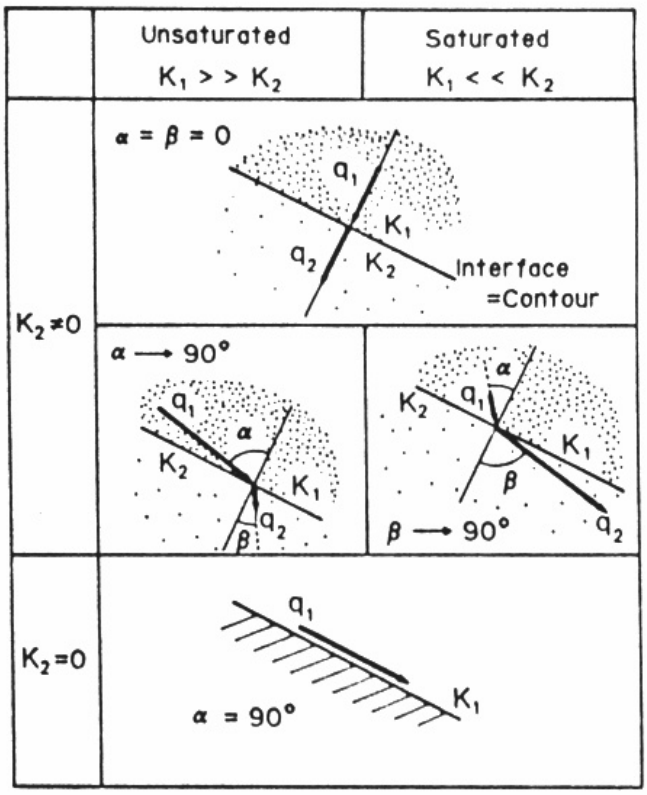


**Figure 2.10 Figure Presents the Difference in the Refraction of Flow Between a Saturated and Unsaturated Layered System for Different Hydraulic Conductivities (after Miyazaki, 1988)**

Figure 2.11 shows a schematic view of downward flow, unsaturated lateral flow (A), saturated lateral flow (B), and partial flow (C) at the inclined interface between fine and coarse-grained materials. Saturated lateral water flow in the second coarse layer accumulates and some water will drop vertically as partial water flow (C).

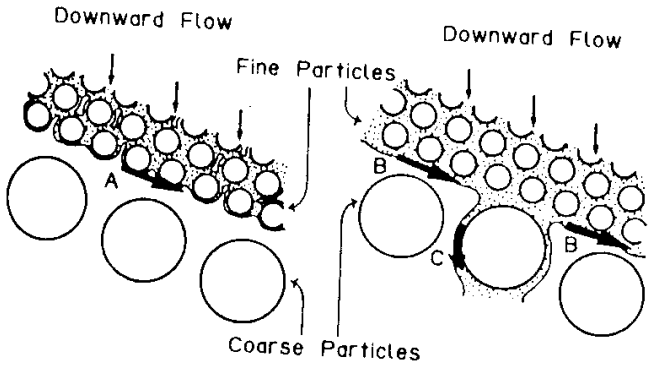


**Figure 2.11 Figure Shows the Schematic Relation between Downward Flow, Unsaturated Lateral Flow (A), Saturated Lateral Flow (B) and Partial Flow (C) at the Inclined Interface between Fine Particles and Coarse Materials (after Miyazaki, 1988)**

When a coarse-grained layer is sandwiched between two fine-grained layers, the wetting front apparently ceases and lateral flow occurs at the inclined interface between the top fine-grained and coarse-grained layer during infiltration. The lateral flow of water also occurs at the inclined interface during steady state percolation. The combination of refraction with partial water flow (C) is an important concept with respect to the flow of water in highly heterogeneous soil slopes.

Stormont (1995) confirmed the work of Miyazaki (1988) in his study on the effect of constant anisotropy on capillary barrier performance. Stormont (1995) indicated that the consequence of anisotropy in a fine-grained layer is that infiltration at the top of the fine-grained layer might be deflected from the vertical. Downward moving water should be diverted laterally as it approaches the fine-coarse interface. Lateral diversion along the fine-grained layer results in an increasing water content in the down dip direction. Eventually, there will be a location near the fine-coarse contact that becomes sufficiently wet that a quantity of water equal to the infiltration rate will move into the coarse-grained layer.

Stormont (1995) concluded that an anisotropic fine-grained layer could improve the performance of a capillary barrier in two ways. First, the increased rate of lateral divergence in an anisotropic capillary barrier will tend to keep the fine-grained layer drier and consequently less likely to become wet and vulnerable. Second, for any infiltration rate under comparable antecedent conditions, an anisotropic capillary barrier will have a greater divergence length than a comparable isotropic barrier.

The above research relates to a dipping layered system of end-dumped waste rock. The steeper angles in the waste rock dump will increase the effect gravity will have on the infiltrating water. The fine-coarse contact between waste rock layers will also facilitate the movement of unsaturated flow down the slope. This also means that a coarse-grained layer will remain dry until the fine-grained layer above nears saturation.

Aubertin et al. (1997) performed a numerical modelling study of unsaturated flow in inclined layers. The authors investigated the influence of the slope angle and the length of the inclined layer using a 2-dimensional numerical model. The numerical model consisted of a 3-layer cover placed on tailings with a 2 and 4% slope, and with a 10 and 50-meter slope length. The authors also noted that larger slope angles could be used to study dikes and waste dumps. The authors also warned of the danger of misinterpreting a one-dimensional model of a cover system.

The result obtained by Aubertin et al. (1997) showed that the hydrogeological conditions in an inclined and layered unsaturated soil system were influenced by several factors. The factors suggested were the capillary properties of the different materials (including a possible anisotropy), the system geometry (layer thickness, length, and slope angle), the hydraulic regime and the water balance components (precipitation, evaporation, infiltration, and runoff).

The physics of flow for the problem of inclined systems was shown by Aubertin et al. (1997). If the hydraulic pressure corresponding elevation to the difference between the upper and lower part of a continuous system approached the air entry value (AEV) of the fine-grained material, then the top portion may become unsaturated. In the case analyzed, it was important to ensure a high degree of saturation along the slope of a cover system to prevent gas transport across the cover. In a tall steep layered system, fine layers could desaturate rapidly over longer contact lengths.

Desaturation of the soil depends upon the slope length and the slope angle. Increasing the air entry value (AEV) of the fine-grained material also helps maintain a more stable water content profile. Aubertin et al. (1997) noted that there is a complex but definite relationship between the soil-water characteristic curve (SWCC) of the soil and the slope length, angle, and moisture distribution in covers.

Stormont and Anderson (1999) conducted infiltration tests on soil columns to investigate the capillary barrier effect of an underlying coarse-grained layer. The results showed that water movement across the interface occurred when the suction head at the interface reached the breakthrough head of the coarser lower soil layer. The breakthrough head was defined as the suction head at which the coarse-grained layer first began to conduct seepage, regardless of the infiltration rate or the properties of the overlying fine-grained soil layer.

Stormont and Anderson (1999) also noted that after eight test-cycles, the breakthrough head did not change substantially, and an effective capillary barrier was restored after each breakthrough. It was also noted that the more uniform and coarser the lower soil layer, the more effective the capillary barrier. The suction head profile during these tests was controlled by the properties of the fine-grained upper layer and by the infiltration rate until the soil near the interface reached the breakthrough head. The authors showed the importance

of the materials used for a cover system and the effect of the materials on the performance of the cover system.

Bussière et al, (1999) studied the capillary barrier effects with respect to the slope angle. The study was conducted for barriers to be used as a gas barrier for reactive mine tailings. The authors showed the results of a numerical study that illustrated the influence of the slope angle on the capillary barrier behavior of different materials.

The Bussière et al, (1999) numerical model study is one of the more complete studies found in the research literature. The numerical study was conducted using Seep/W finite element model for saturated and unsaturated flow (Geo-Slope, 1995). The model simulated was the cross-section of an actual mine site with a slope length of 50 meters and an angle of 18°. The mesh density used was much finer at the top than it was inside the tailings. The intention was to have greater precision in the numerical prediction without having a model that was too computationally demanding. The numerical model was then verified using measured values from instrumentation placed in situ.

The study showed that the water content profile was significantly influenced by the position under consideration along the slope. Thus, it was necessary to evaluate the impact of the geometry on the performance of a cover. The study also confirmed earlier findings that a finer-grained material with a high air entry value will hold water better than a coarser-grained material with a lower air entry value.

## 2.7 Summary and Need for Further Research

The primary rational for this study was to develop appropriate methods for predicting the hydrologic behaviour of waste rock dumps. The key objective of this present work is to study, layered systems within waste rock piles where infiltration flows preferentially through the dump.

Previous studies carried out by Newman (1999) and Bussière et al, (1999) demonstrated that the preferential flow in coarse and fine-grained materials under unsaturated conditions could be simulated using the Seep/W model (Geo-slope, 1995). The previous studies were directed at either vertical (Newman, 1999) or relatively flat (Bussière et al, 1999) layered systems. In the subsequent chapters of the thesis, the Seep/W model will be used to attempt to predict unsaturated flow patterns through interbedded layers of coarse and fine-grained materials. The first part of this chapter introduced the physical problem of ARD and showed that limited research has been done in the area of predicting flow through end-dumped waste rock piles. There is an important need to be able to predict, control, and possibly design waste rock dumps that transmit infiltration water through preferred pathways. Mehling et al. (1997) proposed blending and layering waste rock to delay, mitigate, or prevent acid generation. This method proposed blending or layering acid and non-acid generating waste rock to produce an environmentally benign composite. Attempts to verify the theory were limited by an extremely limited database of case studies.

The examinations of Mehling et al. (1997) on available hard rock case studies, indicated that:

1. Blending did not reduce sulphide oxidation rates in the potentially acid material unless highly reactive neutralizing material (lime) was applied, and the blending was near ideal, as in column or humidity cell tests.
2. Layering did not reduce sulphide oxidation rates in potentially acid material, even when layers were less than 10 cm thick.

Mehling et al. (1997) identified several problems that future researchers should study. The first two problems were i) developing intimate contact between the mixed materials to achieve a benign composite at a practical cost, and ii) relating laboratory test results to the field. The third area of concern identified was related to the prediction of preferential flow through acid producing layers. The third problem is the major focus of this thesis.

The Mehling et al. (1997) study also suggested hauling limestone to a mine site and blending it with reactive waste rock, provided it was economical. It might even be more economical to grind reactive and non-reactive waste rock to specified grain sizes, and then layer these materials. The blending of layers was found to be ineffective at 10-cm thicknesses (Mehling et al., 1997). The layering of coarse-grained reactive with fine-grained non-reactive waste rock can also induce preferential flow with a greater layer thickness, although thicker layers would make construction easier.

The current study builds on a combination of the observations made in the field by Herasymuik (1996) and the laboratory and modelling study of Newman (1999). Newman (1999) successfully predicted the behaviour of a vertical system. Typically, real systems are inclined. The current study extends the Newman (1999) study to higher and steeper systems such as those observed by Herasymuik (1996).

# CHAPTER 3

# THEORETICAL BACKGROUND

## 3.1 Introduction

The previous chapter described the physical problem to be solved, a conceptual interpretation of the physical problem, a review of past research studies and the methodology required to solve the problem. The specific tools to solve the problem are the related theory and governing equations. These tools convert the conceptual model to a mathematical model and a modelling program. This chapter summarizes the saturated/unsaturated soil theory necessary to describe the physical problem and introduces the governing equations.

## 3.2 Unsaturated Soil Theory

The flow of water in waste rock piles is important because of both its potential environmental impacts and its influence on slope stability. Waste rock piles are designed and constructed on the ground surface to prevent the retention of water behind or above the embankment face (Nelson and McWhorter, 1985). As a result, most waste rock piles, except for localized saturated zones, are unsaturated. Waste rock piles may receive water from several sources, and do not function under steady state seepage conditions. Water is generally introduced periodically (i.e., rainfall, snowmelt, runoff etc.) and an understanding of the principles of unsteady state unsaturated water movement, as it pertains to acid rock drainage (ARD), is critical.

The following sections describe the theoretical background of unsaturated soil theory required to develop the equations for the mathematical model.

### 3.2.1 Properties of Unsaturated Soils

Unsaturated soils consist of four phases: air, water, soil particles, and the contractile skin as shown in Figure 3.1 (Fredlund and Rahardjo, 1993). Fredlund and Rahardjo (1993) stated, “The primary property that influences the soil is the ability of the contractile skin to exert surface tension and consequently it behaves like an elastic membrane under tension.”

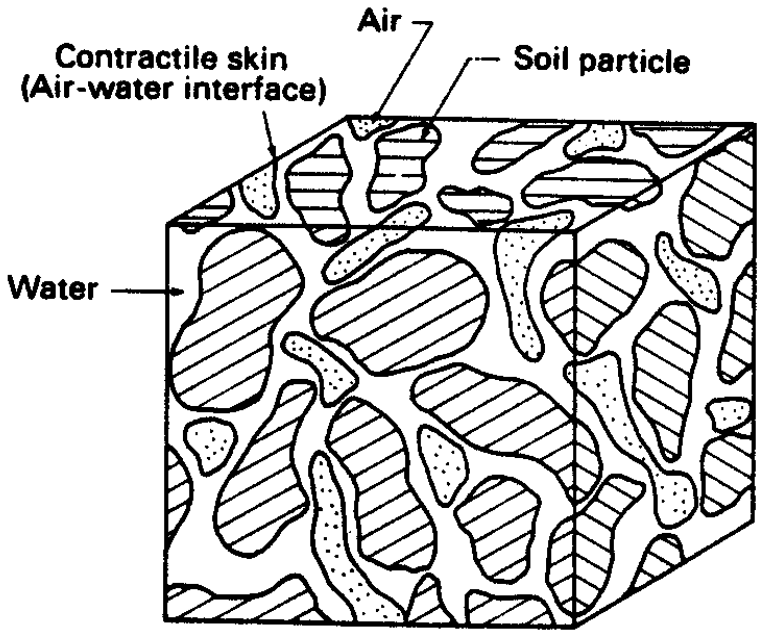


**Figure 3.1 An Element of Unsaturated Soil Showing Continuous Air Phase (after Fredlund and Rahardjo, 1993)**

The surface tension of the contractile skin results from different intermolecular forces acting on the molecules at the air-water interface compared to the forces acting on the water molecules in the interior of the water (Fredlund and Rahardjo, 1993). The contractile skin behaves like an elastic membrane with different pressures on each side. The pressure differences create a curved membrane with the concave curvature towards the larger exerting pressure. Fredlund and Rahardjo (1993) stated, “The surface tension produced by the differences in pressure exerted on the curved membrane or contractile skin

relates to the radius of curvature of the surface." Figure 3.2 illustrates the pressures and surface tension acting on a curved membrane.

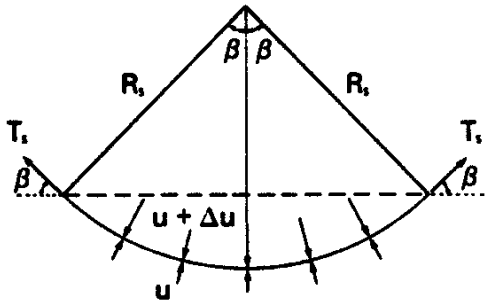


**Figure 3.2 Pressures and Surface Tension Acting on a Curved Surface (after Fredlund and Rahardjo, 1993)**

Fredlund and Rahardjo (1993) stated, "Pressures u and u + $\Delta$u are acting on the membrane with a radius of curvature $R_s$ and a surface tension of $T_s$. Unsaturated soils are subjected to an air pressure $u_a$ that is greater than the water pressure $u_w$. The difference between the air pressure and water pressure is referred to as the matric suction ($u_a - u_w$)." This pressure difference causes the contractile skin to curve according to the Equation 3.1. "When the air and water pressure become equal, the radius of curvature approaches infinity resulting in zero matric suction and a flat air-water interface."

$$(u_a - u_w) = 2T_s/R_s \qquad (3.1)$$

A term that needs to be defined is soil suction. Fredlund and Rahardjo (1993) stated, "Soil suction refers to the free energy state of the soil water measured in terms of the partial vapour pressure of the soil water. Total suction is the addition of capillary forces and dissolved salts in unsaturated soil, and is represented by matric and osmotic suction…." From Figure 3.2, "…it can be seen that matric suction is related to capillarity. The pore spaces in a porous media act as capillary tubes that cause water to rise above the water table. This zone is referred to as the capillary fringe. Although the pores are saturated, the

pressure heads are less than atmospheric or negative in this zone. As pore water pressure becomes increasingly negative the pores begin to drain and adsorptive forces between soil particles may assist in sustaining high negative water pressures at low water contents…." Figure 3.3 illustrates this principle with a capillary tube model using different radii of curvature. "The relative humidity in the soil also decreases as a result of increases in matric and osmotic suction. Matric suction is zero at 100% relative humidity."

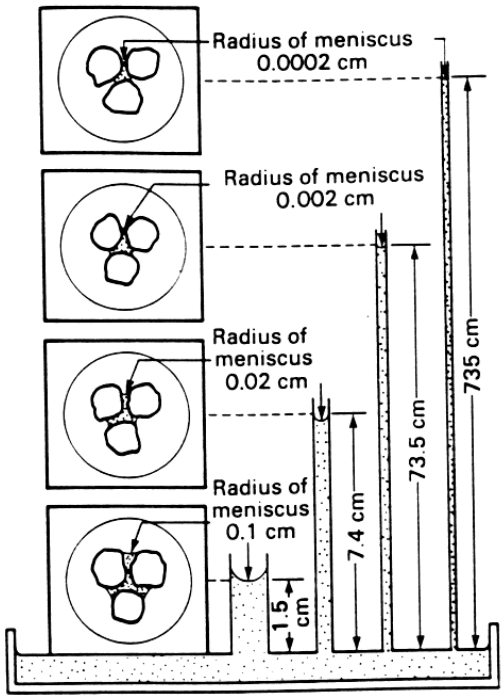


**Figure 3.3 Capillary Tubes, Illustrating the Air-Water Interface at Different Radii of Curvature in Soil (after Fredlund and Rahardjo, 1993)**

### 3.2.2 Unsaturated Liquid Water Flow

For saturated and unsaturated soils, the driving potential causing water to flow is known as hydraulic head. Hydraulic head is defined as the sum of the elevation head and pressure head and is presented in Equation 3.2 (Fredlund and Rahardjo, 1993).

$$h = z + u_w / p_w g \quad (3.2)$$

Above the water table, the pressure heads are negative whereas below the water table pressure heads are positive. In the field, piezometers are used to provide a measurement of hydraulic head in saturated material. In the unsaturated zone however, hydraulic head is determined indirectly through the measurement of the suction head or negative pore-water pressure using a tensiometer. Water will flow from a point of high hydraulic head to a point with low hydraulic head regardless of whether the pore-water pressure is negative or positive (Fredlund and Rahardjo, 1993).

Darcy's Law describes water flow in soils. Darcy's Law states that the flow of water through a soil is proportional to the hydraulic gradient by the following equation:

$$n_w = -K_w \, \partial h_w / \partial y \quad (3.3)$$

where: $n_w$ = flow rate of water (specific discharge),
$-K_w$ = hydraulic conductivity with respects to the water phase, and
$\partial h_w / \partial y$ = hydraulic gradient in the y direction.

The specific discharge $n_w$ has the dimension of a velocity or flux and is sometimes referred to as the Darcy velocity or flux (Freeze and Cherry, 1979). Darcy's law can also be written as:

$$Q = -KiA \quad (3.4)$$

where: Q = discharge,
i = hydraulic gradient, and
A = cross-sectional area.

Darcy's law is also valid for flow through unsaturated soil; although, the hydraulic conductivity is no longer constant. Under saturated conditions, the hydraulic conductivity is approximately constant. In unsaturated conditions, the hydraulic conductivity is a function of the water content and matric suction.

Higher water contents result in more pores filled with water. Water flows through pores filled with water and therefore, under unsaturated condition, fewer pores are available for flow. As a result, lower water contents correspond to lower values of hydraulic conductivity. During the drainage of a saturated soil, air begins to enter the large pore spaces first and water flow is forced to move along the more tortuous path in the smaller pores (Fredlund and Rahardjo, 1993). The hydraulic conductivity will decrease rapidly as the volume of pore space occupied by water decreases.

Fredlund and Rahardjo, (1993) stated that, “The soil water characteristic curve (SWCC) represents the volumetric water content as a function of matric suction. The SWCC is important in describing how a soil stores water under negative pore-water pressures. The air entry value (AEV) can be determined from the SWCC. The AEV is defined as the matric suction value that must be exceeded to have air enter the voids of the soil. The AEV is a function of the maximum pore size of the soil.” Figure 3.4 shows a typical SWCC. The residual degree of saturation or water content is defined as the degree of saturation or the water content at which an increase in matric suction does not produce a significant change in the degree of saturation or water content (Fredlund and Rahardjo, 1993).

The hydraulic conductivity function is expressed by the hydraulic conductivity versus suction or pore-water pressure. Figure 3.4 shows three typical curves. These curves are commonly determined from the soil-water characteristic curve. There are several methods that allow for the calculation of the hydraulic conductivity function. The Fredlund et al (1994) method was used for this study.

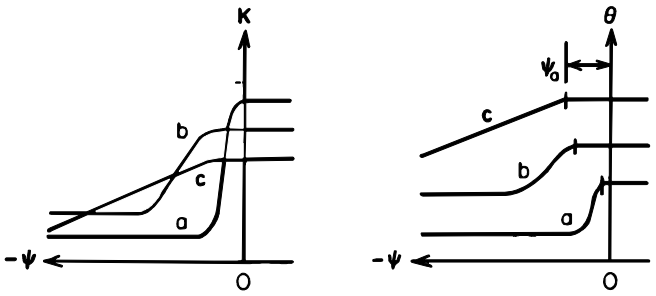


**Figure 3.4 Characteristic Curves for Volumetric Water Content and Hydraulic Conductivity as a Function of Negative Pressure Head (after Freeze and Cherry, 1979). (a) Uniform Sand; (b) Silty Sand; (c) Silty Clay**

### 3.3 Finite Element Method

The finite element method is one tool that can be used to solve the governing equations. The application of the finite element method requires the discretization of the soil mass into elements. Triangular and quadrilateral shapes of elements are commonly used for two-dimensional problems. Each element is made up of points call nodal points. The hydraulic head at each nodal point is obtained by solving the governing flow equation and applying the boundary conditions (Fredlund and Rahardjo, 1993).

The two-dimensional finite element software package used to solve the mathematical model and governing equation for this study is Seep/W (Geo-Slope, 1995). The governing differential equation for 2-dimensional saturated/ unsaturated flow used in the formulation of Seep/W is as follows:

$$\frac{\partial}{\partial x}\left(k_x \frac{\partial h}{\partial x}\right)+\frac{\partial}{\partial y}\left(k_y \frac{\partial h}{\partial y}\right)+Q=\frac{\partial \Theta}{\partial t} \qquad (3.5)$$

where: h = total head
$k_x$ = hydraulic conductivity in the x-direction
$k_y$ = hydraulic conductivity in the y-direction
Q = applied boundary flux
Θ = volumetric water content
t = time

Equation 3.5 states that the difference between the flow (flux) entering and leaving an elemental volume at a point in time is equal to the change in the volumetric water content. In other words, the sum of the rates of change of flows in the x and y-directions plus the external applied flux is equal to the rate of change of the volumetric water content with respect to time

Under steady state conditions, the flux entering and leaving an elemental volume is the same at all times. The right side of the equation consequently vanishes and the equation reduces to:

$$\frac{\partial}{\partial x}\left(k_x \frac{\partial h}{\partial x}\right)+\frac{\partial}{\partial y}\left(k_y \frac{\partial h}{\partial y}\right)+Q=0 \qquad (3.6)$$

A soil element with infinitesimal dimensions illustrated the derivation of Equation 3.6 for steady-state system is presented in Figure 3.5.

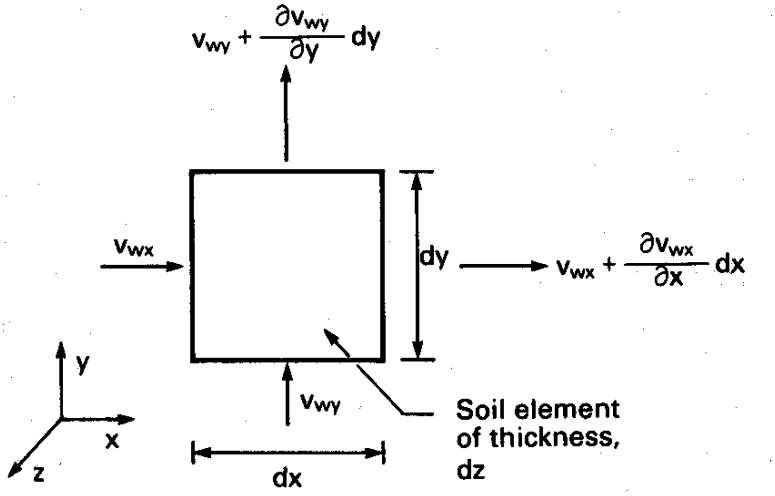


**Figure 3.5 Two-Dimensional Water Flow through an Unsaturated Soil Element (after Fredlund and Rahardjo, 1993)**

### 3.4 Modified Kisch Solution

The finite element method combined with a software package like Seep/W (Geo-slope, 1995), provides a comprehensive numerical tool. However, it is possible to use a finite difference method with hand calculations to provide a clearer understanding of the processes that are taking place. The following section summarizes the finite difference solution that was used to model preferential flow in waste rock layers.

Kisch (1959) considered the problem of reducing water losses from reservoirs by using a lining of compacted clay. It was assumed that water flow was vertical and solutions were obtained for the equation of steady-state saturated and unsaturated flow through non-homogeneous soils. The equations provided the relationship between the water head in the blanketed reservoir and seepage losses.

The Kisch method of analysis is based on the equation for unsaturated steady flow using Darcy's law, and is presented in Equation 3.7.

$$q = K\frac{\partial h}{\partial z} \tag{3.7}$$

where: $q$ = discharge per unit area normal to flow,
$K$ = saturated or unsaturated permeability (with dimensions $LT^{-1}$),
$h$ = hydraulic head (with dimensions $L$), and
$z$ = vertical coordinate increasing upwards (i.e., in the direction opposite to the flow.

The hydraulic head, *h* is defined by Equation 3.8. For unsaturated flow, the pressure head is a function of the water content (i.e., there is no pressure transfer).

$$h = p + z \tag{3.8}$$

where: $p$ = pore-water pressure head.

Using Equations 3.7 and 3.8, and assuming *q* is constant for steady-state:

$$\frac{\partial p}{\partial z} = \frac{q}{K} - \frac{\partial z}{\partial z} \text{ or } \frac{\partial p}{\partial z} = \frac{q}{K} - 1 \tag{3.9}$$

Equation 3.9 is referred to as the Kisch solution (However, soil scientist refer to Equation 3.9 as the Richard's Equation). In Equation 3.9, Kisch assumed the there was only vertical flow and therefore the gradient, $\partial z / \partial z$ is equal to one. In a sloping system the distance between two nodes is no longer $\partial z$ but $\partial l$, and

$$\partial l = \partial z / \sin a \tag{3.10}$$

where: $\alpha$ = the slope angle.

Substituting Equation 3.10 into 3.9 results in an equation for both saturated and unsaturated flow for a sloping system.

$$\frac{\partial p}{\partial l} = \frac{q}{K} - \frac{\partial z}{\partial l} \tag{3.11}$$

Note that Equation 3.11 becomes the same as Equation 3.9 when $a = 90^{o}$.

To solve Equations 3.9 and 3.11, the relationship between $K$ and $p$ must be known. By knowing the hydraulic conductivity function with respect to pressure head (meters), a table of values can be set up on a spreadsheet. The Kisch solution is solved by plotting the function $Y = (q/K - 1)^{-1}$ as a function of $p$. The area under the curve between two values of $p$ is equal to the distance between the points where $p$ is equal to these two values. The function, $Y$, approaches infinity as the calculated hydraulic conductivity approaches the applied flux (i.e., *K* approaches *q*), and as $z$ increases $p$ will go to a constant value (i.e., $\partial p$

approaches 0 as *z* increases). The constant value of $p$ corresponds to $K$ equal to $q$.

The above theory can be applied to a sloping layered system of fine and coarse-grained material (refer to Figure 3.6). The bottom boundary condition can be chosen for a variety of situations. The water table at the bottom boundary can be defined as having a pressure head of 0-meters, and a hydraulic conductivity equivalent to the saturated hydraulic conductivity. Using the Kisch formulation, the pressure head profile can be calculated for each column for a specified *q* with respect to the incremental elevation changes by moving up through the column. However, it is necessary to calculate the pressure head profile for the system (i.e., both columns together). The system pressure head is assumed to be equal horizontally at each vertical node for each column. To solve for the system pressure head, the system hydraulic conductivity can be calculated using Equation 3.12, (Freeze and Cherry, 1979).

$$K_{ll} = \frac{(K_c \times b_c) + (K_f \times b_f)}{b_c + b_f} \qquad (3.12)$$

where: $K_{ll}$ = the hydraulic conductivity where the flow is parallel to the soil columns,

$K_c$, = the hydraulic conductivity of the coarse and fine soil types respectively, and

$b_c$, = the thickness of coarse and fine soil types respectively.

The equations presented above are arranged in a manner that can be solved using an iterative procedure with respect to incremental elevation changes (i.e., $\partial$ e separated by $\partial$

Selecting a value for $\partial$

One hundred nodes were used for simulations. Once the initial bottom boundary -meters for a water table), the applied

flux, the thickness of each column, and the angle of the system is specified. The system angle can be varied from the vertical (90º) to 45º.

Equations 3.11 and 3.12 can be solved for the change in pressure head. The change in pressure head is added to the previous head, and a new iteration with a new hydraulic conductivity for each soil type is then solved at the next node. The new hydraulic conductivities are solved by using a table of the material properties and a simple linear interpolating function to solve for values between known points. As the pressure head and hydraulic conductivity of the system are solved, the pressure head and hydraulic conductivity for the individual soil types are independently solved. From the information obtained, the system gradient and individual fluxes at each node can be calculated. The system gradient for each node is calculated by solving the right hand side of Equation 3.11. The hydraulic conductivity, gradient, and area are known for each layer. Therefore, the flux at each node for each layer can be solved using Darcy's Law. The sum of the flux in each layer is equal to the total applied flux.

Figure 3.6 illustrates the modified Kisch solution using the finite difference method (FDM). The FDM profiles show how two single one-dimensional columns are combined to make a pseudo-two dimensional column with two distinct layers. The FDM pressure profiles show how the pressure heads calculated for each node combined to form the system pressure head profile (*hp*). The FDM sloped profile shows the dimensions used to define the algorithms for sloping the solution (i.e., Equation 3.10). The flux profiles show the calculated flux results in each layer of the system calculated from the bottom boundary condition (i.e., $h = 0$).

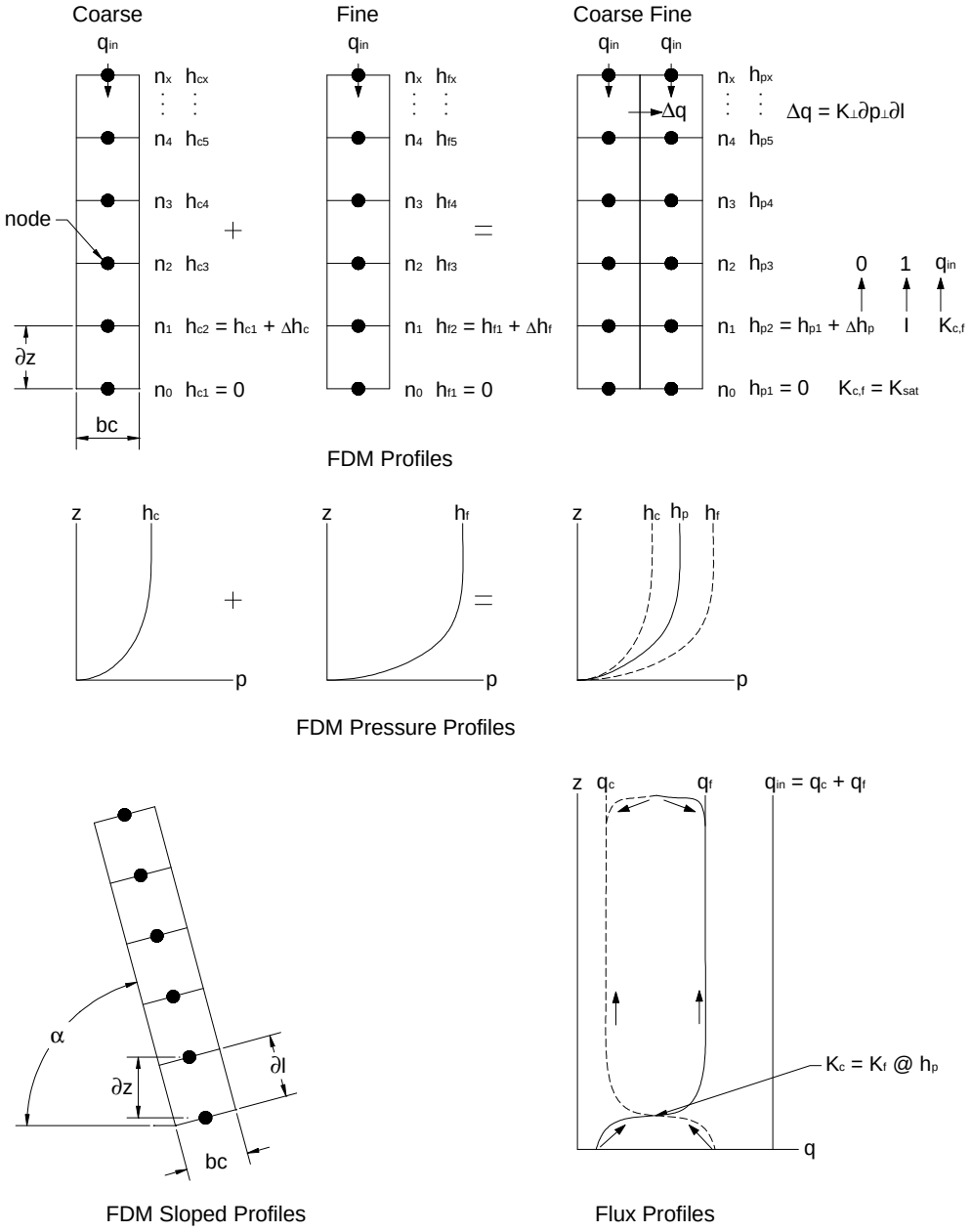


**Figure 3.6 Schematic of the Modified Kisch Solution Using the Finite Difference Method**

The above system of equations and iterative process can be solved for a layered system with preferential flow from the bottom boundary condition to the point where the change in pressure head approaches zero. However, the applied flux flows from the top to the bottom of the column. Separate sets of equations are required in order to describe how the applied flux flows preferentially on the top half of the columns

The flux is applied evenly across the top of both one-dimensional columns and the infiltrating flux flows in preferential pathways via lateral movement. The flux applied equally at the top node of both soil types results in pressure heads and hydraulic conductivities at the top nodes corresponding to the hydraulic conductivity curves of the individual soil type. The pressure head in individual soil layers and the hydraulic conductivity converged to the point where the change in pressure head approaches zero. Convergence is reached by laterally transferring a quantity of flux from the coarse-grained soil layer to the fine-grained layer. The amount of flux transferred is a function of the hydraulic conductivity and the pressure head difference between the two soil types. The flow is perpendicular to the applied flux. The perpendicular hydraulic conductivity of the system is calculated using Equation 3.13 (Freeze and Cherry, 1979).

$$K_{\perp} = \frac{b_c + b_f}{b_c / K_c + b_f / K_f} \tag{3.13}$$

Equation 3.14 calculates the change in flux in transferring from one column to another.

$$\Delta q = K_{\perp} \partial p_{\perp} \partial l \tag{3.14}$$

where: $\partial p_{\perp}$ = the difference in pressure head between the coarse-grained and fine-grained column at a given node.

The calculated change in flux is then added to the fine-grained column and subtracted from the coarse-grained column. Given the new flux at the nodes in each column, the next iteration of hydraulic conductivities can be calculated using Equation 3.15.

$$K_{c,f} = \frac{q_{c,f} / \sin a}{b_{c,f}} \tag{3.15}$$

Calculating the coarse-grained and fine-grained pressure heads from the new hydraulic conductivities completes the iteration. The iterations are calculated with the use of a table of values and a simple linear interpolating function. Further iterations cause the change in flux and the difference in pressure heads to approach zero. Eventually, the fluxes and pressure heads equal the values calculated by the first set of equations presented. Figure 3.6 also illustrates the distribution of the applied flux (i.e., the top boundary condition) in the FDM and flux profiles of the system. The modified Kisch solution spreadsheets are presented in Appendix C.

This chapter has outlined the necessary theoretical background needed to solve the physical problem described in Chapter 2. The following chapter outlines the attempts to solve the physical model using the governing equations of flow and modelling programs using both the Seep/W model and the modified Kisch solution.

# CHAPTER 4

# NUMERICAL MODELLING PROGRAM

## 4.1 Introduction

The theory required to describe the conceptual model mathematically was outlined in Chapter 3. This chapter will build on the previous chapters and develops a solution for the physical model.

A pilot program to numerically model flow through waste rock was conducted prior to the work presented in this thesis. The pilot program was designed to model, using the Seep/W model, observations made by Herasymuik (1996). However, modelling a waste rock pile proved to be extremely difficult. Several problems or combinations of problems were identified. To solve these problems, the model was simplified.

The simplifications implemented provided poor results. A base line model of a known solution was needed. As noted in Chapter 2, Newman (1999) completed a study of preferential flow between adjacent coarse-grained and fine-grained materials.

The objective of the pilot program was to determine whether the overall objective (i.e. numerically modelling flow through a layered waste rock system) was possible and to identify and overcome the difficulties encountered. The resulting parametric study established a base line model that was systematically increased in complexity. The objective of the parametric study was to identify

how flow occurred through waste rock layers and how flow would behave as the model grew in complexity.

The parametric study identified several anomalies in the model and the numerical modelling method. Therefore, an extensive sensitivity analysis using the Seep/W model was developed to explore selected areas of interest. The sensitivity analysis is presented in Appendix B. The use of the simpler modified Kisch solution was explored to see if a comparable solution could be obtained, and to develop a better understanding of the basic principals involved in solving the problem.

## 4.2 Pilot Program

Chapter 2 described in detail the observations made by Herasymuik (1996) at Golden Sunlight Mine in Montana, USA, and those outlined by MEND (1995). Herasymuik (1996) developed a conceptual model of the hydrogeology of the waste rock pile, based on field observations. Herasymuik (1996) observed that the waste rock at Golden Sunlight Mine was placed in high wedge-dump and terraced-dump configurations and were constructed by end-dumped waste rock in several lifts. The top and bottom of each lift had a fine-grained horizontal layer associated with heavy truck traffic. In most cases, the traffic layers were observed to be near saturation. The variation in texture between the waste rock layers was sufficient to result in preferential flow through the waste rock pile. A photograph showing the observations at GSM can be seen in Figure 4.1.

The pilot program resulted from the need to numerically simulate the hydrogeology of an end dumped waste rock pile. The model considered only the flow of liquid water through the waste rock pile. Chemical reactions and gas flow were not considered. The criteria for the model involved a compromise between accuracy and simplicity. The model could not be too complex or it would be impossible to solve, however the model could not be overly simple or it would not achieve the objective of the program. Figure 4.1 shows the highly structured end-dumped waste rock pile, and illustrates how the physical

phenomenon was converted into a numerical model. First, the boundary conditions were identified. A boundary was placed between each layer, and the top and bottom of all the layers. A decision was made regarding the number of layers that should be included in the model (i.e., where to place the left and right boundaries). The use of four to eight layers was deemed reasonable, to minimize the effects that the boundaries would have on the interaction of the internal layers, without an excessive number of layers increasing the computational effort by an unreasonably amount.

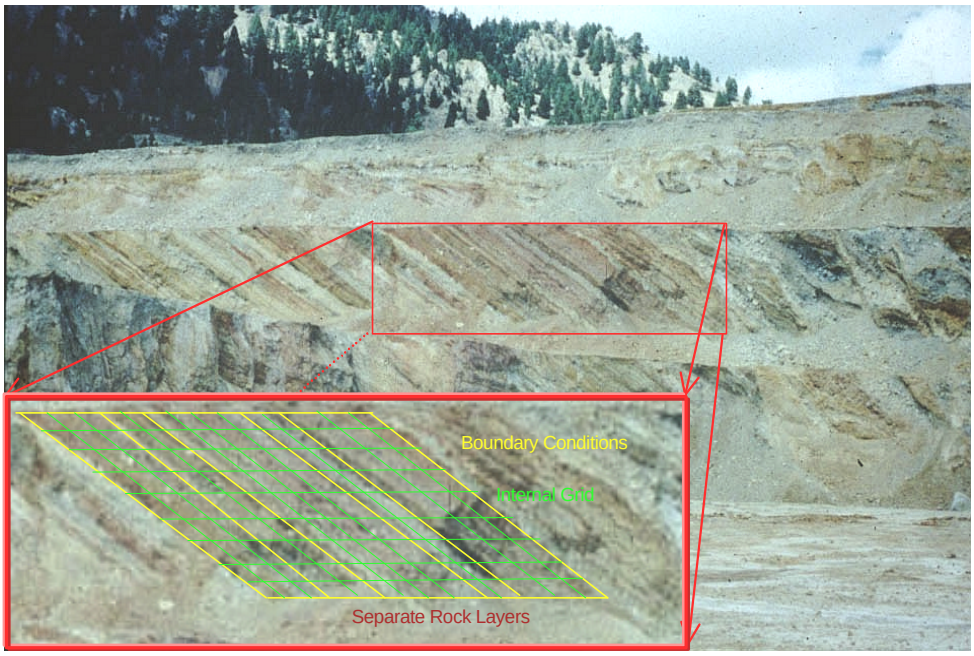


**Figure 4.1 Simplification of Layered Waste Rock System**

Based on these factors, a numerical model was developed for a twenty-meter lift. The model used the 2-D finite element-modelling package Seep/W (Geo-Slope, 1995). It was initially anticipated that simple boundary conditions and material properties were all that would be required for the analysis. Materials were chosen with properties similar to the waste rock samples available for laboratory testing. The materials selected for the analyses were those used by

Newman (1999). Beaver Creek sand was chosen to represent fine waste rock layers. Silica sand was selected for the coarse waste rock layers, and a compacted till was chosen for the tight traffic layer. The hydraulic conductivity functions of the materials selected are shown in Figure 4.2.

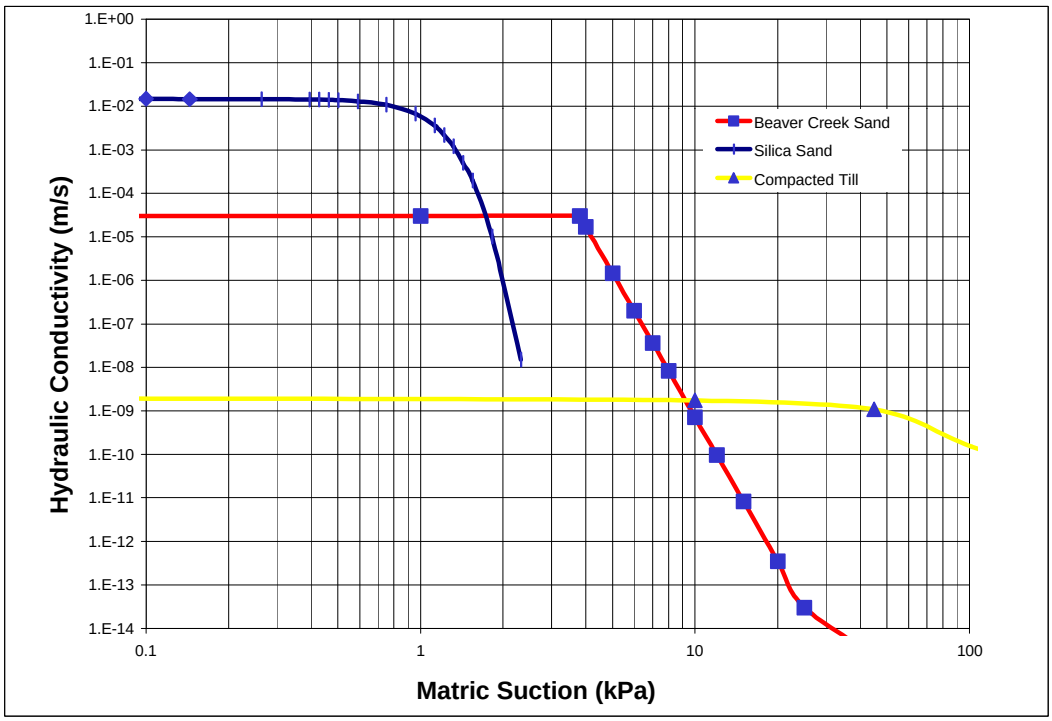


**Figure 4.2 Hydraulic Conductivity Functions for the Initial Pilot Model**

The initial model used for the pilot program had seven alternating coarse and fine-grained layers sloped at 50º from the vertical. Each layer had a thickness of 1-meter in the horizontal. The till layer was placed at the base of the alternating layers and was 1-meter thick in the vertical. A water table was established with a zero head boundary condition at the base of the till layer. A flux boundary condition of $10^{-5}$ m/s was applied at the top of the alternating layers. The sloped edge was set to a zero flux boundary condition, which was reviewed by elevation (i.e., if $K = K_{sat}$, $h = 0$), for a given distance up the slope. The review boundary was used to check for seepage at the toe or up the slope. The initial

model developed with the specified boundary conditions is presented in Figure 4.3.

The initial numerical model was subsequently a greatly simplified representation of the conceptual model proposed by Herasymuik (1996). However, the model proved extremely difficult to solve. The main problem involved trying to achieve convergence in the numerical solution.

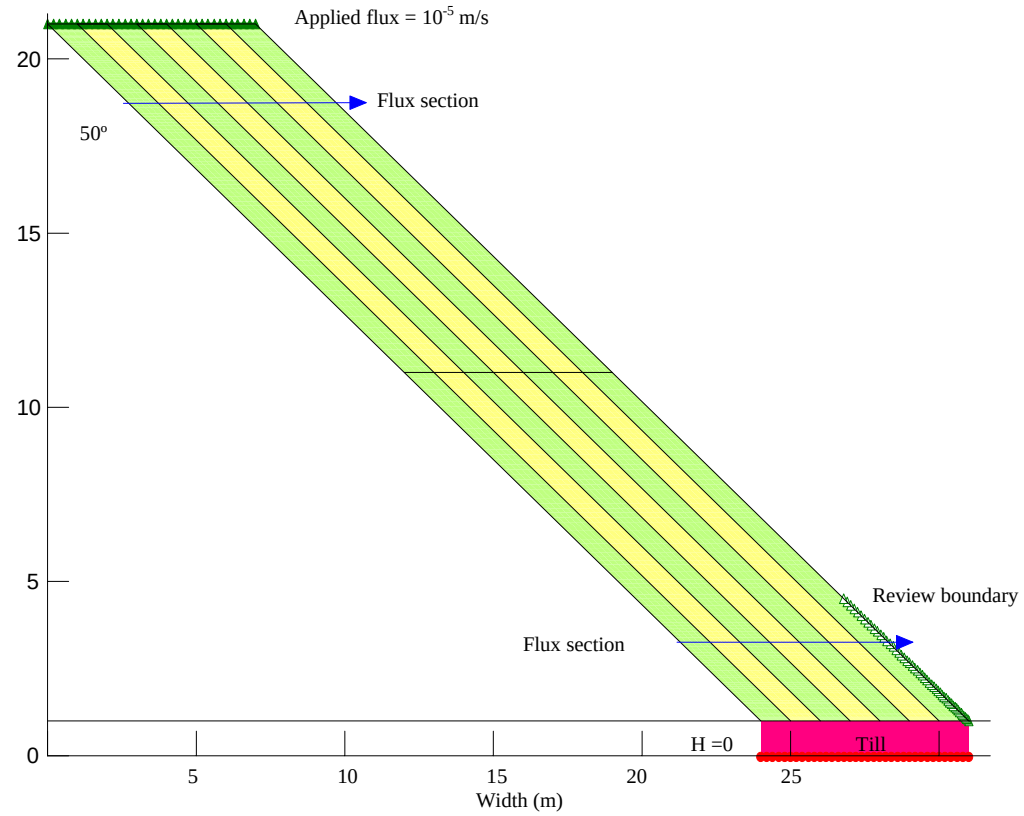


**Figure 4.3 Initial Model Developed and Analyzed**

Several variations for the input parameters were used in an attempt to achieve convergence. The following points summarize the variations used for input parameters:

1. Increasing/decreasing the number and thickness of layers;
2. Raising/lowering the flux review boundary on the slope;
3. Adjusting convergence criteria;
4. Using different fluxes at ground surface;

5. Increasing/decreasing the mesh density;
6. Using different materials;
7. Exchanging layers; and
8. Transient runs.

When a variation or combination of variations did not result in a satisfactory answer, a new simulation would begin with a simpler model than that presented in Figure 4.3. Seventeen different modelling simulations were attempted. Some of the models showed limited success upon completion. The major conclusion of the pilot program was that there was a need to start from a known solution and then increase in complexity. The results would allow one problem to be isolated at a time rather than deal with several problems at once. Newman et al (1997) and Newman (1999) undertook the only known study of this nature. These studies evaluated flow through vertical coarse and fine-grained layers. Building from these studies to more complex cases that better represented a waste rock pile resulted in a more detailed parametric study.

### 4.3 Parametric Study

The parametric study was designed as a continuation of the Newman (1999) study discussed in Chapter 2. The first step was to establish model parameters, and then adapt the Newman (1999) study accordingly. To understand the interaction of multiple adjacent layers, four layers were used rather than two used by Newman (1999). Additional layers increased the computational effort. Newman (1999) showed that preferential flow through the fine-grained layer occurred for any flux less than the saturated hydraulic conductivity of that layer. Therefore, an initial applied flux ($q$) of $10^{-5}$ m/s was selected. All attempts to use the annual precipitation of approximately $7.7E10^{-9}$ m/s at the Golden Sunlight Mine resulted in non-convergence of the solution. The bottom boundary condition was a water table with a pressure head ($h$) equal to zero. The lateral perimeters of the model were set as no flow boundaries. The total thickness of the model was 1-meter with each layer 0.25-meter thick. The mesh density ranged from 20 to 16 elements per meter in the horizontal and 20 to 17 elements per meter in the vertical. A flux section was used to calculate the

seepage flow across selected sections. The model profile included six flux sections. One flux section was used at the top and bottom of the model to check water balance. The remaining four sections were used in the mid-section of the profile to measure the flux in each layer. Figure 4.4 shows the two-meter vertical (or 90º) model. The alternating fine (F) and coarse (C) layers are designated along with the flux section arrows. Note that no vertical cutoff section was used as in the Newman (1999) study. The alternating layers were allowed to interact along the full length of contact.

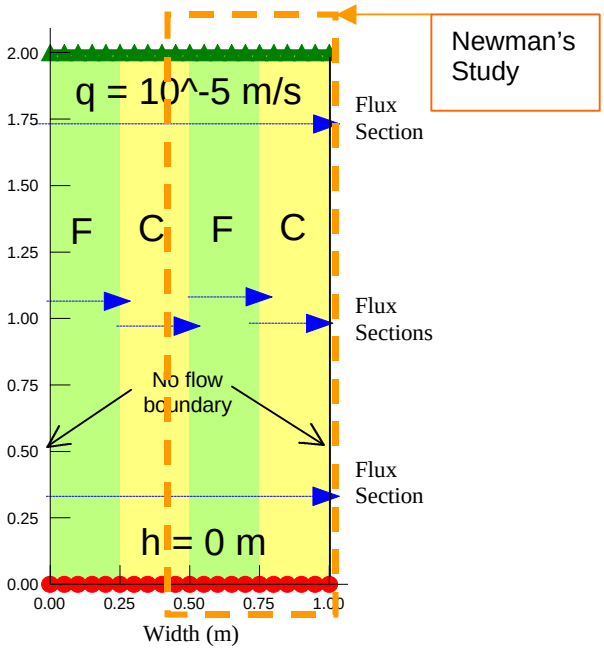


**Figure 4.4 Two-meter 90° Profile Adopted from Newman's Study**

The materials used in the modelling study were changed from those used by Newman (1999). The fine-grained material was changed from Beaver Creek sand, shown in Figure 4.2, to a fine-grained waste rock, as described by Herasymuik (1996) for Golden Sunlight Mine. The hydraulic conductivity function for the fine-grained layer material was computed using the Fredlund et al (1994) method, based on the SWCC and saturated hydraulic conductivity measured by Herasymuik (1996).

The coarse-grained layer used by Newman (1999) was also modified. The pilot program showed that the initial silica sand hydraulic conductivity function was too steep. The steep function resulted in large changes in hydraulic conductivity for small changes in pressure head. These changes made reaching convergence problematic for the taller/higher suction profiles. In order to solve the convergence problems for all profiles, a shallower function was used for the silica sand. The hydraulic characteristic curves for both materials and the applied flux used in the parametric study are shown in Figure 4.5.

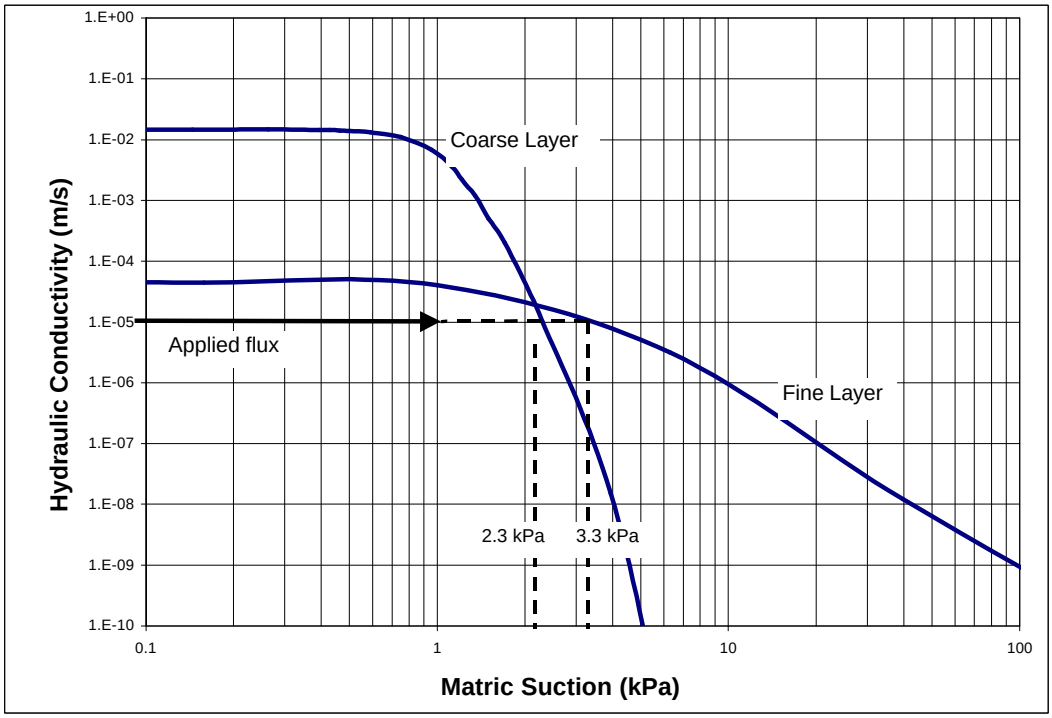


**Figure 4.5a Hydraulic Conductivity Functions For Coarse and Fine-Grained Layers Adopted for the Parametric Study**

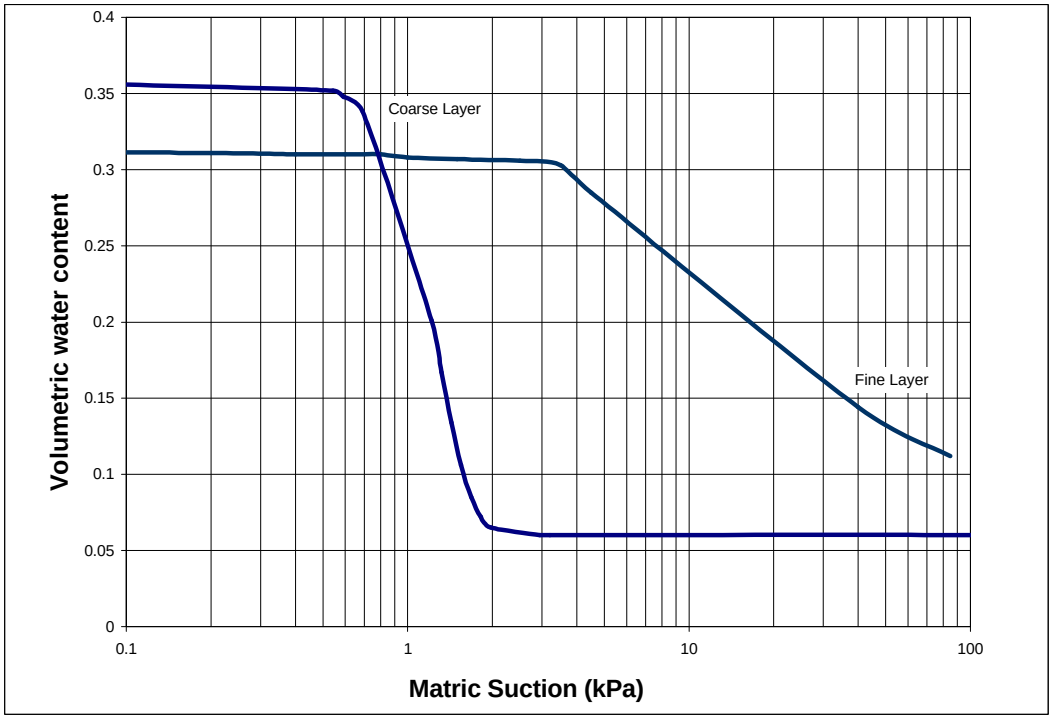


**Figure 4.5b Soil Water Characteristic Curves For Coarse and Fine-Grained Layers Adopted for the Parametric Study**

Systematic incremental changes to the initial 1-meter vertical model were progressively implemented to reach the targeted 20-meter sloped system. The height and slope of the model was varied according to the parametric study shown as flow chart in Figure 4.6. First, the one-meter profile was modelled for all the slope angles starting with vertical layers (no slope). Once all the slope angles for a particular height were completed, the profile height was increased by multiples of two.

A successful model simulation was defined as obtaining numerical convergence within a specified tolerance. According to Geo-Slope (1995), Seep/W solves the finite element equations by computing the head at each node. The head at each node is dependent on the material properties of the material, although the correct material properties are not known at the start of an analysis. Therefore, an iterative procedure is used to determine the heads within the profile.

The iterative process means that the final solution must achieve convergence under the selected convergence criteria. It is possible for an analysis to satisfy the defined convergence criteria, while at the same time not accurately representing the material properties used in the simulation. Therefore, convergence of the analysis must be verified using an alternative method (Geo-Slope, 1995).

Convergence for the current study was determined by two different methods for each simulation. The first method was a vector norm versus iteration graph as provide by Seep/W (Geo-Slope, 1995). As the solution converges, the difference between consecutive vector norms will decrease to an acceptable tolerance. The second method also used a graphical method. The graph was generated by plotting the hydraulic conductivity values calculated by Seep/W at each node against the input hydraulic conductivity functions of both the fine-grained and coarse-grained materials. The calculated hydraulic conductivities should plot on or near the materials hydraulic conductivity functions to ensure that convergence has occurred. Both methods must meet the given tolerance to ensure complete convergence of the problem solution.

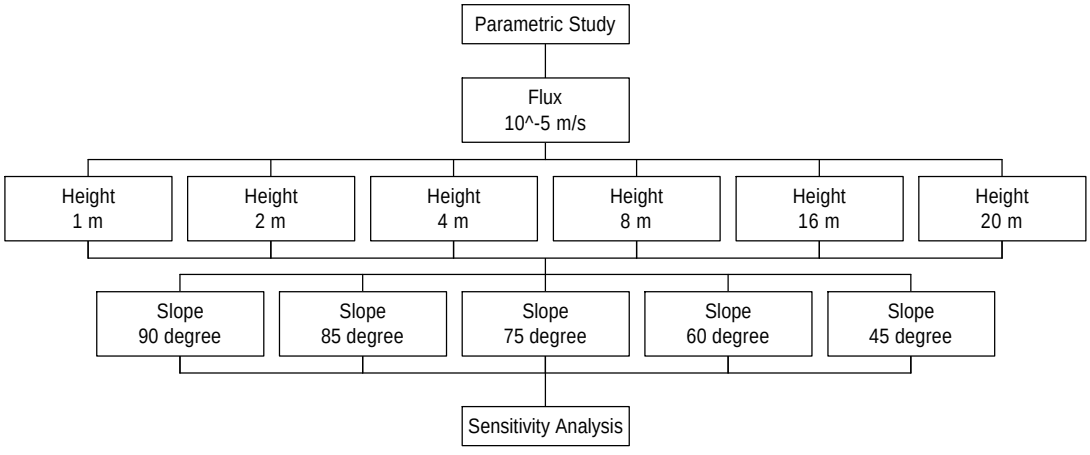


**Figure 4.6 Parametric Study**

The parametric study presented in Figure 4.6 shows the various cases simulated during the study. The modelling program ran steady-state models using the commercial numerical analysis package Seep/W (Geo-Slope, 1995) and produced solutions with convergence for 30 different model simulations. However, lowering the applied flux to simulate the annual precipitation rate at Golden Sunlight Mine ($7.7E10^{-9}$ m/s) resulted in most of the models failing to achieve convergence.

To understand the problems encountered with the convergence issues that resulted from varying input parameters, an investigation was undertaken in the form of an extensive sensitivity analysis. The sensitivity analysis studied the effects of convergence criteria, mesh design, material properties, and transient modelling on the finite element solution. The investigation was "package-specific," in other words, it was designed specifically to test and evaluate variations in the input parameters that are specified for the Seep/W model. The objective of the sensitivity analysis was to provide resolutions to solve the problems encountered during the pilot program and the parametric study. However, the investigation provided to be a considerable effort and showed the limitations of the commercial numerical analysis package chosen as the primary tool to solve the problem.

The understanding of the precise algorithms of the commercial package Seep/W was found to be limited to the published documents. A full understanding of exactly where the model failed could not accurately be determined nor corrected. The review of the literature did not show any details of the "trials and tribulations" of other numerical modellers but concentrated only on their successful numerical models. An extensive discussion on the methods used and the various outcomes during the sensitivity analysis is presented in Appendix B to aid future researchers.

To develop a further understanding of the strongly heterogeneous nonlinear problems a return to first principles was necessary.

### 4.4 Modified Kisch Solution

The use of an alternative numerical method of solution was also investigated to provide further insight to the problem and to independently verify the results of the finite element method. A finite difference method (FDM) was described in Chapter 3 and was used to solve the preferential flow problem. Current finite difference methods can be used to solve for head loss throughout a one or two-dimensional system. Analyzing two soil columns of different materials, the head loss in each column can be calculated independently. However, by using a system of equations for parallel and perpendicular flow in materials of different hydraulic conductivities, the separate columns can be joined. The solution becomes a modified form of the Kisch (1959) solution. The modifications provided an algorithm that made it possible to incline the two-column system to simulate a slope. This was illustrated in Figure 3.6.

The algorithm and equations for the FDM were combined using a spreadsheet. The spreadsheet used six work sheets: Properties, Calc, Data, Conductivities, Heads, Flux, and Gradient. The spreadsheet required the following input parameters from the user:

1. The hydraulic conductivity functions for the coarse and fine-grained materials, (*K*);
2. The angle the system is sloped at, ($\alpha$);
3. The thickness of each layer, (*bc, bf*);
4. The space between each node, (*dz*);
5. The top boundary condition, i.e., applied flux, (*q*); and
6. The bottom boundary condition.

The hydraulic conductivity functions for each soil type were entered in the "properties" sheet with respect to matric suction, (kPa). The matric suction was then converted to pressure head in meters, and the functions were placed in a format suitable for a lookup table (used later to extrapolate a value between two known values). The remaining parameters were entered into the “calculation”

sheet. The “data” sheet was used to organize the results into output plots, and the remaining sheets show the calculated results in graphic form for hydraulic conductivity, pressure heads, flux, and gradient for the individual layers and/or the system.

The “calculation” sheet is subdivided into several categories: input parameters, pressure head, hydraulic conductivity, change in pressure head, gradient, and flux. The input parameters are entered in a small table. The pressure heads were solved at each node for: independent flow (subscript *i*) for both the coarse layer (subscript *c*) and the fine layer (subscript *f*), (*hci, hfi*); for lateral or perpendicular flow (subscript *p*), (*hcp, hfp*); and for the system, (*hp*). The hydraulic conductivity (subscript *k*) was solved at each node for: independent flow, (*kci, kfi*); lateral flow, (*kcp, kfp*); independent flow as a function of the system pressure heads, (*kc(hp), kf(hp)*); flow parallel to the system, (*kll*); and flow perpendicular to the system, (*kp*). The change in pressure heads were solved at each node for: the system, (*dhp*) and independently, (*dhpc, dhpf*). The hydraulic gradient was calculated at each node for the system, (*I*). The flux was calculated at each node for independent flow (*qci, qfi*). The change in flux for perpendicular flow was calculated, (*dq*), and added and subtracted to the applied flux in the coarse and fine layer (*qcp,qfp*) respectively, to emulate lateral flow.

The input parameter for nodal spacing, *dz* was important for obtaining accuracy in the solution and defining the total system height. For example, a nodal spacing of 0.1-meter resulted in a system height of 10-meters (i.e., for 100 nodes used). The top boundary condition was the applied flux (qin), and the bottom boundary condition was defined as a water table (i.e., $h = 0$ and therefore $K = Ksat$).

The spreadsheet program used the equations and methodology presented in Chapter 3 to calculate the FDM solution. Using the material properties, five

different head profiles were computed. The first two profiles were based on the Kisch (1959) solution, for the coarse and fine-grained materials, (*hci, hfi*). The layers were analyzed as individual systems (i.e., a column of fine-grained material only). The third profile combined the separate profiles into a head profile for the system of two adjacent layers of coarse and fine-grained materials, (*hp*). Recall that the first three pressure head profiles were calculated from the bottom boundary condition at elevation zero up through the profile at each node to the top node (defined by *dz* multiplied by the number of nodes in the system). The remaining two head profiles, (*hcp, hfp*) are based on the results of the first two profiles, (*hci, hfi*) at the top node of the system, and calculated the lateral flow (or the flow perpendicular to the applied flux) from the coarse to fine-grained material at each node sequentially from the top through to the bottom of the system.

The pressure heads were solved by calculating the change in pressure head for the current nodal elevation and adding the change to the current pressure head to solve for the next nodal elevation (refer to Figure 3.6). The change in pressure head was calculated by knowing the initial pressure head and hydraulic conductivity in each soil column. Once the change in pressure head was added to the previous head, a new iteration with a new hydraulic conductivity for each soil type was then solved at the next node. The new hydraulic conductivities are solved by using the lookup table of material properties. Since the newly calculated pressure head will often be between two defined pressure heads in the material properties table, a simple linear interpolating function was used to solve for the new hydraulic conductivity valve as a function of the new pressure head. From the calculated pressure heads and hydraulic conductivities, the system gradient and individual fluxes at each node were then calculated.

The output of the FDM included four graphs (presented in Chapter 5). The first graph compared the calculated hydraulic conductivities to the hydraulic

conductivity functions of each soil type. The remaining graphs present the head, flux, and gradient profiles calculated respectively.

Several comparison simulations were undertaken to evaluate the results from the FEM (e.g., Seep/W) with the results from the FDM solution (modified Kisch). The simulations used different heights and slopes, for a two-layered system of coarse and fine-grained materials. Note that this was different than the parametric study conducted with the Seep/W.

The initial profile height chosen was 8-meters but this was lowered to 2-meter and 1.14-meters. The 2-meter height was used to decrease the nodal spacing in the finite difference solution. The 1.14-meter profile was used to compare the results with the Newman (1999) study. The following slope angles were modelled; namely 90°, 75°, and 45°. Two sets of coarse and fine-grained materials were used (i.e., modified silica sand (silica2) and TP5GS1 from earlier work, and the silica and Beaver Creek sand from the Newman (1999) study). The results for the finite different method study are presented in Chapter 5.

## 4.5 Chapter Summary

The previous chapters introduced the physical problem and described the methodology required to solve the physical problem by first conceptualizing the problem and then converting the problem to the fundamental mathematical equations. Chapter 4 described the numerical computer programs and methods used to meet the objective and scope of the thesis. The parametric program studied the effect of increasing height and inclination of a two-soil four-layered waste rock system. The finite difference method using the modified Kisch solution investigates the physical problem with an independent and fundamental approach.

Chapter 5 presents the solutions, analyses, and discussion related to the questions that were formulated. Chapter 6 summarizes the modelling programs and makes recommendations for future research.

# CHAPTER 5

# PRESENTATION OF RESULTS, ANALYSIS, AND DISCUSSION

## 5.1 Introduction

The steady state and transient numerical modelling was completed using the two-dimensional saturated/unsaturated flow, finite element computer package called Seep/W (Geo-slope, 1995). The parametric study undertook steady state modelling and produced solutions with convergence for 30 model simulations. The results from the modified Kisch solution, introduced as an alternate numerical solution, were used to compare and help verify results from the finite element method. Chapter 5 presents the results of the modelling studies introduced in Chapter 4. However, Chapter 5 begins with a short discussion outlining the major issues discovered during this study and summarizes the sensitivity analysis presented in Appendix B. During the course of this study, approximately 200 simulations were investigated. A list of all relevant simulations and the results are presented in the Appendices.

## 5.2 Non-convergence and the Result of the Sensitivity Analysis

Numerical modelling for the parametric study was preceded by pilot program that moved through a long modelling process with many unsuccessful model simulations using various parameters and combinations. Chapter 4 discussed the need to restart the modelling process at a known solution and conduct a parametric study. However, with the parametric study, issues with respect to convergence criteria, mesh design, and material properties proved to be critical. For example, the first coarse-grained material selected worked well for all profile heights below 8-meters but not for any taller profiles. The applied flux of $10^{-5}$ m/s worked well for all models studied but the use of any lower flux would result in non-convergence.

To better understand the anomalies encountered and to acquire a better understanding of the key parameters of the commercial numerical analysis package Seep/W used to solve physical problem, a sensitivity analysis was undertaken and presented in Appendix B. The main objective of the sensitivity analysis was to determine which input parameters affected convergence most and how to better manage these parameters and improve convergence. The key conclusions determined from the sensitivity analysis are outlined below:

1. Numerical models are extremely sensitive to very large or small numbers.

2. The convergence criteria are critical in obtaining a solution to the problem. Insufficient iterations or high rates of change in the solver caused non-converged solutions. A tight convergence criterion did slow the solver considerably but produced a reliable solution.

3. The study of the mesh design showed that tighter nodal spacing in areas of higher activity and/or removing elements with low flow has a direct effect on improving convergence.

4. The material properties specified for the layers were shown to be the most important factor. Reducing the slope of the hydraulic conductivity function can dramatically increase the convergence of the model. However, by doing so, results in the model deviating from the real system being modelled and therefore an acceptable compromise needs to be achieved to keep the model solvable and accurate within a selected tolerance.

5. The major breakthrough of the sensitivity analysis came with further manipulation of the hydraulic conductivity function for the coarse-grained material. The problem of the steep slope for the hydraulic conductivity function specified for the coarse-grained material was solved by progressively decreasing the slope of the hydraulic conductivity function at $10^{-8}$ m/s (for applied fluxes of $10^{-7}$ m/s or less). The slope of the function with values of matric suction greater than the air entry value was reduced into three sections with decreasing slopes. The first section of the slope was set equal to the original silica2, the second section of the slope was only slightly reduced, and the third section of the slope was inclined to match the hydraulic conductivity function for the fine-grained material. By doing so, the difference between the two functions became a constant. The general principle behind these changes was to ease convergence while not affecting flux in the system significantly (i.e. preferential flow still occurs in the correct distribution and convergence criteria were met).

6. The use of transient modelling was explored, however the sensitivity analysis showed that problems with the time expansion caused instability in the

system. The transient modelling proved to be the most inefficient method to solve the solution studied due to the amount of time required to solve a single model.

The selected parameters and the resulting flux in each layer at mid height for all significant models simulated in the sensitivity analysis were tabulated and are presented in the Appendix B. The results of the parametric studied presented in the following section were obtained using material properties and applied flux, based on the sensitivity analysis, that allowed Seep/W to achieve converged solutions.

**5.3 Parametric Study**

Velocity vectors, pressure head contours, seepage flux across selected sections, and two convergence graphs were obtained for each solution. Figure 5.1 shows the resulting fluxes (m/s), pressure head contours (m), and velocity vectors for the 4-meter high, 90º and 60º slopes. These results are typical in appearance to the other solutions, and were therefore selected for presentation. The computed velocity vectors show preferential flow of the applied flux through the fine material in the system. Initially a flux of $10^{-5}$ m/s was applied evenly across the top of the slope. Figure 4.5a shows where the applied flux intersects the hydraulic conductivity function for each material. It can be seen that the fine material is more conductive than the coarse material for all values of matric suction greater than 2.3 kPa. The system gradient favors a flux movement from the coarse layers into the fine layers. Figure 5.1 shows that the velocity vectors do not drain evenly from the sloped profile. This phenomenon has been shown by the conceptual model presented by Herasymuik (1996).

Herasymuik (1996) suggested that water would not flow through the coarse-grained layers when the value of the matric suction was greater than the value corresponding to residual water content. It was suggested that liquid would gather into a water droplet and when the droplet becomes sufficiently heavy, it will travel vertically. The vertical movement of water is gravity driven and depends on the slope, the material properties (e.g., grain size, hydraulic

conductivity), and the dimensions of the system. The Seep/W software (Geo-slope, 1995) assigns a fixed residual hydraulic conductivity to the movement of flow from the coarse-grained layer to the fine-grained layer.

The hydraulic conductivity functions for the coarse and fine layers, together with the applied flux, determine where preferential flow will occur through the fine-grained layers. Figure 5.1 shows preferential flow as a crossover of flow from the coarse to the fine-grained layers. The flow crossover stabilizes in each layer before reaching the mid-section of the profile. The flow crosses back into the coarse layers as it approaches the specified zero head at the bottom boundary. As the pressure head increases and exceeds –0.23 m (-2.3 kPa), the coarse layers becomes the preferential conduit. Hence, flow crosses back to the coarse-grained layers before exiting the system.

The flux sections characterize the amount of seepage across selected cross-sections in the system. The top and bottom flux sections, used to check water balance, show a negligible difference in flux. The intermediate flux sections for the 60º model in Figure 5.1 gave values of 63% ($6.3E10^{-6}$), 10% ($1.0E10^{-6}$), 27%($2.7E10^{-6}$), and 0%($2.7E10^{-10}$) of the total flux in each layer, going from left to right. The lower flux corresponds to the lower pressure head contours in the coarse-grained layers. It can also be seen that the pressure heads are lowest at the top of the vertical system and decrease rapidly from left to right across the sloped systems. The low-pressure heads in the outer coarse-grained layer result in a zone that does not transmit seepage.

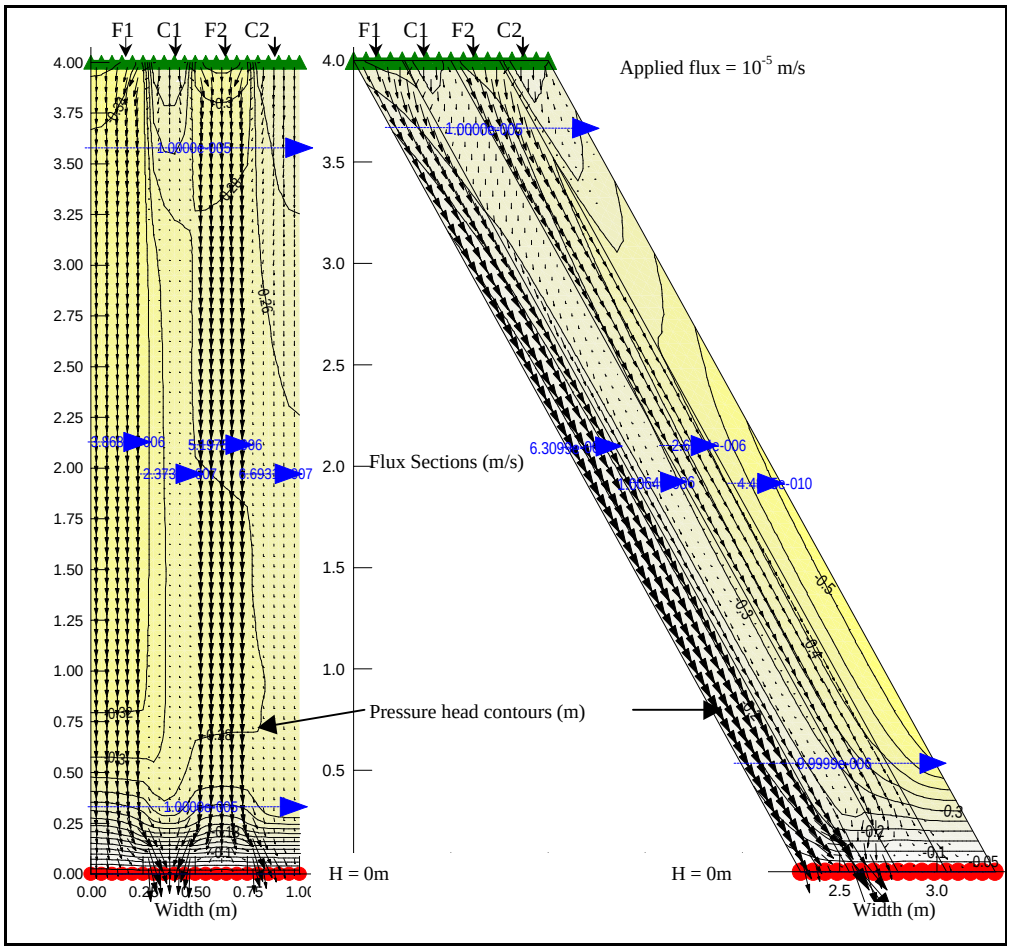


**Figure 5.1 Seep/W result for four-meter 90º and 60º profiles**

The soil-water characteristic curve (SWCC) presented in Figure 4.5b is not required to achieve a solution for the steady-state model. However, using the SWCC provides a measure of storage in the sloping profiles. When the first fine-grained layer (F1) becomes saturated, the first coarse-grained layer (C1) will stop draining into F1, and will increase in degree of saturation. Therefore, if F1 is thicker, it can store more water.

Several graphs were prepared to better show the effects of storage and gravity on the flux pathway, for a sloping layered system. Figure 5.2 shows the flux passing the mid-section of F1. The curves indicate the change in flux for each layer as the slope angle decreases from vertical (90º) to 45º for each height.

Figure 5.2 shows that the flux in F1 increases consistently as the height of the system increases, regardless of the slope angle. The increase is proportional to the increase in contact length between the layers. There was a negligible increase in flux between the 16 and 20-meter high systems for all slope angles. The maximum flux for each height was reached at a slope of 60º. However, the flux decreases for all heights for the 45º slope. It is difficult to provide a reason why the flux decreases for the 45º slope. If the fine layer reaches saturation, the flux would have reached a constant value similar to that for the 60º slope. One possible explanation is as follows: As the system slope becomes closer to 45º, the reduction in hydraulic gradient reduces the saturated flow in the first fine-grained layer (F1) and hence reduces vertical drainage from the adjacent first coarse-grained layer (C1). The associated increase in pressure head enabled the coarse layer to carry more of the flux. Further study between the 60º and 45º slopes would be required to determine the angle at which the pressure heads increased sufficiently to affect the relative flow rates.

Figure 5.3 shows the flux passing the mid-section of the first coarse-grained layer (C1). The flux is no longer proportional to the height increase. In fact, the flux is relatively constant as the height of the system increases and Figure 5.3 shows an exponential increase in flux as the slope increases. The flux in the first coarse-grained layer is at a maximum value for the 45º slope. This is consistent with the reduction in flux in the first fine-grained layer at 45º as shown in Figure 5.2. However, for all other angles both the first fine and coarse-grained layers show an increase in flux. Therefore, the increased flux must have come from the upper coarse and fine-grained layers, F2 and C2, respectively.

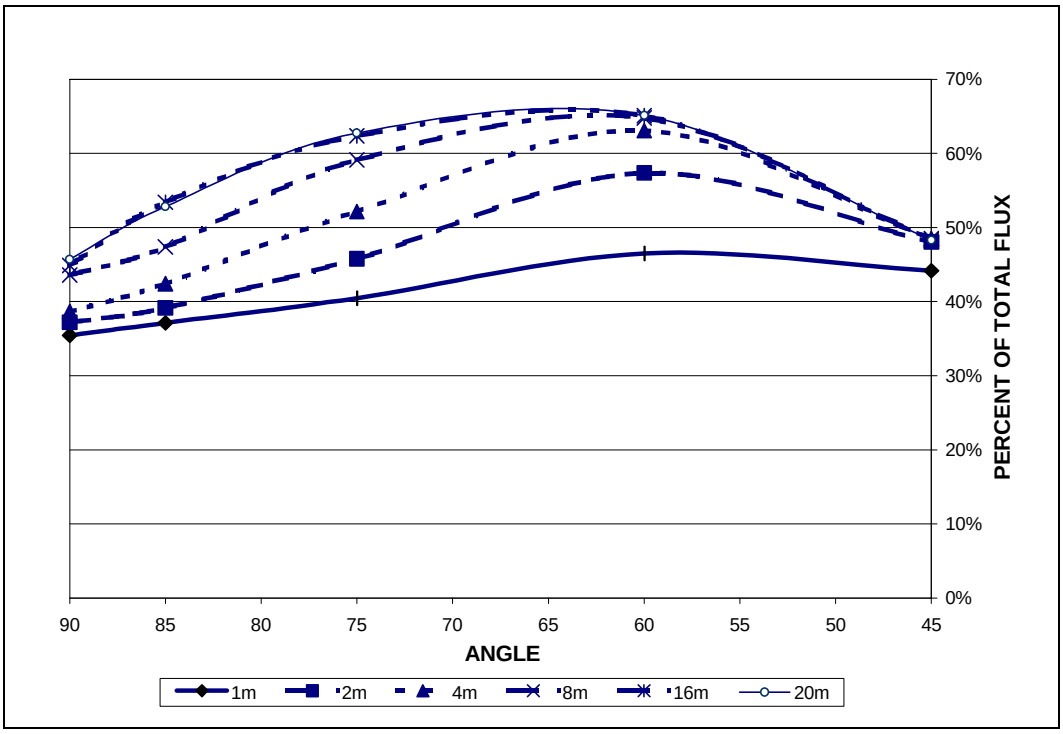


**Figure 5.2 Change in Flux Passing Layer, 'F1' at Mid Height**

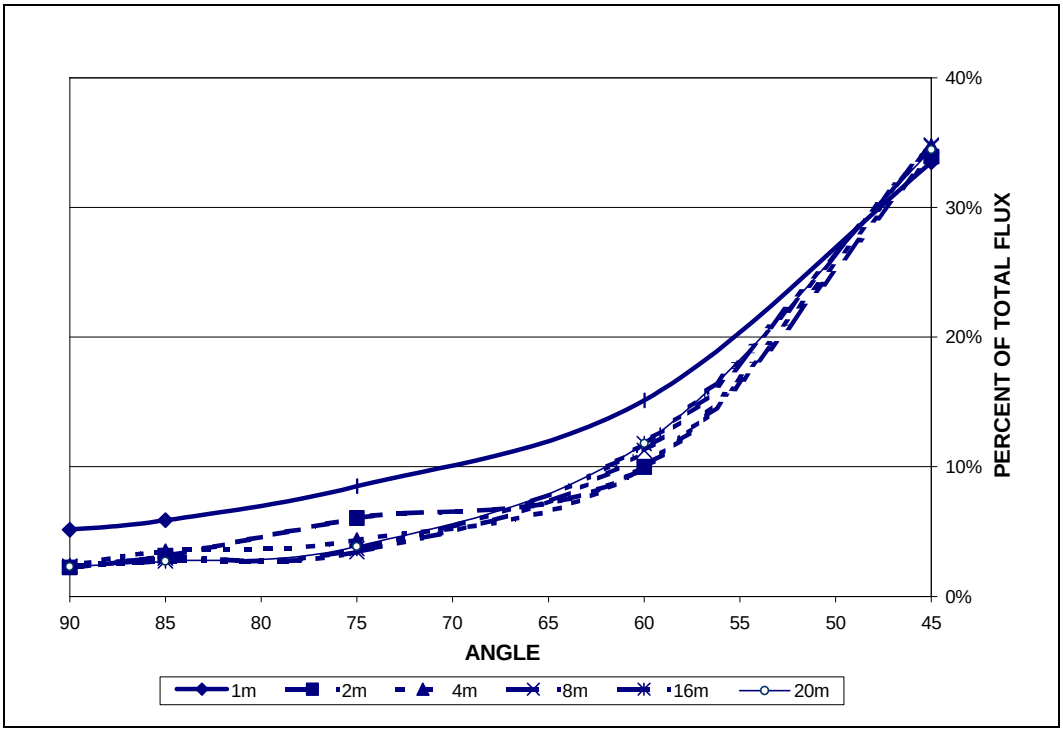


**Figure 5.3 Change in Flux Passing Layer, 'C1' at Mid Height**

Figure 5.4 shows the flux passing the mid-section of the second fine-grained layer (F2). In general, the layer F2 transmits more than half of the flux at 90º. However, as the slope angle decreases the flux steadily decreases. The proportional decrease in flux with slope angle explains the flux increase in the lower coarse and fine-grained layers.

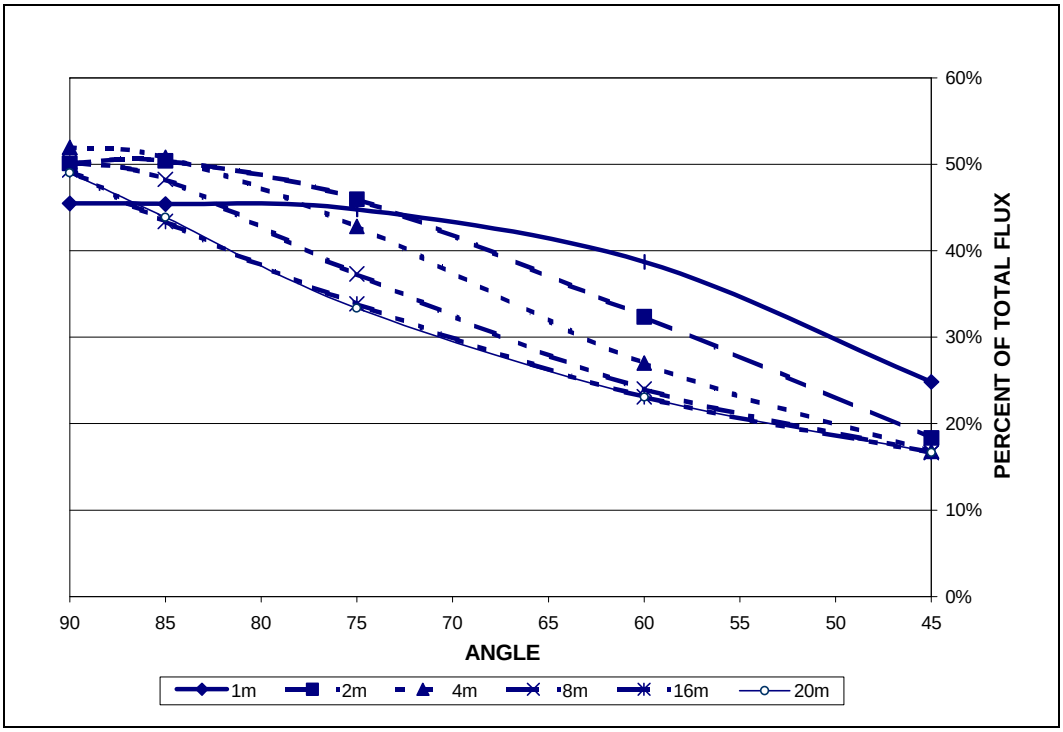


**Figure 5.4 Change in Flux Passing Layer, 'F2' at Mid Height**

Newman (1999), and Newman et al (1997) explained why the flux crosses over from the coarse layers to the fine-grained layers, in a two-layer system. It is also important to understand how preferential flow at the top of the profile behaves with multiple layers as shown in Figure 5.5 for the vertical profiles. The outside two elements in C1 evenly contribute seepage to the bordering fine-grained layer elements. The second coarse-grained layer borders only one fine-grained layer and drains two elements into the fine layer. Therefore, C1 will drain more quickly than C2 as shown in Figure 5.6, where C1 transports less seepage than C2 by mid height. However, both C1 and C2 drain to the same flux for the 20-meter vertical profile as shown in Figure 5.7. The observation indicates that the layers will reach equilibrium for the taller profiles (i.e., larger contact length). At the end of the initial crossover, the second fine layer transmits more flux than

the first fine layer. As the slope decreases from the vertical, the flux balance moves to the lower layers as shown in Figure 5.6.

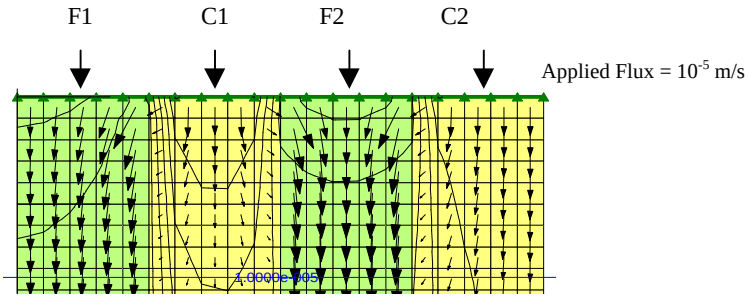


**Figure 5.5 Top Half Meter of 4-meter Vertical Solution**

Figure 5.6 shows the overall results of the 4-meter system for each slope. The figure shows the relative proportion of the flux in each layer. The logarithm of hydraulic conductivity is plotted on the secondary axis of Figure 5.6. The plotted values for the logarithm of hydraulic conductivity are the logarithm of the lowest hydraulic conductivity calculated by Seep/W for a particular simulation. The trend of the logarithm for hydraulic conductivity confirms that the slope angle was directly proportional to the resulting pressure heads and corresponding hydraulic conductivity. The lowest value of pressure head and the corresponding hydraulic conductivity was located on the top of the coarse-grained layers in the vertical profiles and on the mid-section of C2 in the sloped systems (refer to Figure 5.1).

Figure 5.7 shows the overall results of the 20-meter system for each slope. The 20-meter profile has a higher elevation head and contact length between layers. The results are similar to the 4-meter high system, except for the flux values in fine-grained layers. It appears that the longer contact length results in more of a flux transfer from F2 to F1 as the slope angle is increased. However, the fluxes in all the layers are identical at the 45º slope angle. The coarse-grained layers in the 20-meter high system begin with the same flux but C2 quickly drains to residual water content with a flux-approaching zero. Note that the greatest change in the logarithmic of hydraulic conductivity was found for all heights to be between the 85º and 60º slopes.

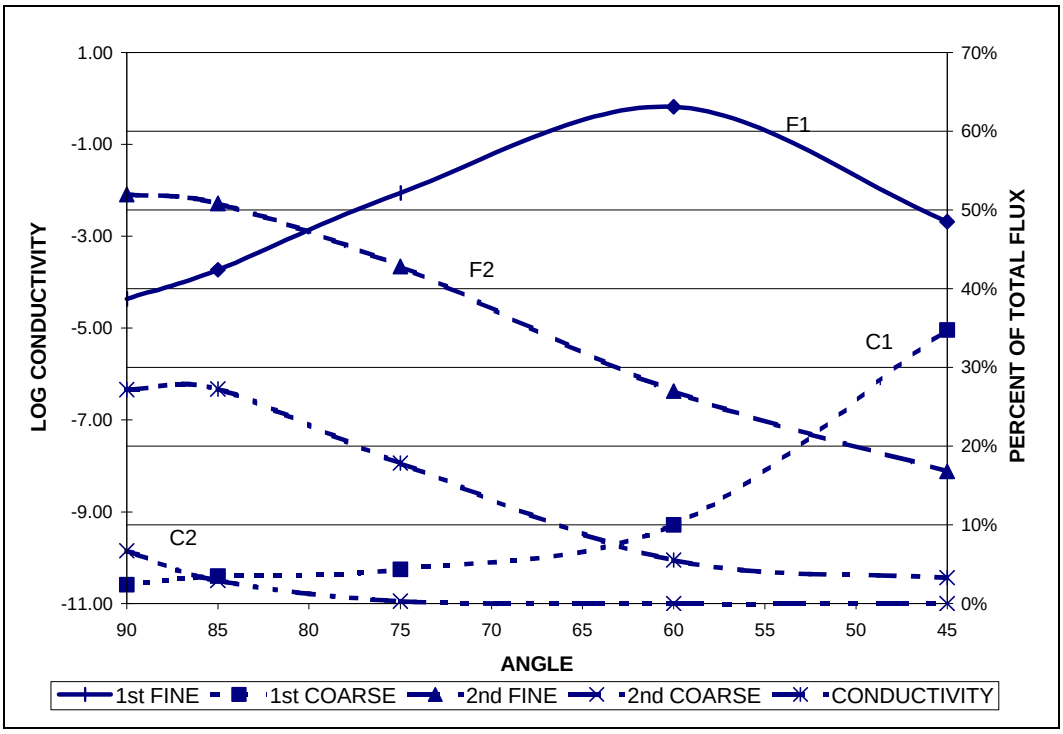


**Figure 5.6 Flux and Hydraulic Conductivity Change for the Four Meter System at Mid Height**

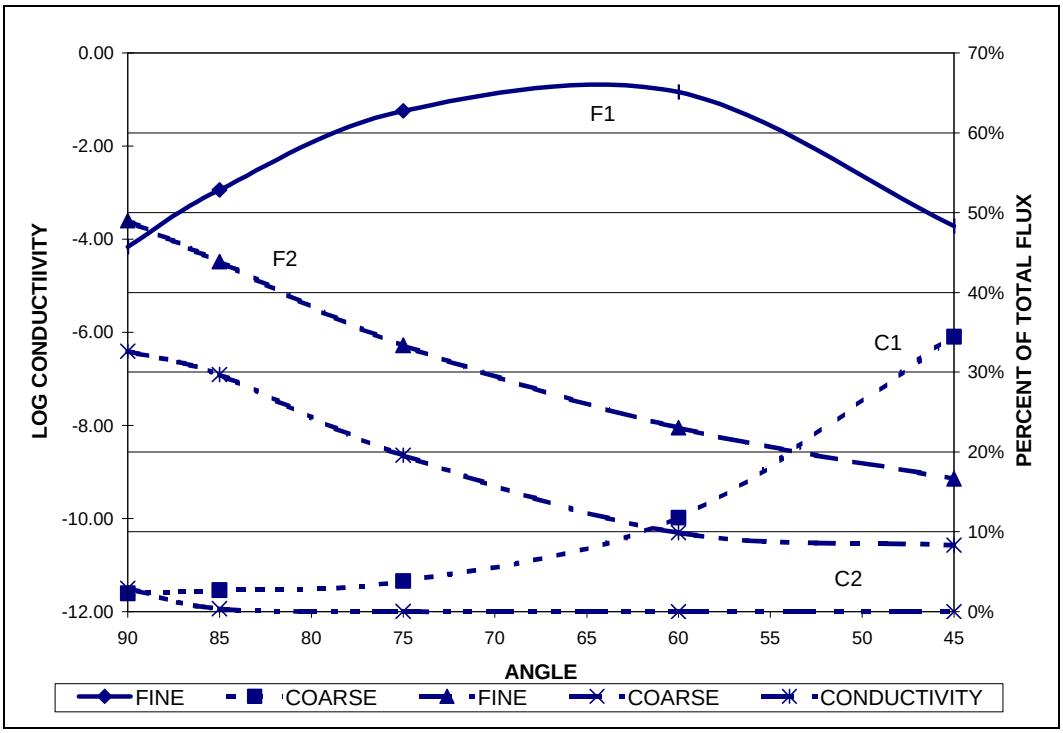


**Figure 5.7 Flux and Hydraulic Conductivity Change for the Twenty-Meter System at Mid Height**

The results of the parametric study showed preferential flow in inclined waste rock layers as described by Herasymuik (1996) and demonstrated by Newman (1999) for the vertical system. The detailed results for all the models simulated are presented in Appendix A. The parametric study demonstrated that flow in a multi-layered waste rock dump is a function of inclination, contact length between the layers, and coarse and fine-grained material hydraulic properties, in addition to mechanism of preferential flow stated by Newman (1999).

## 5.4 Modified Kisch Solution

The modified Kisch solution using the finite difference method (FDM) was developed to explore an alternative solution for preferential flow in an unsaturated layered system. Chapter 3 outlined the theoretical aspects of the problem and Chapter 4 described the procedure for the investigation. The following section will describe the operation of the modified Kisch solution and compare the results with the solutions obtained from the finite element method (FEM) solution (Seep/W).

A 2-meter and a 1.14-meter, two layer, vertical system were used for the analysis. Within the solution, the layers could be specified as coarse over fine or fine over coarse-grained material. The fine-grained layer material selected for analysis was TP5GS1 and the coarse-grained layer material selected was silica2. Table 5.1 presents the input parameters for the analysis.

**Table 5.1 Input Parameter for The Modified Kisch Solution**

| | | |
|---|---|---|
| Height: | 2.00 | m |
| Angle ($\alpha$) | 90 | ° |
| Thickness of coarse layer (*bc*) | 0.05 | m |
| Thickness of fine layer (*bf*) | 0.05 | m |
| Distance from each node (*dz*) | 0.02 | m |
| Angled distance from each node (*dl*) | 0.02 | m |
| Applied flux (*qin*) | -1.00E-05 | m/s |

The thickness of the coarse and fine-grained layers were defined as *bc* and *bf,* respectively. The distance between nodes was defined by *dz* and multiplied by the number of nodes to give the total height. For the simulated sloped systems, *dl* will be greater than *dz* (*dl* is a function of *dz* and the angle). The input flux was represented by *qin*. Note that the negative sign indicates the flux was moving down through the system (i.e., the negative direction).

As previously explained in Chapters 3 and 4, the FDM program calculated the change in pore-water pressure between elevations from the bottom to the top and then from the top back to the bottom. The FDM program first solved for hydraulic conductivity, flux, and gradient in each layer and then solved for the variables at each node using the average heads. The results are presented in four plots: pressure head versus elevation, flux versus elevation, gradient versus elevation, and computed hydraulic conductivities versus material conductivities. The results for the vertical 2-meter system are presented in Figures 5.8 through 5.11.

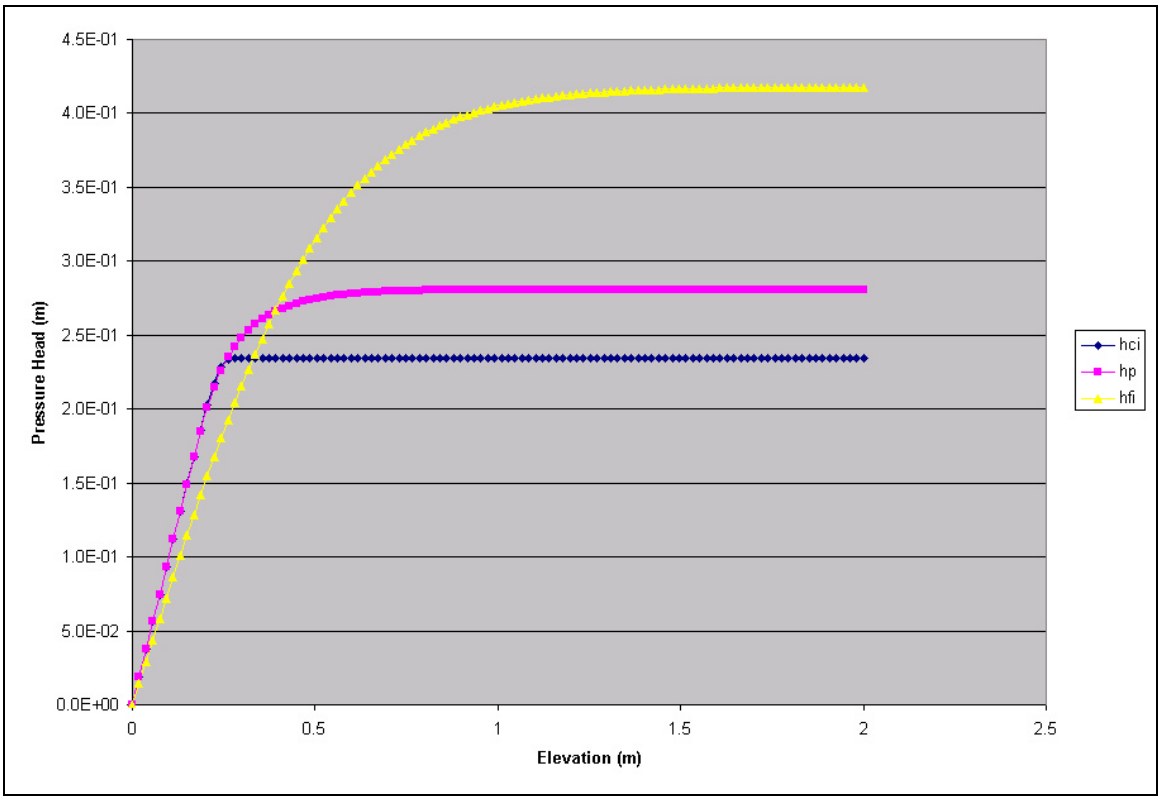


**Figure 5.8 Pressure Heads Calculated for the Vertical 2-Meter System Showing the Pressure Heads for the Coarse (*hci*) and Fine (*hfi*) Layers and for the Combined System (*hp*)**

Figure 5.8 shows the pressure heads calculated where *hci* was the coarse-grained layer, *hf*i was the fine-grained layer, and *hp* was the pore-water pressure heads for the system (i.e., the combined result of both fine and coarse-grained layers). Figure 5.9 presents the calculated fluxes in the system from bottom to top defining the bottom cross-over of flux for preferential flow and from top to bottom defining the upper cross-over of flux for preferential flow.

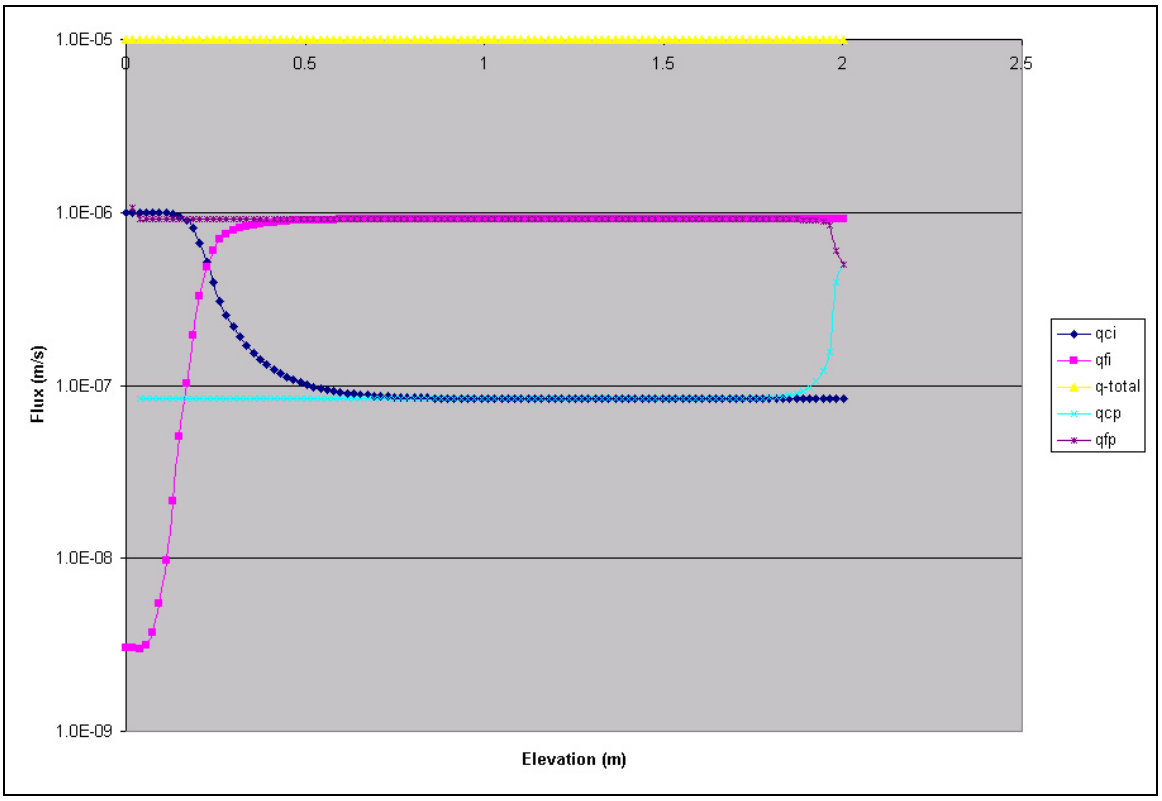


**Figure 5.9 Fluxes Calculated for the Vertical 2-Meter System Showing the Flux in the Coarse (*qci, qcp*), Fine (*qfi, qfp*), and Combined Total Flux (*q-total*)**

Note that fluxes are defined for the full height of the system; however to fully define preferential flow the system must be calculated in two halves. The fluxes at elevations 0 to 1-meter are defined in the coarse and fine-grained layers by *qci* and *qfi*, respectively. The fluxes at elevations 2-meter to 1-meter are defined in the coarse and fine-grained layers by *qcp* and *qfp*, respectively. Figure 5.10 presents the calculated gradients from the bottom to the top of the system.

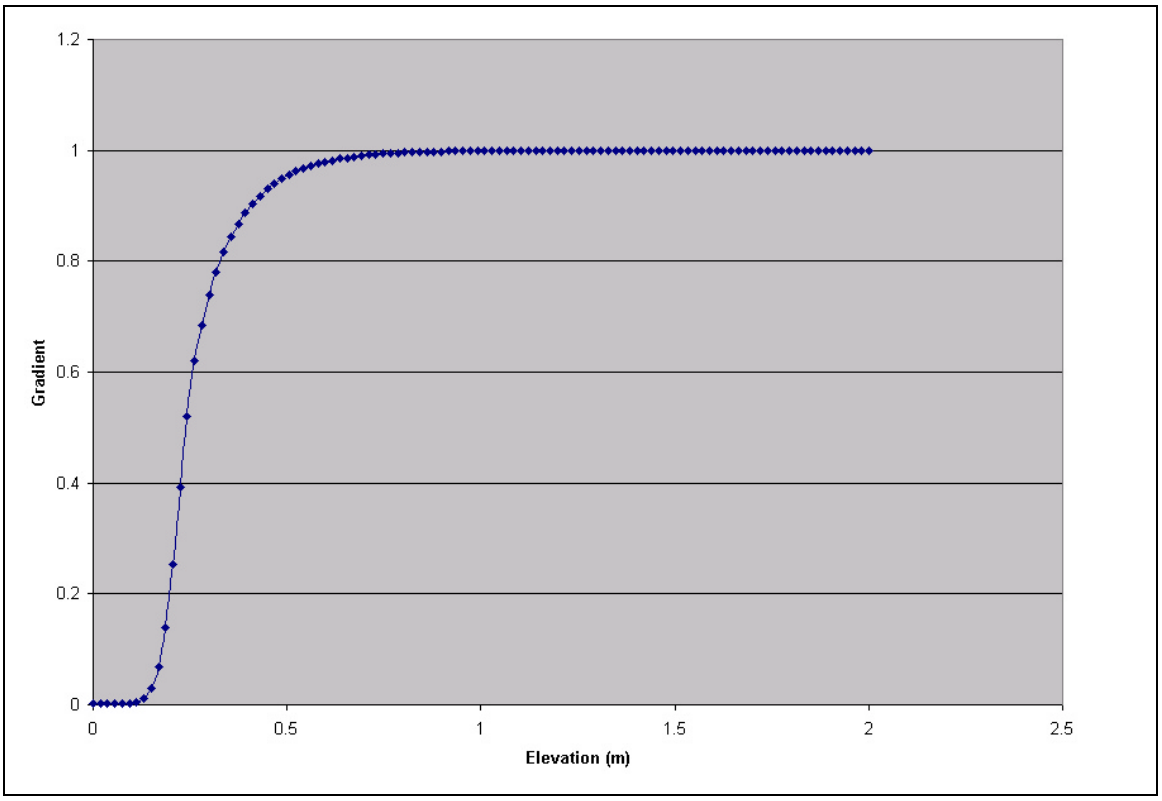


**Figure 5.10 Gradients Calculated for the Vertical 2-Meter System with the Applied Flux of $10^{-5}$ m/s.**

The gradient is the change in pore-water pressure head with respect to the change in elevation. Figure 5.10 shows that the gradient quickly increased from 0 to 1 between 0-meter to 1-meter of elevation. The computed results for the combined flow system suggested that a change in pore-water pressure equaled a change in gradient, which corresponded to a change in hydraulic conductivities and therefore a change in flux within the layers. In other words, the system reached hydraulic equilibrium with respect to elevation (i.e., *dz*) via preferential flow (i.e., change in flux between layers). To ensure convergence, the calculated conductivities were compared against those of the material properties. Figure 5.11 presents the FDM calculated conductivities plotted against those specified for the material properties.

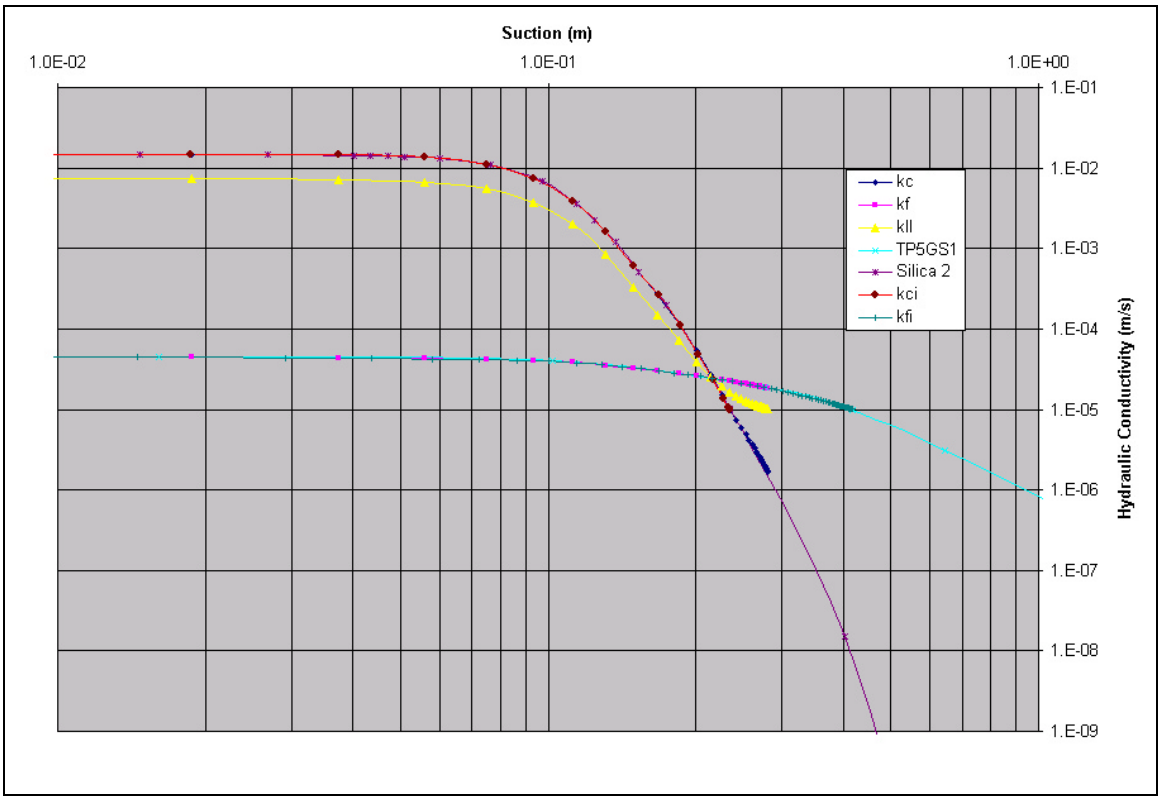


**Figure 5.11 Hydraulic Conductivities Calculated for the Vertical 2-Meter System Plotted Versus the Material Hydraulic Conductivity Functions**

It is apparent in Figure 5.11 that the computed hydraulic conductivities match the given properties. This was attributed to the accuracy of the model and the simple interpolating function used. It is important to note that five hydraulic conductivities and functions are presented in Figure 5.11. The first three were calculated from the bottom to the top, where the calculated hydraulic conductivities for the coarse and fine-grained layers were *kc* and *kf*, respectively, and the combined system hydraulic conductivity was *kll*. Note that *kll* ends at the pressure head of 2.8-meters and the hydraulic conductivity of $10^{-5}$ m/s, while *kc* and *kf* end at different hydraulic conductivities but the same pore-water pressure head. The calculated hydraulic conductivities from the top to the bottom in the coarse and fine-grained layer were *kci* and *kfi* respectively. In this case, the conductivities end at $10^{-5}$ m/s but at different pore-water pressure heads.

Several models were analyzed using the FEM (Seep/W) and compared to the results from the modified Kisch solution. Three 2-meter system models were analyzed with slopes of 90, 75, and 45°, and with TP5GS1 and silica2 as the fine and coarse-grained materials. Three systems models, one 1.14-meter at 90° and two 2-meter at 75° were analyzed respectively with Beaver Creek sand and silica2 as the fine and coarse-grained materials. The second 90° model was set up to compare with the results of Newman (1999) (i.e., a 1.14-meter vertical column). The results of the first set of three models are presented in Figures 5.12 to 5.14 and show the calculated fluxes of both solutions. All of the Seep/W solutions passed the convergence criteria outlined earlier and are represented in the figures as “Coarse” and “Fine.”

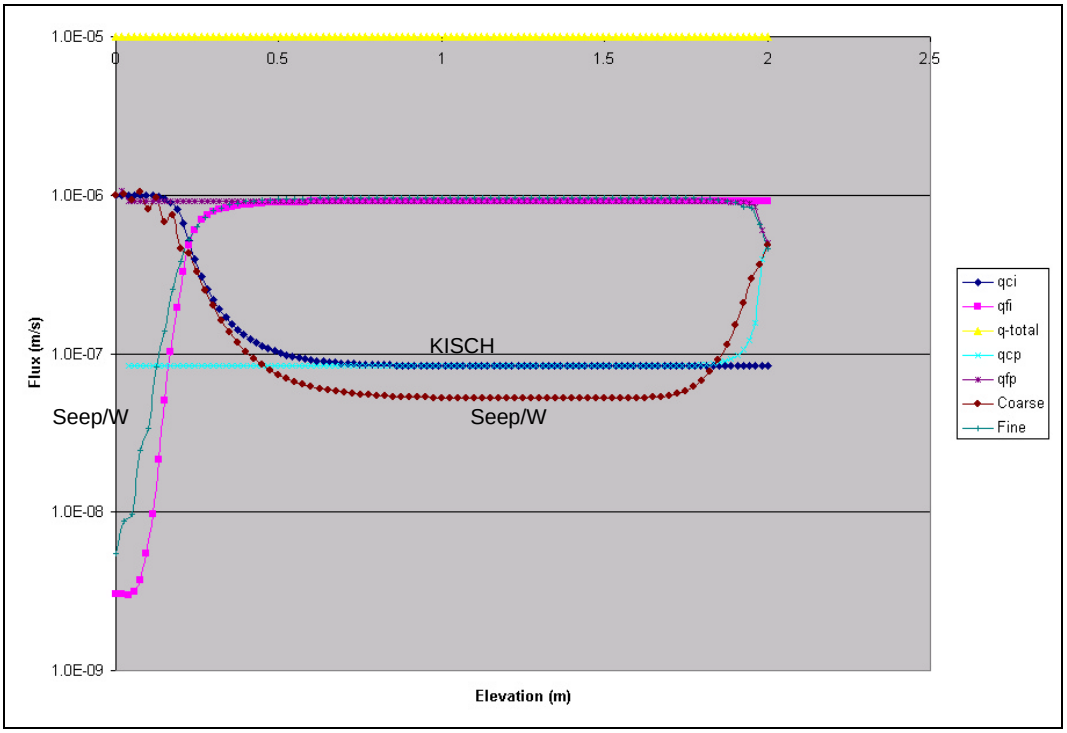


**Figure 5.12 Darcy Flux Calculated for the Vertical 2-Meter System for Modified Kisch and Seep/W Solutions**

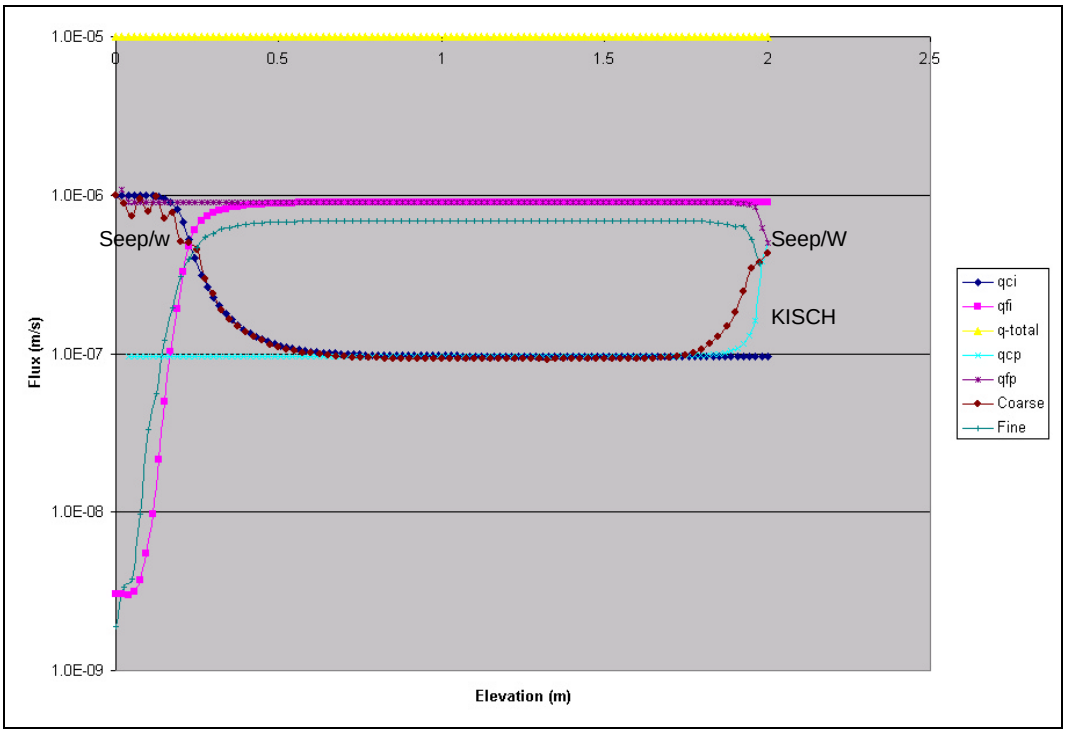


**Figure 5.13 Darcy Flux Calculated for the 75°, 2-Meter System for Modified Kisch and Seep/W Solutions**

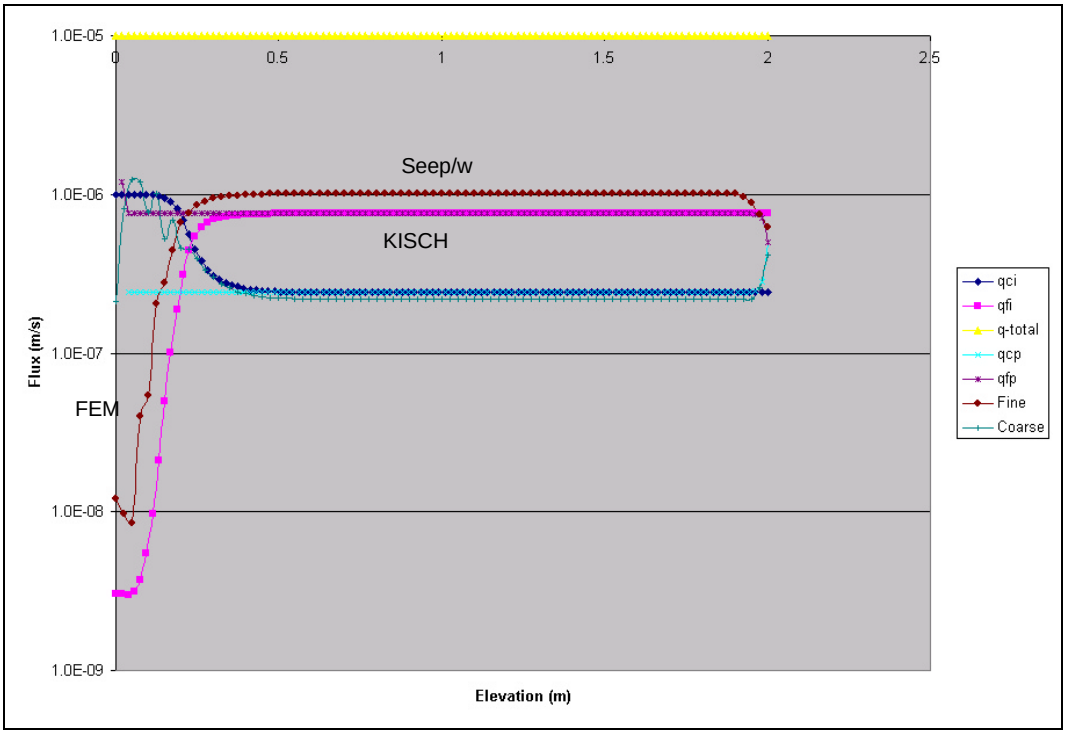


**Figure 5.14 Darcy Flux Calculated for the 45°, 2-Meter System for Modified Kisch and Seep/W Solutions**

The results for the first three models presented in Figure 5.12 through 5.14, compared well. There was a slight fluctuation in the computed values for the fine-grained material results as the model was inclined from the vertical. Note that at the bottom crossover portion of the Seep/W solution does not have as smooth a curve as that calculated with the Modified Kisch solution.

The second set of three models (i.e., one 1.14 and two 2-meter) used the steeper Beaver Creek sand function for the fine-grained material. The results of the second set of models are presented in Figures 5.15 to 5.17 and show the calculated fluxes/velocities of both the modified Kisch (FDM) and FEM solutions. It is important to note that all of the FEM solution passed the convergence criteria outlined earlier. The results are presented in Figures 5.15 through 5.17 as “Coarse” and “Fine.”

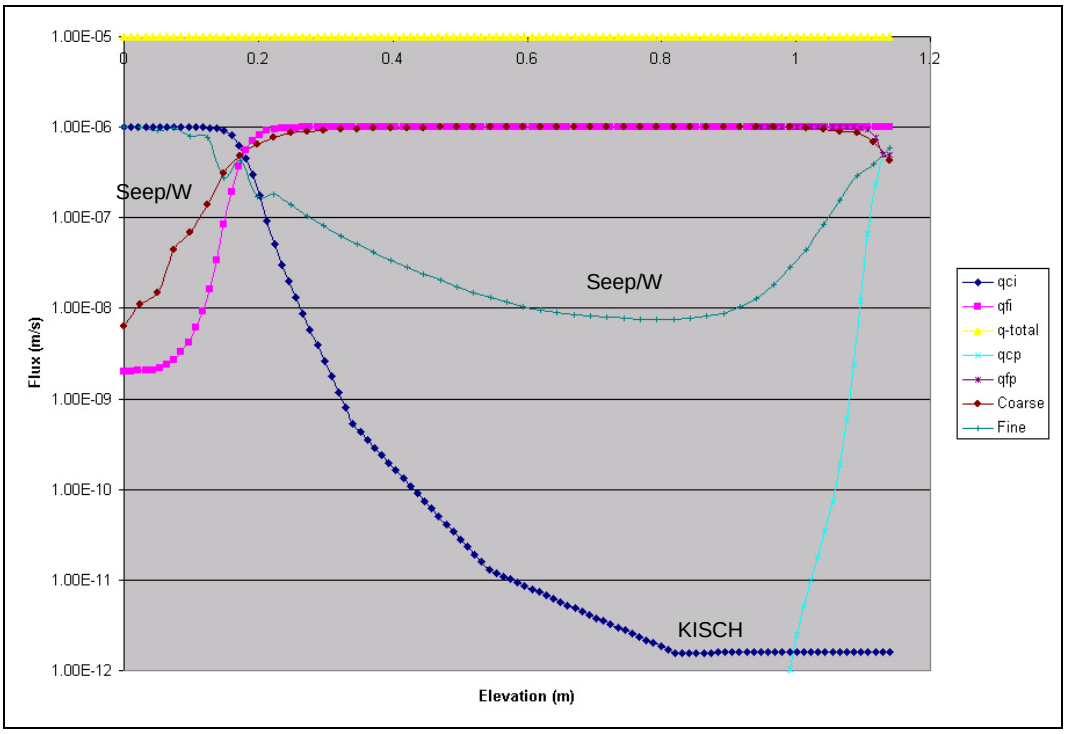


**Figure 5.15 Darcy Flux Calculated for the Vertical, 1.14-Meter System for Modified Kisch and Seep/W Solutions**

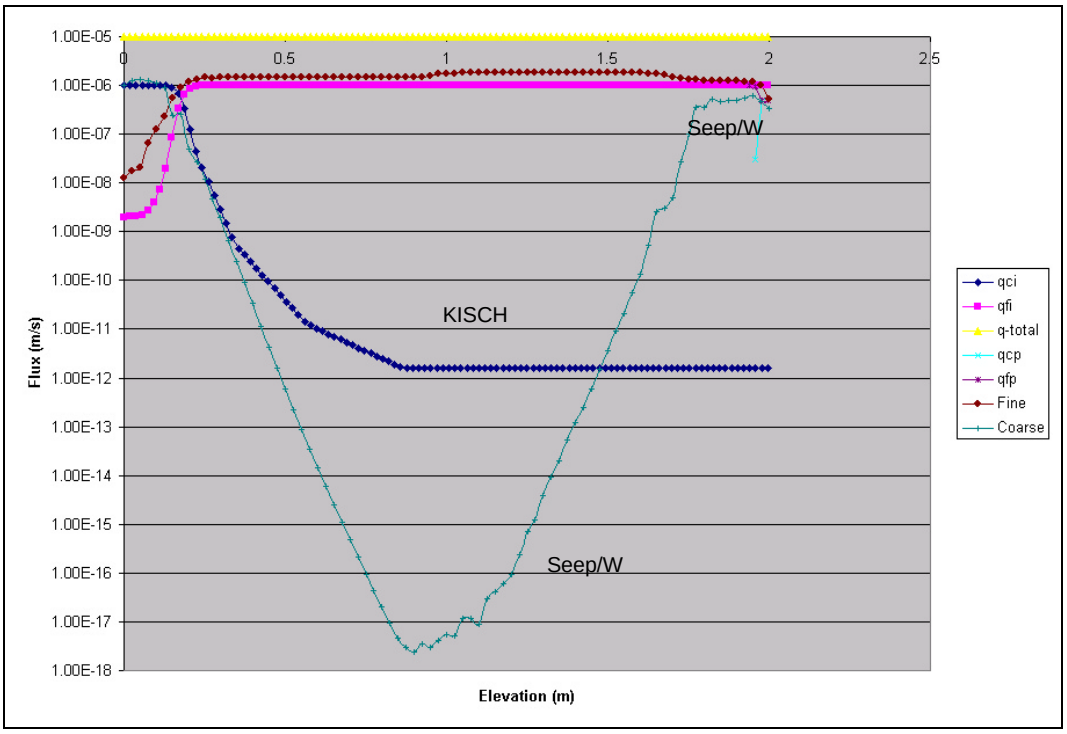


**Figure 5.16 Darcy Flux Calculated for the 75°, 2-Meter System for Modified Kisch and Seep/W Solutions**

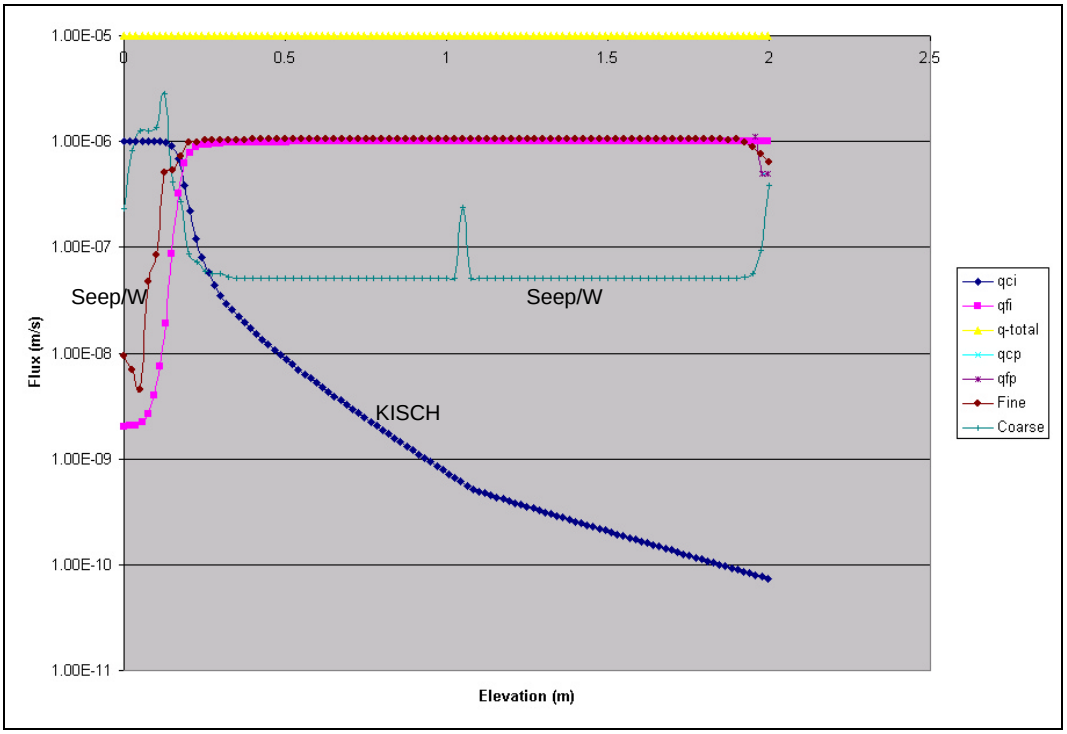


**Figure 5.17 Darcy Flux Calculated for the 45°, 2-Meter System for Modified Kisch and Seep/W Solutions**

The results of the second set of models did not compare as well as the previous set. The FDM solution for the coarse-grained layer did not match that of the FEM solution and the top to bottom calculations were erroneous. To help understand the difference from the first set of models to the second set, the calculated pressure head, gradients, and conductivities were studied and are presented in Figures 5.18 to 5.20.

Compared to the first set of materials used, (i.e., TP5GS1 and silica2) the pore-water pressure heads shown in Figure 5.18 for the second set are more linear and rigid. Figure 5.19 presents the calculated gradients. Note the double hump in the curve indicating that, unlike the first model, (i.e., shown in Figure 5.10) the second model did not reach a gradient of 1 before the midpoint. Figure 5.20 presents the given and calculated hydraulic conductivities. Note the distinct break in the curve of the fine-grained function at the air entry value (AEV).

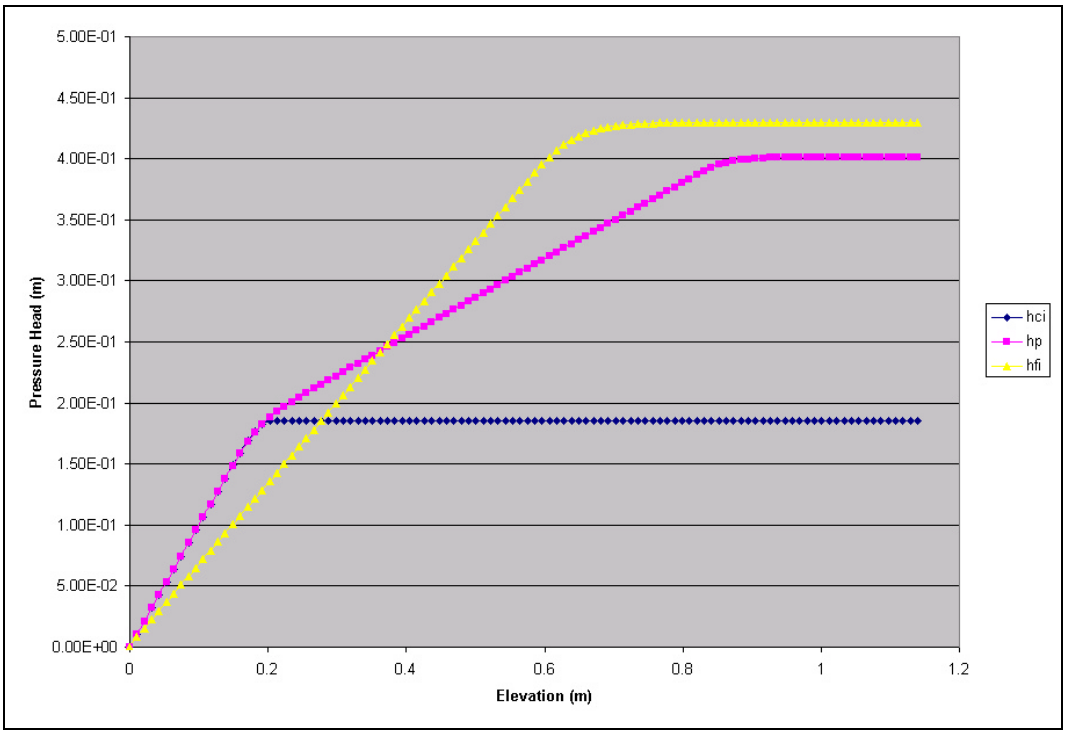


**Figure 5.18 Pressure Heads Calculated for the Second Vertical 1.14-Meter System Using Beaver Creek and Silica Sand**

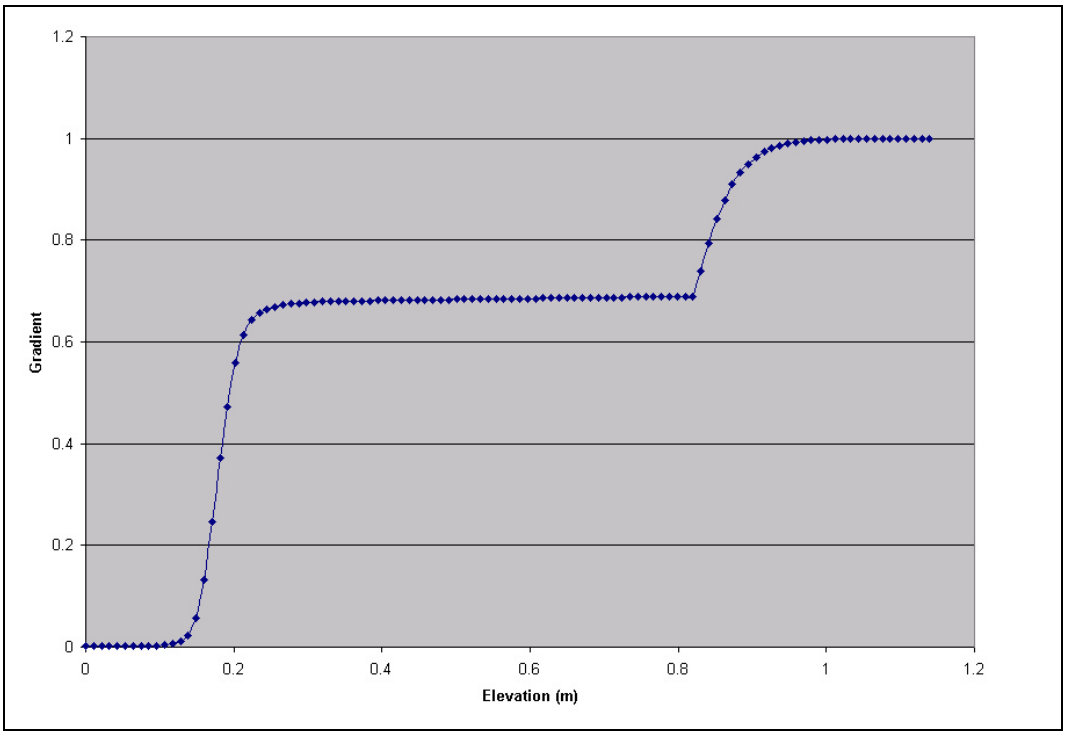


**Figure 5.19 Gradients Calculated for the Second Vertical 1.14-Meter System Using Beaver Creek and Silica Sand**

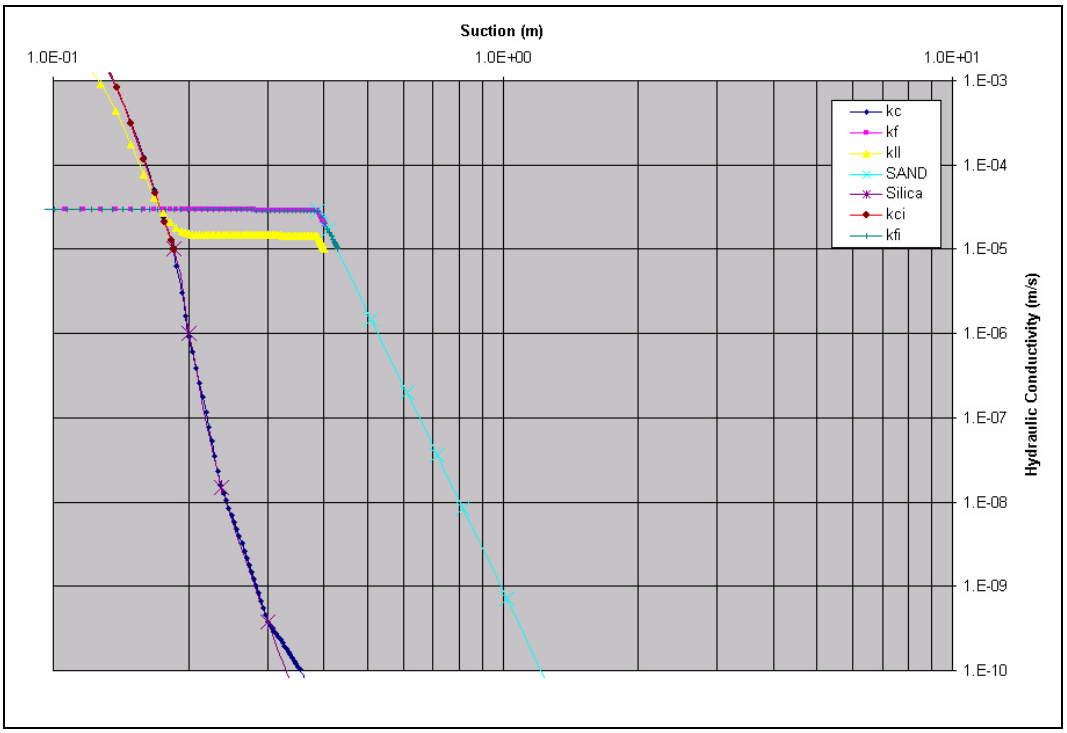


**Figure 5.20 Hydraulic Conductivities Calculated for the Second Vertical 1.14-Meter System Using Beaver Creek and Silica Sand**

The overall results were that the first set of three models using silica2 and TP5GS1 for materials compared well to the FEM solutions; however, the second set of models using silica2 and Beaver Creek sand failed to arrive at a complete solution due to the steep and sudden change in the Beaver Creek sand hydraulic conductivity function. It appeared that the interpolating function was unable to correctly select points along the function and therefore introduced error into the calculations making the top to the bottom solution erroneous.

Other issues were noted with the modified Kisch (1959) solution (FDM). It was observed that the solution was improved by defining tighter nodal spacing and by adding more points in the hydraulic conductivity functions for both materials, or by redefining the hydraulic conductivity functions as a mathematical function. However, there were two main problems with the FDM. First, the linear method by which the FDM was calculated depended solely on the previously calculated value. The FDM can take an error and carry that error to the remaining calculations, or compound the error. In many cases, the investigator will have difficulties in determining an error existed let alone debugging the error. The second and most important problem with the FDM was the same problem encountered with the FEM, which was that dividing and multiplying by very small numbers resulted in numeric instability. In the case of the current FDM study, the instability was dependent on the input parameters, each of which could create instability equally. In this study, a balance had to be reached between the calculations made from the bottom to top (parallel equations, i.e., Equation 3.12) and those made from the top to the bottom (perpendicular equations, i.e., Equation 3.13). For example, defining small nodal spacing and layer thickness would increase the accuracy for the parallel equations but would rapidly decrease the accuracy for the perpendicular equations. Achieving a reasonable balance was possible but it limited the versatility and range of the problems that can be studied with the FDM. This was evident in the second set of models analyzed.

## 5.5 Pilot Program Revisited

As discussed in Chapter 4, the nature of this thesis resulted from choosing a starting point, encountering considerable difficulties and having to take several large step backwards before being able to take small successful steps forward again. Upon completion of the sensitivity analysis (Appendix B) and the finite difference numerical method, the lessons learned were applied to the model used in the original pilot program (refer to Figure 4.3). Using an applied flux of $10^{-5}$ m/s and the original silica2 material properties, a 20-meter tall profile inclined at 50° was developed. The model consisted of seven alternating 1-meter thick fine and coarse-grained layers. A 1-meter thick compacted till layer was specified under the fine and coarse-grained layers to simulate a compacted traffic layer of a lower construction bench. The zero pore-water pressure boundary condition was specified at the bottom of the till layer, and a review boundary was placed on the slope of the model to define possible seepage. The nodal spacing was reduced between different layers and at the top boundary. Convergence criteria used for the parametric study were applied. The model was allowed to run for several days and as new review boundaries were calculated the iterations were repeated. The results of the model with pressure contours and velocity vectors are presented in Figure 5.21. The model was found to achieve full convergence.

The results in Figure 5.21 show that the applied flux flowed preferentially. It appeared that the amount of flux was sufficient to reduce the head in the fine-grained layer, which allowed flow back into the coarse-grained and through to the first fine-grained layer. The first fine layer became saturated to the point where it was unable to accept more flux. The first coarse-grained layer transmitted the remaining flux to the bottom of the system.

The bottom section of the system showed the development of a perched water table. The flow in each fine-grained layer crossed over to the adjacent coarse-

grained layers. A perched water table was created due to the lower permeability of the till and the water flowed laterally through all layers to the toe of the slope.

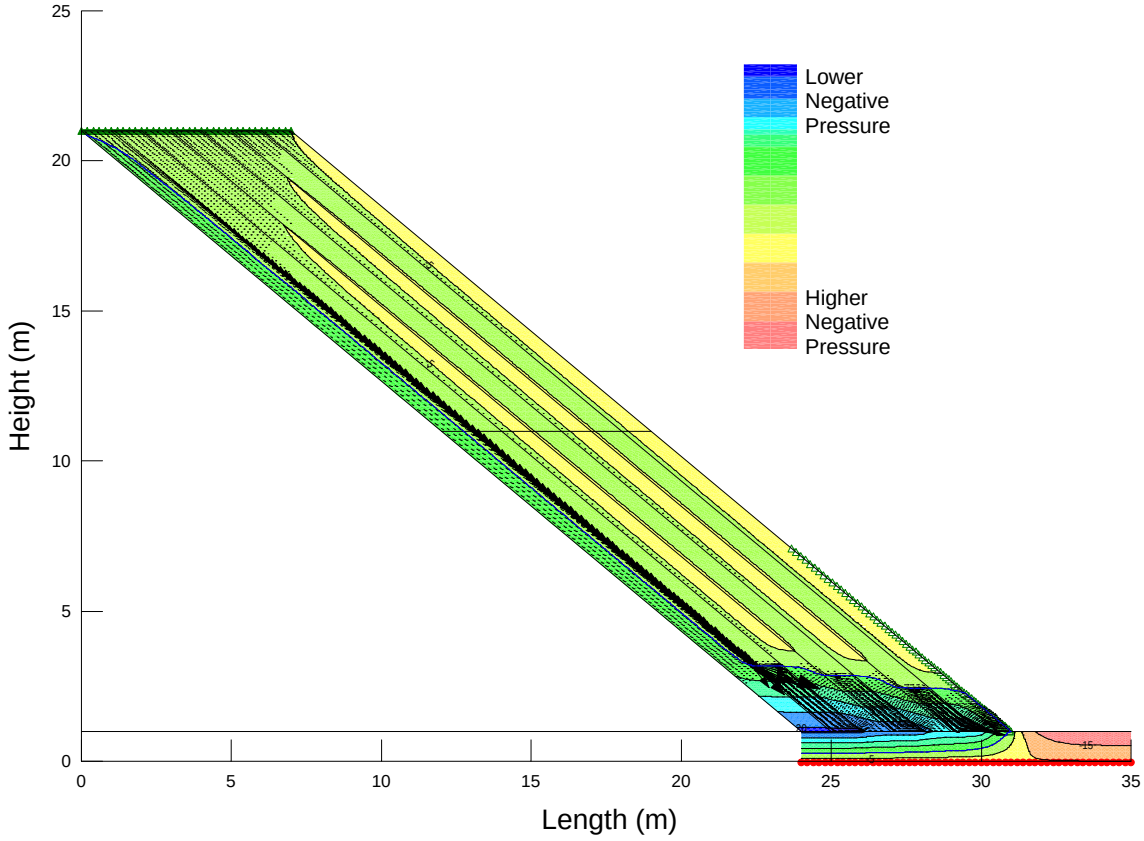


**Figure 5.21 Result of the 50° 20-meter Multi-Layered System with the Applied Flux of $10^{-5}$ m/s**

The positive model result described above prompted an additional model simulation with the annual precipitation at Golden Sunlight Mine for the applied flux (i.e., $7.7E10^{-9}$ m/s). The modified multi-sloped silica2 hydraulic conductivity function developed during the sensitivity analysis and results presented in Figure B21, was used. The results with pore-water pressure contours and velocity vectors are presented in Figure 5.22. Note that this model also achieved full convergence within a reasonable period of computational time.

The results presented in Figure 5.22 showed that preferential flow fully developed with the low applied flux and selected material properties. All flux from the coarse-grained layer crossed over to the fine-grained layers and the

flux was transmitted to the bottom of the system through the fine layers. Due to the low flux, a significant perched water table did not developed at the bottom contact with the till layer. However, seepage did flow toward the slope at the review boundary, and exit out.

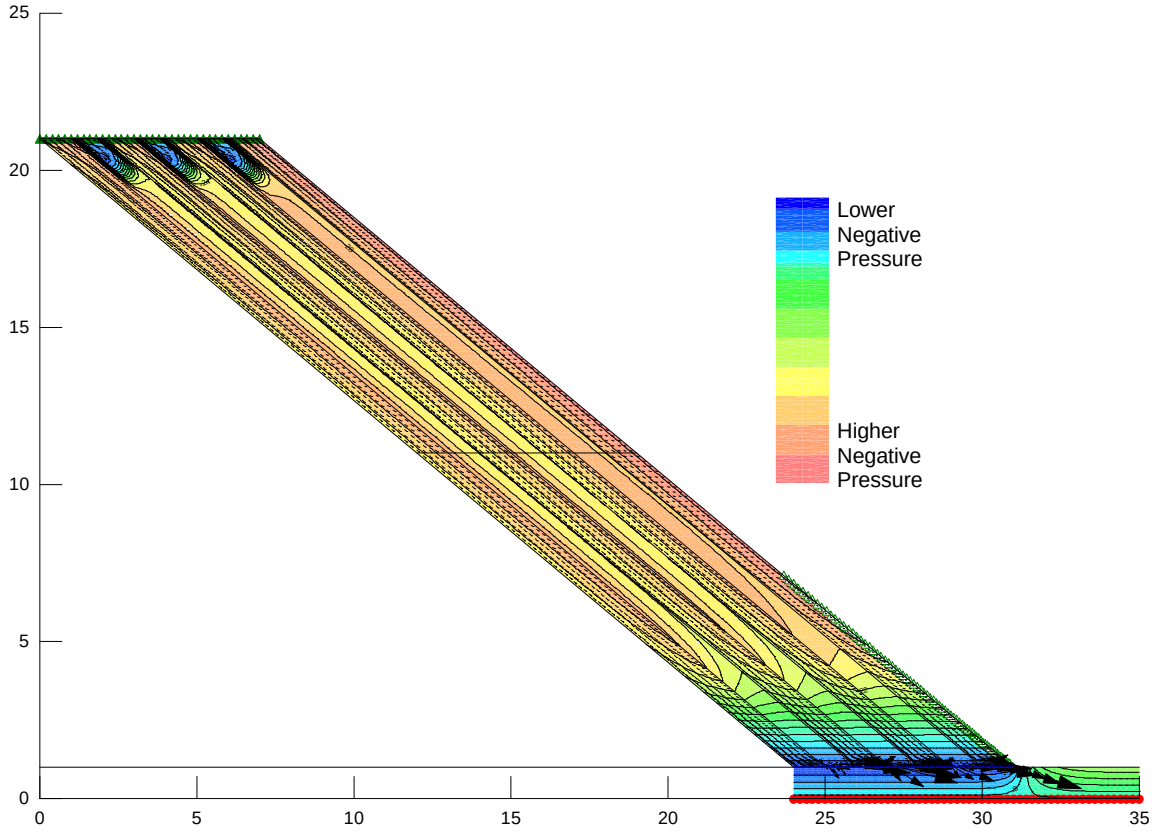


**Figure 5.22 Result of the 50° 20-meter Multi-Layered System with the Applied Flux of 7.7e10$^{-9}$ m/s**

The results present in Figure 5.22 were not expected to be accomplished during this study. The successful work of Newman (1999) led to a successful parametric study, modified Kisch (1959) solution, and sensitivity analysis (Appendix B) that developed the understanding of the tools available to numerically solve the problem. The results from this study can now be a platform for future research.

# CHAPTER 6

# SUMMARY, CONCLUSION, & RECOMMENDATIONS

## 6.1 Summary and Conclusion

The previous chapters described the modelling process beginning with the identification of a real life seepage problem (the physical problem) through to the conceptualization of the problem as a series of basic components. The conceptual model was transformed to a mathematical model by defining the governing equations, and solving the mathematical model using both a finite element method (i.e., Seep/W) and a finite difference method (i.e., modified Kisch solution), along with verification of the results. This chapter will summarize the lessons learned from the problems encountered in the pilot program, the parametric study, and the development of the modified Kisch solution.

The negative results of the pilot program led to the development of a parametric study. The results of the parametric study (section 5.3) showed that numerical modelling programs could support the conceptual model developed by Herasymuik (1996), and the mechanics of preferential flow described by Newman (1999). The numerical simulation results presented are preliminary in nature and are not intended to fully describe seepage in unsaturated waste rock dumps with dipping layers of variable textures. However, the results of the analysis illustrated complexity of unsaturated flow hydrogeology in waste rock dumps, and some key trends. The process of starting with a simple solution and increasing the complexity incrementally yielded not only valuable insight into the problem, but gave a higher platform in which to start future studies that are more ambitious.

The parametric study showed that preferential flow in inclined waste rock layers could be modelled numerically. Preferential flow was found to be a function of the material properties, geometry, and pressure heads in the system, and the applied flux into the system. Preferential flow was also found to be influenced by the inclination of the waste rock layers, as well as the contact length between the fine and coarse layers.

It was concluded that preferential flow was a function of several variables that dictated where the preferential conduit would occur and how much flux would be transmitted. A unique solution exists for each set of variables specified. Not only did the parametric study reveal that the problem being solved was non-linear, but also that it was a coupled problem in such a way that the variables appeared inter-dependent on each other.

The modified Kisch (1959) solution using the finite difference method was explored and a surprisingly straightforward solution to preferential flow in a two-soil two-layered system was discovered. The modified Kisch solution can characterize preferential flow through the system by utilizing the five pressure head profiles calculated. As the applied flux enters the top of the system, the flux was divided between the layers, based on the last two head profiles and the law of conservation of mass. The division of flux was found to characterize the initial crossover of flux shown by Newman (1999). A third head profile was used to characterize the center and bottom sections of the system. It was shown at the vertical midway point of the system, the gradient was equal to unity, and no transfer of flux was observed. As the elevation decreased, the pressure head in the system increases to zero and the head in the system will reach a point where both the coarse and fine-grained material have the same hydraulic conductivity for the same pressure head. At this point, the coarse-grained material becomes more conductive and the majority of the flux will crossover into the coarse-grained layer.

The results of the modified Kisch solution were academic in nature; however working through the mathematics provided further insight to the relationships between the individual layers as they interact as a system. The modified Kisch solution can be used to compare two soil properties before turning to the Seep/W. In addition, the system of equations and algorithms can be further improved to increase efficiency.

By following the methodology for numerical modelling outlined in Chapter 2, an understanding of the numerical model was further developed with respect to both the physical and mathematical models.

Based on the lessons learned from the numerical modelling programs, the original model in the pilot program was repeated with positive results. The results of the simulations showed that with the very low applied flux of $7.7E10^{-9}$ m/s, flow through a seven-layered system would quickly move to the fine-grained layer and travel exclusively in the fine-gained layers. Only when the pore-water pressure heads increased would the flow transfer back into the coarse-grained material layers and eventually exit the system. The result was significant with respect to reducing matric suction and possible slope stability issues.

## 6.2 Need for Future Research

Little research has been devoted to the prediction and analysis of seepage through waste rock dumps. This study investigated preferential flow in vertical to inclined waste rock layers with horizontal segregation (i.e., fine-coarse-fine-coarse). The conceptual model described by Herasymuik (1996) indicated that as waste rock is end dumped, the waste rock segregates, and the coarser-grained material rolls further down the dump than the finer-grained material. This results in layering not only horizontally but also vertically, as finer material will be retained more near the top of the dump than at the bottom. This sorting can explain the observation of a wetting front on the top third of an end-dumped waste rock bench. MEND (1995) also noted that the finer material would remain

in the top third of the waste rock dump. The added complexity of the problem with respect to the vertical segregation and further horizontal segregation (i.e., more that two materials) of waste rock layers was not investigated in this study and is recommended for future study.

The current study also investigated many of the problems related to using numerical modelling as a predictive design tool. The major problems resulted from the negative pressure heads and corresponding low values of hydraulic conductivity encountered in the taller profiles while using steep hydraulic conductivity functions and low applied fluxes. It has to be noted that the numerical modelling package (Seep/W) used was not designed to deal with the extreme conditions encountered in this study. A balance between applying accurate material properties and changing the material properties to ease numerical instability has to be reached in case-by-case bases. As noted earlier in the thesis, if a very low hydraulic conductivity function value contributes significantly to numerical instability and insignificantly to flow, the slope of the hydraulic conductivity function should be increased to assist numerical stability but also be kept from significantly changing the flow distribution within the system.

In general, commercial seepage modelling packages are powerful and useful tools that are designed to adequately accommodate a wide range of geotechnical problems. The study showed that Seep/W may not be the best-suited tool to analyze unsaturated seepage through sloping waste rock layers. However, numerical modelling is a process and working through the process helps to enhance engineering judgment. The Seep/W model provided an adequate solution for a simplified simulation of unsaturated seepage through waste rock layers. The modified Kisch solution independently verified the solution and provided additional confidence for the results of Seep/W model. However, several improvements in numerical modelling coding, pre-processing, and computing power must occur before further developments can proceed. In

addition, laboratory studies for a multi-layer waste rock system should be conducted to verify the current study as well as design new studies as numerical modelling coding specific for unsaturated seepage through waste rock layers.

A possible application of the numerical modelling includes the slope stability analysis for the waste rock dumps and the design of an engineered waste rock pile in which non-reactive fine-grained material borders a reactive coarse-grained waste rock. The results of the present study show it is possible to simulate unsaturated flow through the fine-grain material, leaving the coarse-grain material void of significant flux. The result would be a system that may greatly reduce drainage through acid generating material.

## LIST OF REFERENCES

Aubertin, M., Chapuis, R.P., Bouchentouf, A., and Bussière, B., 1997. Unsaturated flow modelling of inclined layers for the analysis of covers. Proceedings of the fourth-international conference on acid rock drainage, Vancouver, B.C. May 31-June 6, vol. II, pp. 731-746.

Barbour, S.L., 1998. Numerical Modelling for Geotechnical/Geoenvironmental Engineering. Course notes for CE 898. Department of Civil Engineering, University of Saskatchewan, Saskatoon, Canada.

Bussière, B., Aubertin, M., Chapuis, R.P., 1997. Écoulement non saturé à travers les couvertures avec effets de barrière Capillaire (CEBC): Modélisation physique et numérique avec application au drainage minier acide. Technical Report EPM/RT-97/03, École Polytechnique de Montréal, 202 pages.

Bussière, B., Aubertin, M., Chapuis, R.P., 1999. Numerical study of the hydraulic behaviour of inclined covering systems aimed at limiting the flux of oxygen. In: Proceedings of the 52nd Geotechnical Conference, pp. 373-380.

Dawson, R. and Morgenstern, N.R., 1995. Liquefaction flowslides in Western Canadian coal mine waste dumps. (prepared for the CANMET-Western Research Centre.) AGRA Earth and Environmental Ltd., Calgary, Alta.

Fredlund, D.G. and Rahardjo, H.R., 1993. Soil mechanics for unsaturated soils. John Wiley & Sons, New York. N.Y.

Fredlund, D.G., Xing, A., and Huang, S., 1994. Predicting the permeability function for unsaturated soils using the soil-water characteristic curve. Canadian Geotechnical Journal, (31): pp. 533-546.

Freeze, R.A, and Cherry, J.A., 1979. Groundwater. Prentice Hall, Englewood Cliffs, NJ.

Frind, E.O., Gillham, R.W., and Pickens, J.F., 1976. Application of unsaturated flow properties in the design of geologic environments for radioactive waste storage facilities. In: Proceedings of the First International Conference on Finite Elements in Water Resources, Princeton, N.J.

Geo-slope International Ltd., 1995. Seep/W User's Manual. Geo-Slope International Ltd., Calgary, AB.

Herasymuik, G.M., 1996. Hydrogeology of a sulphide waste rock dump. M.Sc. Thesis, University of Saskatchewan, Saskatoon, Saskatchewan, Canada.

Hillel, D., 1971. Soil and water: physical principles and processes. Academic Press, New York.

Horton, J.H. and Hawkins, R.H., 1965. Flow path of rain from the soil surface to the water table. Soil Science (100) No.6: pp. 337-383.

Kisch, M., 1959. The theory of seepage from clay-blanketed reservoirs. Geotechnique, Volume 9, pp. 9-21.

Kumar, M.S.M., Prasad, K.S.H., and Sekkar, M. 1995. A finite analytic model for analysis of recharge through unsaturated soil. Unsaturated soils/sols non-satures, Alonso & Delage (eds.) Balkema, pp. 1092-1100.

Larson, T.H., Keefer, D.A., Albrecht, K.A., and Cartwright, K., 1988. Infiltration through layered soil trench covers: Response to an extended period of rainfall. Journal of Contaminant Hydrology, Volume 3, pp. 251-261.

Mehling, P.E., Day, S.J., and Sexsmith, K.S., 1997. Blending and layering waste rock to delay, mitigate or prevent acid generation: a case study review.

MEND Associate Project, 1995. Hydrogeology of waste rock dumps. Final Report to Department of Natural Resources Canada.

Mercer and Faust, 1981. Ground-water modelling. National Water Well Association.

Miyazaki, T., 1988. Water flow in unsaturated soil in layered slopes. Journal of Hydrology, Volume 102, pp. 201-214.

National Research Council, 1990. Groundwater models – Scientific and regulatory applications. National Research Council.

Nelson and McWhorter, 1985. Water movement. In Design of non-impounding mine waste dumps, M.K. Carter Ed. American Institute of Mining, Metallurgical and Petroleum Engineers Inc., New York.

Newman, L.L., 1999. A mechanism for preferential flow in vertically layered unsaturated systems. M.Sc. Thesis, University of Saskatchewan, Saskatoon, Saskatchewan, Canada.

Newman, L.L, Herasymuik, G.M., Barbour, S.L., Fredlund, D.G., and Smith, T., 1997. The hydrogeology of waste rock dumps and a mechanism for unsaturated preferential flow. Proceedings of the forth-international conference on acid rock drainage, Vancouver, B.C. May 31-June 6, vol. II, pp. 553-565.

Oldenburg, C.M. and Pruess, K., 1993. On numerical modelling of capillary barriers. Water Resources Research, Volume 26, Number 1, pp. 1-8.

Ross, B., 1990. The diversion capacity of capillary barriers. Water Resources Research, Volume 26, Number 10 pp. 2625-2629.

Selim, H.M., 1987. Water flow in layered soils with sloping surfaces. Journal of Irrigation and Drainage Engineering, Volume 114, Volume 3, pp. 442-462.

Spitz and Moreno, 1996. Practical guide to groundwater and solute transport modelling. John Wiley & Sons, Inc.

Steenhuis, T.S., Parlange, J.Y., and Kung, K.J.S., 1991. Comment on "The diversion capacity of capillary barriers" by B. Ross. Water Resources Research, Volume 27, Number 8, pp. 2155-2156.

Stormont, J.C., 1995. The effect of constant anisotropy on capillary barrier performance. Water Resources Research, Volume 31, Number 3, pp. 783-785.

Stormont, J.C. and Anderson, C.E., 1999. Capillary barrier effect from underlying coarser soil layer. Journal of Geotechnical and Geoenvironmental Engineering, pp. 641-648.

Swanson, D.A., 1995. Predictive modelling of moisture movement in engineered soil covers for acid generating mine waste. M.Sc. Thesis, University of Saskatchewan, Saskatoon, Saskatchewan, Canada.

Topp, G.C. and Miller, E.E., 1966. Hysteretic moisture characteristics and hydraulic conductivity of glass bead media. Soil Science Society of America Journal, Volume 30, pp. 156-162.

Tsai, W.F. and Chen, C.J., 1993. Finite analytic numerical solutions for unsaturated flow with irregular boundaries. Journal of Hydraulic Engineering, ASCE, Volume 119, Number 11, pp. 1274-1298.

Wallach, R and Zaslavsky, D., 1991. A closed-form equation for predicting the hydraulic Conductivity of unsaturated soils. Soil Science Society of American Journal, Volume 119, Number 11, pp. 1274-1298.

Yeh, T.C.J., Guzman, Al., Srivestava, R., and Gagnard, P.E., 1994. Numerical Simulation of the wicking effect in liner Systems. Ground Water, Volume 32, Number 1, pp. 2-11.

Zaslavsky, D. and Sinai, G., 1981. Surface hydrology: IV – Flow in sloping, layered soil. Journal of the Hydraulics Division, ASCE, Volume 107(HY1), pp. 53-64.

# APPENDIX A

# PARAMETRIC STUDY

The parametric study involved the solution of steady state models and yielded solutions with convergence for 30 model simulations. The results of the parametric study with respect to the increasing model height and the lowest log hydraulic conductivity calculated for the models are presented in Table A1 below. Table A1 presents the percentage of the total flux in each layer for each inclination at each height modelled.

**Table A1 Result of The Parametric Study with Respects to Model Height**

| 1m | | | | | |
|---|---|---|---|---|---|
| LAYER | ANGLES | | | | |
| | 90 | 85 | 75 | 60 | 45 |
| 1ST FINE | 35.48% | 37.11% | 40.46% | 46.48% | 44.17% |
| 1ST COARSE | 5.14% | 5.88% | 8.50% | 15.12% | 33.49% |
| 2ND FINE | 45.48% | 45.38% | 44.79% | 38.73% | 24.83% |
| 2ND COARSE | 13.78% | 11.39% | 6.28% | 1.36% | 0.01% |
| CONDUCTIVITY | -5.80 | -5.79 | -5.92 | -6.96 | -8.38 |

| 2m | | | | | |
|---|---|---|---|---|---|
| LAYER | ANGLES | | | | |
| | 90 | 85 | 75 | 60 | 45 |
| 1ST FINE | 37.21% | 39.16% | 45.80% | 57.36% | 48.05% |
| 1ST COARSE | 2.23% | 3.15% | 6.04% | 10.00% | 33.93% |
| 2ND FINE | 50.10% | 50.38% | 45.96% | 32.35% | 18.34% |
| 2ND COARSE | 9.90% | 5.43% | 1.67% | 0.96% | 0.00% |
| CONDUCTIVITY | -6.30 | -6.08 | -6.89 | -8.89 | -10.34 |

| 4m | | | | | |
|---|---|---|---|---|---|
| LAYER | ANGLES | | | | |
| | 90 | 85 | 75 | 60 | 45 |
| 1ST FINE | 38.69% | 42.40% | 52.17% | 63.10% | 48.50% |
| 1ST COARSE | 2.37% | 3.50% | 4.36% | 10.00% | 34.74% |
| 2ND FINE | 51.98% | 50.81% | 42.83% | 26.99% | 16.79% |
| 2ND COARSE | 6.69% | 2.93% | 0.30% | 0.00% | 0.00% |
| CONDUCTIVITY | -6.34 | -6.33 | -7.94 | -10.05 | -10.44 |

**Table A1 Result of the parametric study with respects to model height (continued)**

| 8m | | | | | |
|---|---|---|---|---|---|
| LAYER | ANGLES | | | | |
| | 90 | 85 | 75 | 60 | 45 |
| 1ST FINE | 43.57% | 47.36% | 59.14% | 64.81% | 48.50% |
| 1ST COARSE | 2.33% | 2.95% | 3.46% | 11.26% | 34.82% |
| 2ND FINE | 50.31% | 48.25% | 37.32% | 23.99% | 16.66% |
| 2ND COARSE | 3.77% | 1.30% | 0.06% | 0.00% | 0.00% |
| CONDUCTIVITY | -6.35 | -6.70 | -8.74 | -10.24 | -10.48 |

| 16m | | | | | |
|---|---|---|---|---|---|
| LAYER | ANGLES | | | | |
| | 90 | 85 | 75 | 60 | 45 |
| 1ST FINE | 44.90% | 53.40% | 62.38% | 65.08% | 48.33% |
| 1ST COARSE | 2.30% | 2.73% | 3.70% | 11.79% | 34.71% |
| 2ND FINE | 49.33% | 43.40% | 33.87% | 23.11% | 16.65% |
| 2ND COARSE | 3.25% | 0.48% | 0.03% | 0.00% | 0.13% |
| CONDUCTIVITY | -6.39 | -7.11 | -8.62 | -10.28 | -10.51 |

| 20m | | | | | |
|---|---|---|---|---|---|
| LAYER | ANGLES | | | | |
| | 90 | 85 | 75 | 60 | 45 |
| 1ST FINE | 45.70% | 52.83% | 62.75% | 65.11% | 48.29% |
| 1ST COARSE | 2.31% | 2.71% | 3.86% | 11.81% | 34.45% |
| 2ND FINE | 49.00% | 43.86% | 33.37% | 23.06% | 16.68% |
| 2ND COARSE | 2.95% | 0.39% | 0.03% | 0.00% | 0.00% |
| CONDUCTIVITY | -6.40 | -6.91 | -8.64 | -10.30 | -10.57 |

The results of the parametric study with respects to the increase inclination and the lowest log conductivity calculated for the model of the models is presented in Table A2 below. Table A2 presents the flux in each layer for each height at each model inclination.

**Table A2 Result of The Parametric Study with Respects to Model Inclination**

| 90 Degrees | | | | | | |
|---|---|---|---|---|---|---|
| LAYER | HEIGHTS | | | | | |
| | 1 | 2 | 4 | 8 | 16 | 20 |
| 1ST FINE | 35.48% | 37.21% | 38.69% | 43.57% | 44.90% | 45.80% |
| 1ST COARSE | 5.14% | 2.23% | 2.37% | 2.33% | 2.30% | 2.30% |
| 2ND FINE | 45.48% | 50.10% | 51.98% | 50.31% | 49.33% | 49.10% |
| 2ND COARSE | 13.78% | 9.90% | 6.69% | 3.77% | 3.25% | 2.77% |
| CONDUCTIVITY | -5.80 | -6.30 | -6.34 | -6.35 | -6.39 | -7.86 |
| **85 Degrees** | | | | | | |
| LAYER | HEIGHTS | | | | | |
| | 1 | 2 | 4 | 8 | 16 | 20 |
| 1ST FINE | 37.11% | 39.16% | 42.40% | 47.36% | 53.40% | 52.83% |
| 1ST COARSE | 5.88% | 3.15% | 3.50% | 2.95% | 2.73% | 2.71% |
| 2ND FINE | 45.38% | 50.38% | 50.81% | 48.25% | 43.40% | 43.86% |
| 2ND COARSE | 11.39% | 5.43% | 2.93% | 1.30% | 0.48% | 3.93% |
| CONDUCTIVITY | -5.79 | -6.08 | -6.33 | -6.70 | -7.11 | -6.91 |
| **75 Degrees** | | | | | | |
| LAYER | HEIGHTS | | | | | |
| | 1 | 2 | 4 | 8 | 16 | 20 |
| 1ST FINE | 40.46% | 45.80% | 52.17% | 59.14% | 62.38% | 62.75% |
| 1ST COARSE | 8.50% | 6.04% | 4.36% | 3.46% | 3.70% | 3.86% |
| 2ND FINE | 44.79% | 45.96% | 42.83% | 37.32% | 33.87% | 33.37% |
| 2ND COARSE | 6.28% | 1.67% | 0.30% | 0.06% | 0.03% | 0.03% |
| CONDUCTIVITY | -5.92 | -6.89 | -7.94 | -8.74 | -8.62 | -8.64 |
| **60 Degrees** | | | | | | |
| LAYER | HEIGHTS | | | | | |
| | 1 | 2 | 4 | 8 | 16 | 20 |
| 1ST FINE | 46.48% | 57.36% | 63.10% | 64.81% | 65.11% | 65.11% |
| 1ST COARSE | 15.12% | 10.00% | 10.00% | 11.26% | 11.81% | 11.81% |
| 2ND FINE | 38.73% | 32.35% | 26.99% | 23.99% | 23.06% | 23.06% |
| 2ND COARSE | 1.36% | 1.61% | 0.00% | 0.00% | 0.00% | 0.00% |
| CONDUCTIVITY | -6.96 | -8.89 | -10.05 | -10.24 | -10.30 | -10.30 |
| **45 Degrees** | | | | | | |
| LAYER | HEIGHTS | | | | | |
| | 1 | 2 | 4 | 8 | 16 | 20 |
| 1ST FINE | 44.17% | 48.05% | 48.50% | 48.50% | 48.33% | 48.29% |
| 1ST COARSE | 33.49% | 33.93% | 34.74% | 34.82% | 34.71% | 34.45% |
| 2ND FINE | 24.83% | 18.34% | 16.79% | 16.66% | 16.65% | 16.68% |
| 2ND COARSE | 0.01% | 0.00% | 0.00% | 0.00% | 0.13% | 0.00% |
| CONDUCTIVITY | -8.38 | -10.34 | -10.44 | -10.48 | -10.51 | -10.57 |

The results of Table A1 are plotted and presented in Figures A1 to A6 below. The figures show the flux in each layer (secondary axis) and the lowest calculated log conductivity (primary axis) as the model is inclined for each modelled height.

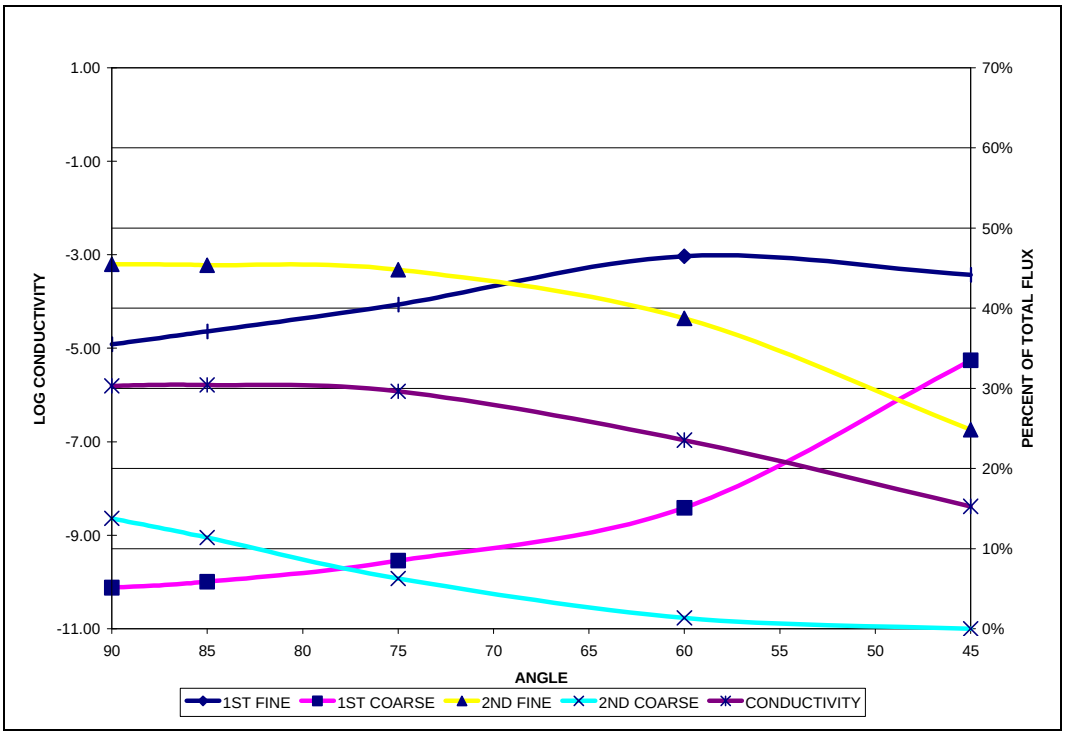


**Figure A1 The Results of the 1-meter Model with respect to Inclination**

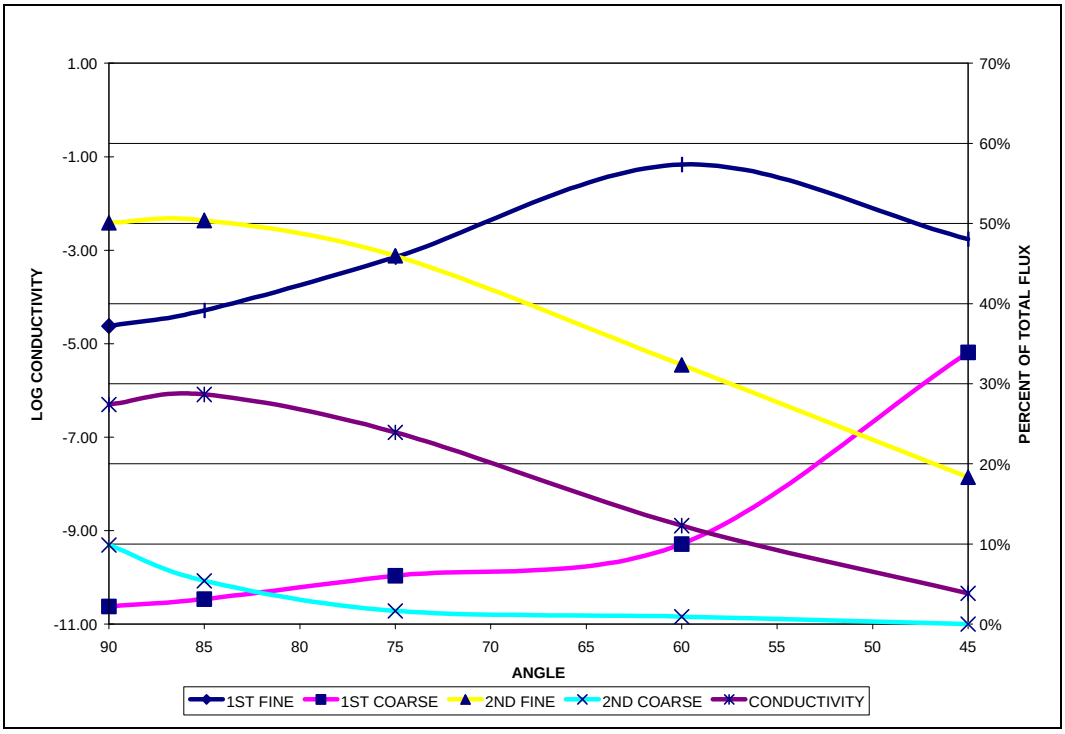


**Figure A2 The Results of the 2-meter Model with Respect to Inclination**

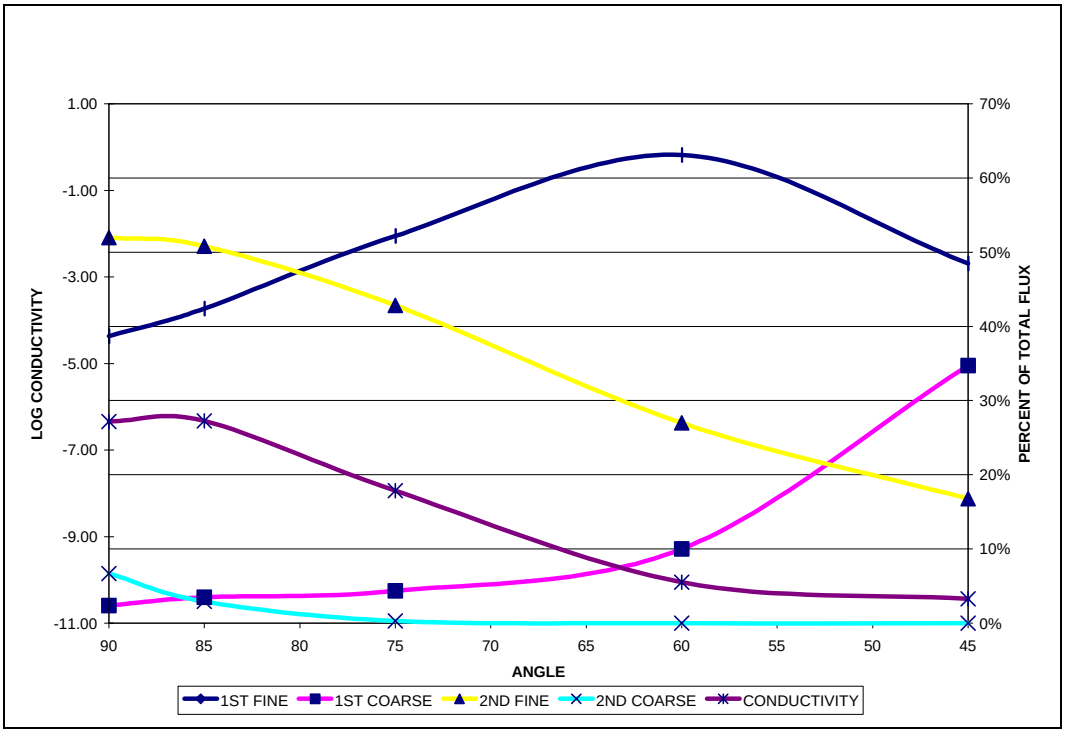


**Figure A3 The Results of the 4-meter Model with Respect to Inclination**

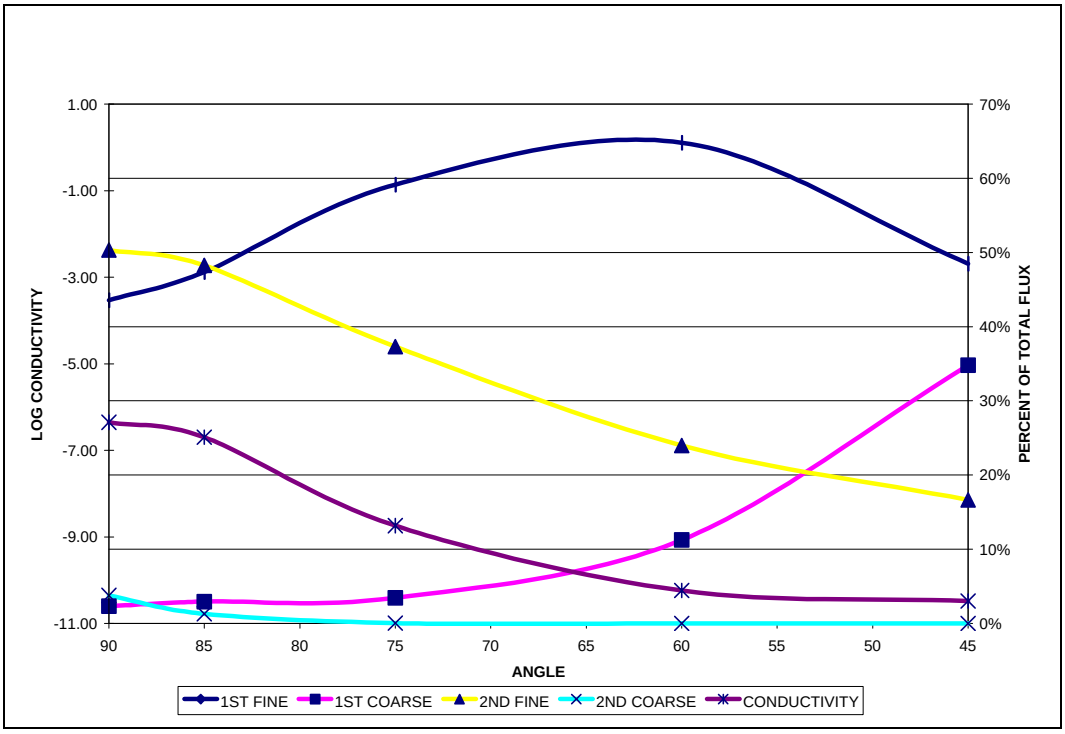


**Figure A4 The Results of the 8-meter Model with Respect to Inclination**

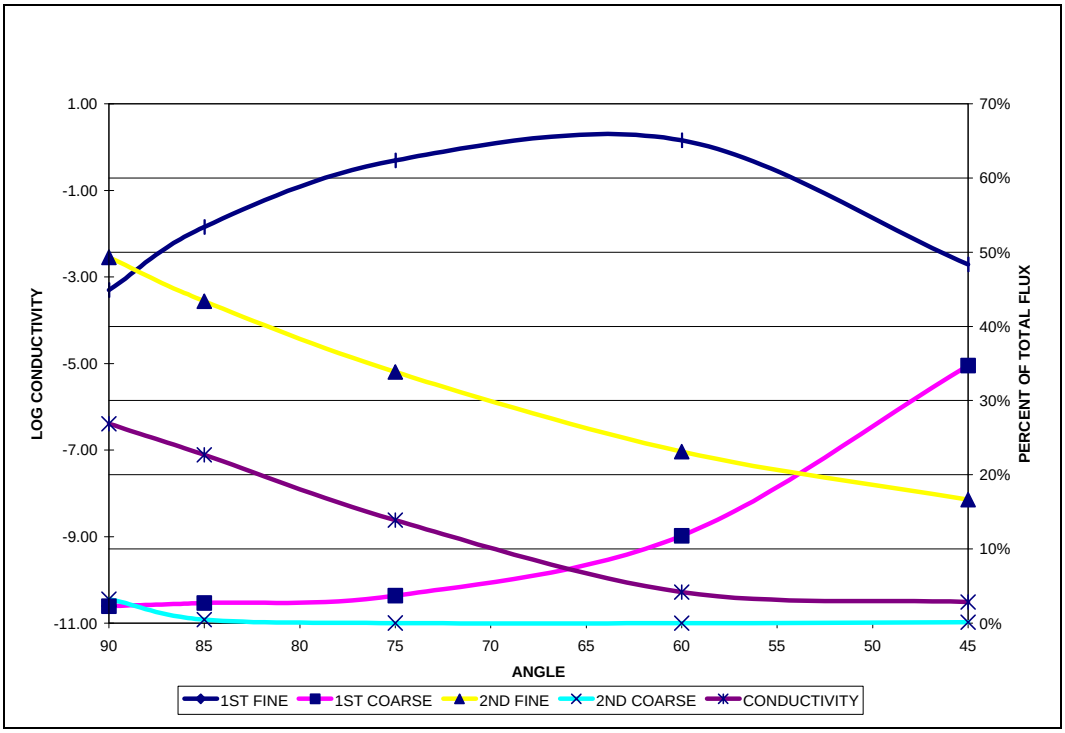


**Figure A5 The Results of the 16-meter Model with Respect to Inclination**

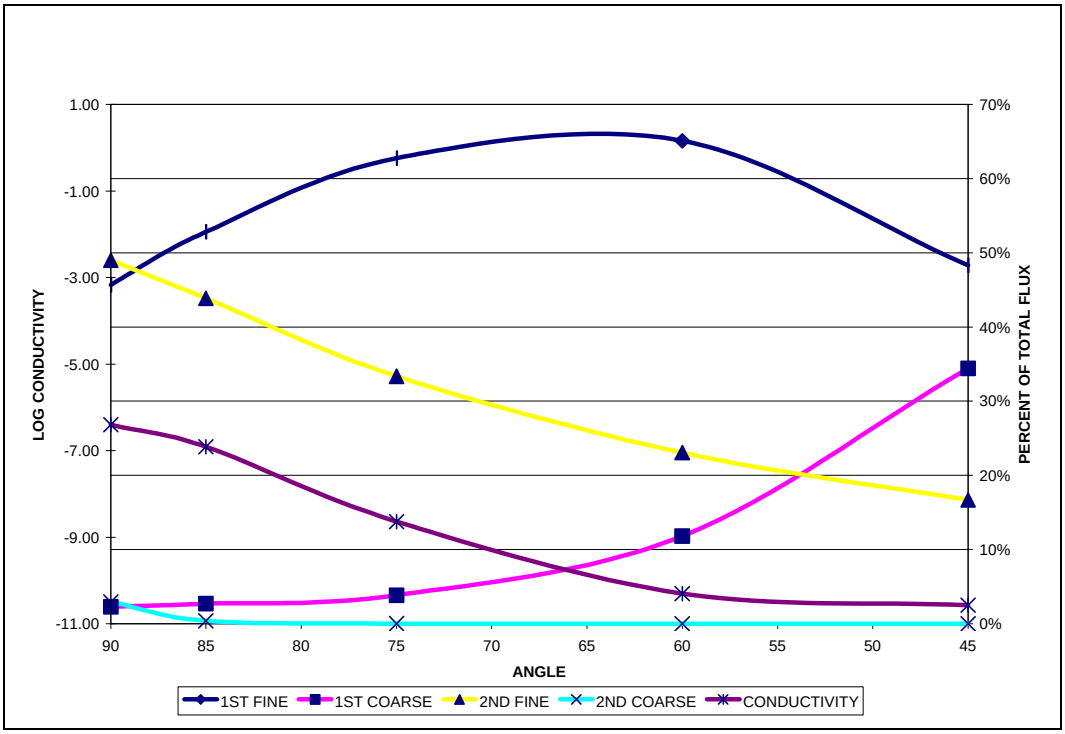


**Figure A6 The Results of the 20-meter Model with Respect to Inclination**

The results of Table A2 are plotted and presented in Figures A7 to A11 below. The figures show the flux in each layer (secondary axis) and the lowest calculated log conductivity (primary axis) for each modelled height, as the model is inclined.

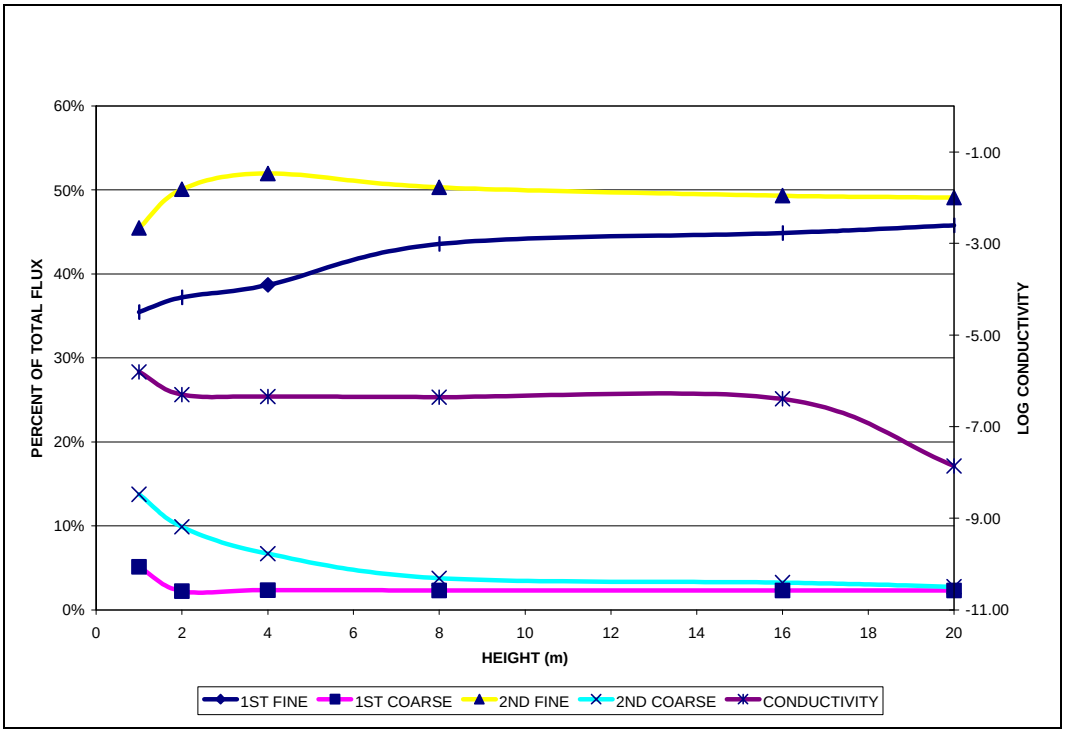


**Figure A7 The Results of the 90° Model with Respect to Height**

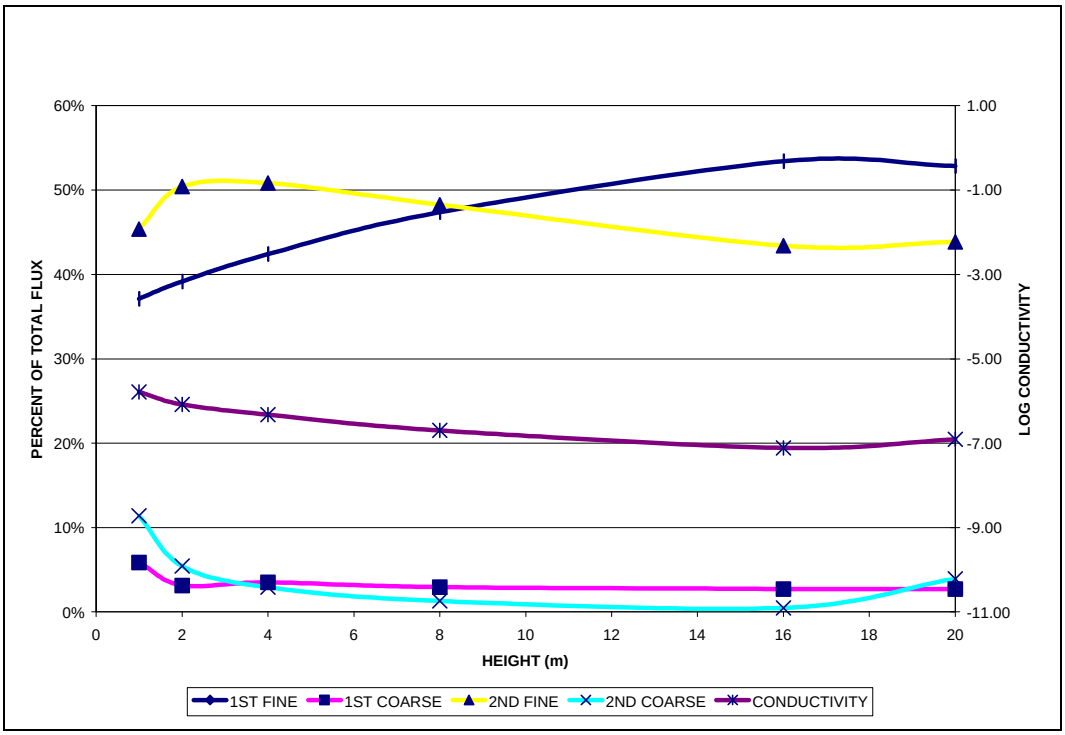


**Figure A8 The results of the 85° Model with Respect to Height**

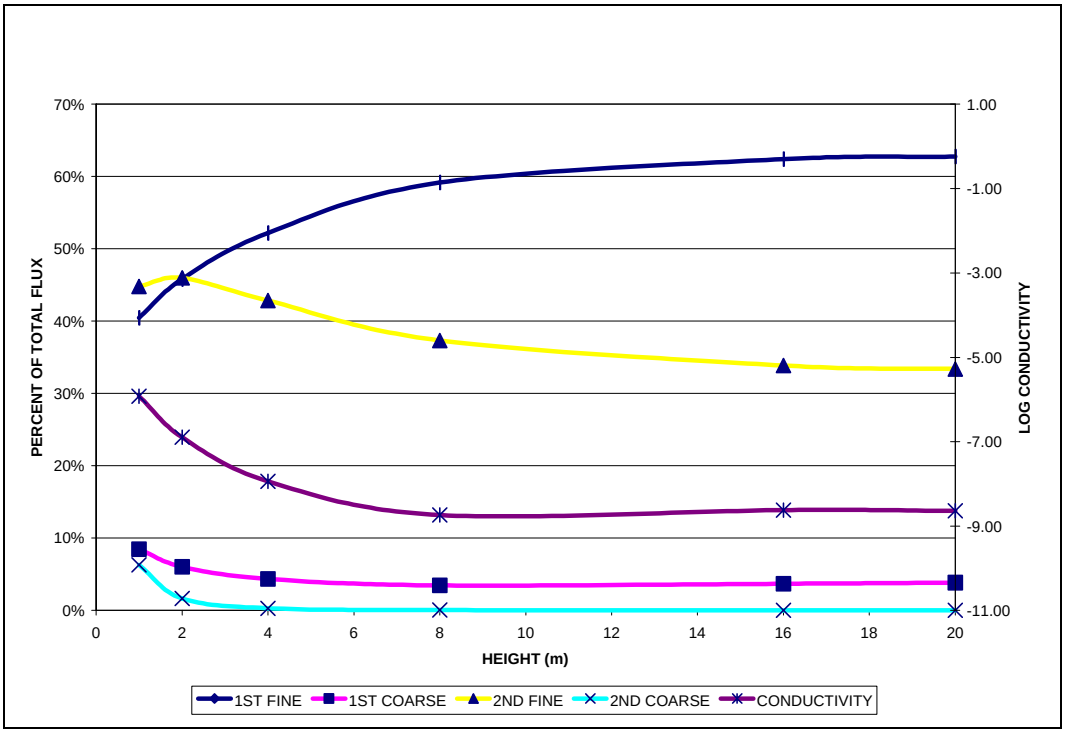


**Figure A9 The Results of the 75° Model with Respect to Height**

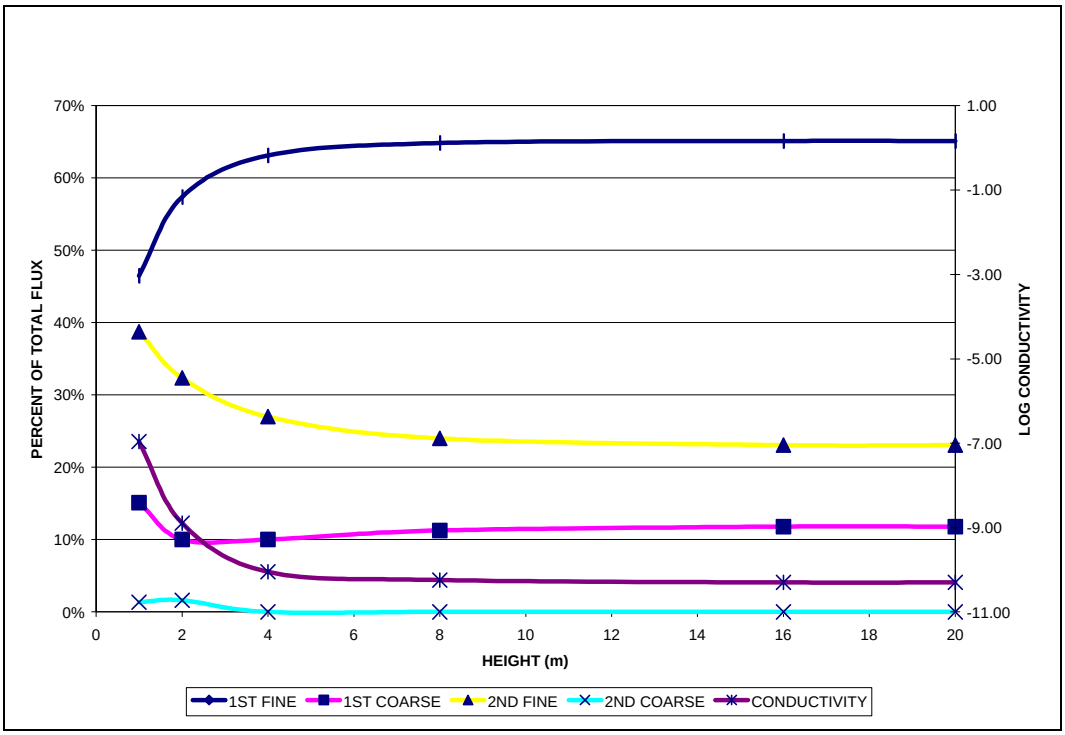


**Figure A10 The Results of the 60° Model with Respect to Height**

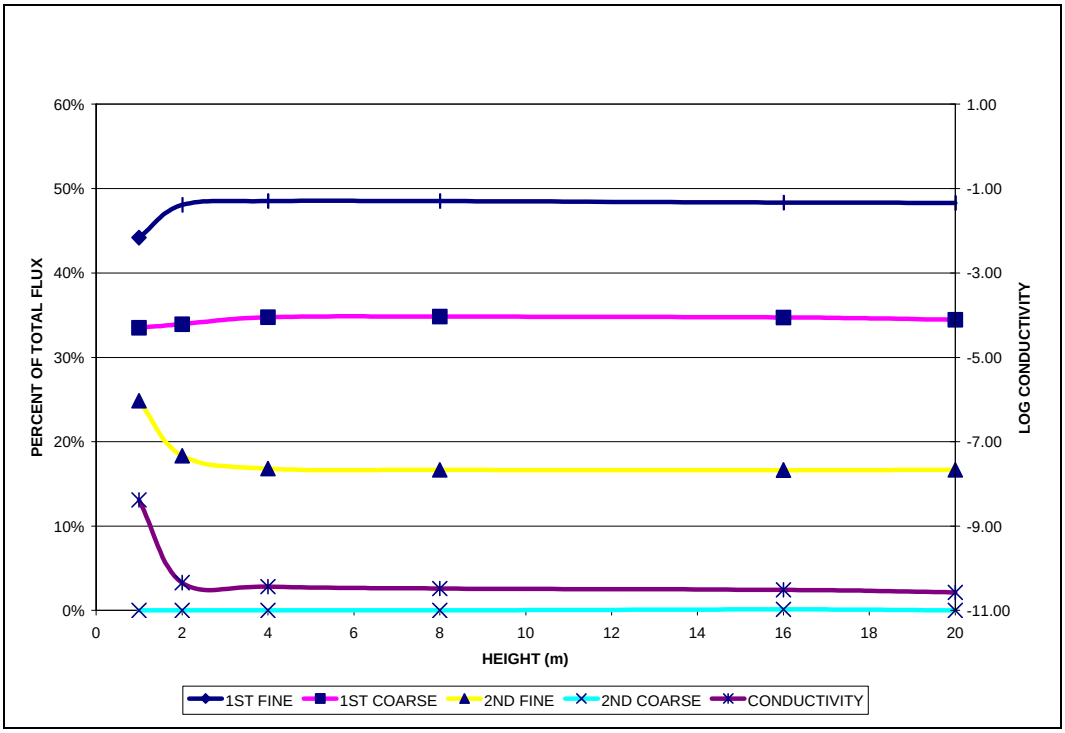


**Figure A11 The Results of the 45° Model with Respect to Height**

# APPENDIX B

# SENSITIVITY ANALYSIS

## B1 Introduction

The numerical modelling for the parametric study began with the completion of the pilot program that moved through a long modelling process with many unsuccessful model simulations with various parameters and combinations attempted. To better understand the anomalies encountered and to acquire a better understanding of the key parameters of the commercial numerical analysis package, Seep/W used to solve physical problem, a sensitivity analysis was undertaken. The sensitivity analysis determined the effect that the convergence criteria, mesh design, material properties, and transient simulations had on the computed solutions.

## B2 Numerical Modelling Program

The main objective of the sensitivity analysis was to determine which input parameters affected convergence and how to manage these parameters to improve convergence. The 8-meter column at an angle of 75º was used for most of the analyses. This system represented an intermediate height and slope to model, and required only one run of the program to solve. However, other heights and slopes were also explored further. The applied fluxes used for the analyses varied from $10^{-3}$ to $10^{-7}$ m/s. These fluxes were chosen to provide regimes between fully and partially saturated. Major factors assessed with the sensitivity analysis were: convergence criteria, mesh design, material properties, and transient modelling effects. The sensitivity analysis program is presented in Figure B1.

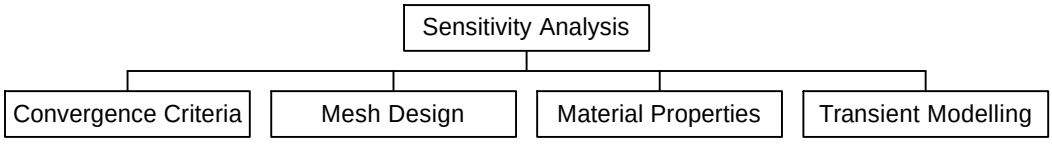


**Figure B1 Sensitivity Analysis Factors**

The sensitivity analysis was not carried out for all possibilities. Each category was subdivided into major variables and for these variables; only a limited range of values was studied. The topics covered are described in the following subsections.

### B2.1 Convergence Criteria

The modeller has several techniques that can be used to influence the way a finite element program calculates a solution. In the Seep/W (Geo-Slope, 1995) package, five major parameters can be varied. The combination of values chosen for each parameter directly affects the solver. The convergence parameters are:

1. Maximum number of iterations;
2. Tolerance;
3. Maximum change;
4. Rate of change; and
5. Minimum change.

The parameter for the maximum number of iterations limits the number of iterations used to obtain a solution. The tolerance parameter is used to select the percentage difference in the norm of the nodal head vector between two successive iterations. The iteration process stops if the percentage difference is less than the specified tolerance. If the percentage difference is greater than the tolerance, the iteration process continues until it reaches the maximum number of iterations.

The next three parameters refer to changes in conductivity (in orders of magnitude). Geo-Slope (1995) states that, “The maximum conductivity change parameter is the maximum change in the (log base 10) of the hydraulic conductivity between two successive iterations. A value of 1 (the default value) means the hydraulic conductivity can change as much as 1 order of magnitude between iterations. The ‘rate of conductivity change’ parameter controls the rate at which maximum change diminishes with each oscillation reversal in the convergence process. A value of 1.1, for example, means that after the first

oscillation reversal, the maximum change is reduced to 0.91 (i.e., 1.0/1.1). After the next oscillation reversal, maximum change is reduced to 0.83 (i.e., 0.91/1.1) and so forth until the maximum change is less than the minimum change. The minimum conductivity change parameter puts a lower limit on the value to which maximum change can diminish. A value of $10^{-4}$ means that the change in hydraulic conductivity from one iteration to the next is $10^{-4}$ orders of magnitude."

The convergence criteria must be selected based on the model complexity and observations of the solver performance. If the vector norms calculated by the solver do not appear to converge, a tighter convergence criterion may be required. The convergence criteria for the parametric study was based on the lessons learned from the pilot program.

The initial models of the pilot program began with the default convergence criteria. As the models proved difficult to solve, tighter and tighter convergence criteria were used. The tightest convergence criterion was required for the taller profiles. The shorter profiles initially used less tight and faster convergence criterion. However, it was discovered that by using different rate of change parameters, different pressure heads would be calculated for a model. Based on this discovery, the tighter convergence criterion was used for all models simulated in the parametric study. This increased the overall computation time, but insured that all the solutions had a similar base. The convergence criterion chosen is presented in Table B1.

**Table B1 Convergence Parameters for The Parametric Study**

| Convergence parameter | Value |
|---|---|
| Maximum number of iterations | 999 |
| Tolerance (%) | $10^{-5}$ |
| Maximum change | 0.1 |
| Rate of change | 1.01 |
| Minimum change | $10^{-5}$ |

The taller profiles required up to 3000 iterations before convergence was attained. Since the maximum number of iterations allowed by the program were 999, the taller profiles required three consecutive analyses, using the previous results as the initial conditions for the following model. Sensitivity analyses related to the convergence parameters were analyzed and the results are presented in section B3.

### B2.2 Mesh Design

Guidelines for mesh design are discussed in Seep/W manual. In general, it is good practice to reach a balance between the ease of mesh generation and efficiency processing, and mesh size should be inversely proportional to the change of gradient (Geo-Slope, 1995).

The parametric study used two standard mesh designs. The designs consisted of quadrilateral elements. The first design was used for the initial, relatively short, vertical systems up to the eight-meter high profiles. The first design consisted of 5 elements for the base of each layer and 20 elements for each meter in height. However, the vertical 16-meter profile required twice the number of elements as the 8-m profile. The extra elements increased the computational time and produced instability in the solver (for some cases). The results from the pilot program showed that an extremely fine mesh density resulted in floating point errors in the program solver, and not enough elements resulted in poor results. To solve this problem a mesh with a 4 element wide by 17 element high per meter design was used for all remaining systems. The mesh with this lower density design proved to be most successful.

The sensitivity analysis investigated changing the nodal spacing in the mesh design. The following mesh designs were included in the sensitivity analysis:

1. Comparison of results between a sloped 45º profile with an internal mesh angles of 45º and 90º;
2. Modifications to the mesh with tighter nodal spacing at the top and bottom boundaries, and at the interfaces between layers;
3. Use of secondary nodes; and
4. Removing elements from the mesh.

Two methods for sloping the profiles were adopted from the parametric study program. The first method was the simplest. It involved matching the internal angles of the mesh elements with the slope of the system. For the 45º profiles, the internal angle of the mesh element was 45º. However, the use of any internal angle less than 90º will decrease computational efficiency. An angle of 45º provided the minimum acceptable performance for a quadrilateral element (Geo-Slope, 1995). The second method of sloping profiles keeps the internal element angles at 90º. This method involves using the vertical profile, and pinning the top left node. The entire profile would be rotated to the desired slope. However, considerable effort was required to define these meshes. Therefore, a balance between ease of mesh generation and efficiency processing was reached by using the first method (matching elements to the slope). A sensitivity analysis was used to compare results between a sloped 45º profile with internal mesh angles of 45º and 90º. The results of the simulations are presented in the following section.

During the modelling, several areas of the mesh were identified as possible problem areas. These areas included the top and bottom boundary conditions, the area where the flux crosses over to another layer, the interface between layers, and the low pressure head regions.

The boundary conditions are areas of the model that are forced to have certain head or flux values. If these values are unrealistic or extreme in anyway, stress is placed on the system and non-convergence results. The crossover areas are regions of high computational activity and need to be defined correctly. The interface between layers is marked by a node, which is shared by two very

different materials. An extreme pressure head difference in hydraulic properties (i.e., K), between the two layers creates area of instability. In general, to help ease the distress in these regions, a closer nodal spacing or mesh density can be used. By knowing the problem regions in a model, a custom-made mesh design can be developed with closer nodal spacing in the problem areas to speed computations in other areas. Defining this mesh was simplified by the size ratio option found in Seep/W version 4.0 and higher (Geo-Slope, 1995).

The size ratio specifies the element distribution along each side of the multiple element regions. The size ratio is the ratio of the length of the last element to that of the first element along a side (Geo-Slope, 1995). A modified mesh was developed with nodal spacing that was tight at the top and bottom and looser in the middle of the system. A tight mesh was also used at the interfaces but a looser mesh was used at the center of a layer. A sensitivity analysis using the modified mesh was conducted and the results are presented in section B3.

The use of secondary nodes and higher integration orders was also investigated during in the mesh sensitivity analysis. The typical quadrilateral element consisted of four nodes. A quadrilateral element with secondary nodes consists of eight nodes. Secondary nodes with a higher integration order of nine rather than four are recommended for nonlinear problems (Geo-Slope, 1995). The nature of the problem being solved was nonlinear and secondary nodes should assist in convergence. However, secondary nodes were not used for the parametric study due to the increase in computational time required to solve the problem. In addition, the models from the parametric study were able to converge without the use of the secondary nodes.

Secondary nodes were used to solve the non-convergence produced by the applied fluxes of $10^{-6}$ m/s or less. These low flux values produced lower pressure heads and hydraulic conductivities in the system, and the solution using the standard quadrilateral element with four nodes (the standard mesh)

was unable to converge. The analysis of the low flux problem with secondary nodes was conducted and results are presented in section B3.

The remaining modification to the standard mesh came as a simplification. Observations from the parametric study showed that the outside two elements of the outside layers did not contribute flux to the interior elements. This was particularly noticeable in the vertical profiles. Removing these outside elements decreased the computational time, and removed areas of higher suction (related to the lack of flow in these areas) that contributed to higher instability. For the inclined profiles, the low flow and higher negative pressure areas are located in both coarse layers. Removing elements from the coarse layers without affecting the overall flow pattern may result in removing non-convergent nodes. A number of analyses were completed to verify the possibility of improving the convergence by removing elements. The results of the simulations are presented in section B3.

### B2.3 Material Properties

To model a natural system or an aspect of a natural system, the results depend heavily upon how close the specified parameters are to that of the natural system. The properties required for each material are the hydraulic conductivity function and the soil-water characteristic curve (SWCC) as presented in Figure 4.5a and 4.5b respectively. The SWCC was required for the transient analyses, but it was also needed to calculate the volumetric water content contours in the steady-state models.

When modelling granular materials such as waste rock, the material properties have a steep function. Steep functions add to the problem of non-convergence. Non-convergence is due to the non-linearity of the hydraulic conductivity function with respect to matric suction. For example, a pressure head change of 1-meter changes the hydraulic conductivity in the coarse-grained layer by $10^{15}$ m/s (refer to Figure 4.5a). A small pressure head change therefore results in a

hydraulic conductivity change of several orders of magnitude. The result is that the vector norm jumps from one extreme to another for consecutive iterations and fails to converge. Customizing the mesh design and convergence criteria for the problem is one possible solution. However, if this does not work, a compromise has to be reached between keeping material properties as realistic as possible and achieving an acceptable solution.

The sensitivity analysis for the material properties was directed at two parts. The first part studied modifying the coarse material hydraulic conductivity function with respect to the ease of convergence. The second part studied the effects of closing the gap between the coarse-grained and fine-grained materials hydraulic conductivity functions. This effectively reduced the order of magnitude difference between the hydraulic conductivity for the materials. Geo-Slope (1995) also suggests breaking a steep hydraulic conductivity function into a series of short flatter segments while keeping the overall shape of the original hydraulic conductivity function. This method was not investigated in this study.

The first coarse–grained material used in the pilot program and the initial parametric study was silica sand (Figure 4.2). However, for all models over 5-meters, convergence could no longer be achieved. Convergence was only achieved when the silica sand was modified. The initial silica sand was designated as silica1 and the modified sand was designated silica2 (coarse-grained material in Figure 4.5). The slope of the permeability function for the initial coarse material “silica1” was changed between the air entry value (AEV) and residual value of $10^{-17}$ m/s by adjusting the residual matric suction from 4 kPa to 10 kPa. To provide a better understanding of the effects of changing the conductivity curve, four conductivity functions at different slopes were studied and compared. The curves studied were silica1, silica2, and two intermediate curves (silica1a and silica1b) and are presented in Figure B2.

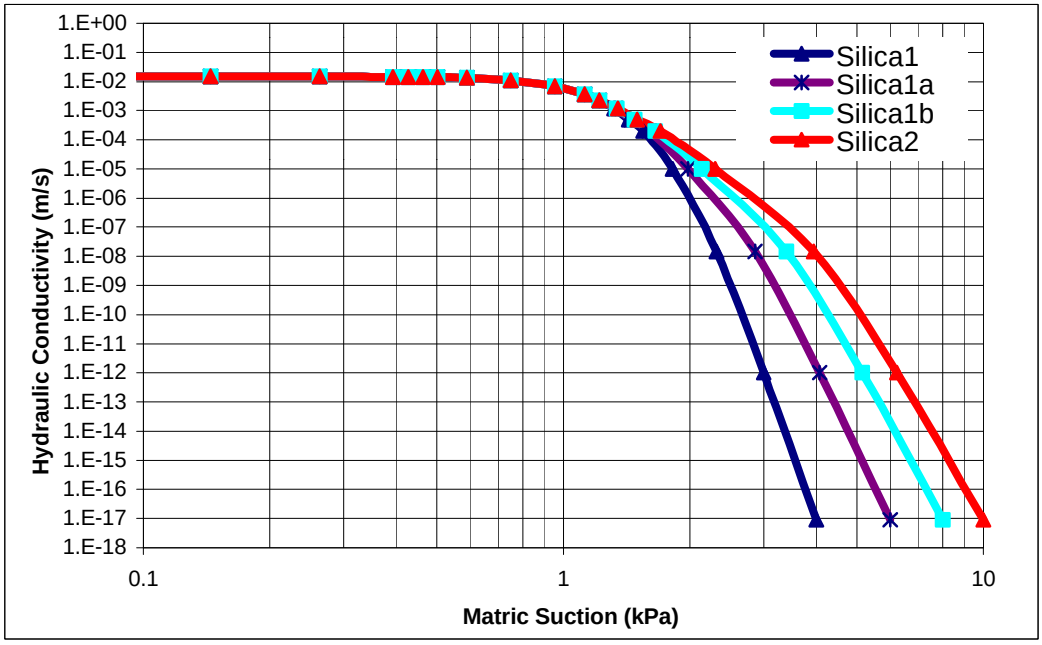


**Figure B2 Sensitivity Analysis of Coarse Material**

The second method considered reducing the difference between the fine and coarse-grained materials. Figure 4.5a shows that as the matric suction increases so does the difference between the hydraulic conductivity functions of fine and coarse-grained materials. Reducing the difference between the two functions was conducted in three ways. The first way was to replace the fine-grained material of TP5GS1 with Beaver Creek sand (Figure 4.2). Beaver Creek sand properties are more similar to the coarse-grained material than those of TP5GS1 are. The second way was to introduce a material that would bridge the difference between the coarse and fine-grained materials (i.e., a transitional material). The use of a transitional material indicated that the change from one layer to another is more gradual. In addition, it is possible that a transitional material could bridge the difference in pressure heads between the layers and therefore assist convergence. The transitional material developed for this study is presented in Figure B3. The third way involved increasing the residual hydraulic conductivity of the coarse-grained material.

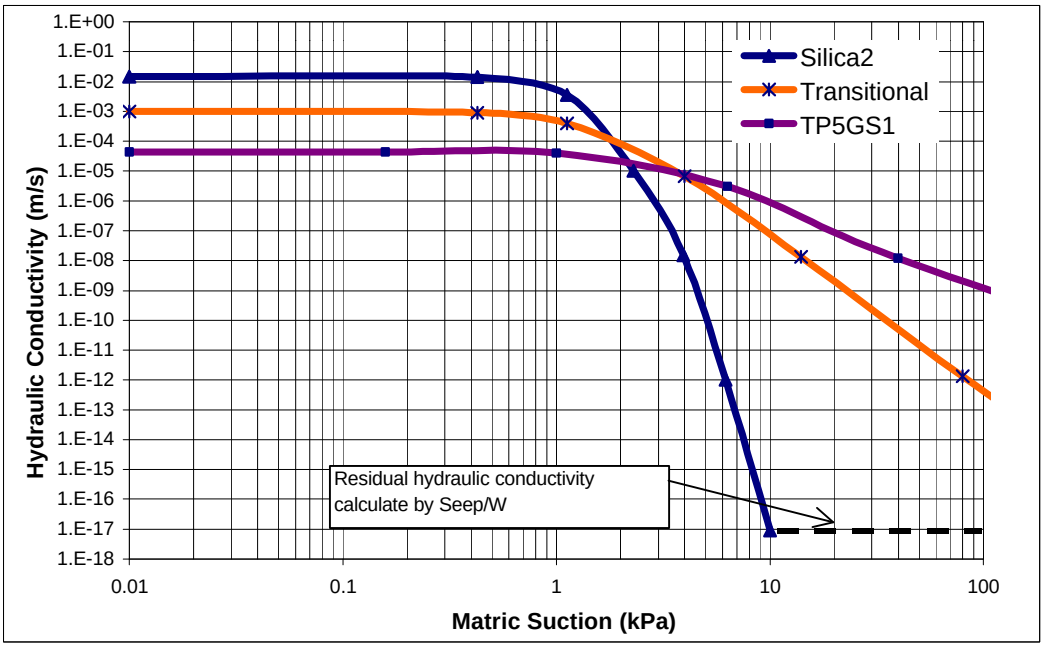


**Figure B3 Hydraulic Conductivity Function for The Transitional Material**

During the low applied flux modelling simulations, another material property problem was encountered. An applied flux of $10^{-7}$ m/s corresponded to a matric suction of 20 kPa in the fine-grained material (Figure 4.5a). However, a matric suction of 20 kPa has no corresponding hydraulic conductivity in the coarse-grained material. The coarse-grained material was not defined for any values of matric suction greater than 10 kPa. Therefore, Seep/W reacts by assigning nodes with matric suctions greater than 10 kPa to a horizontal line as shown in Figure B3. This line begins at the residual value of $10^{-17}$ m/s and may vary from 10 to 1000 kPa in some cases.

The difference between a material with a residual hydraulic conductivity of $10^{-12}$ m/s rather than $10^{-17}$ m/s does not significantly affect the flux in that material. However, it may assist convergence. Sets of models were defined with the coarse-grained material having a residual value of hydraulic conductivity equal to $10^{-17}$, $10^{-12}$, $10^{-9}$, $10^{-8}$, and $10^{-7}$ m/s. These models were checked for improvement in convergence with minimal change in the original flux distribution

in the system. Finding a balance between convergences and allowing flow through areas that would not otherwise carry seepage was investigated.

The above runs were completed with the residual hydraulic conductivities as a horizontal line. The problem with the horizontal residual hydraulic conductivity was that the solver could calculate a constant residual value for any pressure head greater than the actual residual. This may destabilize the rest of the system. A better solution was to match the residual slope of the coarse-grained material hydraulic conductivity curve to that of the fine-grained material. The sloped residual will define a unique hydraulic conductivity for each pressure head for the coarse material. The growing difference between the functions for a given matric suctions reaches a constant value and this should assist the solver in reaching convergence. Another possibility is to have the residual values of both the fine and coarse-grained materials slope to meet at $10^6$ kPa. Therefore, the difference in both curves will decrease to zero with greater applied suction.

The modelling results when using Beaver Creek sand for the fine-grained material, a transitional material, and a residual slope for the coarse material are all presented in section B3.

### B2.4 Transient Models

An alternative method of solving a steady-state problem was to use a transient model. The transient model stepped the time forward using small time steps. This initiates a system to accept the imposed boundary conditions. The time steps were then increased until the model reached a steady-state condition. A steady-state condition occurred when the flux entering and leaving an element in a model were equal for all times. The other advantage of a transient model was that each time step provides a solution and a further understanding of the process at work in the system. However, transient models have several disadvantages.

As discussed in Chapter 3, the transient governing differential equation requires two more variables than the steady-state equation. These variables are the rate of change of volumetric water content and time. The volumetric water content is defined by the SWCC (see Figure 4.5b) for each material used. The time is defined in the program as time steps.

The SWCC for the coarse-grained material was similar to its hydraulic conductivity function. Both curves are functions of matric suction, and both curves are steep. Therefore, the problems encountered with a steep hydraulic conductivity function can also be expected to occur for a steep SWCC. For example, a small pressure change will result in a large storage change, as well as a large hydraulic conductivity change. Satisfying two steep curves complicates convergence.

Another disadvantage of the transient models was the time required to solve the simulations. Each time step is treated as though it were a steady-state run (i.e., it will run for the full number of iterations defined in the convergence criteria). Therefore, a transient run with 50 time steps, using the convergence criteria of the steady-state model in the parametric study will finish after 50,000 iterations.

Seep/W (Geo-Slope, 1995) outlines the following criterion to generate a time sequence:

1. The number of increments;
2. The starting time;
3. The initial increment size;
4. The amount by which the time increment should increase with each step (i.e., expansion factor); and
5. The maximum increment size.

The time steps are measured in seconds. A typical time step sequence would be to start small and then use the expansion function to reach a maximum increment size (e.g., one day). That maximum increment size is then used for

the remaining time steps. The time sequence used for most of the transient models is shown in Table B2

**Table B2 Time Sequence Used for Transient Models**

| TIME STEP PARAMETER | VALUE |
|---|---|
| Number of Time Steps | 25 |
| Starting Time | 0 seconds |
| Initial Increment Size | 5 seconds |
| Expansion Factor | 1.5 |
| Maximum Increment Size | 86400 seconds |

After the SWCC and time sequences are defined, the transient model will run as defined. There are several combinations of methods to analyze a transient model. The first method, where the input parameters are used to attempt a solution, involves taking an initial system and forcing the applied flux through the system. An alternate method is to use a steady-state simulation to saturate the system by using a boundary condition at the top of the pile equal to the elevation head or using a flux equal to $K_{sat}$. The results can then be defined as an initial condition. Using this initial condition, a transient model can allow drainage from the initial condition to a residual value before the desired flux is applied. Alternatively, a transient model can drain to the desired flux. This means that a saturated flux is applied to the model and the flux reduces with time to the unsaturated flux. Since the saturated system does not pose a convergence problem, the alternative method would be expected to converge. Once the desired flux is reached, time steps can be added to achieve steady-state conditions. Transient modelling with a standard or modified mesh can be simulated with different fluxes and materials. The results of the transient sensitivity analyses are presented in section B3.

## B3 Presentation of Results, Analysis and Discussion

The need for a sensitivity analysis became evident when the top boundary condition for the parametric study model was lowered from a flux of $10^{-5}$ m/s to a value equal to the average precipitation of the Golden Sunlight Mine of 243 mm per year (i.e., 7.7E$10^{-9}$ m/s; Swanson, 1995). In general, the results of the model simulations were a complete failure to achieve convergence. Convergence improved as the flux increased; however, only a flux of $10^{-5}$ m/s was found to give convergence for all profiles. This corresponds to a precipitation of 300 meters per year, which does not represent conditions found in nature.

A sensitivity analysis was conducted using the 8-meter profile from the parametric study with the input fluxes of $10^{-3}$, $10^{-6}$, and $10^{-7}$ m/s. For the $10^{-3}$ m/s flux, all the profiles converged and seepage was mainly through the coarse-grained layers (i.e., matric suction was less than -2.3 kPa). For the $10^{-7}$ m/s flux none of the profile solutions converged. The results for the $10^{-6}$ m/s flux showed that as the profile inclined from 90º to 45º, convergence would improve. The 90º, 85º, and 75º profiles did not converge, the 60º profile showed poor convergence and while the 45º profile showed good convergence. The key difference between the profiles was that high negative pressures developed in the coarse-grained material increased as the slope angle increased. For example, the minimum hydraulic conductivity for the 45º profile was 5.0E$10^{-14}$ m/s while the minimum hydraulic conductivity for the 60º profile was 9.0E$10^{-15}$ m/s.

The conclusion that can be drawn from the parametric study was that as the profile height increased, the pore-water pressure in the profile was reduced, causing non-convergence in the solution. Lowering the specified flux produced a similar result to increasing the profile height. It was of interest in the $10^{-6}$ m/s flux model that the seepage through the coarse-grained material decreased to zero, as the model was inclined steeper than 75º. Usually non-convergence

was related to a low flow through the coarse-grained layers (i.e., very low hydraulic conductivity) resulting from low pore-water pressures in the layers. The only exception occurred when a model converged with a minimum conductivity of $5.0E10^{-14}$ m/s in the coarse-grained material. However, convergence was not achieved when the minimum hydraulic conductivity of $9.0E10^{-15}$ m/s was calculated. The question that arises as to whether this means that $10^{-14}$ m/s is the lower limit for the model, or the program solver, or just for the material properties? It was not possible to obtain a definitive answer to this question.

The main objective of the sensitivity analysis was not only to determine which input parameters affected convergence but also to determine how to combine these parameters to improve convergence. The following sections explore a limited number of variables for selected profiles.

### B3.1 Convergence Criteria

The convergence criterion directs the procedure used in the finite element method (FEM) to calculate a solution. In the finite element program (Seep/W) the five parameters associated with the convergence criteria are:

1. Maximum number of iterations;
2. Tolerance;
3. Maximum change (in calculated hydraulic conductivity);
4. Rate of change; and
5. Minimum change.

The initial models of the pilot program lead to the convergence criteria shown in Table 4.1. It was also noted in the parametric study that different pore-water pressure heads would be calculated for the same model by varying only the rate of change parameters. To investigate this and other possible effects of varying the convergence criteria, the sensitivity analysis used an applied flux of $10^{-5}$ m/s for the 8-meter, 85º profile with eight different combinations of convergence criteria, as presented in Table B3. Figure B6 illustrates the general configuration of geometry and the alternating fine and coarse-grained layers for this model.

**Table B3 Convergence Parameters for Sensitivity Analysis**

| Convergence Parameter | Test #1 | Test #2 | Test #3 | Test #4 | Test #5 | Test #6 | Test #7 | Test #8 |
|---|---|---|---|---|---|---|---|---|
| Max. Number of Iterations | 999 | 100 | 10 | 100 | 500 | 500 | 500 | 500 |
| Tolerance (%) | $10^{-5}$ | 1 | 1 | 0.1 | $10^{-3}$ | $10^{-3}$ | $10^{-3}$ | $10^{-5}$ |
| Max Change | 0.1 | 1 | 1 | 1 | 0.5 | 0.1 | 0.1 | 0.1 |
| Rate of Change | 1.01 | 1.1 | 1.1 | 1.15 | 1.05 | 1.05 | 1.01 | 1.01 |
| Minimum Change | $10^{-5}$ | $10^{-4}$ | $10^{-4}$ | $10^{-4}$ | $10^{-5}$ | $10^{-5}$ | $10^{-5}$ | $10^{-5}$ |

Test numbers 1, 7, and 8 resulted in convergence. Test numbers 5 and 6 resulted in poor convergence, and test numbers 2, 3, and 4 resulted in non-convergence. Using test number 1 as the base line test, only tests number 7 and 8 had similar results, which indicated that there were sufficient iterations to converge and that the tolerance of $10^{-3}$ was sufficient to achieve convergence. Both test numbers 5 and 6 showed similar convergence patterns indicating that the rate of change factored more than the maximum change defined. Test number 3 did not converge due to an insufficient number of iterations, while the high tolerance and rate of change of test number 2 resulted in a high degree of non-convergence, as the solver appeared to diverge from the solution. Test number 4 also failed due to the high rate of change defined.

Table B4 summarizes the results of the fluxes flowing through each layer at mid height for each test. The non-converged tests have results that vary greatly from each other and from test number 1 while test number 5 and 6 are similar to each other but are different from the known solution (i.e., test number 1 from the parametric study). Tests numbers 7 and 8 with good convergence have the same results as the known solution.

**Table B4 Convergence Sensitivity Analysis Results**

| Layer (%) | Test #1 | Test #2 | Test #3 | Test #4 | Test #5 | Test #6 | Test #7 | Test #8 |
|---|---|---|---|---|---|---|---|---|
| First Fine | 47.4 | 42.2 | 0.3 | 45.6 | 54.9 | 50.5 | 47.5 | 47.5 |
| First Coarse | 2.9 | 25.2 | 92.3 | 12.4 | 2.9 | 5.8 | 2.9 | 2.9 |
| Second Fine | 48.3 | 34.5 | 0.4 | 31.4 | 43.7 | 41.9 | 48.3 | 48.3 |
| Second Coarse | 1.3 | 1.1 | 6.9 | 10.0 | 0.9 | 1.8 | 1.2 | 1.2 |
| Results | Good | None | None | Poor | Poor | Good | Good | Good |

It is important to note that a further sensitivity analysis with respect to convergence criteria should be conducted for each analysis conducted to achieve the optimum possible balance of speed and accuracy.

### B3.2 Mesh Design

The sensitivity analysis looked into changing the nodal spacing in the mesh. The following mesh designs were included in the sensitivity analysis:

1. Comparison of results between a 45º profile with an internal mesh angle of 45º (used in the parametric study) and 90º;
2. Modify the mesh with tighter nodal spacing at the top and bottom boundaries, and at the interface between layers;
3. Use of secondary nodes; and
4. Removing elements/nodes from the mesh.

The 45º profile with an internal mesh angle of 90º was used to compare convergence results with the standard mesh and both meshes are presented in Figure B4.

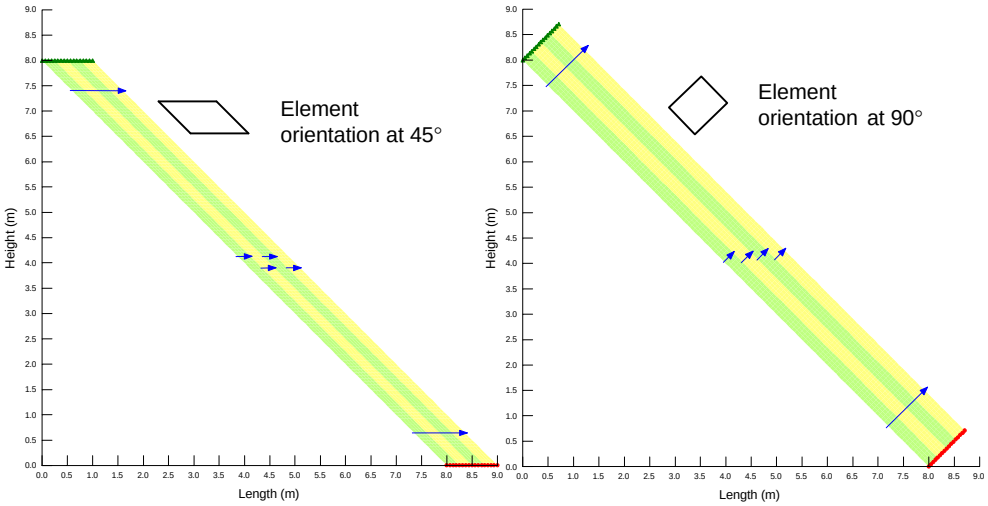


**Figure B4 45º Profile with an Internal Mesh Angle of 45º on the Left and 90º on the Right**

The model was analyzed for fluxes of $10^{-5}$, $10^{-6}$, and $10^{-7}$ m/s. Both $10^{-5}$ m/s flux models converged, however the fluxes through each layer were different as shown in Table B5. The $10^{-6}$ m/s flux converged for the 45º element mesh and poor convergence was achieved for the 90º element mesh. Both meshes with the $10^{-7}$ m/s flux models did not converge.

**Table B5 Comparison of Results Between Internal Mesh Angles of 45º and 90º**

| Mesh Element angle (flux) | First Fine (%) | First Coarse (%) | Second Fine (%) | Second Coarse (%) | Convergence Achieved |
|---|---|---|---|---|---|
| 45º Mesh ($10^{-5}$) | 48.5 | 34.8 | 16.7 | 0 | Yes |
| 90º Mesh ($10^{-5}$) | 69.2 | 15.6 | 15.3 | 0 | Yes |
| 45º Mesh ($10^{-6}$) | 44.1 | 0 | 56.0 | 0 | Yes |
| 90º Mesh ($10^{-6}$) | 42.5 | 0 | 57.5 | 0 | Poor |
| 45º Mesh ($10^{-7}$) | 41.3 | 0 | 59.3 | 0 | No |
| 90º Mesh ($10^{-7}$) | 38.0 | 0 | 61.9 | 0 | No |

It was observed in the parametric study that the 45º profiles for all heights showed a distinct decrease of flux in the F1 layer and an increase flux in the C1 layer. The $10^{-5}$ m/s flux with the internal element angle of 90º (used in the sensitivity analysis) showed that the flux in the F1 and coarse-grained layers continue to gradually increase in flux and did not decrease in flux as shown in Figure 5.6 and 5.7 of the parametric study. These results were unexpected and bring into question the results observed in the parametric study for the 45º profiles.

The internal mesh angle of 45º may have resulted in the F1 layer to prematurely be unable accept more flux from the C1 layer. This would indicate that the pressure in the F1 layer did exceed the -2.3 kPa required to have preferential flow, therefore the flux did not fully cross over. The fact that the top right tip of the 90º element model was approximately 0.7-meters higher than the 45º element could also have result in different internal pore-water pressures. This may be the reason why the $10^{-6}$ m/s flux converged for the 45º slope and only achieved poor convergences for the 90º slope. The results for the models with pore-water pressure contours for the converged solutions at fluxes equal to $10^{-5}$ and $10^{-6}$ m/s and the non-converged solution at $10^{-7}$ m/s are presented in Figure B5.

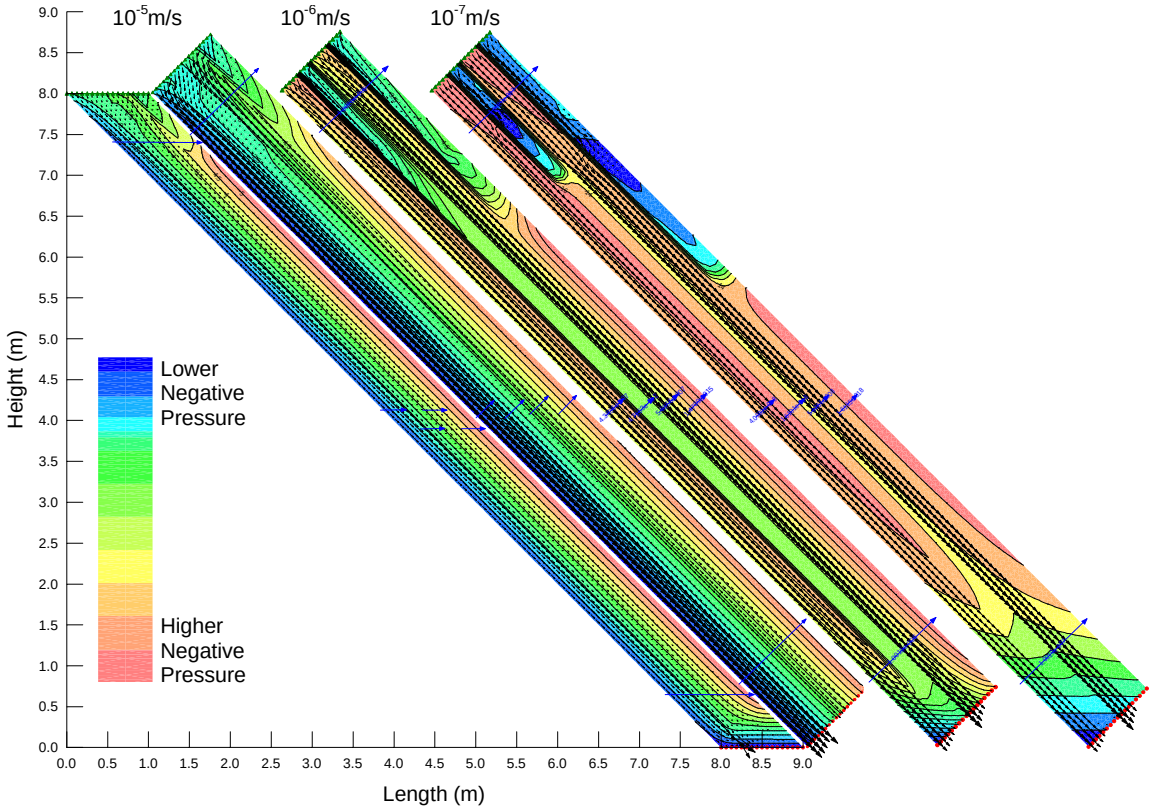


**Figure B5 Computed Results for the 45º Profile with an Internal Mesh Angle of 45º at $10^{-5}$ m/s flux, and 90º at $10^{-5}$, $10^{-6}$, and $10^{-7}$ Fluxes with Pore-Water Pressure Contours**

The far right profile in Figure B5 shows the standard mesh with the internal elements angle of 45° at a flux of $10^{-5}$ m/s, and the remaining meshes from right to left are the computed results for the input fluxes of $10^{-5}$, $10^{-6}$, and $10^{-7}$ m/s, respectively with the modified mesh the 90° elements. The pore-water pressure contours in Figure B5 shows that a lower negative pore-water pressure region (i.e., closer to zero) developed in the top half of the coarse-grained layers for the $10^{-7}$ m/s model that did not converge. The lower negative pore-water pressure regions noted do not appear in the $10^{-5}$ m/s flux models that achieved convergence. This area appears to may have contributed to the non-convergence of the $10^{-7}$ m/s model.

Figure B6 shows a modified mesh with tighter nodal spacing at the top and bottom boundaries, and at the interface between layers using the 8-meters and the 75º profile. The modified mesh used three different flux rates of $10^{-5}$, $10^{-6}$, and $10^{-7}$ m/s to check for improvements in convergence compared with the standard mesh results from the parametric study.

The results showed that the convergence of the models became poorer as the flux rate was lowered. A small improvement was observed when compared with the standard mesh results. Table B6 compares the resulting flux in each layer between the standard meshes and the modified meshes for each flux. There was little change between each mesh except for the $10^{-6}$ m/s model and this might be the result of the non-converged solution.

**Table B6 Comparison of Results Between The Standard and Modified Meshes**

| Mesh (Flux) | First Fine (%) | First Coarse (%) | Second Fine (%) | Second Coarse (%) |
|---|---|---|---|---|
| Standard ($10^{-5}$) | 59.1 | 3.5 | 37.3 | 0.1 |
| Modified ($10^{-5}$) | 59.2 | 3.5 | 37.2 | 0.1 |
| Standard ($10^{-6}$) | 37.6 | 0 | 62.2 | 0 |
| Modified ($10^{-6}$) | 42.5 | 0 | 57.5 | 0 |
| Standard ($10^{-7}$) | 37.6 | 0 | 62.4 | 0 |
| Modified ($10^{-7}$) | 38.0 | 0 | 61.9 | 0 |

Figure B6 shows the modified mesh and the computed results for three different models with pore-water pressure contours and fluxes through each layer.

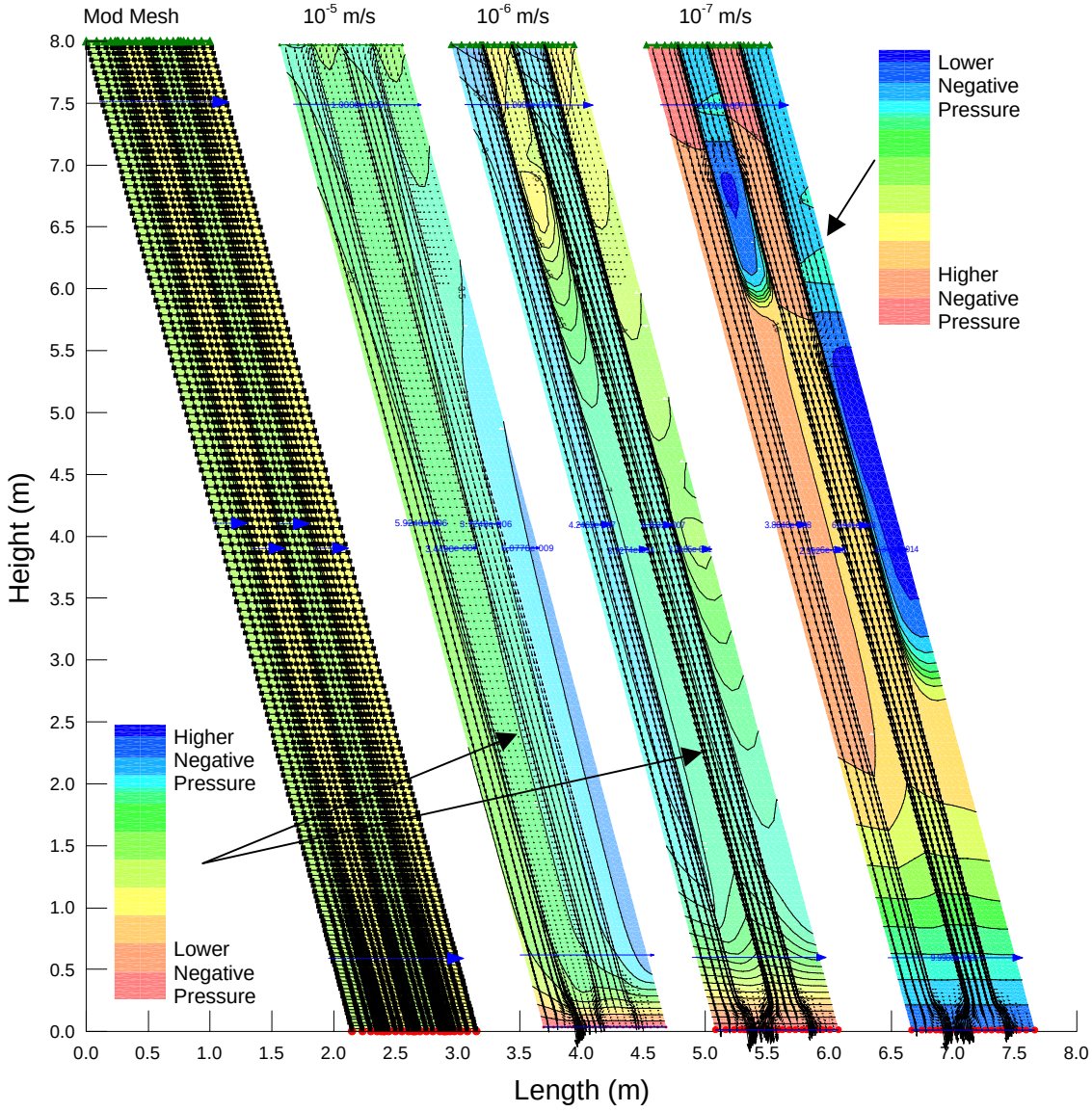


**Figure B6 Result of the Modified Mesh for $10^{-5}$, $10^{-6}$, and $10^{-7}$ Fluxes with Pore-water Pressure Contours**

The left most profile shows the modified mesh, and the next meshes from left to right are the results with pore-water pressure contours for the $10^{-5}$, $10^{-6}$, and $10^{-7}$ m/s applied fluxes, respectively. It can be seen that as the flux is reduced, the pore-water pressure in the profiles decreases. In addition, the flow vectors at low flow are concentrated along the more closely spaced elements along the interface between the different materials. The pore-water pressure contours in

Figure B6 show two lower negative-pressure regions that developed near the base in the coarse-grained layers at $10^{-7}$ m/s flux. The lower negative pore-water pressure region does not appear in the $10^{-5}$ m/s flux model; however, the $10^{-6}$ m/s flux model shows signs of lower negative pore-water pressure regions developing. It appears that the higher negative pore-water pressure regions not only contribute to non-convergence of the model but also are more significant in the less inclined models when compared to Figure B5. Note that some pore-water pressure regions are –2 kPa to 0 kPa, and should be able to transport water seepage but do not appear to do so.

It was discussed in section B2 that secondary nodes and higher integration order might assist in obtaining convergence. A mesh with secondary nodes was developed for the 8-meter 75° profile. The secondary node mesh used three different applied fluxes (i.e., $10^{-5}$, $10^{-6}$, and $10^{-7}$ m/s) to check for improvements in convergence as compared to the standard mesh.

The results showed that convergence of the models became poorer as the flux was lowered. No notable improvement was observed when comparisons were made with the standard mesh results. Table B7 compares the resulting flux in each layer between the standard and secondary node meshes for each flux. It was observed that the results for the $10^{-6}$ and $10^{-7}$ m/s flux models are different for each mesh used but similar when the fluxes differ but mesh configurations remain the same. The difference between the models can be explained by the models not reaching convergence and the difference between the order of integration used by the solver.

**Table B7 Comparison of Results Between the Standard and Modified Mesh with Secondary Nodes**

| Mesh (Flux) | First Fine (%) | First Coarse (%) | Second Fine (%) | Second Coarse (%) |
|---|---|---|---|---|
| Standard ($10^{-5}$) | 59.1 | 3.5 | 37.3 | 0 |
| Secondary ($10^{-5}$) | 59.1 | 3.4 | 37.4 | 0.1 |
| Standard ($10^{-6}$) | 37.6 | 0 | 62.2 | 0 |
| Secondary ($10^{-6}$) | 41.2 | 0 | 58.8 | 0 |
| Standard ($10^{-7}$) | 37.6 | 0 | 62.4 | 0 |
| Secondary ($10^{-7}$) | 41.9 | 0 | 58.1 | 0 |

Figure B7 shows the secondary node mesh and the computed results for the three different fluxes with pore-water pressure contours and fluxes through each layer.

The left most profile shows the standard mesh with the secondary nodes added, and the next meshes from left to right are the results for the $10^{-5}$, $10^{-6}$, and $10^{-7}$ m/s input fluxes, respectively, with pore-water pressure contours. The results were similar to those obtained with the modified mesh. As the flux was reduced the pore-water pressures in the profile became lower, (except in the areas of non-convergence where the pressures actually increased), and the flow vectors were concentrated along the interface between the different materials. The pore-water pressure contours in Figure B7 showed two low negative pore-water pressure regions in the $10^{-7}$ m/s model that developed in the coarse-grained layers, similar to the results in Figure B6.

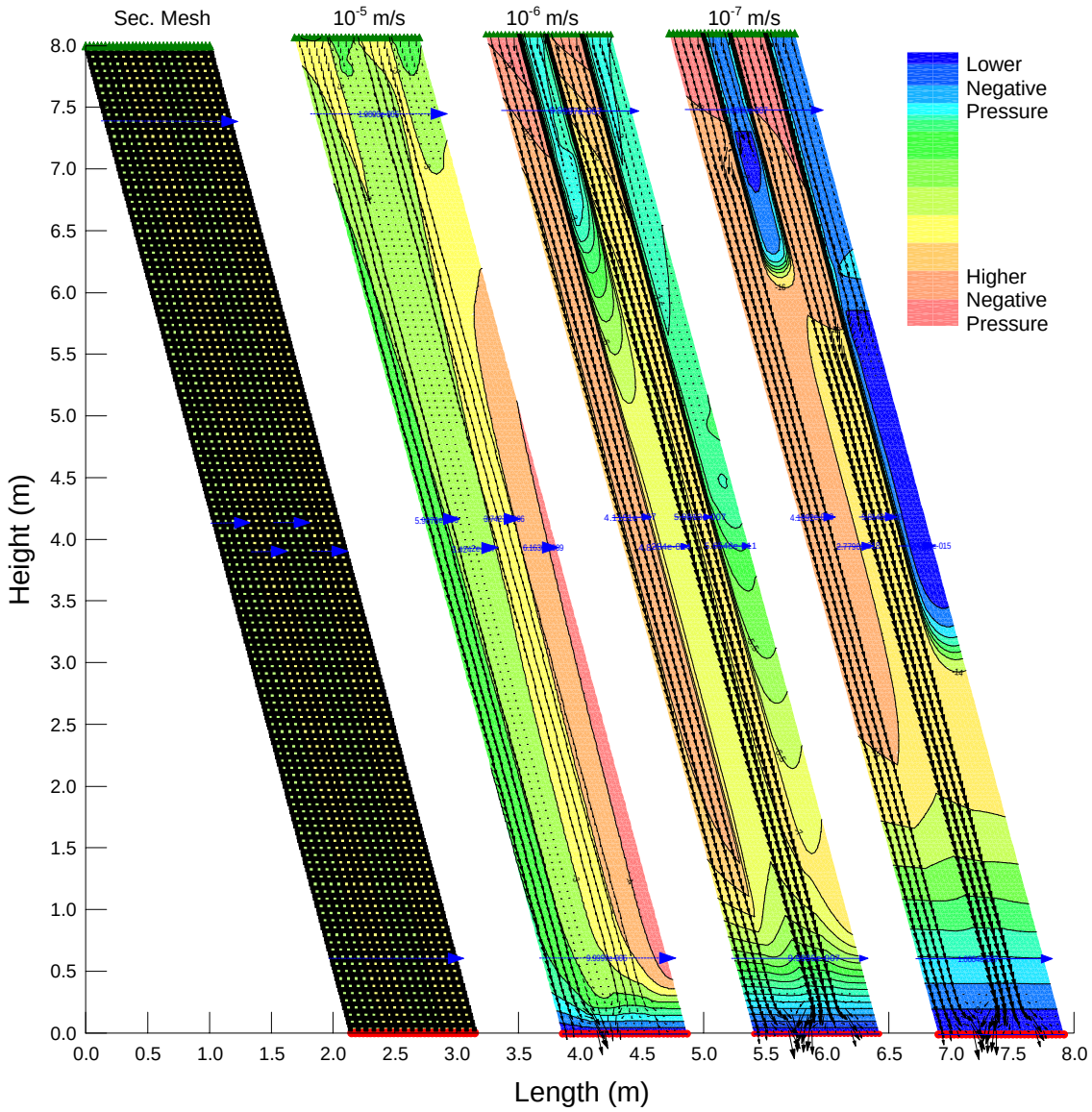


**Figure B7 Result for Computed Mesh with Secondary Nodes for $10^{-5}$, $10^{-6}$, and $10^{-7}$ m/s Applied Fluxes with Pore-Water Pressure Contours**

The lower negative pore-water pressure regions for the $10^{-7}$ m/s applied flux observed in the results of Figures B5, B6, and B7 can be related to the non-convergence in the elements. These areas do not have seepage and according to the hydraulic conductivity function for the coarse-grained layer presented in Figure 4.5a, the pore-water pressures of 0 to 2.0 kPa correspond to a hydraulic conductivity of $1.0E10^{-2}$ to $5.5E10^{-5}$ m/s, respectively. However, the calculated

conductivity provided by the Seep/W model for the lower negative pore-water pressure regions in the $10^{-7}$ m/s applied flux model were between $10^{-8}$ to $10^{-12}$ m/s. Therefore, the pore-water pressures solved for the $10^{-7}$ m/s flux were not correct in the lower negative pore-water pressure regions noted. The error for the $10^{-6}$ m/s flux models was not as great but it still contributed to the non-convergences of most of the models.

Section B2 also discussed how convergence might be improved by removing the nodes/elements where high negative pore-water pressures resulted in a negligible flux and corresponded to extremely low hydraulic conductivities that resulted in non-convergence. Several meshes were developed with the removal of elements/nodes from the standard mesh. The new meshes are referred to as simplified meshes. The first mesh was developed with the removal of the two outside column of elements between the first fine and second coarse-grained layers. The results from the parametric study showed that these elements did not contribute to preferential flow as shown in Figure B8 below. There is a line of symmetry where the flow vectors do not cross of flow toward the center of the mesh. It was evident that these elements did not interact in the vertical profiles, and the non-interaction was also observed in the inclined profiles to a lesser degree. A model with the flux equal to $10^{-7}$ m/s, using the simplified mesh, was analyzed and results are presented in Figure B9

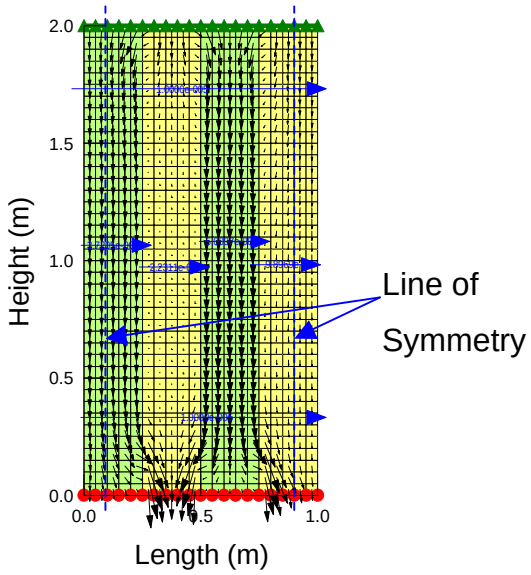


**Figure B8 Result from the Parametric Study 2-Meter (Standard Mesh) with $10^{-5}$ m/s Applied Flux Model**

Based on the results presented in Figures B5 through B7, several lower negative pore-water pressure regions developed where lower pore-water pressures were not expected. Believing that these areas were due to non-convergence, a second simplified mesh was developed by removing the outer three columns of elements from the C2 layer. The inside coarse elements were left to interact with the bordering fine-grained layer and enough elements were left on the top and bottom boundaries to leave room for preferential flow. A model with a $10^{-6}$ m/s flux was analyzed and the results are presented in Figure B9. In addition, a third model was developed which simplified the second mesh further by removing the inside two columns of elements from the center of the first coarse layer. Models with a flux set equal $10^{-6}$ and $10^{-7}$ m/s flux were analyzed and compared for improvements in convergence. The results are presented in Figure B9.

The resulting convergences from the simplified meshes are plotted in Figure B10. The improvement in convergence was observed by lowering the density of the non-converged nodes in the plot. Figures B10a to B10c show the results for

the $10^{-6}$ m/s flux with the standard mesh, a simplified mesh with elements removed from the second coarse-grained layer, and a simplified mesh with elements removed from both coarse-grained layers, respectively. Figures B10d to B10f show the computed results for the $10^{-7}$ m/s flux and the standard mesh, a simplified mesh with two outside elements removed in the first fine and second coarse-grained layers and a modified material property which is discussed in the following section, and a simplified mesh with elements removed from both coarse-grained layers, respectively. In summary, it can be seen in Figures 10d to 10f that the difficulty in achieving convergence at low flux (i.e., $10^{-7}$ m/s) is caused by the steep hydraulic conductivity function for the coarse material. The valves of hydraulic conductivity calculated by the Seep/W solution do not correspond to the material property function.

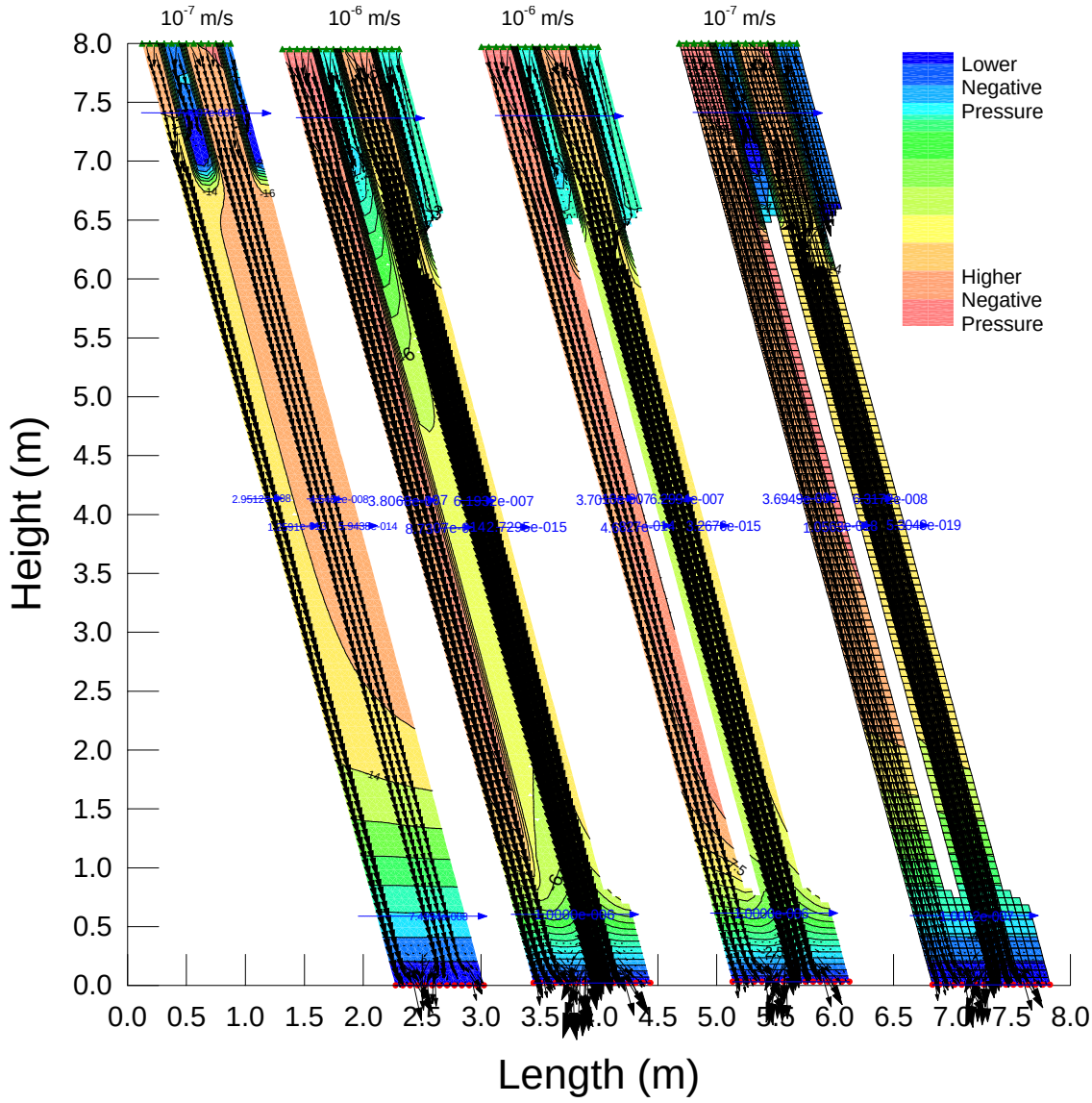


**Figure B9 Computed Result for Three Simplified Meshes (outside two elements removed, second coarse elements removed, and elements removed from both coarse layers) with $10^{-7}$, $10^{-6}$, $10^{-6}$, and $10^{-7}$ m/s Applied Fluxes (from left to right)**

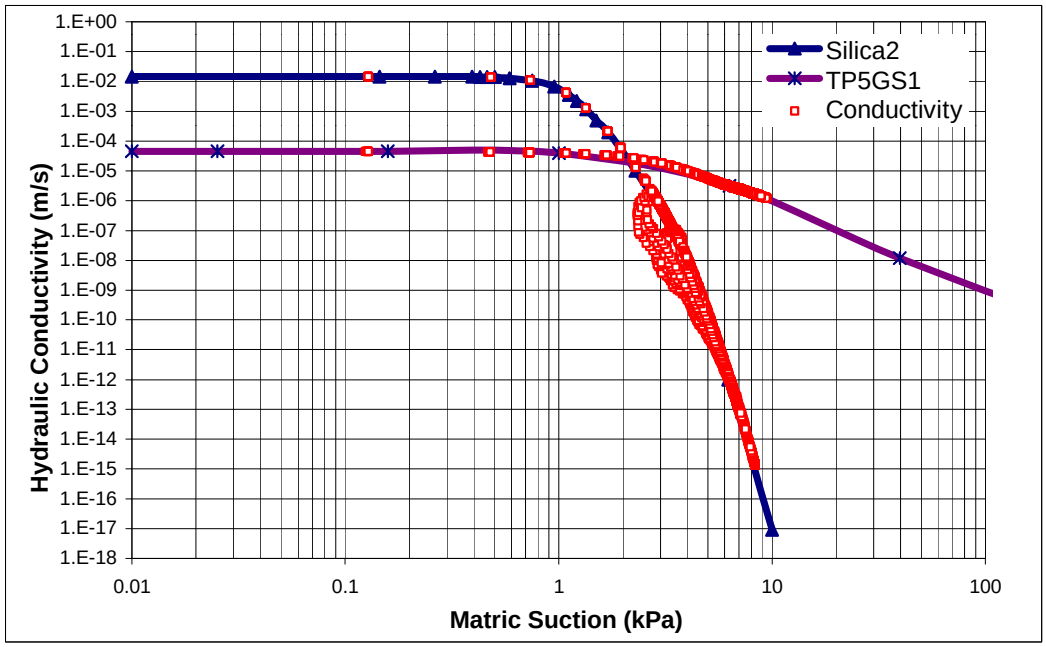


**Figure B10a Convergence Results for The $10^{-6}$ m/s Model with The Standard Mesh**

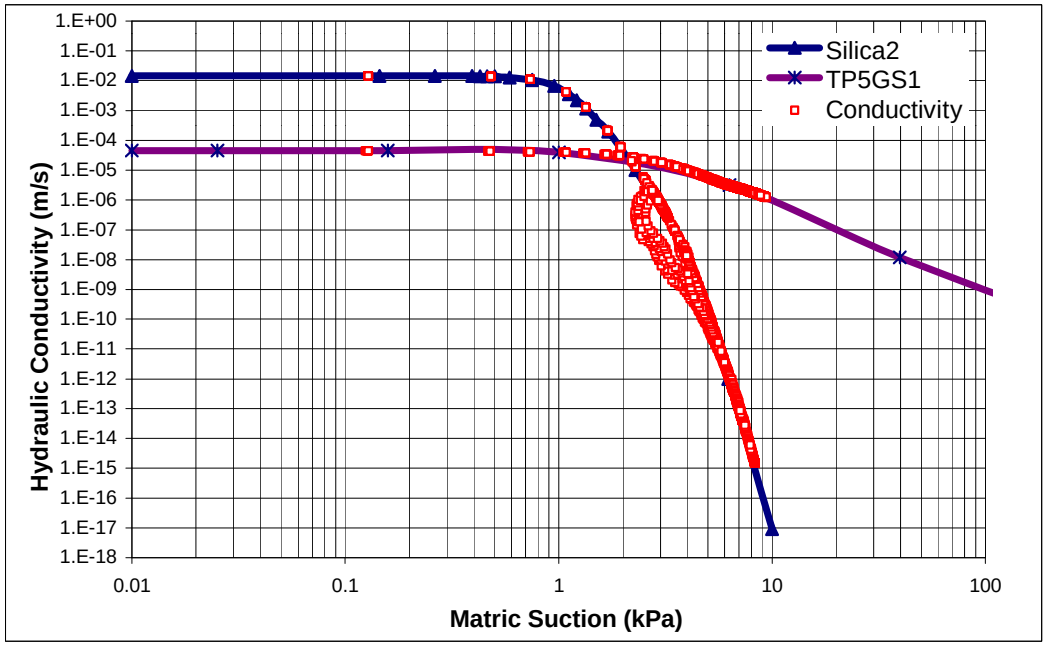


**Figure B10b Convergence Results for The $10^{-6}$ m/s Model with The Elements Removed from Second Coarse Layer**

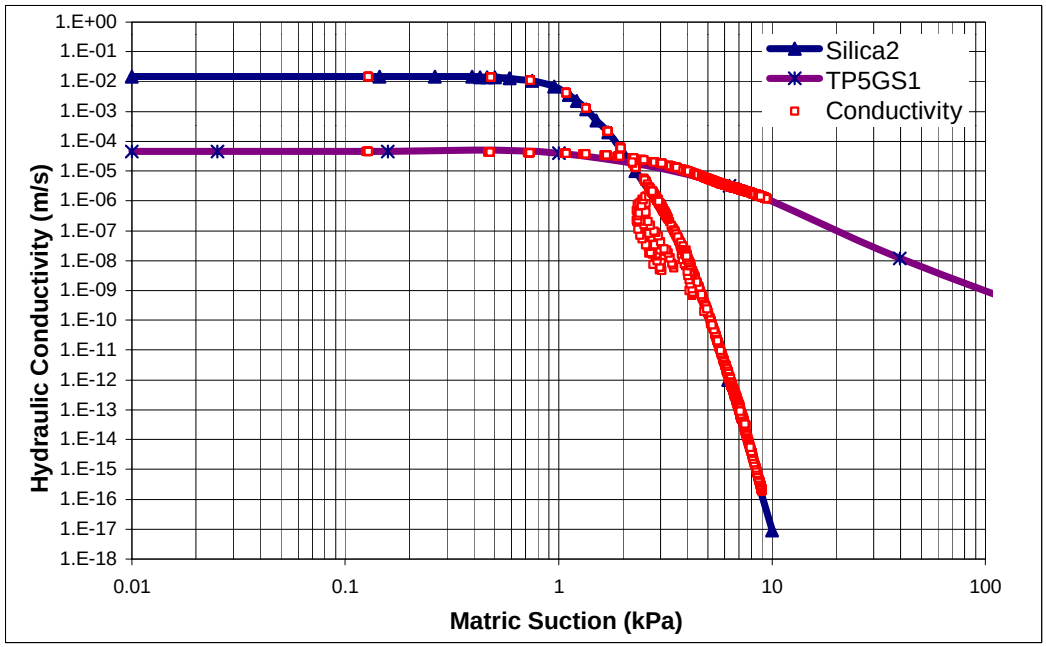


**Figure B10c Convergence Results for The $10^{-6}$ m/s Model with The Elements Removed from Both Coarse Layers**

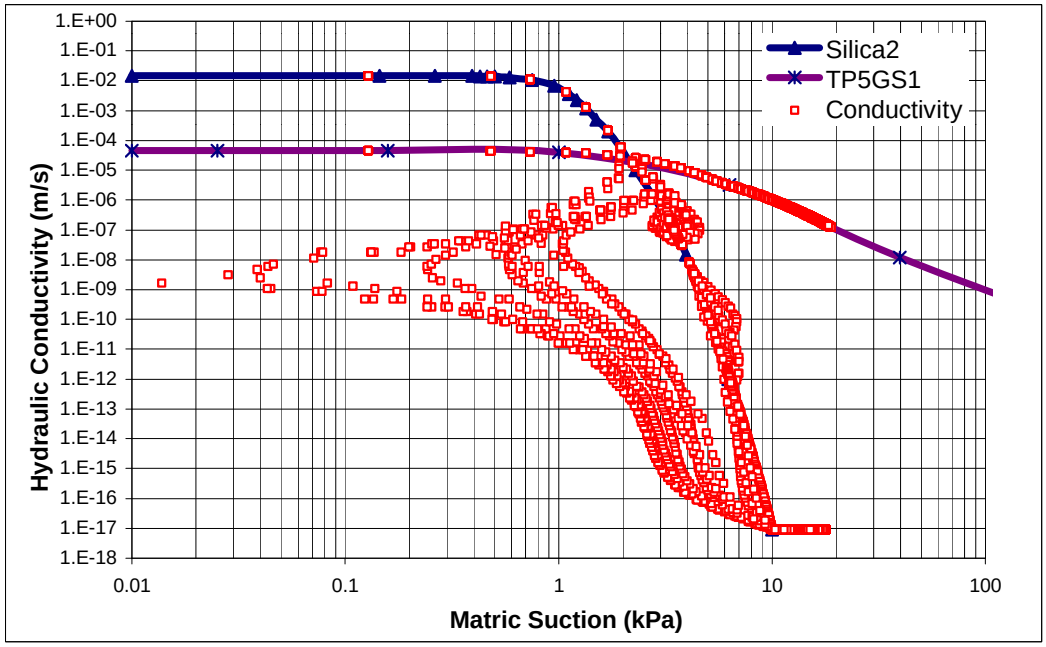


**Figure B10d Convergence Results for The $10^{-7}$ m/s Model with The Standard Mesh**

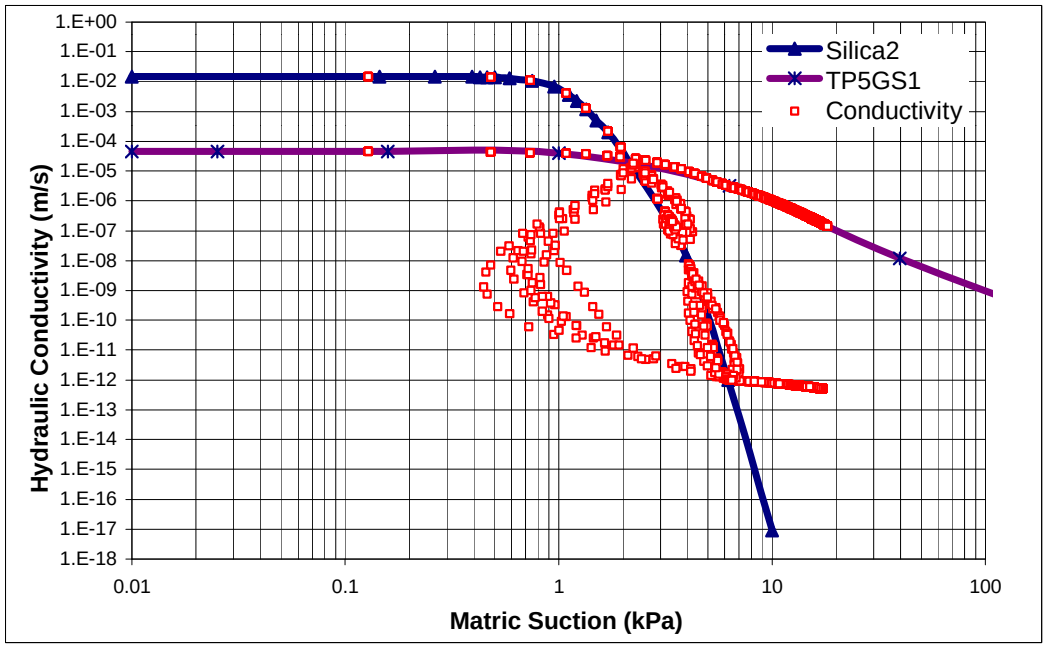


**Figure B10e Convergence Results for The $10^{-7}$ m/s Model with The Elements Removed from The Outside Fine and Coarse Layers**

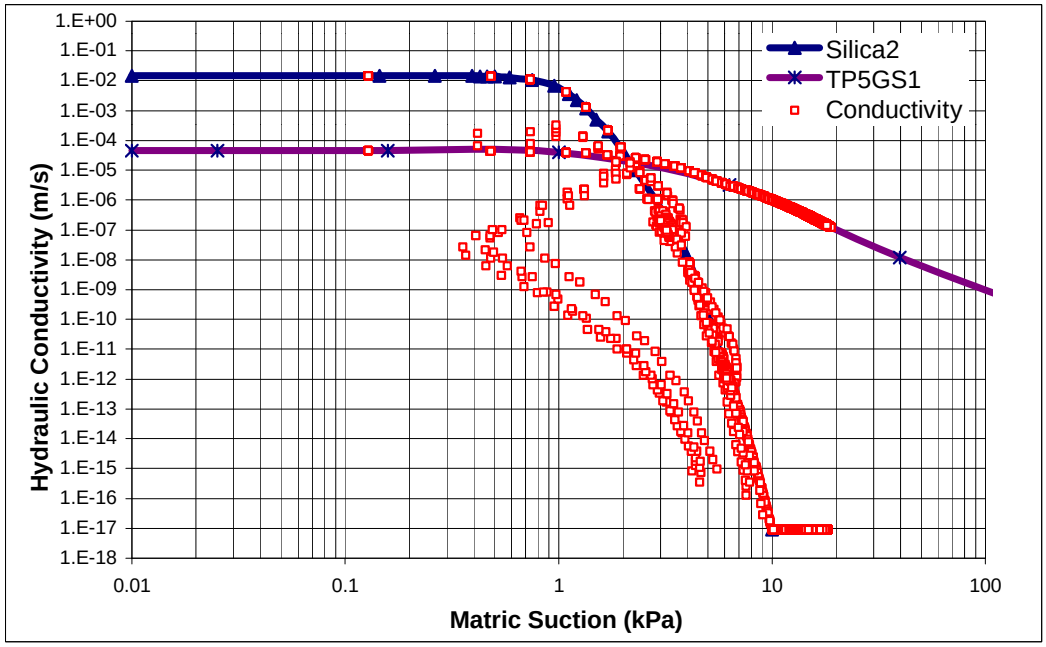


**Figure B10f Convergence Results for The $10^{-7}$ m/s Model with The Elements Removed from Both Coarse Layers**

The $10^{-6}$ m/s flux convergence results with the standard mesh showed slight to moderate non-convergence. The conductivity points in Figure B10a show the calculated hydraulic conductivity for each model. The size and density of the scatter pattern from the given coarse-grained layer hydraulic conductivity was the measure of convergence. Figure B10b shows that the removal of the outside elements in the second coarse-grained layer improved convergence in the lower portion of the curve, but widened the scatter pattern in the upper portion of the curve. Figure B10c shows that the removal of elements in the first coarse-grained layer greatly improved convergence (or the appearance of convergence). However, several non-converged points still exist in elements in the upper portion of the model.

The convergence results for the $10^{-7}$ m/s flux with the standard mesh showed a high level of non-convergence in a distinct scatter pattern (Figure B10d). Figure B10e shows that removing the outside two columns of elements from both sides reduced the scatter pattern. The use of a modified (i.e. reduced residual hydraulic conductivity function) material property may also affect the reduction in the scatter pattern. Figure B10f shows that the removal of elements from both coarse-grained layers resulted in a similar but greatly reduced scatter pattern. However, several non-converged points still exist.

To ensure that the flux in each layer of the system was not significantly affected by removing elements/nodes, a $10^{-5}$ m/s flux model was analyzed and compared with the converged solution from the standard mesh. In addition, the results from the $10^{-6}$ and $10^{-7}$ m/s flux models with elements removed from both coarse-grained layers were also compared and are presented in Table 5.6.

**Table B8 Comparison of Computed Results Between Standard and Simplified Mesh with Elements Removed From Both Coarse Layers**

| Mesh (Flux) | First Fine (%) | First Coarse (%) | Second Fine (%) | Second Coarse (%) |
|---|---|---|---|---|
| Standard ($10^{-5}$) | 59.1 | 3.5 | 37.3 | 0.06 |
| Simplified ($10^{-5}$) | 52.4 | 3.1 | 44.5 | 0.1 |
| Standard ($10^{-6}$) | 37.6 | 0 | 62.2 | 0 |
| Simplified ($10^{-6}$) | 37.0 | 0 | 63.0 | 0 |
| Standard ($10^{-7}$) | 37.6 | 0 | 62.4 | 0 |
| Simplified ($10^{-7}$) | 37.0 | 0 | 63.2 | 0 |

The results presented in Figure B9 indicated that the remaining coarse elements in the top portion of the $10^{-6}$ and $10^{-7}$ m/s flux models still show regions of higher than expected pore-water pressures. Figure B10 indicated that removing elements in the coarse-grained layers did improve convergence significantly, however, several non-convergent elements/nodes were still evident. The non-convergent areas appeared to be in the upper portion of the models where preferential flow occurs. Further fine-tuning of the mesh can be made for each different input flux to continue to improve convergence, however elements with flow vectors should not be removed or else there would be a deviation from the known solution.

Comparing the flux flowing in each layer showed surprisingly little change in the non-converged $10^{-6}$ and $10^{-7}$ m/s flux models; however, there was a 7 percent change in the converged $10^{-5}$ m/s flux models after elements from the first coarse-grained layer were removed. It is interesting that the difference occurred in the fine-grained layers. Figure B11 presents the results for the $10^{-5}$ m/s flux model with the standard and simplified meshes.

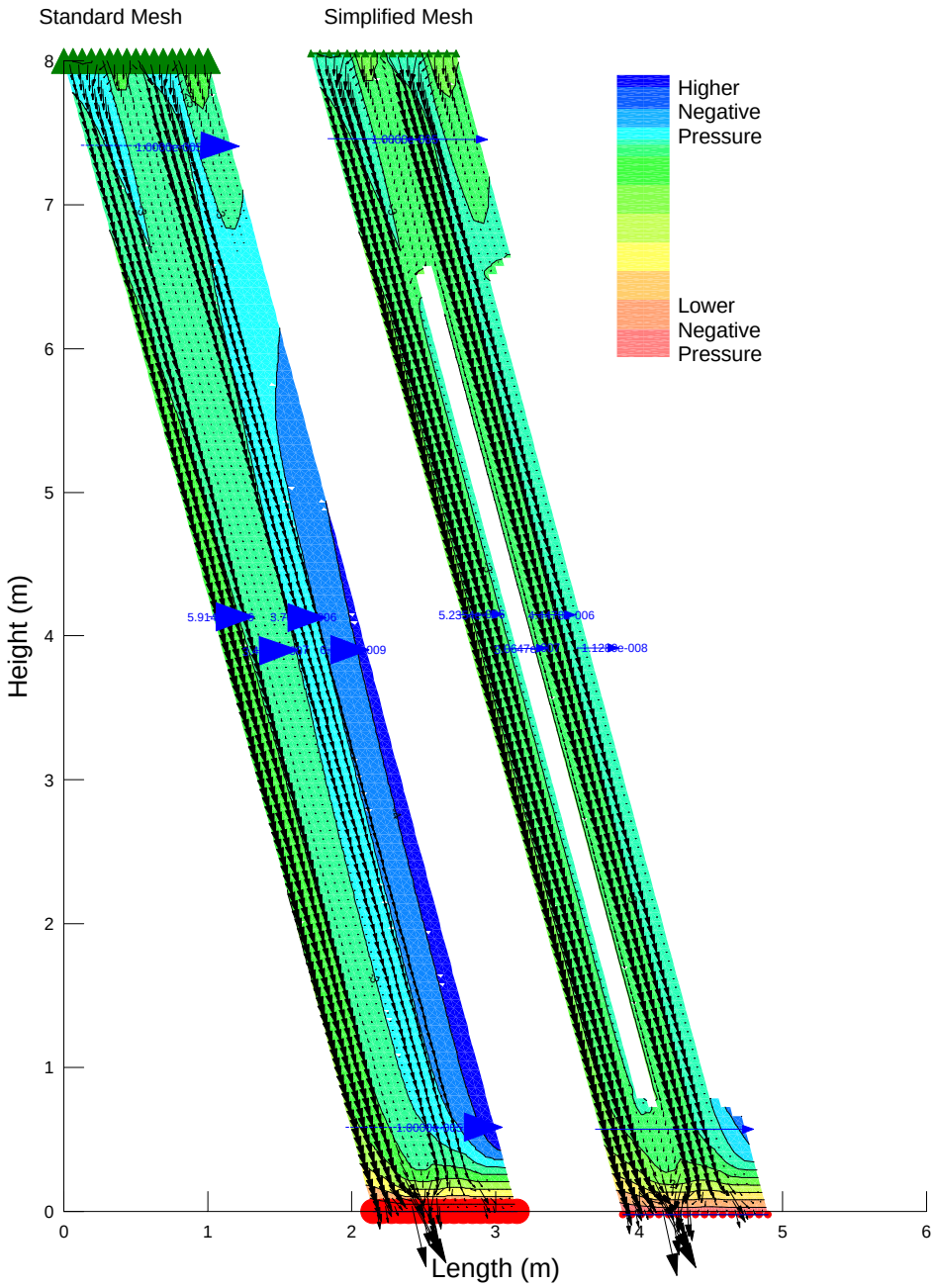


**Figure B11 Computed Results from the $10^{-5}$ m/s Applied Flux Model with the Standard Mesh on the Left and Simplified Mesh on the Right**

The pressure contours in Figure B11 indicate that the higher negative pore-water pressure zone in the standard mesh did not occur in the simplified mesh. The preferential flow zones in the top portion of both meshes appear to be similar. Since the change in flux showed an increase in both the second fine

and coarse-grained layers, it can be concluded that removing elements from the first coarse-grained layer not only disrupted the flow vectors abruptly but may also prevent further crossover flow between the upper two layers. This flow would otherwise have occurred in the converged $10^{-5}$ m/s solution but not in the non-converged $10^{-6}$ and $10^{-7}$ m/s models. A possible reason for no change in flow in the $10^{-6}$ and $10^{-7}$ m/s flux models was due to the insignificant amount of flux flowing in the coarse-grained layers for the non-converged solution. It could also indicate that the preferential flow cross over of flux is completed before the removed elements are encountered.

### B3.3 Material Properties

The sensitivity analysis for material properties concentrated on studying the effects on convergence issues for modifying the steep hydraulic conductivity function of the coarse-grained material, as well as changing the materials properties, and decreasing the difference between the materials properties used.

It was previously mentioned that in the parametric study, the coarse-grained material (i.e., silica1) did not converge after increasing the model over a certain height. The only solution to the problem was obtained by modifying the property curve for the coarse-grained material to that of silica2. To study the effects of changing the slope of the soil property curve for hydraulic conductivity, two intermediate curves were developed and the four curves were presented in Figure 4.8. The results of the analysis are presented in Figure B12.

The results in Figure B12 indicate that as the slope of the hydraulic conductivity curve was decreased there was marked improvement in convergence. Even the first incremental slope change showed a vast improvement in convergence of the problem solution.

For a given finite element mesh and set of convergence parameters, the hydraulic conductivities calculated by the program solver are directly dependent on the specified material properties of the fine-grained material for the given applied flux. In this case, the $10^{-5}$ m/s flux will correspond to a matric suction in the fine-grained material of approximately 3.5 kPa with a corresponding hydraulic conductivity of $10^{-5}$ m/s (i.e., equal to the applied flux). It can be seen on Figure B12 that the corresponding hydraulic conductivity in the coarse-grained material changes more than three orders of magnitude at a suction of 3.5 kPa, from silica1 to silica1a, less than two orders of magnitude from silica1a to silica1b, and less than one order of magnitude from silica1b to silica2. The matric suctions varies only 1 kPa between silica1 to silica2.

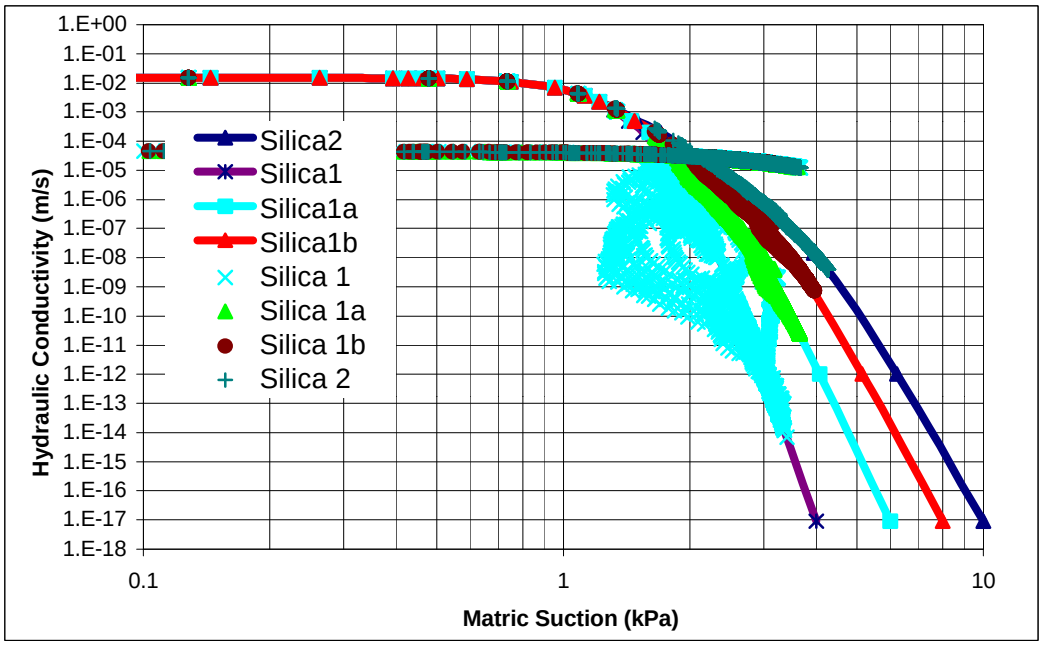


**Figure B12 Result from the Sensitivity Analysis of the Coarse Material Using $10^{-5}$ m/s Applied Flux.**

Once again, the results indicated that low calculated value of hydraulic conductivities for coarse elements/nodes are proportional to non-convergence in those elements/nodes. The non-converged nodes are on the left side of the curve, indicating lower than expected pressure, which explained the low pore-

water pressure zones in the results previously presented for the areas with $10^{-6}$ and $10^{-7}$ m/s flux (i.e., Figures B6 through B9). It also explained the absence of flow vectors in these zones. Since the solution did not converge, the actual material properties for the coarse-grained material were not properly represented and therefore the calculated conductivities in the non-converged patterns replaced the correct hydraulic conductivity function within the particular solution, thus implying that there was no longer a unique solution for each pressure. A matric suction of 2 kPa could correspond to a wide range of hydraulic conductivity values. Hence, the low-pressure areas where no flow vectors were apparent had a relatively lower hydraulic conductivity than the surrounding element/nodes.

Figure B13a and B13b compare the $10^{-5}$ and $10^{-7}$ m/s flux results, respectively, for the standard mesh with the same parameters used for the parametric study.

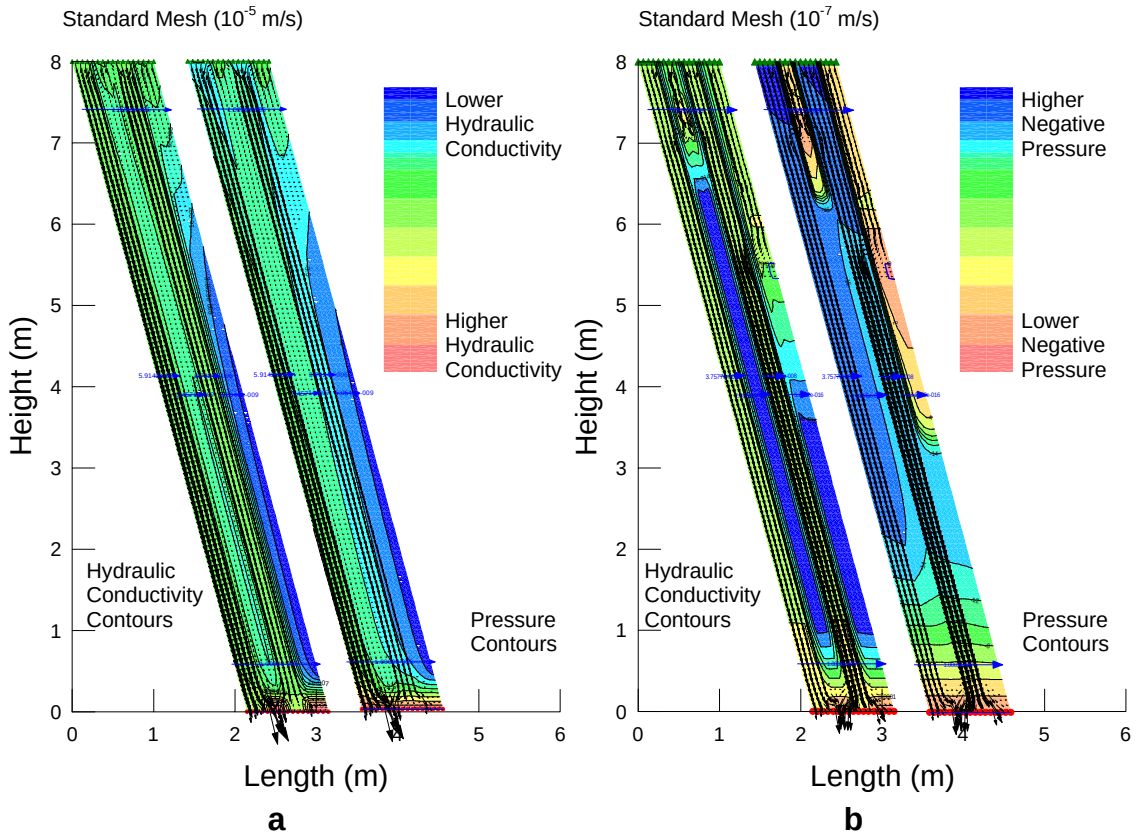


**Figure B13 Result from the Converged (a) $10^{-5}$ m/s and Non-Converged (b) $10^{-7}$ m/s Applied Flux Models with Calculated Hydraulic Conductivities and Pressure Contours**

Figure B13a presents the converged results of the $10^{-5}$ m/s flux model analyzed in the parametric study with pore-water pressure contours. The mesh to the left shows the contours of the calculated hydraulic conductivities and the mesh to the right shows the contours of the calculated pressures. Note that the contour shades of the each mesh are closely related (i.e., the higher negative pore-water pressures are corresponding with the lower conductivities values). In this figure, the darker shade corresponds to the higher negative pore-water pressures and lower hydraulic conductivity values. The higher negative pore-water pressures were clearly shown to be in the second coarse-grained layer. The second coarse-grained layer had higher negative pore-water pressure values than the first coarse-grained layer due to its position over all the other layers. The pore-

water pressures and hydraulic conductivities in all the layers quickly increased in the lower portion of the mesh as the pore-water pressure increased from the –2.5 kPa to 0 kPa specified at the bottom boundary.

The $10^{-7}$ m/s flux solution shown in Figure B13b does not show the uniformity presented in Figure B13a. The lower calculated hydraulic conductivities are in the coarse-grained layers. However, the calculated higher negative pore-water pressures are in the first two layers. A large region can be observed where the first fine and coarse-grained layers share the same pore-water pressures for the same elevations. Based on the discrepancies from the contours in each mesh it can be concluded that the $10^{-7}$ m/s flux has not only failed to converge but identifies the mode of failure. By plotting the calculated hydraulic conductivities and pressures against the material properties, combined with the hydraulic conductivity and pore-water pressure contours in Figure B13b, it can be concluded that the values of hydraulic conductivity are calculated correctly and the velocity vectors are a function of the calculated hydraulic conductivities and therefore are also correct. In addition, the pore-water pressures were not calculated correctly and therefore the calculated hydraulic conductivities are plotted incorrectly (i.e., not on the given function). Also, note that the pattern produced by the non-converged solution is inconsistent with the material properties (refer to Figure 5.16). The pattern may be the result of incorrect pore-water pressures calculated for nodes at different elevations and proximity to the fine and coarse-grained material boundary. The reason why the pore-water pressures are greater than the material properties rather than lower or evenly distributed is unknown.

It was discussed in section B2 that reducing the difference between the coarse and fine-grained material properties may assist in the convergence of the solution. This theory was investigated using silica1 as the coarse-grained material and changing TP5GS1 to a uniform sand (e.g. Beaver Creek sand) for the fine-grained layer. The model analyzed was an 8-meter model inclined 75°

with secondary nodes. Note that the similar model with silica1 and TP5GS1 at $10^{-5}$ m/s flux failed to converge in the parametric study. The result of the new analysis is presented in Figure B14.

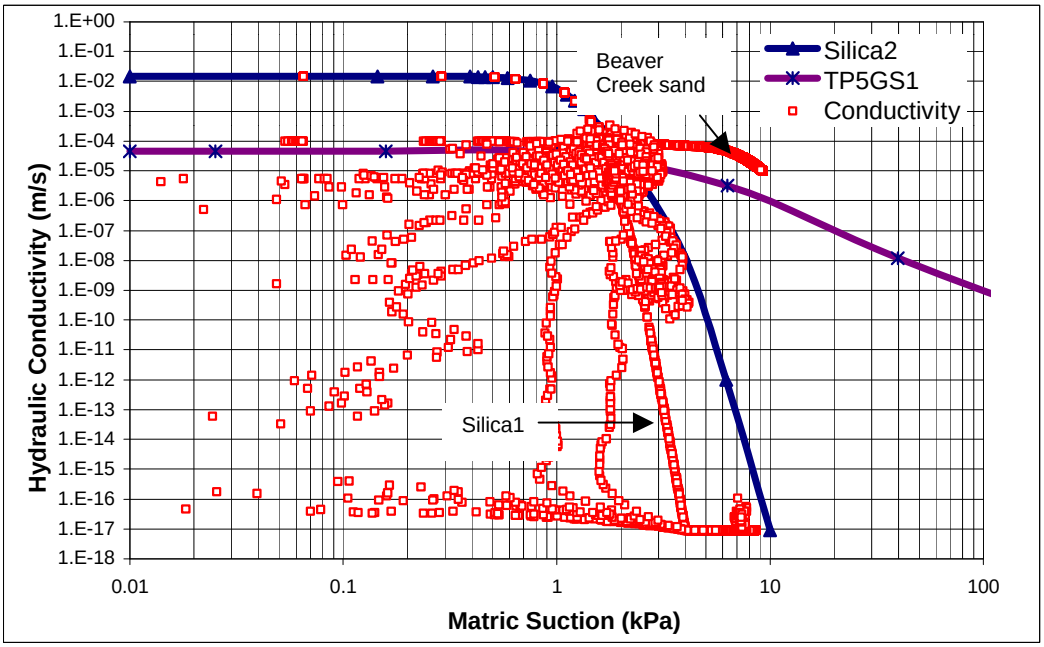


**Figure B14 Result From the $10^{-5}$ m/s Flux Model with Silica1 and Uniform Beaver Creek Sand Material Properties Used for the Coarse and Fine Layers Respectively**

The results indicated that the solution continued to fail to converge in the coarse-grained layer but the fine-grained layer material did reach convergence. Assuming that the silica1 was still too steep to achieve convergence, silica2 was used with the uniform sand in an attempt to improve convergence for the $10^{-7}$ m/s flux model. The result of the analysis is presented in Figure B15. The result also indicated non-convergence.

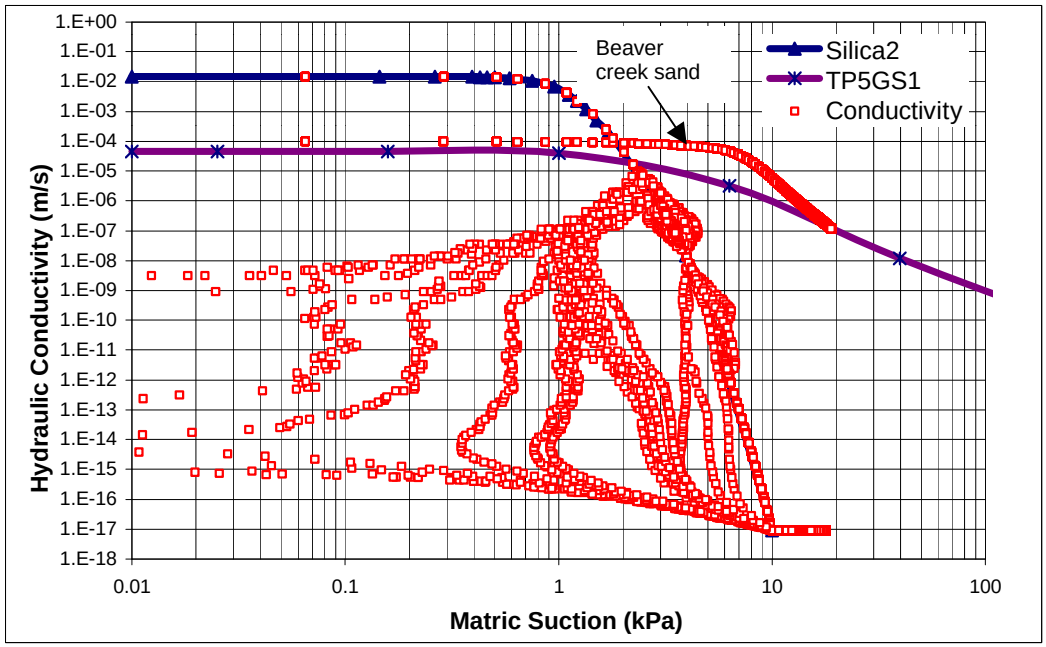


**Figure B15 Computed Result From the $10^{-7}$ m/s Flux Model with Silica2 and Uniform Sand Material Properties Used for the Coarse and Fine Layers Respectively.**

The purpose of the analyses presented in this section was to determine if by changing the material properties of the fine-grained layer to something slightly closer to the coarse-grained layer could positively affect the results of the non-convergent models. The analyses showed that non-convergence still occurred. This was not to say that further investigation might yield results that are more favorable. However, the more the material properties are manipulated, the farther the analyses deviate from reality.

Section B2 also discussed the possibility of using a transitional layer with soil properties between those of the coarse and fine-grained layers. It can be argued that non-convergence was the result of the abrupt changes in pore-water pressures due to the sharing of nodes along the boundary of the fine and coarse-grained layers. The transitional layer has a material property function midway between the coarse and fine-grained material properties. The transitional layer should, in theory, be a buffer to ease the transition from one

layer to the other. Note that the transitional layer was not intended to represent actual field conditions encountered in the Golden Sunlight Mine (GSM), but was used as a modelling technique.

The transitional layer was used for the modified mesh and the standard mesh with secondary nodes for the $10^{-7}$ m/s flux model. Figure B16 illustrates the transitional layer between the coarse and fine-grained layers in the standard mesh with secondary nodes, and the calculated pore-water pressure contours. Figures B17 and B18 present the calculated hydraulic conductivities for the standard mesh with secondary nodes and the modified mesh.

The results indicate that the use of a transitional layer for both meshes failed to reach convergence. However, the standard mesh with secondary nodes showed improvement. Both the fine-grained and transitional layers converged but the coarse-grained layer showed only slight improvements that can be attributed to replacing coarse elements/nodes with the transitional elements layer material. A further investigation could consider a sensitivity analysis on different hydraulic conductivity function slopes for the transitional material until the transitional material fails to converge or the coarse-grained material converges. This extension of the investigation was not pursued.

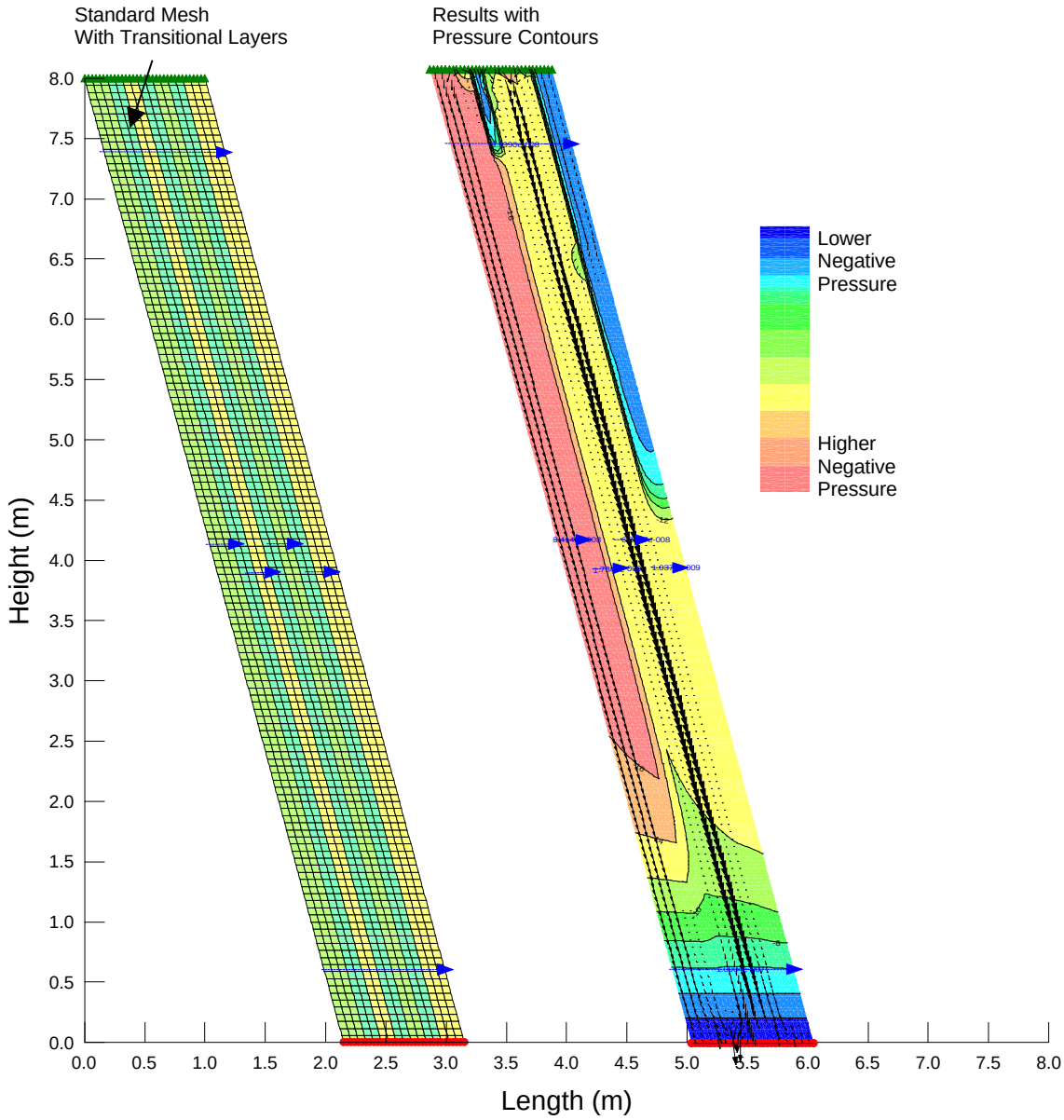


**Figure B16 Mesh and Computed Pressure Contours for the Case with the Transitional Layers in a Standard Mesh with Secondary Nodes for the $10^{-7}$ m/s Applied Flux Model.**

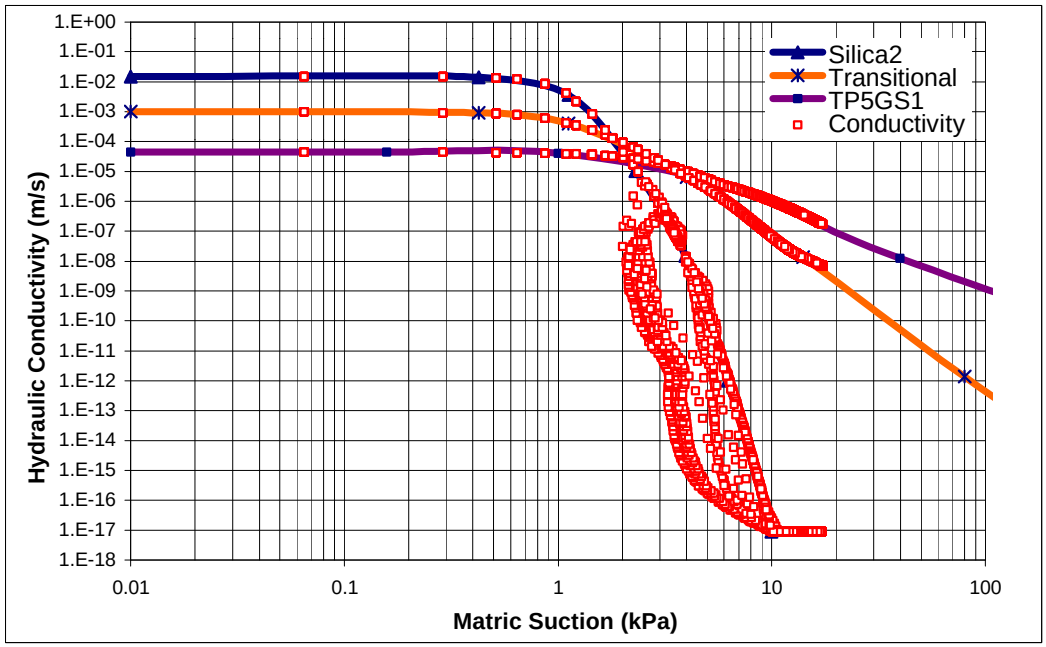


**Figure B17 Result from the $10^{-7}$ m/s Flux Model with Transitional Layer and the Standard Mesh with Secondary Nodes.**

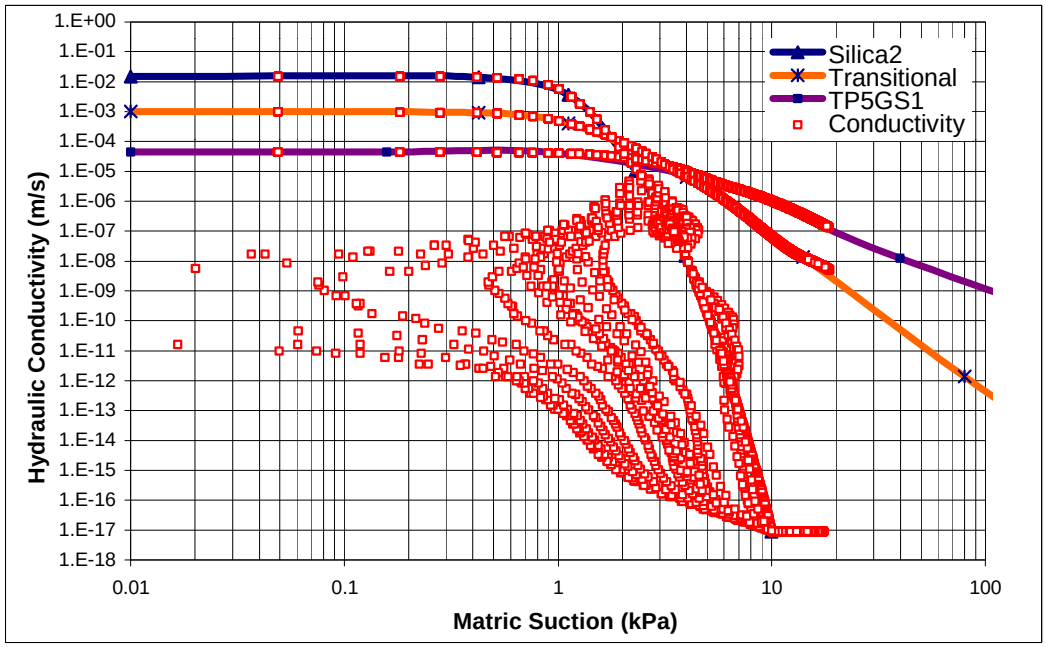


**Figure B18 Result from the $10^{-7}$ m/s Input Flux Model with Transitional Layer and the Modified Mesh.**

The final section of the material sensitivity analysis investigated the further manipulation of the hydraulic conductivity function of the coarse-grained layer. It had been observed that the coarse-grained material with lower hydraulic conductivities failed to converge. It was also known that the coarse-grained material was unable to transport significant flux at the lower conductivities and pore-water pressures, as compared to the fine-grained material at the same pore-water pressures. Therefore, it was not necessary to define the coarse-grained hydraulic conductivity function down to $10^{-17}$ m/s if $10^{-12}$ m/s might give a better result. However, increasing the residual hydraulic conductivity by too much may lead to changing the flux distribution between the layers (i.e., a false solution). The sensitivity analysis looked at three possible solutions:

1. Raising the conductivity function residual value further up the curve;
2. Raising and sloping the residual section of the function; and
3. Raising and sloping the function into three distinct sections.

The result of increasing the residual hydraulic conductivity for the same case shown in Figure B16 was plotted showing the convergence pattern calculated is presented in Figure B19. Figure B19a shows the case with a $10^{-12}$ m/s residual conductivity where the model failed to converge. The convergence pattern plotted was similar to that for the original material function except that a horizontal line of calculated conductivities equal to the $10^{-12}$ m/s is plotted for the pore-water pressure range between -6 and -11 kPa. There was no change in the flux distribution between the layers.

Figure B19b shows the results for the case with a $10^{-9}$ m/s residual conductivity. The results indicated that the non-convergence had been greatly reduced, however more flux was found entering into the coarse-grained layers. Figure B19c and B19d show the results using residual conductivities of $10^{-8}$ and $10^{-7}$ m/s, respectively. The results showed that both models converged, however the flux in the coarse-grained layer had increased significantly. The $10^{-7}$ m/s residual hydraulic conductivity function failed to achieve preferential flow. All flux results are presented in section B6.

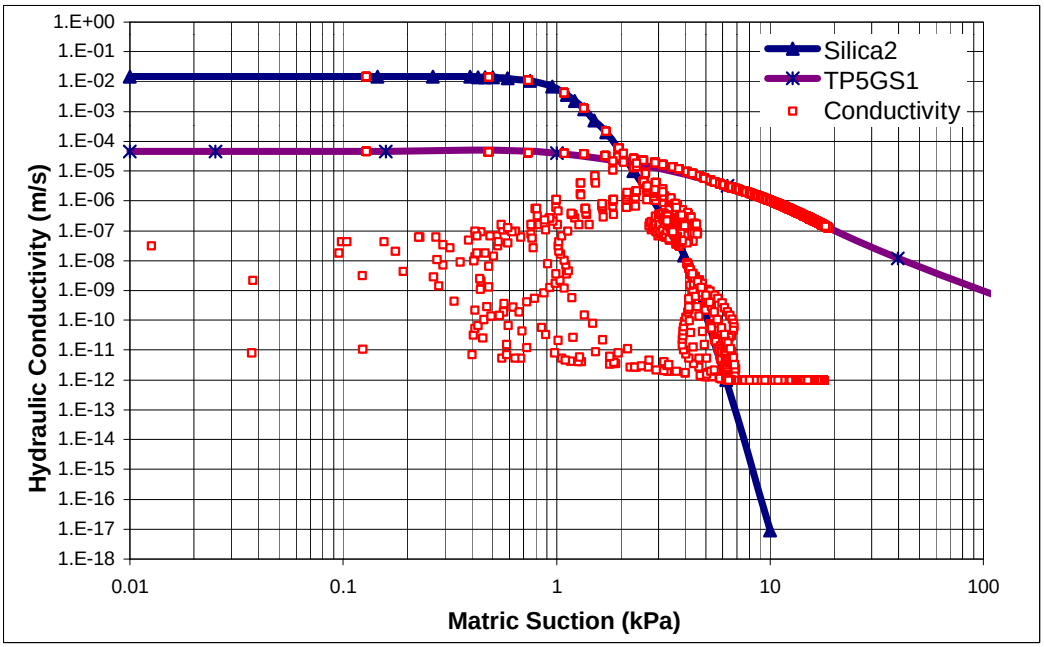


**Figure B19a The Result from the $10^{-7}$ m/s Applied Flux Models with The $10^{-12}$ m/s Residual Hydraulic Conductivity for the Coarse Layer**

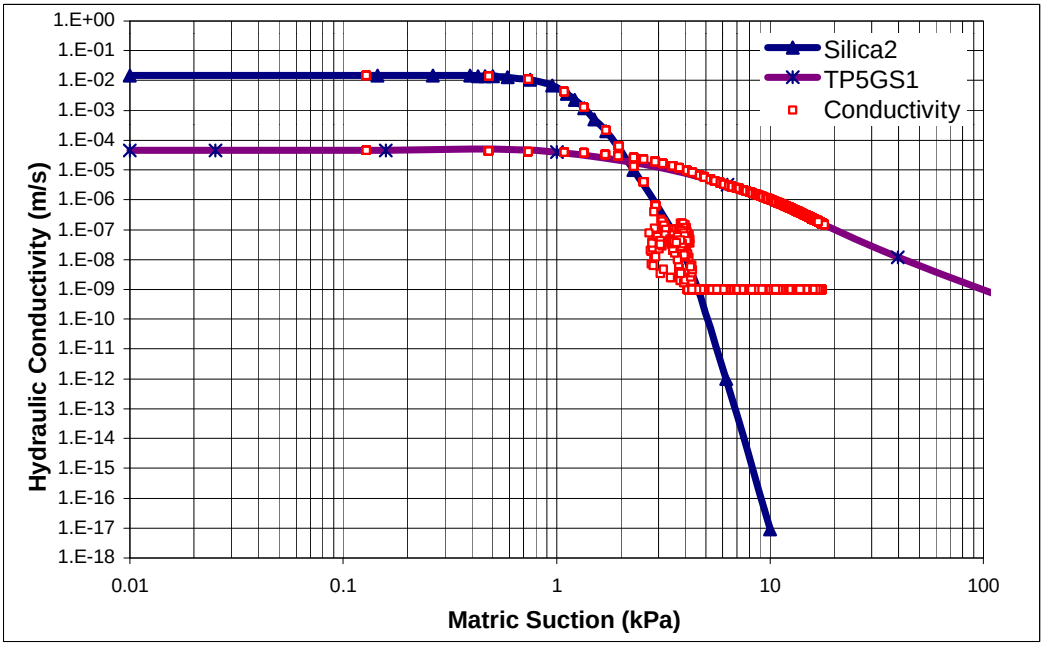


**Figure B19b The Result from the $10^{-7}$ m/s Applied Flux Models with The $10^{-9}$ m/s Residual Hydraulic Conductivity for the Coarse Layer**

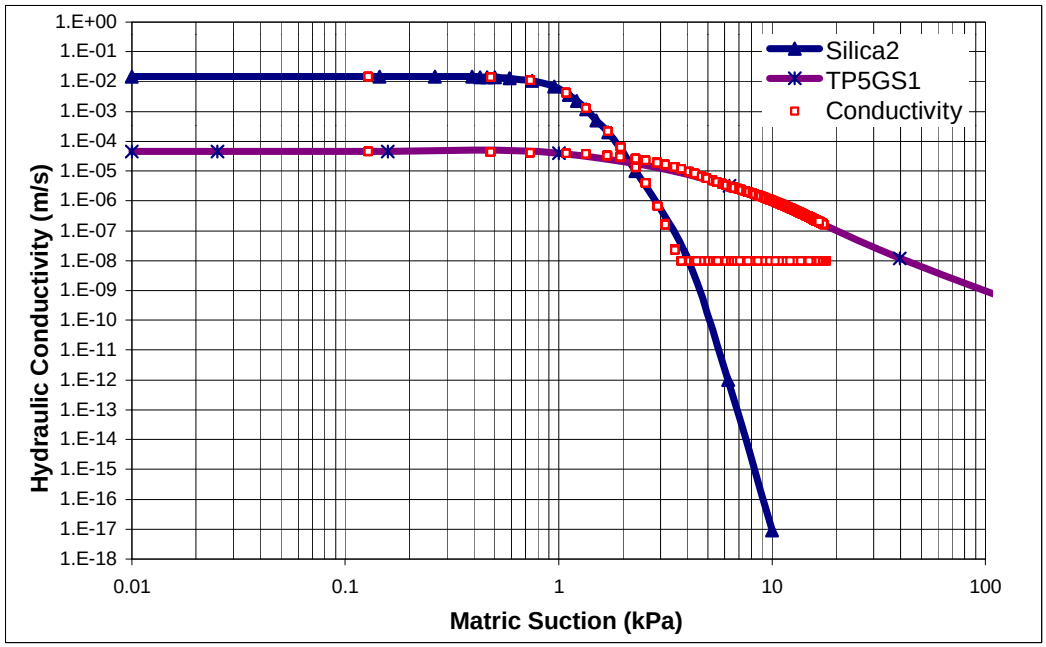


**Figure B19c The Result from the $10^{-7}$ m/s Applied Flux Models with The $10^{-8}$ m/s Residual Hydraulic Conductivity for the Coarse Layer**

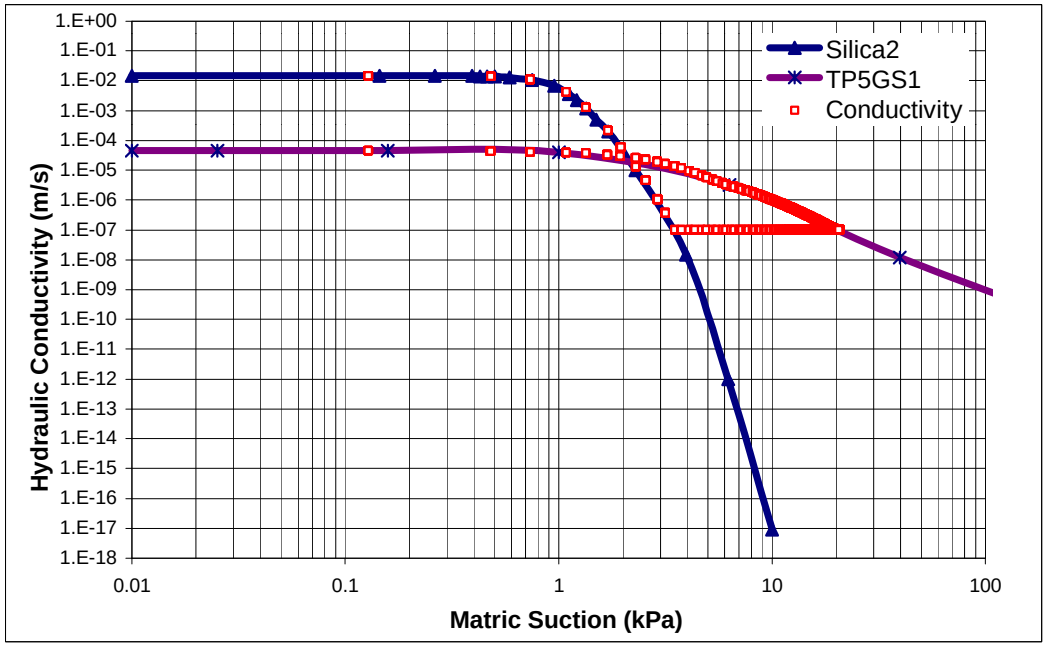


**Figure B19d The Result from the $10^{-7}$ m/s Applied Flux Model with The $10^{-7}$ m/s Residual Hydraulic Conductivity for the Coarse Layer**

The computed results for increasing the residual hydraulic conductivity indicated that coarse-grained material would either not converge or would give a false solution. To resolve this dilemma, further analyses focused on the calculated horizontal line that develops at the residual value. The coarse-grained material was not defined past the residual hydraulic conductivity and residual pore-water pressure; however, the solver calculates hydraulic conductivities past the residual pore-water pressure. To solve this problem a sloped residual section of the hydraulic conductivity function was developed, thereby forcing the solver to see a unique conductivity for each pore-water pressure. A material property with a curved residual function segment beginning at $10^{-12}$ and $10^{-8}$ m/s is presented in Figure B20a and B20b. The residual function segment curve was reduced by an order of magnitude and the result is present in Figure B20c.

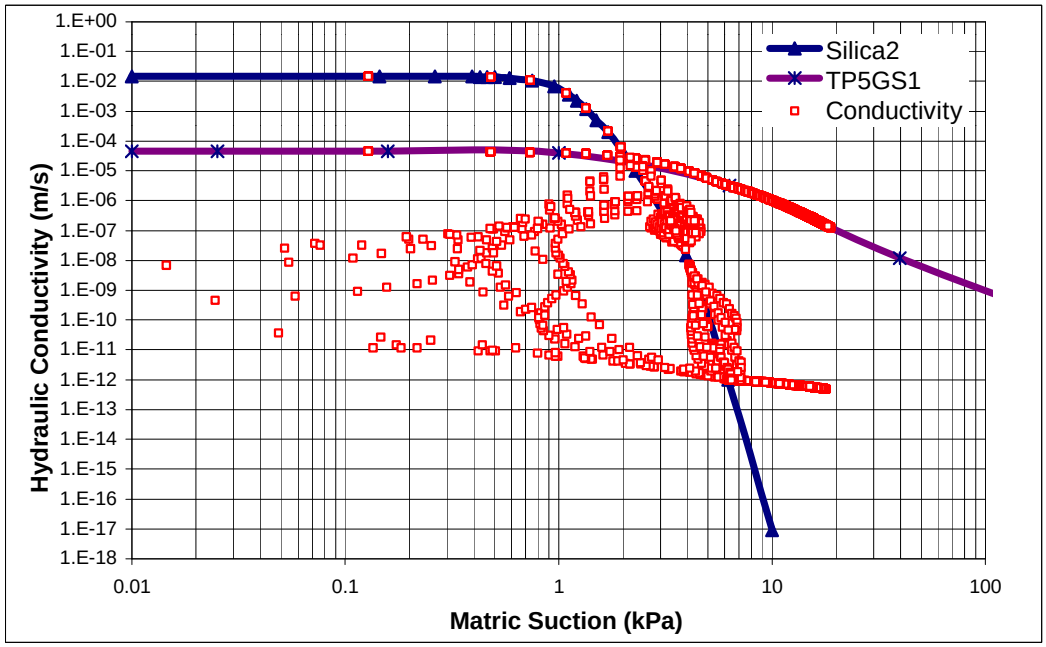


**Figure B20a The Result from the $10^{-7}$ m/s Applied Flux Model with The Residual Hydraulic Conductivity of The Coarse layer Curved From $10^{-12}$ m/s**

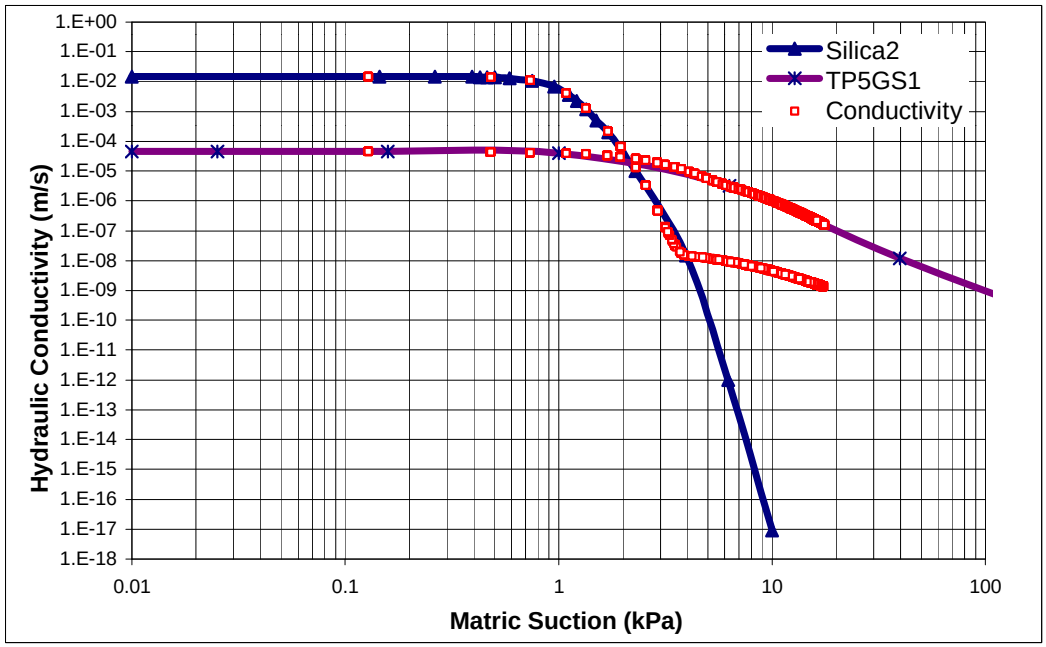


**Figure B20b The Result from the $10^{-7}$ m/s Applied Flux Model with The Residual Hydraulic Conductivity of The Coarse layer Curved From $10^{-8}$ m/s**

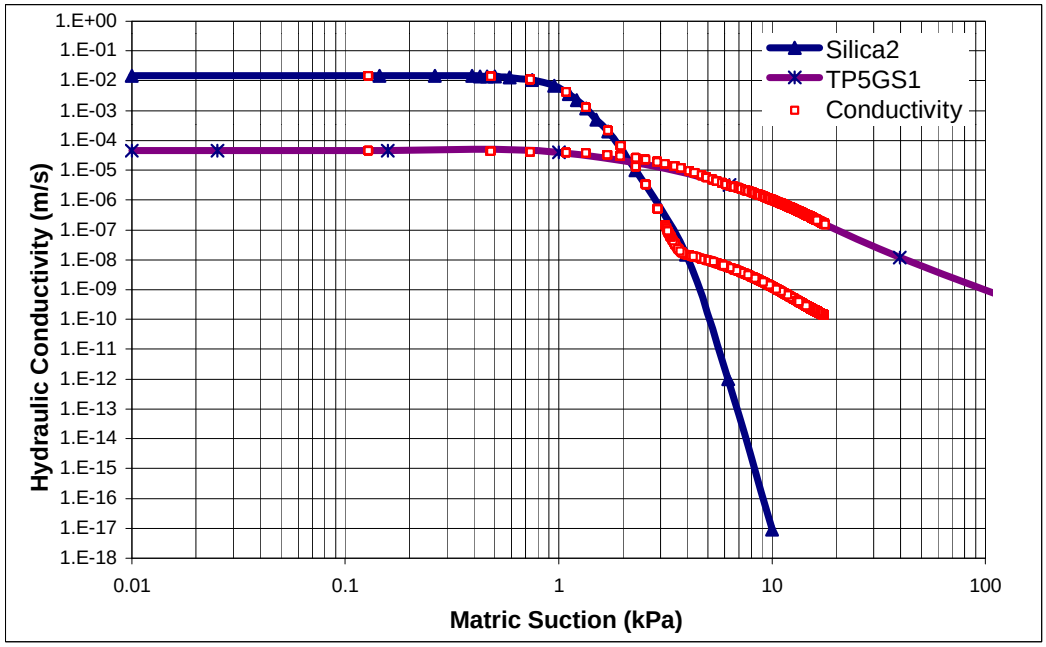


**Figure B20c The Result from the $10^{-7}$ m/s Applied Flux Model with The Residual Hydraulic Conductivity of The Coarse layer Curved From $10^{-8}$ m/s with Increased Slope to The Function**

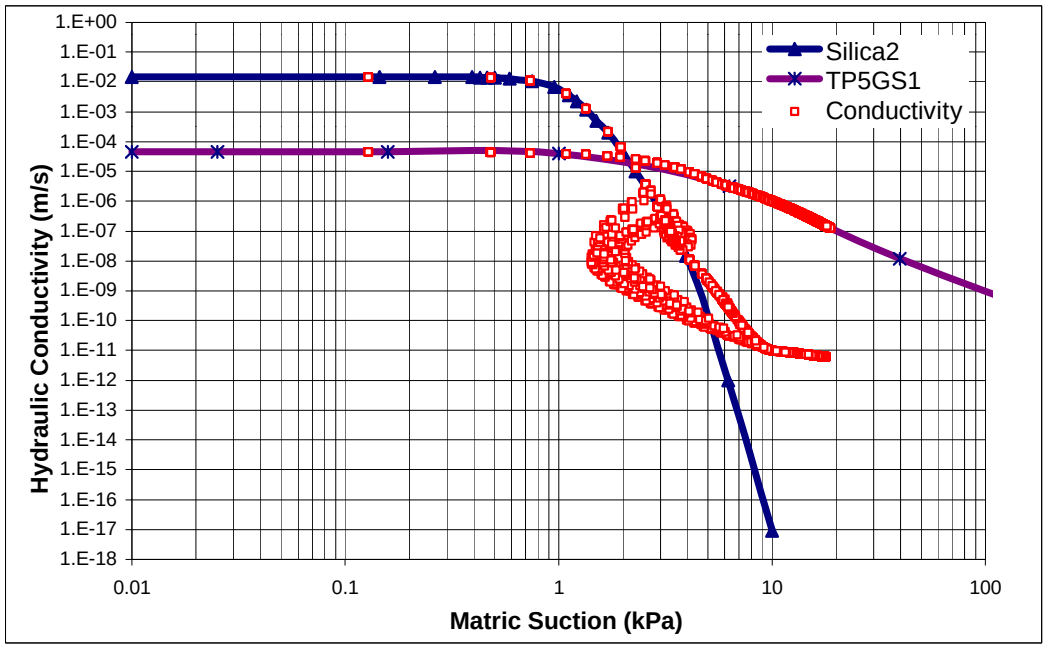


**Figure B20d The Result from the $10^{-7}$ m/s Applied Flux Model with The Residual Hydraulic Conductivity of The Coarse layer Curved From $10^{-8}$ m/s and From $10^{-11}$ m/s.**

The results of Figure B20a to B20c were similar to those shown in Figure B19 (i.e., Figure B20a failed while Figures B20b and B20c had too much flow in the coarse-grained layers). The third alternative was to change the slope of the existing hydraulic conductivity function in two places. The slope of the new conductivity function was altered at $10^{-8}$ m/s by decreasing the slope of the function slightly. The second change in slope was placed at a residual value of $10^{-11}$ m/s and had a slope similar to that of the previous models. The results are presented in Figure B20d.

The computed results plotted on Figure B20d show non-convergence. Note that the calculated conductivities were in a tighter pattern than previously. For a final analysis, the change in slope at the residual value was changed to $10^{-10}$ m/s and a simulation with a flux of $10^{-7}$ m/s flux was evaluated.

The results presented in Figure B21a indicated convergence (i.e., the calculated hydraulic conductivities for the simulation matches the specified function not presented in Figure B21) and no significant increase in the flux was observed in the coarse-grained layers. To confirm the stability of the new function, the simulation was re-analyzed with a $10^{-8}$ m/s flux. The results presented in Figure B21b once again indicated convergence with a similar flux distribution. It appeared that the key to solving the convergence issues was to reshape the hydraulic conductivity function for the coarse-grained materials in such a way as to strike a balance between achieving convergence (accuracy) and having the model represent reality (physical admissible solution). Note that the lowest hydraulic conductivities calculated in both fine and coarse-grained materials share the same value of matric suction. This was not the case in most of the models analyzed.

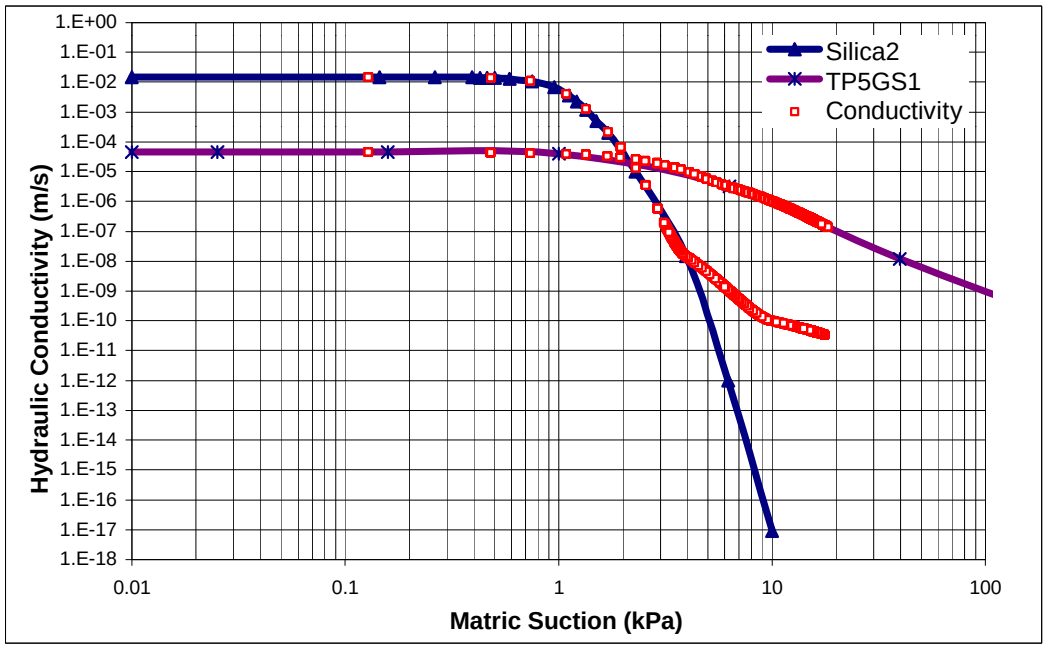


**Figure B21a The Result From the Dual Change in Slope for Residual Hydraulic Conductivity in the Coarse Layer Hydraulic Conductivity Function at $10^{-8}$ and at $10^{-10}$ m/s, with an Applied Flux of $10^{-7}$ m/s**

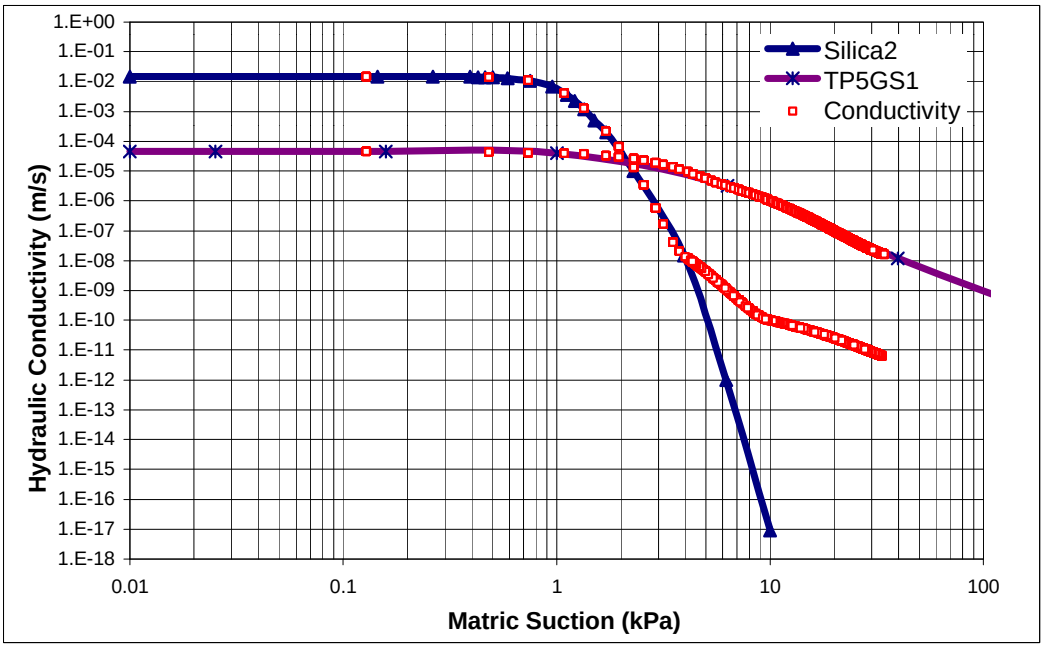


**Figure B21b The Result From the Dual Change in Slope for Residual Hydraulic Conductivity in the Coarse Layer Hydraulic Conductivity Function at $10^{-8}$ and at $10^{-10}$ m/s, with an Applied Flux of $10^{-8}$ m/s**

## B3.4 Transient Models

The final sensitivity analysis topic that was investigated involved the use of transient models. Chapter 3 outlined the theoretical aspects of the transient finite element formulation, and section 2B specified the methodology for modelling a steady state problem with transient models. Three variations were explored:

1. Applying the desired flux and stepping into time (1 model required);
2. Saturating the system, draining the system to residual volumetric water contents and then applying the desired flux (3 models required); and
3. Saturating the system and then draining the system from a saturated flux at to the desired unsaturated flux (2 models required).

The first obstacle encountered with the transient models was checking for convergence. It appeared that the solver did not calculate conductivities in the same way as for the steady state method. Plotting the calculated conductivities against the actual hydraulic conductivities of the materials resulted in agreement on every occasion. Plotting the calculated volumetric water contents against the

actual soil-water characteristic curves (SWCC) also showed agreement. This observation left only the vector norm versus iteration graph and an analysis of the solution to determine whether the model achieved convergence.

Several analyses were conducted using the first method listed. However, a steady state solution with the desired fluxes was not achieved. The problem was determined to be in the method of analysis. Effectively, the model defined a mesh with predetermined properties and no activity, and then at time zero, a flux was forced into the system. The input flux resulted in low pore-water pressures, low conductivities, and low volumetric water contents on the top elements. As time goes on the flux was continually forced down the system. The end results deviated from the known solution solved in the parametric study.

The second method eliminated the flaw in the first method by running previous models such that at time zero the mesh was at a residual volumetric water content and pore-water pressure. The sensitivity analysis investigated the 8-meter, 75° profile with the standard and modified meshes at $10^{-5}$ and $10^{-7}$ m/s input fluxes. To test the transient method, the coarse-grained material used for the analysis was the steeper silica1 function. Figure B22 shows the results of the analysis as the system was saturated then drained and the input fluxes are subsequently applied.

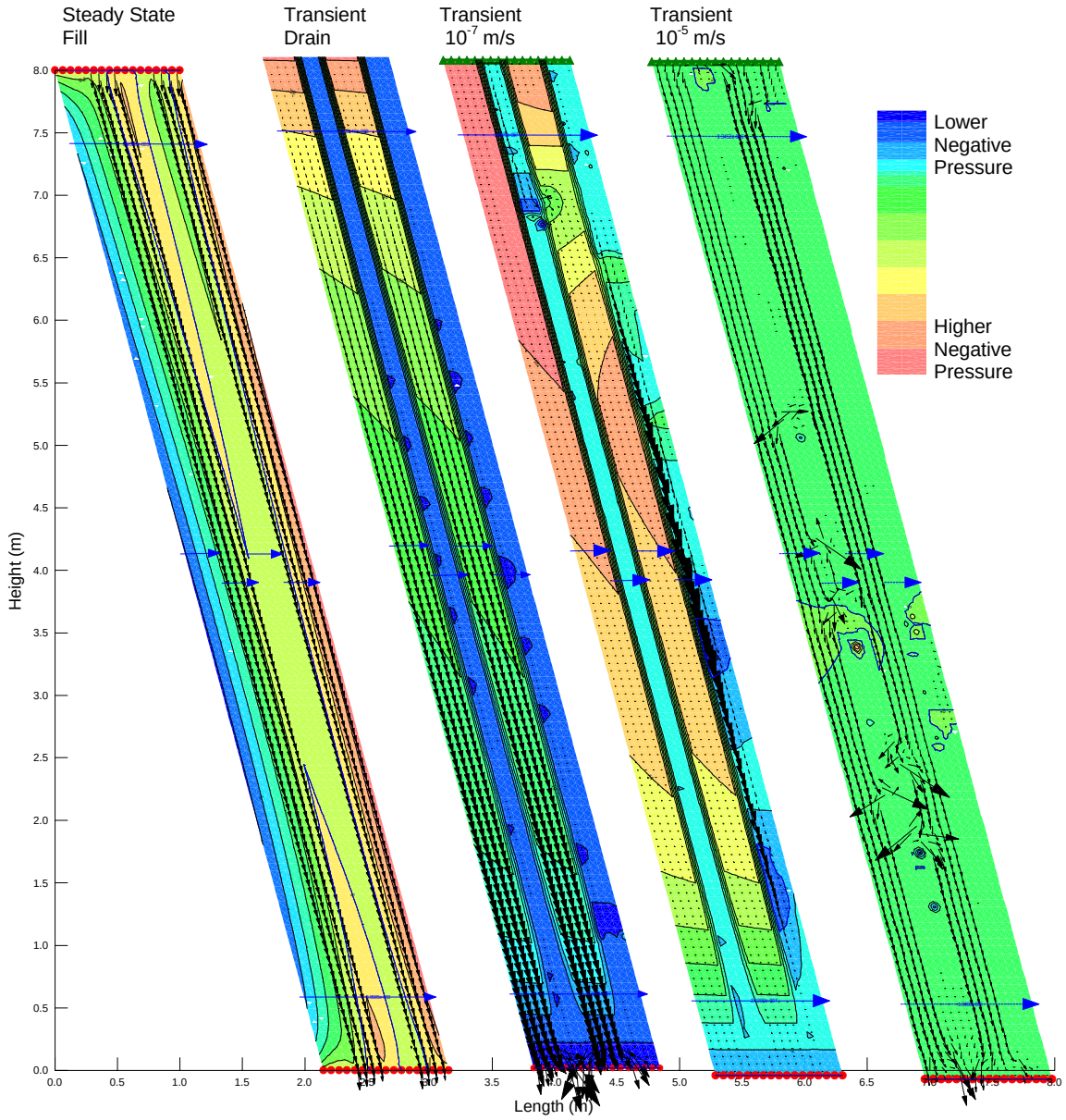


**Figure B22 Computed Pressure Contours and Flow Vectors From the Transient Analysis of the Standard Mesh Showing from Left to Right the Saturation of the System, the Transient Draining of the System, the Addition of Transient Applied Flux of $10^{-7}$ and $10^{-5}$ m/s**

Figures B23 and B24 present the computed pore-water pressure versus distance and vector norm versus iteration graphs, respectively. Note that Figure B23a shows the decrease in computed pore-water pressures within the cross-section of the system as time advances in the $10^{-7}$ m/s model. Figure B23b is the same for the $10^{-5}$ m/s model but there is an error in the final time step.

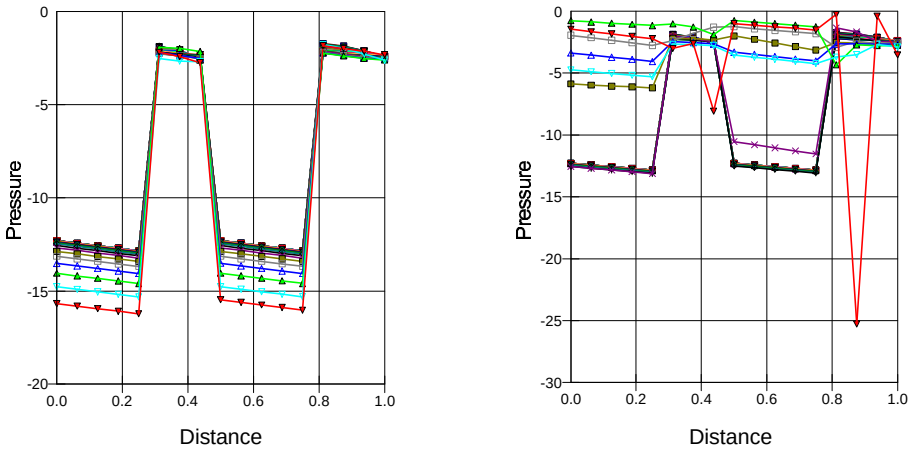


**a** **b**

**Figure B23 Computed Pressure Versus Distance For Each Time Step Across the Center of the Profile for the Transient Analysis Standard Mesh with Applied Fluxes of a) $10^{-7}$ and b) $10^{-5}$ m/s**

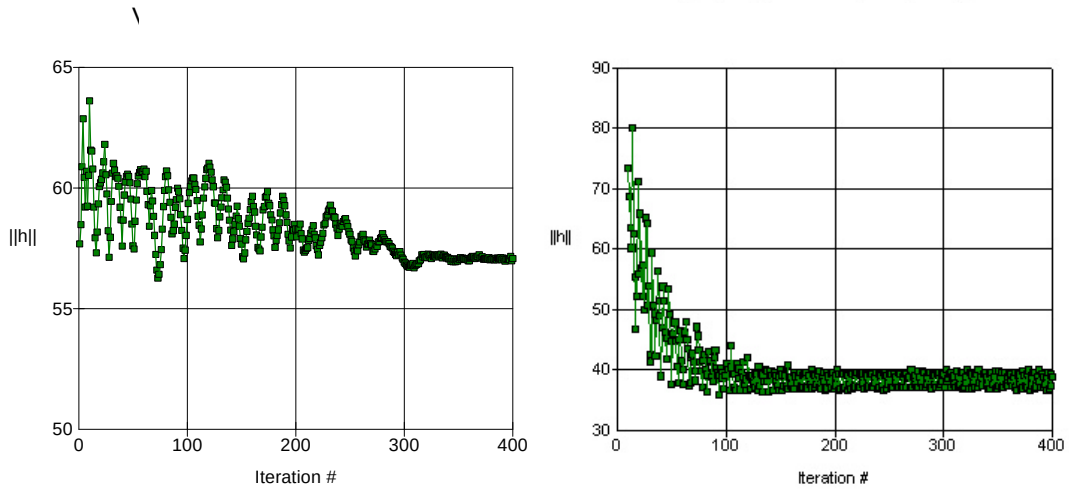


**a** **b**

**Figure B24 Computed Vector Norms vs. Iterations from Time Step #25 of the Transient Analysis Mesh with Applied Fluxes of a) $10^{-7}$ and b) $10^{-5}$ m/s**

The overall results shown in Figures B23 and B24 indicated that the $10^{-7}$ m/s flux model converged while the $10^{-5}$ m/s flux model did not converge. However, inspecting the computed pore-water pressure contours in Figure B22 both models appeared to be incorrect. The $10^{-7}$ m/s model may have required further time steps before reaching steady state and an established solution.

The results of the analysis using the modified mesh are presented in Figures B25 and B26.

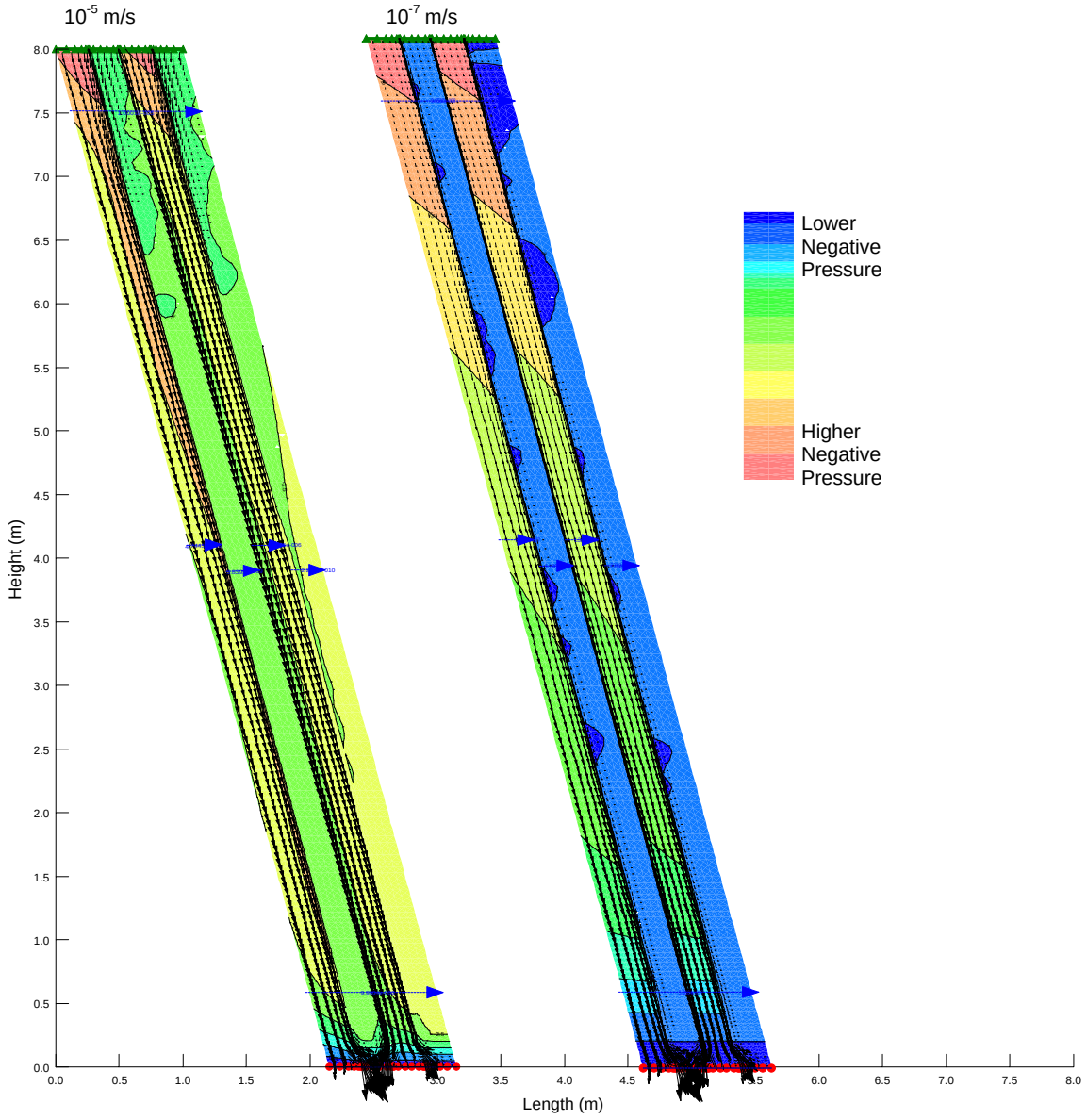


**Figure B25 Computed Pressure Contours and Flow Vectors From the Transient Analysis of the Modified Mesh Showing from Left to Right the Transient Applied Fluxes of $10^{-5}$ and $10^{-7}$ m/s**

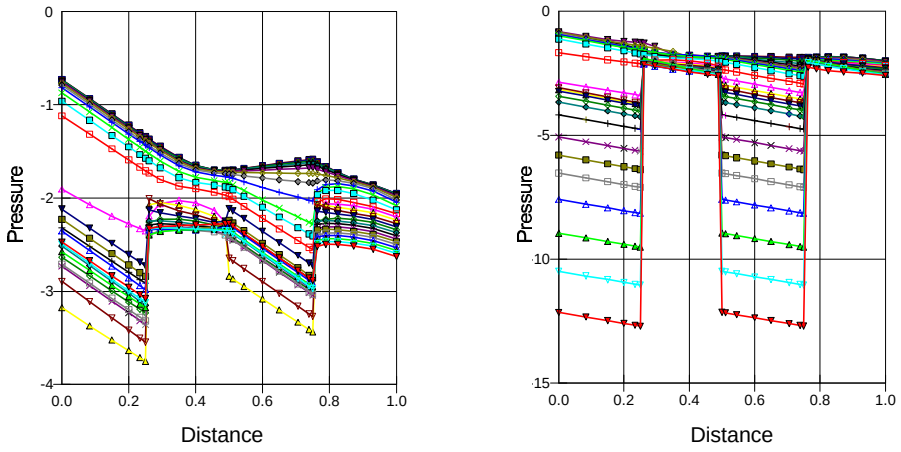


**a** **b**

**Figure B26 Computed Pressure vs. Distance For Each Time Step Across the Center of the Profile for the Transient Analysis Modified Mesh With Applied Fluxes of a) $10^{-5}$ and b) $10^{-7}$ m/s**

The results from the modified mesh showed that both models converged. The results indicated that the transient method could achieve the desired results, however, a steady state was not achieved. The reason why the modified mesh showed improved convergence compared to the standard mesh appeared to be due to the increased number of nodes in the cross-section at the boundary between the coarse and fine-grained layers.

A third transient analysis was conducted for the modified mesh with $10^{-7}$ m/s input fluxes. A boundary function was used to define an input flux that would decrease in value as the solver stepped forward in time. At the final time step, the flux would be equal to $10^{-7}$ m/s. The initial condition was the saturated system, which then drained with respect to time as the boundary function was applied. Figure B27 presents the resulting plots for pressure and volumetric water content versus distance of the cross-section across the center of the system.

The analysis did not reach steady state within the specified number of time steps. The resulting vector norms versus iteration were found to converge for all time steps except the last one, (i.e., time step #25). The flux vectors and pore-water pressure contours for the time step #25 solution was found to be erratic.

Figure B27a showed that the pore-water pressures dropped from 0 kPa to –10 kPa, with the largest changes occurring in the last two time steps. The last time steps showed more than a 5 kPa difference between the second coarse-grained layer and the adjacent fine-grained layers. Figure 5.27b shows the volumetric water content of the layer at 0 kPa. It can be seen that with time the volumetric water content decreased significantly more in the coarse-grained layers due to the steeper SWCC of the material. At the final time step, both coarse-grained layers were at the same volumetric water content but not the same pore-water pressure. Recalling that the material properties specified for the coarse-grained material, (i.e., silica1) were only defined to a pore-water pressure of –4 kPa, hence the calculated –10 kPa pressures in first coarse-grained layer may be the result of the non-convergent vector norms.

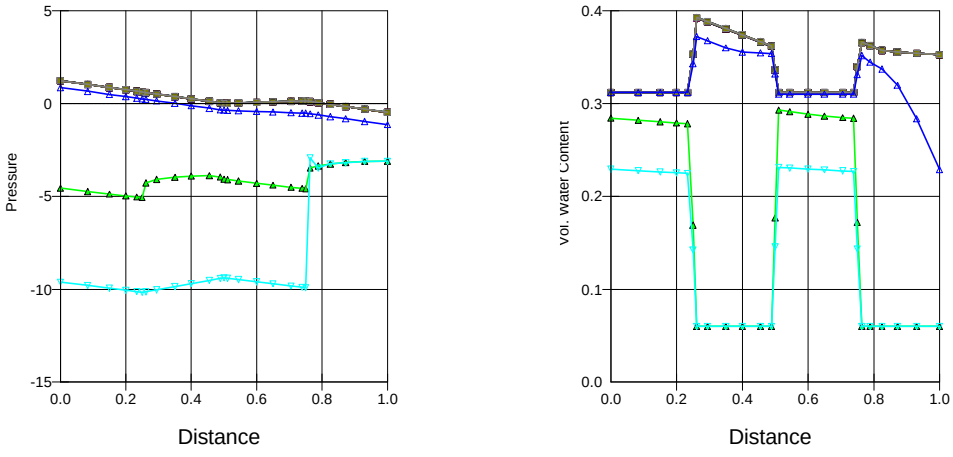


**a** **b**

**Figure B27 Computed Transient Analysis of the Modified Mesh with Applied Fluxes of $10^{-7}$ m/s Across the Center of the Profile a) Pressure vs. Distance b) Volumetric Water Content vs. Distance**

In summary, the overall results of the transient analyses were positive. It was found that difficult steady state problems could be solved with a transient analysis with progressive time steps until the steady state system was achieved. The disadvantage of the method was the amount of computational time involved and the apparent instability of the model, which was observed. The instability appeared to occur towards the last few time steps where the time steps were largest. In addition, verifying the solution for each time step using the transient method was difficult since the calculated conductivities versus material properties cannot be plotted. The only method to verify the result was by analyzing each vector norm versus iteration plot during or after running the model and then viewing the flux vectors and pore-water pressure contours for each time step (i.e., #25 in this case study) to determine if the solution was reasonable.

## B4 Summary, Conclusion and Recommendations

The sensitivity analysis manipulated key parameters for the finite element method/program and discovered which parameters are more critical than others for the purpose of solving the numerical model in terms of convergence and efficiency.

Both the unsuccessful and successful results of the sensitivity analysis provided further insight into numerical modelling and the problem. The first lesson learned was that the efficiency of the model should be improved only after the model becomes solvable. Solutions for the more difficult models could have been obtained earlier if less attention was given to streamlining the model for quicker results. Several specific conclusions are outlined below.

1. Numerical models are extremely sensitive to very large or small numbers. Since the numerical method solves non-linear problems linearly, dividing and/or multiplying by extreme large or small numbers can cause instability in the solver resulting in poor solutions. In addition, variations of the applied flux demonstrated the sensitivity of the model with respect to the calculated

values of hydraulic conductivities. The lower the applied flux, the lower the calculated values of hydraulic conductivities.

2. The convergence criteria proved critical in obtaining a solution to the problem. Insufficient iterations or high rates of change in the solver caused non-converged solutions. However, a tight convergence criterion slowed the solver considerably but produced a reliable solution. The convergence criterion developed for the parametric study appears to be the best for solving the non-linear problem studied.

3. The mesh design showed that changing the internal angle of the elements or using secondary nodes proved only limited improvements for the solution compared to the results for the standard mesh in the parametric study. However, the modified mesh with tighter nodal spacing in areas of higher activity, or removing elements with low flow appeared to have a more direct effect on improving convergence. In general, the removal of elements must be accomplished so as not to disturb the internal flow regime of the system. This implies knowing or previously calculating the result to a certain degree.

4. The material properties specified for the layers were shown to be the most important factor. Reducing the slope of the hydraulic conductivity function can dramatically increase the convergence of the model. However by doing so, the results of the model deviate from the real system being modelled.

5. It was thought that reducing the difference between the fine and coarse-grained material properties could ease convergence. The use of materials with less contrast and/or the use of a transitional material layer with both modified and secondary node meshes resulted in limited improvements. However, different variations, not investigated, may provide better results.

6. The major breakthrough of the sensitivity analysis came with further manipulation of the hydraulic conductivity function for the coarse-grained material. The slope of the function with values of matric suction greater than the air entry value was reduced into three sections with decreasing slope. The first section of the slope was set equal to the original silica2, the second section of the slope was only slightly reduced, and the third section of the slope was inclined to match the hydraulic conductivity function for the fine-grained material. By doing so, the difference between the two functions became a constant. The general principle behind these changes was to ease convergence while not affecting flux in the system significantly (i.e. preferential flow still occurs in the correct distribution and convergence criteria was met).

7. The use of transient modelling was explored. The sensitivity analysis showed that it was possible to step forward in time to reach a steady state solution for the model. However, problems with the time expansion were

observed when the larger time expansions caused instability in the system. The transient modelling proved to be the most inefficient method of solution studied due to the amount of time required to solve a single model.

The input parameters and resulting flux in each layer for all significant models simulated in the sensitivity analysis were tabulated and are presented in the following section.

## B5 Sensitivity Analysis Output

Table B9 presents the results for the flux, convergence, and mesh sensitivity analysis simulations, and Table B10 presents the results for the material and transient sensitivity analysis simulations. Note that the input parameters for the transient simulations were defined in Table B2.

The following material names corresponds with the material properties used in Seep/W and in the tables below (i.e., soil name (hydraulic conductivity number used, SWCC number used)):

- silica1 (13, 13)
- silica 2 (19, 13)
- TP5GS1 (14, 14)
- Beaver Creek sand (8, 8)
- transitional material (20, 19)

The modified hydraulic conductivity functions for the reduced residual hydraulic conductivities used for silica2 were noted in the tables below as follows: Silica2 (19) at residual hydraulic conductivity (R) at the log conductivity of $10^{-9}$ m/s (:9), i.e., 19(R:9). The two reduced sloped functions were defined using two residual values. For example, 19(R:11-12) would indicated that the silica2 function slope was reduced at $10^{-11}$ m/s and then again at $10^{-12}$ m/s.

**Table B9 The Input Parameters and Results of All Significant Models Studied in the Flux, Convergence, and Mesh Sensitivity Analysis**

| | | | | | | Convergence Criteria | | | | | | Materials | | | | | | Flux Results | | | | |
|---|---|---|---|---|---|---|---|---|---|---|---|---|---|---|---|---|---|---|---|---|---|---|
| | | | | | | | | Conductivity Change (in Orders of Magnitude) | | | | | | | | | | | | | | |
| File Name | Height (m) | Slope (Deg) | Mesh Design | TBC (m/s) | BBC (m) | Maximum Iterations | Tolerance (%) | Maximum Change | Rate of Change | Minimum Change | Analysis Control | Coarse Conductivity | Coarse SWCC | Fine Conductivity | Fine SWCC | Transitional Conductivity | Trans. SWCC | 1st Fine | 1st Coarse | 2nd Fine | 2nd Coarse | Convergence Achieved |
| **Flux** | | | | | | | | | | | | | | | | | | | | | | |
| mp20d6q2 | 8 | 90 | Std | 1.00E-03 | 0 | 999 | 1.00E-05 | 0.1 | 1.01 | 1.00E-05 | SS | 19 | 13 | 14 | 14 | 0 | 0 | 1.00 | 60.06 | 1.00 | 38.01 | Y |
| mp20d6q3 | 8 | 90 | Std | 1.00E-07 | 0 | 999 | 1.00E-05 | 0.1 | 1.01 | 1.00E-05 | SS | 19 | 13 | 14 | 14 | 0 | 0 | 34.38 | 0.00 | 65.58 | 0.00 | N |
| mp20d6q4 | 8 | 90 | Std | 1.00E-06 | 0 | 999 | 1.00E-05 | 0.1 | 1.01 | 1.00E-05 | SS | 19 | 13 | 14 | 14 | 0 | 0 | 35.05 | 0.00 | 64.38 | 0.05 | N |
| mp21dq2 | 8 | 85 | Std | 1.00E-03 | 0 | 999 | 1.00E-05 | 0.1 | 1.01 | 1.00E-05 | SS | 19 | 13 | 14 | 14 | 0 | 0 | 1.00 | 63.48 | 1.00 | 34.56 | Y |
| mp21dq3 | 8 | 85 | Std | 1.00E-07 | 0 | 999 | 1.00E-05 | 0.1 | 1.01 | 1.00E-05 | SS | 19 | 13 | 14 | 14 | 0 | 0 | 35.20 | 0.00 | 64.79 | 0.00 | N |
| mp21dq4 | 8 | 85 | Std | 1.00E-06 | 0 | 999 | 1.00E-05 | 0.1 | 1.01 | 1.00E-05 | SS | 19 | 13 | 14 | 14 | 0 | 0 | 35.96 | 0.00 | 60.29 | 2.03 | N |
| mp22dq2 | 8 | 75 | Std | 1.00E-03 | 0 | 999 | 1.00E-05 | 0.1 | 1.01 | 1.00E-05 | SS | 19 | 13 | 14 | 14 | 0 | 0 | 1.00 | 69.56 | 1.00 | 28.47 | Y |
| mp22dq3 | 8 | 75 | Std | 1.00E-07 | 0 | 999 | 1.00E-05 | 0.1 | 1.01 | 1.00E-05 | SS | 19 | 13 | 14 | 14 | 0 | 0 | 37.58 | 0.00 | 62.44 | 0.00 | N |
| mp22dq4 | 8 | 75 | Std | 1.00E-06 | 0 | 999 | 1.00E-05 | 0.1 | 1.01 | 1.00E-05 | SS | 19 | 13 | 14 | 14 | 0 | 0 | 37.62 | 0.00 | 62.19 | 0.05 | N |
| mp23dq2 | 8 | 60 | Std | 1.00E-03 | 0 | 999 | 1.00E-05 | 0.1 | 1.01 | 1.00E-05 | SS | 19 | 13 | 14 | 14 | 0 | 0 | 0.83 | 71.75 | 1.10 | 26.32 | Y |
| mp23dq3 | 8 | 60 | Std | 1.00E-07 | 0 | 999 | 1.00E-05 | 0.1 | 1.01 | 1.00E-05 | SS | 19 | 13 | 14 | 14 | 0 | 0 | 40.17 | 0.00 | 59.81 | 0.00 | N |
| mp23dq4 | 8 | 60 | Std | 1.00E-06 | 0 | 999 | 1.00E-05 | 0.1 | 1.01 | 1.00E-05 | SS | 19 | 13 | 14 | 14 | 0 | 0 | 41.00 | 0.00 | 59.00 | 0.00 | N |
| mp24dq2 | 8 | 45 | Std | 1.00E-03 | 0 | 999 | 1.00E-05 | 0.1 | 1.01 | 1.00E-05 | SS | 19 | 13 | 14 | 14 | 0 | 0 | 0.56 | 90.13 | 1.02 | 8.27 | Y |
| mp24dq3 | 8 | 45 | Std | 1.00E-07 | 0 | 999 | 1.00E-05 | 0.1 | 1.01 | 1.00E-05 | SS | 19 | 13 | 14 | 14 | 0 | 0 | 41.29 | 0.00 | 58.69 | 0.00 | N |
| mp24dq4 | 8 | 45 | Std | 1.00E-06 | 0 | 999 | 1.00E-05 | 0.1 | 1.01 | 1.00E-05 | SS | 19 | 13 | 14 | 14 | 0 | 0 | 44.11 | 0.00 | 55.87 | 0.00 | N |
| **Convergence** | | | | | | | | | | | | | | | | | | | | | | |
| mp21dc1a | 8 | 85 | Std | 1.00E-05 | 0 | 100 | 1 | 1 | 1.1 | 1.00E-04 | SS | 19 | 13 | 14 | 14 | 0 | 0 | 42.20 | 25.20 | 34.50 | 1.10 | N |
| mp21dc3a | 8 | 85 | Std | 1.00E-05 | 0 | 10 | 1.00E+00 | 1 | 1.1 | 1.00E-04 | SS | 19 | 13 | 14 | 14 | 0 | 0 | 0.30 | 92.30 | 0.40 | 6.90 | N |
| mp21dc3b | 8 | 85 | Std | 1.00E-05 | 0 | 100 | 1.00E-01 | 1 | 1.15 | 1.00E-04 | SS | 19 | 13 | 14 | 14 | 0 | 0 | 45.60 | 12.40 | 31.40 | 10.00 | N |
| mp21dc3c | 8 | 85 | Std | 1.00E-05 | 0 | 500 | 1.00E-03 | 0.5 | 1.05 | 1.00E-05 | SS | 19 | 13 | 14 | 14 | 0 | 0 | 54.90 | 2.90 | 43.70 | 0.90 | P |
| mp21dcv1 | 8 | 85 | Std | 1.00E-05 | 0 | 500 | 1.00E-03 | 0.1 | 1.05 | 1.00E-05 | SS | 19 | 13 | 14 | 14 | 0 | 0 | 50.50 | 5.80 | 41.90 | 1.80 | P |
| mp21dcv2 | 8 | 85 | Std | 1.00E-05 | 0 | 500 | 1.00E-03 | 0.1 | 1.01 | 1.00E-05 | SS | 19 | 13 | 14 | 14 | 0 | 0 | 47.50 | 2.90 | 48.30 | 1.20 | Y |
| mp21dcv3 | 8 | 85 | Std | 1.00E-05 | 0 | 500 | 1.00E-03 | 0.1 | 1.01 | 1.00E-05 | SS | 19 | 13 | 14 | 14 | 0 | 0 | 47.50 | 2.90 | 48.30 | 1.20 | Y |
| **Mesh** | | | | | | | | | | | | | | | | | | | | | | |
| meshvt1 | 8 | 75 | Mod | 1.00E-05 | 0 | 999 | 1.00E-05 | 0.1 | 1.01 | 1.00E-05 | SS | 19 | 13 | 14 | 14 | 0 | 0 | 59.20 | 3.50 | 37.20 | 0.10 | Y |
| meshvt1a | 8 | 75 | Mod | 1.00E-06 | 0 | 999 | 1.00E-05 | 0.1 | 1.01 | 1.00E-05 | SS | 19 | 13 | 14 | 14 | 0 | 0 | 42.50 | 0.00 | 57.50 | 0.30 | P |
| meshvt2 | 8 | 75 | Sec | 1.00E-05 | 0 | 999 | 1.00E-05 | 0.1 | 1.01 | 1.00E-05 | SS | 19 | 13 | 14 | 14 | 0 | 0 | 59.10 | 3.40 | 37.40 | 0.00 | Y |
| meshvt2a | 8 | 75 | Sec | 1.00E-06 | 0 | 999 | 1.00E-05 | 0.1 | 1.01 | 1.00E-05 | SS | 19 | 13 | 14 | 14 | 0 | 0 | 41.20 | 0.00 | 58.80 | 0.00 | P |
| meshvt3 | 8 | 75 | Sim | 1.00E-05 | 0 | 999 | 1.00E-05 | 0.1 | 1.01 | 1.00E-05 | SS | 19 | 13 | 14 | 14 | 0 | 0 | 59.22 | 3.46 | 37.28 | 0.03 | Y |
| meshvt3a | 8 | 75 | Sim | 1.00E-06 | 0 | 999 | 1.00E-05 | 0.1 | 1.01 | 1.00E-05 | SS | 19 | 13 | 14 | 14 | 0 | 0 | 38.07 | 0.00 | 61.93 | 0.00 | N |
| meshvt3b | 8 | 75 | Sim | 1.00E-06 | 0 | 999 | 1.00E-05 | 0.1 | 1.01 | 1.00E-05 | SS | 19 | 13 | 14 | 14 | 0 | 0 | 37.01 | 0.00 | 63.00 | 0.00 | N |
| meshvt3c | 8 | 75 | Sim | 1.00E-05 | 0 | 999 | 1.00E-05 | 0.1 | 1.01 | 1.00E-05 | SS | 19 | 13 | 14 | 14 | 0 | 0 | 52.35 | 3.06 | 44.48 | 0.11 | Y |
| meshvt3d | 8 | 75 | Sim | 1.00E-07 | 0 | 999 | 1.00E-05 | 0.1 | 1.01 | 1.00E-05 | SS | 19 | 13 | 14 | 14 | 0 | 0 | 36.95 | 0.00 | 63.17 | 0.00 | N |
| mp24d451 | 8.7 | 45 | @90 | 1.00E-05 | 0 | 999 | 1.00E-05 | 0.1 | 1.01 | 1.00E-05 | SS | 19 | 13 | 14 | 14 | 0 | 0 | 69.20 | 15.60 | 15.30 | 0.00 | Y |
| mp24d453 | 8.7 | 45 | @90 | 1.00E-06 | 0 | 999 | 1.00E-05 | 0.1 | 1.01 | 1.00E-05 | SS | 19 | 13 | 14 | 14 | 0 | 0 | 43.84 | 0.00 | 56.36 | 0.00 | P |
| mp24d454 | 8.7 | 45 | @90 | 1.00E-07 | 0 | 999 | 1.00E-05 | 0.1 | 1.01 | 1.00E-05 | SS | 19 | 13 | 14 | 14 | 0 | 0 | 40.93 | 0.00 | 59.26 | 0.00 | N |
| mp25 | 8 | 75 | Sim | 1.00E-07 | 0 | 999 | 1.00E-05 | 0.1 | 1.01 | 1.00E-05 | SS | 19-MOD | 13 | 14 | 14 | 0 | 0 | 54.52 | 0.00 | 45.48 | 0.00 | N |

**Table B10 The Input Parameters and Results of all Significant Models Studied in the Material and Transient Sensitivity Analysis**

| | | | | | | Convergence Criteria | | | | | | Materials | | | | | | Flux Results | | | | |
|---|---|---|---|---|---|---|---|---|---|---|---|---|---|---|---|---|---|---|---|---|---|---|
| | | | | | | | | Conductivity Change (in Orders of Magnitude) | | | | | | | | | | | | | | |
| File Name | Height (m) | Slope (Deg) | Mesh Design | TBC (m/s) | BBC (m) | Maximum Iterations | Tolerance (%) | Maximum Change | Rate of Change | Minimum Change | Analysis Control | Coarse Conductivity | Coarse SWCC | Fine Conductivity | Fine SWCC | Transitional Conductivity | Trans. SWCC | 1st Fine | 1st Coarse | 2nd Fine | 2nd Coarse | Convergence Achieved |
| **Materials** | | | | | | | | | | | | | | | | | | | | | | |
| mp22dm2 | 8 | 75 | Sec | 1.00E-05 | 0 | 999 | 1.00E-05 | 0.1 | 1.01 | 1.00E-05 | SS | 13 | 13 | 14 | 14 | 0 | 0 | 43.58 | 0.00 | 56.01 | 0.00 | N |
| mp22dm2a | 8 | 75 | Sec | 1.00E-07 | 0 | 999 | 1.00E-05 | 0.1 | 1.01 | 1.00E-05 | SS | 19 | 13 | 14 | 14 | 0 | 0 | 41.89 | 0.00 | 58.14 | 0.00 | N |
| mp22dm2b | 8 | 75 | Sec | 1.00E-05 | 0 | 999 | 1.00E-05 | 0.1 | 1.01 | 1.00E-05 | SS | 19 | 13 | 14 | 14 | 0 | 0 | 59.08 | 3.42 | 37.43 | 0.06 | Y |
| mp22dm2c | 8 | 75 | Sec | 1.00E-05 | 0 | 999 | 1.00E-05 | 0.1 | 1.01 | 1.00E-05 | SS | 13 | 13 | 8 | 8 | 0 | 0 | 41.84 | 0.00 | 58.15 | 0.00 | N |
| mp22dm2d | 8 | 75 | Sec | 1.00E-07 | 0 | 999 | 1.00E-05 | 0.1 | 1.01 | 1.00E-05 | SS | 19 | 13 | 8 | 8 | 0 | 0 | 41.88 | 0.00 | 57.15 | 0.00 | N |
| mp22dm2e | 8 | 75 | Sec | 1.00E-10 | 0 | 999 | 1.00E-05 | 0.1 | 1.01 | 1.00E-05 | SS | 19 | 13 | 8 | 8 | 0 | 0 | 44.36 | 0.00 | 36.58 | 0.00 | N |
| mp22dq3i | 8 | 75 | Std | 1.00E-06 | 0 | 999 | 1.00E-05 | 0.1 | 1.01 | 1.00E-05 | SS | 19(R:11-12) | 13 | 14 | 14 | 0 | 0 | 38.89 | 0.00 | 61.08 | 0.00 | P |
| mp22dq3j | 8 | 75 | Std | 1.00E-07 | 0 | 999 | 1.00E-05 | 0.1 | 1.01 | 1.00E-05 | SS | 19(R:11-12) | 13 | 14 | 14 | 0 | 0 | 37.60 | 0.00 | 62.40 | 0.00 | N |
| mp22dq3k | 8 | 75 | Std | 1.00E-08 | 0 | 999 | 1.00E-05 | 0.1 | 1.01 | 1.00E-05 | SS | 19(R:10-12) | 13 | 14 | 14 | 0 | 0 | 38.97 | 0.00 | 60.98 | 0.00 | Y |
| mp22dq3l | 8 | 75 | Std | 1.00E-07 | 0 | 999 | 1.00E-05 | 0.1 | 1.01 | 1.00E-05 | SS | 19(R:10-12) | 13 | 14 | 14 | 0 | 0 | 38.20 | 0.00 | 61.70 | 0.00 | Y |
| mp22dq3m | 8 | 75 | Std | 1.00E-07 | 0 | 999 | 1.00E-05 | 0.1 | 1.01 | 1.00E-05 | SS | 19(R:8-10) | 13 | 14 | 14 | 0 | 0 | 45.20 | 0.50 | 53.95 | 0.40 | Y |
| mp22dq3n | 8 | 75 | Std | 1.00E-07 | 0 | 999 | 1.00E-05 | 0.1 | 1.01 | 1.00E-05 | SS | 19(R:8-11) | 13 | 14 | 14 | 0 | 0 | 40.00 | 0.00 | 59.90 | 0.00 | Y |
| mp22dq3o | 8 | 75 | Std | 1.00E-07 | 0 | 999 | 1.00E-05 | 0.1 | 1.01 | 1.00E-05 | SS | 19(R:12-14) | 13 | 14 | 14 | 0 | 0 | 37.60 | 0.00 | 62.40 | 0.00 | N |
| mp22dq3u | 8 | 75 | Std | 1.00E-07 | 0 | 999 | 1.00E-05 | 0.1 | 1.01 | 1.00E-05 | SS | 19(R:9) | 13 | 14 | 14 | 0 | 0 | 42.80 | 0.30 | 56.60 | 0.10 | P |
| mp22dq3w | 8 | 75 | Std | 1.00E-07 | 0 | 999 | 1.00E-05 | 0.1 | 1.01 | 1.00E-05 | SS | 19(R:7) | 13 | 14 | 14 | 0 | 0 | 30.90 | 22.10 | 24.50 | 21.80 | Y |
| mp22dq3x | 8 | 75 | Std | 1.00E-07 | 0 | 999 | 1.00E-05 | 0.1 | 1.01 | 1.00E-05 | SS | 19(R:8) | 13 | 14 | 14 | 0 | 0 | 52.60 | 2.40 | 42.70 | 2.30 | Y |
| mp22dq3y | 8 | 75 | Std | 1.00E-07 | 0 | 999 | 1.00E-05 | 1 | 1.01 | 1.00E-05 | SS | 19(R:12) | 13 | 14 | 14 | 0 | 0 | 38.60 | 0.00 | 39.60 | 21.76 | N |
| mp22dq3z | 8 | 75 | Std | 1.00E-07 | 0 | 999 | 1.00E-05 | 0.1 | 1.01 | 1.00E-05 | SS | 19(R:12) | 13 | 14 | 14 | 0 | 0 | 37.10 | 0.00 | 62.30 | 0.00 | N |
| mp22ds1 | 8 | 75 | Std | 1.00E-05 | 0 | 999 | 1.00E-05 | 0.1 | 1.01 | 1.00E-05 | SS | 13 | 13 | 14 | 14 | 0 | 0 | 40.61 | 1.01 | 58.43 | 0.00 | N |
| mp22ds1a | 8 | 75 | Std | 1.00E-05 | 0 | 999 | 1.00E-05 | 0.1 | 1.01 | 1.00E-05 | SS | 13(1a) | 13 | 14 | 14 | 0 | 0 | 48.11 | 0.89 | 50.94 | 0.00 | P |
| mp22ds1b | 8 | 75 | Std | 1.00E-05 | 0 | 999 | 1.00E-05 | 0.1 | 1.01 | 1.00E-05 | SS | 13(1b) | 13 | 14 | 14 | 0 | 0 | 53.93 | 1.32 | 44.65 | 0.02 | Y |
| mp26 | 8 | 75 | Std | 1.00E-07 | 0 | 999 | 1.00E-05 | 0.1 | 1.01 | 1.00E-05 | SS | 19 | 19 | 14 | 14 | 0 | 0 | 37.64 | 0.00 | 62.39 | 0.00 | N |
| mp26a | 8 | 75 | Std | 1.00E-05 | 0 | 999 | 1.00E-05 | 0.1 | 1.01 | 1.00E-05 | SS | 19 | 19 | 14 | 14 | 0 | 0 | 59.30 | 3.70 | 36.98 | 0.00 | Y |
| mp2dm2q3 | 8 | 75 | Std | 1.00E-07 | 0 | 999 | 1.00E-05 | 0.1 | 1.01 | 1.00E-05 | SS | 19 | 13 | 8 | 8 | 0 | 0 | 38.85 | 0.00 | 61.14 | 0.00 | N |
| tranmat | 8 | 75 | Mod | 1.00E-07 | 0 | 999 | 1.00E-05 | 0.1 | 1.01 | 1.00E-05 | SS | 19 | 13 | 14 | 14 | 20 | 19 | 39.56 | 0.49 | 60.11 | 0.13 | N |
| tranmat1 | 8 | 75 | Mod | 1.00E-05 | 0 | 999 | 1.00E-05 | 0.1 | 1.01 | 1.00E-05 | SS | 19 | 13 | 14 | 14 | 20 | 19 | 55.75 | 6.25 | 36.29 | 1.67 | Y |
| tranmat2 | 8 | 75 | Mod | 1.00E-06 | 0 | 999 | 1.00E-05 | 0.1 | 1.01 | 1.00E-05 | SS | 19 | 13 | 14 | 14 | 20 | 19 | 37.17 | 4.20 | 55.82 | 2.78 | N |
| tranmat3 | 8 | 75 | Sec | 1.00E-07 | 0 | 999 | 1.00E-05 | 0.1 | 1.01 | 1.00E-05 | SS | 19 | 13 | 14 | 14 | 20 | 19 | 34.14 | 1.75 | 63.11 | 1.04 | N |
| **Transient** | | | | | | | | | | | | | | | | | | | | | | |
| mp22dhhh | 8 | 75 | Std | 8 m | 0 | 999 | 1.00E-05 | 0.1 | 1.01 | 1.00E-05 | SS | 13 | 13 | 14 | 14 | 0 | 0 | 0.15 | 50.46 | 0.16 | 49.23 | Y |
| mp22dhha | 8 | 75 | Std | 0.00E+00 | 0 | 400 | 1.00E-05 | 1 | 1.05 | 1.00E-05 | Transient | 13 | 13 | 14 | 14 | 0 | 0 | 49.70 | 0.33 | 49.70 | 0.26 | Y |
| mp22dhhb | 8 | 75 | Std | 1.00E-05 | 0 | 400 | 1.00E-05 | 1 | 1.05 | 1.00E-05 | Transient | 13 | 13 | 14 | 14 | 0 | 0 | 48.72 | 0.00 | 51.28 | 0.00 | N |
| mp22dhhc | 8 | 75 | Std | 1.00E-07 | 0 | 400 | 1.00E-05 | 1 | 1.05 | 1.00E-05 | Transient | 13 | 13 | 14 | 14 | 0 | 0 | 3.84 | 0.02 | 4.11 | 92.04 | N |
| mp22dhh1 | 8 | 75 | Mod | 8 m | 0 | 999 | 1.00E-05 | 0.1 | 1.05 | 1.00E-05 | SS | 13 | 13 | 14 | 14 | 0 | 0 | 0.15 | 50.46 | 0.16 | 49.22 | Y |
| mp22dhh2 | 8 | 75 | Mod | 0.00E+00 | 0 | 400 | 1.00E-05 | 1 | 1.05 | 1.00E-05 | Transient | 13 | 13 | 14 | 14 | 0 | 0 | 16.06 | 64.90 | 14.82 | 4.22 | N |
| mp22dhh3 | 8 | 75 | Mod | 1.00E-05 | 0 | 400 | 1.00E-05 | 1 | 1.05 | 1.00E-05 | Transient | 13 | 13 | 14 | 14 | 0 | 0 | 47.46 | 0.04 | 52.50 | 0.00 | Y |
| mp22dhh4 | 8 | 75 | Mod | 1.00E-07 | 0 | 400 | 1.00E-05 | 1 | 1.05 | 1.00E-05 | Transient | 13 | 13 | 14 | 14 | 0 | 0 | 46.68 | 3.97 | 46.74 | 2.61 | Y |

# APPENDIX C

# MODIFIED KISCH SOLUTION

The spreadsheet used to for the finite different method to solve for the modified Kisch solution for preferential flow between two layers is presented in this appendix.

Six models were analyzed using the modified Kisch solution. Three 2-meter systems models were analyzed at 90°, 75°, and 45° with TP5GS1 and silica2 as the fine and coarse materials respectively. Three systems models (one 1.14 and two 2-meter) were analyzed at 90°, 75°, and 45° with beaver creek sand and silica2 as the fine and coarse materials respectively. The input parameters and results of the first set of three models are presented in Tables C1 through C3. The table shows the calculated values for the equations (defined in Chapter 3) at each node for the given elevation. Note that only the top 30 nodes and the bottom 28 nodes are presented for clarity.

The results of the second set of three models are presented in Tables C4 to C6.

## Table C1 The FDM Results for the 90°, 2-Meter System using The Modified Kisch Solution

| # | z | hci | hcp | hp | hfp | hfi | kci | kcp | kc | kf | kfp | kfi | kll | kp | dhp | dhpc | dhpf | l | lcx | lfx | l | dq | qci | qcp | qfi | qfp | q-total |
|---|---|---|---|---|---|---|---|---|---|---|---|---|---|---|---|---|---|---|---|---|---|---|---|---|---|---|---|
| 1 | 0 | 0.00E+00 | #NUM! | 1.00E-04 | #NUM! | 0.00E+00 | 1.48E-02 | #NUM! | 1.48E-02 | 4.50E-05 | #NUM! | 4.50E-05 | 7.42E-03 | #NUM! | -1.87E-02 | -1.87E-02 | -1.45E-02 | -3.73E-01 | 6.76E-04 | 2.22E-01 | 1.35E-03 | #NUM! | 9.97E-07 | #NUM! | 3.03E-09 | #NUM! | 1.00E-05 |
| 2 | 0.019 | 1.87E-02 | 1.32E-02 | 1.88E-02 | 2.81E-01 | 1.45E-02 | 1.46E-02 | -1.39E-06 | 1.46E-02 | 4.46E-05 | 2.14E-05 | 4.50E-05 | 7.34E-03 | -2.98E-06 | -1.87E-02 | -1.87E-02 | -1.45E-02 | -3.73E-01 | 6.83E-04 | 2.22E-01 | 1.36E-03 | 1.53E-08 | 9.97E-07 | -6.97E-08 | 3.03E-09 | 1.07E-06 | 1.00E-05 |
| 3 | 0.037 | 3.74E-02 | 2.81E-01 | 3.74E-02 | 2.81E-01 | 2.91E-02 | 1.45E-02 | 1.67E-06 | 1.45E-02 | 4.35E-05 | 1.83E-05 | 4.40E-05 | 7.25E-03 | 3.06E-06 | -1.87E-02 | -1.87E-02 | -1.44E-02 | -3.73E-01 | 6.91E-04 | 2.27E-01 | 1.38E-03 | 0.00E+00 | 9.97E-07 | 8.35E-08 | 3.00E-09 | 9.16E-07 | 1.00E-05 |
| 4 | 0.056 | 5.61E-02 | 2.81E-01 | 5.61E-02 | 2.81E-01 | 4.35E-02 | 1.34E-02 | 1.67E-06 | 1.34E-02 | 4.25E-05 | 1.83E-05 | 4.32E-05 | 6.74E-03 | 3.06E-06 | -1.87E-02 | -1.87E-02 | -1.44E-02 | -3.73E-01 | 7.44E-04 | 2.31E-01 | 1.48E-03 | 0.00E+00 | 9.97E-07 | 8.35E-08 | 3.15E-09 | 9.16E-07 | 1.00E-05 |
| 5 | 0.075 | 7.47E-02 | 2.81E-01 | 7.48E-02 | 2.81E-01 | 5.79E-02 | 1.11E-02 | 1.67E-06 | 1.11E-02 | 4.16E-05 | 1.83E-05 | 4.24E-05 | 5.57E-03 | 3.06E-06 | -1.87E-02 | -1.87E-02 | -1.43E-02 | -3.73E-01 | 9.00E-04 | 2.36E-01 | 1.79E-03 | 0.00E+00 | 9.96E-07 | 8.35E-08 | 3.73E-09 | 9.16E-07 | 1.00E-05 |
| 6 | 0.094 | 9.34E-02 | 2.81E-01 | 9.35E-02 | 2.81E-01 | 7.22E-02 | 7.43E-03 | 1.67E-06 | 7.42E-03 | 4.06E-05 | 1.83E-05 | 4.17E-05 | 3.73E-03 | 3.06E-06 | -1.86E-02 | -1.87E-02 | -1.42E-02 | -3.73E-01 | 1.35E-03 | 2.40E-01 | 2.68E-03 | 0.00E+00 | 9.95E-07 | 8.35E-08 | 5.44E-09 | 9.16E-07 | 1.00E-05 |
| 7 | 0.112 | 1.12E-01 | 2.81E-01 | 1.12E-01 | 2.81E-01 | 8.64E-02 | 3.92E-03 | 1.67E-06 | 3.92E-03 | 3.84E-05 | 1.83E-05 | 4.10E-05 | 1.98E-03 | 3.06E-06 | -1.86E-02 | -1.87E-02 | -1.41E-02 | -3.72E-01 | 2.55E-03 | 2.44E-01 | 5.06E-03 | 0.00E+00 | 9.90E-07 | 8.35E-08 | 9.72E-09 | 9.16E-07 | 1.00E-05 |
| 8 | 0.131 | 1.31E-01 | 2.81E-01 | 1.31E-01 | 2.81E-01 | 1.01E-01 | 1.63E-03 | 1.67E-06 | 1.63E-03 | 3.54E-05 | 1.83E-05 | 4.03E-05 | 8.33E-04 | 3.06E-06 | -1.85E-02 | -1.86E-02 | -1.41E-02 | -3.70E-01 | 6.14E-03 | 2.48E-01 | 1.20E-02 | 0.00E+00 | 9.79E-07 | 8.35E-08 | 2.13E-08 | 9.16E-07 | 1.00E-05 |
| 9 | 0.15 | 1.49E-01 | 2.81E-01 | 1.49E-01 | 2.81E-01 | 1.15E-01 | 6.13E-04 | 1.67E-06 | 6.19E-04 | 3.27E-05 | 1.83E-05 | 3.80E-05 | 3.26E-04 | 3.06E-06 | -1.81E-02 | -1.84E-02 | -1.38E-02 | -3.63E-01 | 1.63E-02 | 2.63E-01 | 3.07E-02 | 0.00E+00 | 9.50E-07 | 8.35E-08 | 5.01E-08 | 9.16E-07 | 1.00E-05 |
| 10 | 0.168 | 1.68E-01 | 2.81E-01 | 1.67E-01 | 2.81E-01 | 1.28E-01 | 2.61E-04 | 1.67E-06 | 2.66E-04 | 3.02E-05 | 1.83E-05 | 3.58E-05 | 1.48E-04 | 3.06E-06 | -1.74E-02 | -1.80E-02 | -1.35E-02 | -3.49E-01 | 3.83E-02 | 2.79E-01 | 6.75E-02 | 0.00E+00 | 8.98E-07 | 8.35E-08 | 1.02E-07 | 9.16E-07 | 1.00E-05 |
| 11 | 0.187 | 1.86E-01 | 2.81E-01 | 1.85E-01 | 2.81E-01 | 1.42E-01 | 1.11E-04 | 1.67E-06 | 1.17E-04 | 2.79E-05 | 1.83E-05 | 3.37E-05 | 7.24E-05 | 3.06E-06 | -1.61E-02 | -1.70E-02 | -1.32E-02 | -3.22E-01 | 8.98E-02 | 2.96E-01 | 1.38E-01 | 0.00E+00 | 8.07E-07 | 8.35E-08 | 1.93E-07 | 9.16E-07 | 1.00E-05 |
| 12 | 0.206 | 2.03E-01 | 2.81E-01 | 2.01E-01 | 2.81E-01 | 1.55E-01 | 4.82E-05 | 1.67E-06 | 5.29E-05 | 2.60E-05 | 1.83E-05 | 3.18E-05 | 3.94E-05 | 3.06E-06 | -1.40E-02 | -1.48E-02 | -1.28E-02 | -2.79E-01 | 2.07E-01 | 3.14E-01 | 2.54E-01 | 3.18E-24 | 6.70E-07 | 8.35E-08 | 3.30E-07 | 9.16E-07 | 1.00E-05 |
| 13 | 0.224 | 2.18E-01 | 2.81E-01 | 2.15E-01 | 2.81E-01 | 1.68E-01 | 2.32E-05 | 1.67E-06 | 2.66E-05 | 2.45E-05 | 1.83E-05 | 3.01E-05 | 2.55E-05 | 3.06E-06 | -1.14E-02 | -1.07E-02 | -1.25E-02 | -2.28E-01 | 4.30E-01 | 3.32E-01 | 3.92E-01 | 3.18E-24 | 5.21E-07 | 8.35E-08 | 4.79E-07 | 9.16E-07 | 1.00E-05 |
| 14 | 0.243 | 2.28E-01 | 2.81E-01 | 2.26E-01 | 2.81E-01 | 1.80E-01 | 1.38E-05 | 1.67E-06 | 1.52E-05 | 2.33E-05 | 1.83E-05 | 2.85E-05 | 1.92E-05 | 3.06E-06 | -8.98E-03 | -5.11E-03 | -1.21E-02 | -1.80E-01 | 7.27E-01 | 3.51E-01 | 5.20E-01 | 3.18E-24 | 3.95E-07 | 8.35E-08 | 6.05E-07 | 9.16E-07 | 1.00E-05 |
| 15 | 0.262 | 2.33E-01 | 2.81E-01 | 2.35E-01 | 2.81E-01 | 1.92E-01 | 1.07E-05 | 1.67E-06 | 9.85E-06 | 2.24E-05 | 1.83E-05 | 2.70E-05 | 1.61E-05 | 3.06E-06 | -7.10E-03 | -1.22E-03 | -1.18E-02 | -1.42E-01 | 9.35E-01 | 3.70E-01 | 6.20E-01 | 3.18E-24 | 3.06E-07 | 8.35E-08 | 6.94E-07 | 9.16E-07 | 1.00E-05 |
| 16 | 0.281 | 2.35E-01 | 2.81E-01 | 2.42E-01 | 2.81E-01 | 2.04E-01 | 1.01E-05 | 1.67E-06 | 7.47E-06 | 2.17E-05 | 1.83E-05 | 2.57E-05 | 1.46E-05 | 3.06E-06 | -5.88E-03 | -1.86E-04 | -1.14E-02 | -1.18E-01 | 9.90E-01 | 3.90E-01 | 6.85E-01 | 3.18E-24 | 2.56E-07 | 8.35E-08 | 7.44E-07 | 9.16E-07 | 1.00E-05 |
| 17 | 0.299 | 2.35E-01 | 2.81E-01 | 2.48E-01 | 2.81E-01 | 2.16E-01 | 1.00E-05 | 1.67E-06 | 5.94E-06 | 2.12E-05 | 1.83E-05 | 2.44E-05 | 1.35E-05 | 3.06E-06 | -4.90E-03 | -5.14E-05 | -1.10E-02 | -9.79E-02 | 9.97E-01 | 4.10E-01 | 7.38E-01 | 6.36E-24 | 2.19E-07 | 8.35E-08 | 7.81E-07 | 9.16E-07 | 1.00E-05 |
| 18 | 0.318 | 2.35E-01 | 2.81E-01 | 2.53E-01 | 2.81E-01 | 2.27E-01 | 1.00E-05 | 1.67E-06 | 4.91E-06 | 2.07E-05 | 1.83E-05 | 2.32E-05 | 1.28E-05 | 3.06E-06 | -4.10E-03 | -1.40E-05 | -1.07E-02 | -8.20E-02 | 9.99E-01 | 4.30E-01 | 7.81E-01 | 6.36E-24 | 1.92E-07 | 8.35E-08 | 8.08E-07 | 9.16E-07 | 1.00E-05 |
| 19 | 0.337 | 2.35E-01 | 2.81E-01 | 2.57E-01 | 2.81E-01 | 2.37E-01 | 1.00E-05 | 1.67E-06 | 4.19E-06 | 2.03E-05 | 1.83E-05 | 2.22E-05 | 1.23E-05 | 3.06E-06 | -3.45E-03 | -3.82E-06 | -1.03E-02 | -6.90E-02 | 1.00E+00 | 4.51E-01 | 8.16E-01 | 9.53E-24 | 1.71E-07 | 8.35E-08 | 8.29E-07 | 9.16E-07 | 1.00E-05 |
| 20 | 0.355 | 2.35E-01 | 2.81E-01 | 2.61E-01 | 2.81E-01 | 2.48E-01 | 1.00E-05 | 1.67E-06 | 3.66E-06 | 2.00E-05 | 1.83E-05 | 2.12E-05 | 1.18E-05 | 3.06E-06 | -2.91E-03 | -1.04E-06 | -9.88E-03 | -5.82E-02 | 1.00E+00 | 4.72E-01 | 8.44E-01 | 9.53E-24 | 1.55E-07 | 8.35E-08 | 8.45E-07 | 9.16E-07 | 1.00E-05 |
| 21 | 0.374 | 2.35E-01 | 2.81E-01 | 2.64E-01 | 2.81E-01 | 2.58E-01 | 1.00E-05 | 1.67E-06 | 3.27E-06 | 1.98E-05 | 1.83E-05 | 2.03E-05 | 1.15E-05 | 3.06E-06 | -2.47E-03 | -2.83E-07 | -9.49E-03 | -4.94E-02 | 1.00E+00 | 4.93E-01 | 8.68E-01 | 9.53E-24 | 1.42E-07 | 8.35E-08 | 8.58E-07 | 9.16E-07 | 1.00E-05 |
| 22 | 0.393 | 2.35E-01 | 2.81E-01 | 2.66E-01 | 2.81E-01 | 2.67E-01 | 1.00E-05 | 1.67E-06 | 2.97E-06 | 1.96E-05 | 1.83E-05 | 1.95E-05 | 1.13E-05 | 3.06E-06 | -2.10E-03 | -7.69E-08 | -9.10E-03 | -4.20E-02 | 1.00E+00 | 5.13E-01 | 8.88E-01 | 1.59E-23 | 1.32E-07 | 8.35E-08 | 8.68E-07 | 9.16E-07 | 1.00E-05 |
| 23 | 0.411 | 2.35E-01 | 2.81E-01 | 2.68E-01 | 2.81E-01 | 2.76E-01 | 1.00E-05 | 1.67E-06 | 2.74E-06 | 1.94E-05 | 1.83E-05 | 1.87E-05 | 1.11E-05 | 3.06E-06 | -1.79E-03 | -2.09E-08 | -8.71E-03 | -3.58E-02 | 1.00E+00 | 5.34E-01 | 9.04E-01 | 1.59E-23 | 1.24E-07 | 8.35E-08 | 8.76E-07 | 9.16E-07 | 1.00E-05 |
| 24 | 0.43 | 2.35E-01 | 2.81E-01 | 2.70E-01 | 2.81E-01 | 2.85E-01 | 1.00E-05 | 1.67E-06 | 2.55E-06 | 1.92E-05 | 1.83E-05 | 1.80E-05 | 1.09E-05 | 3.06E-06 | -1.53E-03 | -5.69E-09 | -8.31E-03 | -3.06E-02 | 1.00E+00 | 5.55E-01 | 9.18E-01 | 5.72E-23 | 1.17E-07 | 8.35E-08 | 8.83E-07 | 9.16E-07 | 1.00E-05 |
| 25 | 0.449 | 2.35E-01 | 2.81E-01 | 2.71E-01 | 2.81E-01 | 2.93E-01 | 1.00E-05 | 1.67E-06 | 2.40E-06 | 1.91E-05 | 1.83E-05 | 1.74E-05 | 1.08E-05 | 3.06E-06 | -1.31E-03 | -1.55E-09 | -7.93E-03 | -2.62E-02 | 1.00E+00 | 5.76E-01 | 9.30E-01 | 6.67E-23 | 1.12E-07 | 8.35E-08 | 8.88E-07 | 9.16E-07 | 1.00E-05 |
| 26 | 0.468 | 2.35E-01 | 2.81E-01 | 2.73E-01 | 2.81E-01 | 3.01E-01 | 1.00E-05 | 1.67E-06 | 2.28E-06 | 1.90E-05 | 1.83E-05 | 1.68E-05 | 1.06E-05 | 3.06E-06 | -1.12E-03 | -4.21E-10 | -7.54E-03 | -2.24E-02 | 1.00E+00 | 5.97E-01 | 9.40E-01 | 1.14E-22 | 1.07E-07 | 8.35E-08 | 8.93E-07 | 9.16E-07 | 1.00E-05 |
| 27 | 0.486 | 2.35E-01 | 2.81E-01 | 2.74E-01 | 2.81E-01 | 3.09E-01 | 1.00E-05 | 1.67E-06 | 2.19E-06 | 1.89E-05 | 1.83E-05 | 1.62E-05 | 1.05E-05 | 3.06E-06 | -9.62E-04 | -1.14E-10 | -7.16E-03 | -1.92E-02 | 1.00E+00 | 6.17E-01 | 9.49E-01 | 1.37E-22 | 1.04E-07 | 8.35E-08 | 8.96E-07 | 9.16E-07 | 1.00E-05 |
| 28 | 0.505 | 2.35E-01 | 2.81E-01 | 2.75E-01 | 2.81E-01 | 3.16E-01 | 1.00E-05 | 1.67E-06 | 2.11E-06 | 1.88E-05 | 1.83E-05 | 1.57E-05 | 1.05E-05 | 3.06E-06 | -8.27E-04 | -3.11E-11 | -6.79E-03 | -1.65E-02 | 1.00E+00 | 6.37E-01 | 9.56E-01 | 2.00E-22 | 1.01E-07 | 8.35E-08 | 8.99E-07 | 9.16E-07 | 1.00E-05 |
| 29 | 0.524 | 2.35E-01 | 2.81E-01 | 2.76E-01 | 2.81E-01 | 3.23E-01 | 1.00E-05 | 1.67E-06 | 2.04E-06 | 1.87E-05 | 1.83E-05 | 1.52E-05 | 1.04E-05 | 3.06E-06 | -7.11E-04 | -8.46E-12 | -6.43E-03 | -1.42E-02 | 1.00E+00 | 6.56E-01 | 9.62E-01 | 3.05E-22 | 9.81E-08 | 8.35E-08 | 9.02E-07 | 9.16E-07 | 1.00E-05 |
| 30 | 0.542 | 2.35E-01 | 2.81E-01 | 2.76E-01 | 2.81E-01 | 3.29E-01 | 1.00E-05 | 1.67E-06 | 1.98E-06 | 1.87E-05 | 1.83E-05 | 1.48E-05 | 1.03E-05 | 3.06E-06 | -6.11E-04 | -2.30E-12 | -6.08E-03 | -1.22E-02 | 1.00E+00 | 6.75E-01 | 9.67E-01 | 4.39E-22 | 9.60E-08 | 8.35E-08 | 9.04E-07 | 9.16E-07 | 1.00E-05 |
| 81 | 1.496 | 2.35E-01 | 2.81E-01 | 2.81E-01 | 2.81E-01 | 4.17E-01 | 1.00E-05 | 1.67E-06 | 1.67E-06 | 1.83E-05 | 1.83E-05 | 1.01E-05 | 1.00E-05 | 3.06E-06 | -3.34E-07 | 0.00E+00 | -1.12E-04 | -6.69E-06 | 1.00E+00 | 9.94E-01 | 1.00E+00 | 1.28E-13 | 8.35E-08 | 8.35E-08 | 9.16E-07 | 9.16E-07 | 1.00E-05 |
| 82 | 1.515 | 2.35E-01 | 2.81E-01 | 2.81E-01 | 2.81E-01 | 4.17E-01 | 1.00E-05 | 1.67E-06 | 1.67E-06 | 1.83E-05 | 1.83E-05 | 1.01E-05 | 1.00E-05 | 3.06E-06 | -2.89E-07 | 0.00E+00 | -1.03E-04 | -5.78E-06 | 1.00E+00 | 9.94E-01 | 1.00E+00 | 1.87E-13 | 8.35E-08 | 8.35E-08 | 9.16E-07 | 9.16E-07 | 1.00E-05 |
| 83 | 1.533 | 2.35E-01 | 2.81E-01 | 2.81E-01 | 2.81E-01 | 4.17E-01 | 1.00E-05 | 1.67E-06 | 1.67E-06 | 1.83E-05 | 1.83E-05 | 1.01E-05 | 1.00E-05 | 3.06E-06 | -2.49E-07 | 0.00E+00 | -9.44E-05 | -4.99E-06 | 1.00E+00 | 9.95E-01 | 1.00E+00 | 2.75E-13 | 8.35E-08 | 8.35E-08 | 9.16E-07 | 9.16E-07 | 1.00E-05 |
| 84 | 1.552 | 2.35E-01 | 2.81E-01 | 2.81E-01 | 2.81E-01 | 4.17E-01 | 1.00E-05 | 1.67E-06 | 1.67E-06 | 1.83E-05 | 1.83E-05 | 1.00E-05 | 1.00E-05 | 3.06E-06 | -2.15E-07 | 0.00E+00 | -8.67E-05 | -4.31E-06 | 1.00E+00 | 9.95E-01 | 1.00E+00 | 4.03E-13 | 8.35E-08 | 8.35E-08 | 9.16E-07 | 9.16E-07 | 1.00E-05 |
| 85 | 1.571 | 2.35E-01 | 2.81E-01 | 2.81E-01 | 2.81E-01 | 4.17E-01 | 1.00E-05 | 1.67E-06 | 1.67E-06 | 1.83E-05 | 1.83E-05 | 1.00E-05 | 1.00E-05 | 3.06E-06 | -1.86E-07 | 0.00E+00 | -7.95E-05 | -3.72E-06 | 1.00E+00 | 9.96E-01 | 1.00E+00 | 5.90E-13 | 8.35E-08 | 8.35E-08 | 9.16E-07 | 9.16E-07 | 1.00E-05 |
| 86 | 1.59 | 2.35E-01 | 2.81E-01 | 2.81E-01 | 2.81E-01 | 4.17E-01 | 1.00E-05 | 1.67E-06 | 1.67E-06 | 1.83E-05 | 1.83E-05 | 1.00E-05 | 1.00E-05 | 3.06E-06 | -1.61E-07 | 0.00E+00 | -7.30E-05 | -3.21E-06 | 1.00E+00 | 9.96E-01 | 1.00E+00 | 8.64E-13 | 8.35E-08 | 8.35E-08 | 9.16E-07 | 9.16E-07 | 1.00E-05 |
| 87 | 1.608 | 2.35E-01 | 2.81E-01 | 2.81E-01 | 2.81E-01 | 4.17E-01 | 1.00E-05 | 1.67E-06 | 1.67E-06 | 1.83E-05 | 1.83E-05 | 1.00E-05 | 1.00E-05 | 3.06E-06 | -1.39E-07 | 0.00E+00 | -6.70E-05 | -2.77E-06 | 1.00E+00 | 9.96E-01 | 1.00E+00 | 1.27E-12 | 8.35E-08 | 8.35E-08 | 9.16E-07 | 9.16E-07 | 1.00E-05 |
| 88 | 1.627 | 2.35E-01 | 2.81E-01 | 2.81E-01 | 2.81E-01 | 4.17E-01 | 1.00E-05 | 1.67E-06 | 1.67E-06 | 1.83E-05 | 1.83E-05 | 1.00E-05 | 1.00E-05 | 3.06E-06 | -1.20E-07 | 0.00E+00 | -6.15E-05 | -2.39E-06 | 1.00E+00 | 9.97E-01 | 1.00E+00 | 1.86E-12 | 8.35E-08 | 8.36E-08 | 9.16E-07 | 9.16E-07 | 1.00E-05 |
| 89 | 1.646 | 2.35E-01 | 2.81E-01 | 2.81E-01 | 2.81E-01 | 4.17E-01 | 1.00E-05 | 1.67E-06 | 1.67E-06 | 1.83E-05 | 1.83E-05 | 1.00E-05 | 1.00E-05 | 3.06E-06 | -1.03E-07 | 0.00E+00 | -5.64E-05 | -2.07E-06 | 1.00E+00 | 9.97E-01 | 1.00E+00 | 2.72E-12 | 8.35E-08 | 8.36E-08 | 9.16E-07 | 9.16E-07 | 1.00E-05 |
| 90 | 1.664 | 2.35E-01 | 2.81E-01 | 2.81E-01 | 2.81E-01 | 4.17E-01 | 1.00E-05 | 1.67E-06 | 1.67E-06 | 1.83E-05 | 1.83E-05 | 1.00E-05 | 1.00E-05 | 3.06E-06 | -8.92E-08 | 0.00E+00 | -5.18E-05 | -1.78E-06 | 1.00E+00 | 9.97E-01 | 1.00E+00 | 3.99E-12 | 8.35E-08 | 8.36E-08 | 9.16E-07 | 9.16E-07 | 1.00E-05 |
| 91 | 1.683 | 2.35E-01 | 2.81E-01 | 2.81E-01 | 2.81E-01 | 4.17E-01 | 1.00E-05 | 1.67E-06 | 1.67E-06 | 1.83E-05 | 1.83E-05 | 1.00E-05 | 1.00E-05 | 3.07E-06 | -7.71E-08 | 0.00E+00 | -4.75E-05 | -1.54E-06 | 0.00E+00 | -9.50E-04 | 1.00E+00 | 5.85E-12 | 8.35E-08 | 8.36E-08 | 9.16E-07 | 9.16E-07 | 1.00E-05 |
| 92 | 1.702 | 2.35E-01 | 2.81E-01 | 2.81E-01 | 2.81E-01 | 4.17E-01 | 1.00E-05 | 1.67E-06 | 1.67E-06 | 1.83E-05 | 1.83E-05 | 1.00E-05 | 1.00E-05 | 3.07E-06 | -6.65E-08 | 0.00E+00 | -4.36E-05 | -1.33E-06 | 0.00E+00 | -8.72E-04 | 1.00E+00 | 8.59E-12 | 8.35E-08 | 8.37E-08 | 9.16E-07 | 9.16E-07 | 1.00E-05 |
| 93 | 1.72 | 2.35E-01 | 2.81E-01 | 2.81E-01 | 2.81E-01 | 4.17E-01 | 1.00E-05 | 1.68E-06 | 1.67E-06 | 1.83E-05 | 1.83E-05 | 1.00E-05 | 1.00E-05 | 3.07E-06 | -5.75E-08 | 0.00E+00 | -4.00E-05 | -1.15E-06 | 0.00E+00 | -8.00E-04 | 1.00E+00 | 1.26E-11 | 8.35E-08 | 8.38E-08 | 9.16E-07 | 9.16E-07 | 1.00E-05 |
| 94 | 1.739 | 2.35E-01 | 2.81E-01 | 2.81E-01 | 2.81E-01 | 4.17E-01 | 1.00E-05 | 1.68E-06 | 1.67E-06 | 1.83E-05 | 1.83E-05 | 1.00E-05 | 1.00E-05 | 3.07E-06 | -4.96E-08 | 0.00E+00 | -3.67E-05 | -9.92E-07 | 0.00E+00 | -7.34E-04 | 1.00E+00 | 1.86E-11 | 8.35E-08 | 8.39E-08 | 9.16E-07 | 9.16E-07 | 1.00E-05 |
| 95 | 1.758 | 2.35E-01 | 2.81E-01 | 2.81E-01 | 2.81E-01 | 4.18E-01 | 1.00E-05 | 1.68E-06 | 1.67E-06 | 1.83E-05 | 1.83E-05 | 1.00E-05 | 1.00E-05 | 3.08E-06 | -4.28E-08 | 0.00E+00 | -3.37E-05 | -8.57E-07 | 0.00E+00 | -6.73E-04 | 1.00E+00 | 2.73E-11 | 8.35E-08 | 8.41E-08 | 9.16E-07 | 9.16E-07 | 1.00E-05 |
| 96 | 1.777 | 2.35E-01 | 2.80E-01 | 2.81E-01 | 2.81E-01 | 4.18E-01 | 1.00E-05 | 1.69E-06 | 1.67E-06 | 1.83E-05 | 1.83E-05 | 1.00E-05 | 1.00E-05 | 3.09E-06 | -3.70E-08 | 0.00E+00 | -3.09E-05 | -7.40E-07 | 0.00E+00 | -6.18E-04 | 1.00E+00 | 4.04E-11 | 8.35E-08 | 8.44E-08 | 9.16E-07 | 9.16E-07 | 1.00E-05 |
| 97 | 1.795 | 2.35E-01 | 2.80E-01 | 2.81E-01 | 2.81E-01 | 4.18E-01 | 1.00E-05 | 1.70E-06 | 1.67E-06 | 1.83E-05 | 1.83E-05 | 1.00E-05 | 1.00E-05 | 3.10E-06 | -3.19E-08 | 0.00E+00 | -2.83E-05 | -6.39E-07 | 0.00E+00 | -5.67E-04 | 1.00E+00 | 5.98E-11 | 8.35E-08 | 8.48E-08 | 9.16E-07 | 9.15E-07 | 1.00E-05 |
| 98 | 1.814 | 2.35E-01 | 2.80E-01 | 2.81E-01 | 2.81E-01 | 4.18E-01 | 1.00E-05 | 1.71E-06 | 1.67E-06 | 1.83E-05 | 1.83E-05 | 1.00E-05 | 1.00E-05 | 3.12E-06 | -2.76E-08 | 0.00E+00 | -2.60E-05 | -5.52E-07 | 0.00E+00 | -5.20E-04 | 1.00E+00 | 8.91E-11 | 8.35E-08 | 8.54E-08 | 9.16E-07 | 9.15E-07 | 1.00E-05 |
| 99 | 1.833 | 2.35E-01 | 2.80E-01 | 2.81E-01 | 2.82E-01 | 4.18E-01 | 1.00E-05 | 1.73E-06 | 1.67E-06 | 1.83E-05 | 1.83E-05 | 1.00E-05 | 1.00E-05 | 3.15E-06 | -2.38E-08 | 0.00E+00 | -2.39E-05 | -4.76E-07 | 0.00E+00 | -4.77E-04 | 1.00E+00 | 1.34E-10 | 8.35E-08 | 8.63E-08 | 9.16E-07 | 9.14E-07 | 1.00E-05 |
| 100 | 1.851 | 2.35E-01 | 2.79E-01 | 2.81E-01 | 2.82E-01 | 4.18E-01 | 1.00E-05 | 1.75E-06 | 1.67E-06 | 1.83E-05 | 1.82E-05 | 1.00E-05 | 1.00E-05 | 3.20E-06 | -2.06E-08 | 0.00E+00 | -2.19E-05 | -4.11E-07 | 0.00E+00 | -4.38E-04 | 1.00E+00 | 2.03E-10 | 8.35E-08 | 8.76E-08 | 9.16E-07 | 9.12E-07 | 1.00E-05 |
| 101 | 1.87 | 2.35E-01 | 2.78E-01 | 2.81E-01 | 2.83E-01 | 4.18E-01 | 1.00E-05 | 1.79E-06 | 1.67E-06 | 1.83E-05 | 1.82E-05 | 1.00E-05 | 1.00E-05 | 3.26E-06 | -1.78E-08 | 0.00E+00 | -2.01E-05 | -3.55E-07 | 0.00E+00 | -4.02E-04 | 1.00E+00 | 3.15E-10 | 8.35E-08 | 8.96E-08 | 9.16E-07 | 9.10E-07 | 1.00E-05 |
| 102 | 1.889 | 2.35E-01 | 2.77E-01 | 2.81E-01 | 2.84E-01 | 4.18E-01 | 1.00E-05 | 1.86E-06 | 1.67E-06 | 1.83E-05 | 1.81E-05 | 1.00E-05 | 1.00E-05 | 3.37E-06 | -1.53E-08 | 0.00E+00 | -1.84E-05 | -3.07E-07 | 0.00E+00 | -3.69E-04 | 1.00E+00 | 5.03E-10 | 8.35E-08 | 9.28E-08 | 9.16E-07 | 9.07E-07 | 1.00E-05 |
| 103 | 1.907 | 2.35E-01 | 2.75E-01 | 2.81E-01 | 2.86E-01 | 4.18E-01 | 1.00E-05 | 1.96E-06 | 1.67E-06 | 1.83E-05 | 1.80E-05 | 1.00E-05 | 1.00E-05 | 3.53E-06 | -1.32E-08 | 0.00E+00 | -1.69E-05 | -2.65E-07 | 0.00E+00 | -3.38E-04 | 1.00E+00 | 8.43E-10 | 8.35E-08 | 9.78E-08 | 9.16E-07 | 9.02E-07 | 1.00E-05 |
| 104 | 1.926 | 2.35E-01 | 2.71E-01 | 2.81E-01 | 2.90E-01 | 4.18E-01 | 1.00E-05 | 2.13E-06 | 1.67E-06 | 1.83E-05 | 1.79E-05 | 1.00E-05 | 1.00E-05 | 3.80E-06 | -1.14E-08 | 0.00E+00 | -1.55E-05 | -2.29E-07 | 0.00E+00 | -3.10E-04 | 1.00E+00 | 1.54E-09 | 8.35E-08 | 1.06E-07 | 9.16E-07 | 8.94E-07 | 1.00E-05 |
| 105 | 1.945 | 2.35E-01 | 2.65E-01 | 2.81E-01 | 2.99E-01 | 4.18E-01 | 1.00E-05 | 2.43E-06 | 1.67E-06 | 1.83E-05 | 1.76E-05 | 1.00E-05 | 1.00E-05 | 4.27E-06 | -9.87E-09 | 0.00E+00 | -1.42E-05 | -1.97E-07 | 0.00E+00 | -2.85E-04 | 1.00E+00 | 3.39E-09 | 8.35E-08 | 1.22E-07 | 9.16E-07 | 8.78E-07 | 1.00E-05 |
| 106 | 1.964 | 2.35E-01 | 2.41E-01 | 2.81E-01 | 3.75E-01 | 4.18E-01 | 1.00E-05 | 3.11E-06 | 1.67E-06 | 1.83E-05 | 1.69E-05 | 1.00E-05 | 1.00E-05 | 5.26E-06 | -8.52E-09 | 0.00E+00 | -1.31E-05 | -1.70E-07 | 0.00E+00 | -2.61E-04 | 1.00E+00 | 2.40E-08 | 8.35E-08 | 1.56E-07 | 9.16E-07 | 8.44E-07 | 1.00E-05 |
| 107 | 1.982 | 2.35E-01 | 2.35E-01 | 2.81E-01 | 4.18E-01 | 4.18E-01 | 1.00E-05 | 7.90E-06 | 1.67E-06 | 1.83E-05 | 1.21E-05 | 1.00E-05 | 1.00E-05 | 9.56E-06 | -7.36E-09 | 0.00E+00 | -1.20E-05 | -1.47E-07 | 0.00E+00 | -2.40E-04 | 1.00E+00 | 1.05E-08 | 8.35E-08 | 3.95E-07 | 9.16E-07 | 6.05E-07 | 1.00E-05 |
| 108 | 2.001 | 2.35E-01 | 2.35E-01 | 2.81E-01 | 4.18E-01 | 4.18E-01 | 1.00E-05 | 1.00E-05 | 1.67E-06 | 1.83E-05 | 1.00E-05 | 1.00E-05 | 1.00E-05 | 3.06E-06 | -6.36E-09 | 0.00E+00 | -1.10E-05 | -1.27E-07 | 2.99E-01 | 2.73E-02 | 1.00E+00 | 0 | 8.35E-08 | 5.00E-07 | 9.16E-07 | 5.00E-07 | 1.00E-05 |

## Table C2 The FDM Results for the 75°, 2-Meter System using The Modified Kisch Solution

| # | z | hci | hcp | hp | hfp | hfi | kci | kcp | kc | kf | kfp | kfi | kll | kp | dhp | dhpc | dhpf | I | Icx | Ifx | I | dq | qci | qcp | qfi | qfp | q-total |
|---|---|---|---|---|---|---|---|---|---|---|---|---|---|---|---|---|---|---|---|---|---|---|---|---|---|---|---|
| 1 | 0 | 0.00E+00 | #NUM! | 1.00E-04 | #NUM! | 0.00E+00 | 1.48E-02 | #NUM! | 1.48E-02 | 4.50E-05 | #NUM! | 4.50E-05 | 7.42E-03 | #NUM! | -1.87E-02 | -1.87E-02 | -1.44E-02 | -3.73E-01 | 6.76E-04 | 2.22E-01 | 1.35E-03 | #NUM! | 9.97E-07 | #NUM! | 3.03E-09 | #NUM! | 1.00E-05 |
| 2 | 0.019 | 1.87E-02 | 1.32E-02 | 1.88E-02 | 2.76E-01 | 1.44E-02 | 1.46E-02 | -1.68E-06 | 1.46E-02 | 4.46E-05 | 2.24E-05 | 4.50E-05 | 7.34E-03 | -3.63E-06 | -1.87E-02 | -1.87E-02 | -1.44E-02 | -3.73E-01 | 6.83E-04 | 2.22E-01 | 1.36E-03 | 1.78E-08 | 9.97E-07 | -8.11E-08 | 3.03E-09 | 1.08E-06 | 1.00E-05 |
| 3 | 0.037 | 3.74E-02 | 2.76E-01 | 3.74E-02 | 2.76E-01 | 2.88E-02 | 1.45E-02 | 2.00E-06 | 1.45E-02 | 4.35E-05 | 1.87E-05 | 4.40E-05 | 7.25E-03 | 3.61E-06 | -1.87E-02 | -1.87E-02 | -1.43E-02 | -3.73E-01 | 6.91E-04 | 2.27E-01 | 1.38E-03 | 0.00E+00 | 9.97E-07 | 9.65E-08 | 3.00E-09 | 9.03E-07 | 1.00E-05 |
| 4 | 0.056 | 5.61E-02 | 2.76E-01 | 5.61E-02 | 2.76E-01 | 4.31E-02 | 1.34E-02 | 2.00E-06 | 1.34E-02 | 4.25E-05 | 1.87E-05 | 4.32E-05 | 6.74E-03 | 3.61E-06 | -1.87E-02 | -1.87E-02 | -1.42E-02 | -3.73E-01 | 7.44E-04 | 2.31E-01 | 1.48E-03 | 0.00E+00 | 9.97E-07 | 9.65E-08 | 3.15E-09 | 9.03E-07 | 1.00E-05 |
| 5 | 0.075 | 7.47E-02 | 2.76E-01 | 7.48E-02 | 2.76E-01 | 5.73E-02 | 1.11E-02 | 2.00E-06 | 1.11E-02 | 4.16E-05 | 1.87E-05 | 4.25E-05 | 5.57E-03 | 3.61E-06 | -1.87E-02 | -1.87E-02 | -1.41E-02 | -3.73E-01 | 9.00E-04 | 2.35E-01 | 1.79E-03 | 0.00E+00 | 9.96E-07 | 9.65E-08 | 3.73E-09 | 9.03E-07 | 1.00E-05 |
| 6 | 0.094 | 9.34E-02 | 2.76E-01 | 9.35E-02 | 2.76E-01 | 7.15E-02 | 7.43E-03 | 2.00E-06 | 7.42E-03 | 4.06E-05 | 1.87E-05 | 4.17E-05 | 3.73E-03 | 3.61E-06 | -1.86E-02 | -1.87E-02 | -1.41E-02 | -3.73E-01 | 1.35E-03 | 2.40E-01 | 2.68E-03 | 0.00E+00 | 9.95E-07 | 9.65E-08 | 5.44E-09 | 9.03E-07 | 1.00E-05 |
| 7 | 0.112 | 1.12E-01 | 2.76E-01 | 1.12E-01 | 2.76E-01 | 8.55E-02 | 3.92E-03 | 2.00E-06 | 3.92E-03 | 3.84E-05 | 1.87E-05 | 4.10E-05 | 1.98E-03 | 3.61E-06 | -1.86E-02 | -1.87E-02 | -1.40E-02 | -3.72E-01 | 2.55E-03 | 2.44E-01 | 5.05E-03 | 0.00E+00 | 9.90E-07 | 9.65E-08 | 9.72E-09 | 9.03E-07 | 1.00E-05 |
| 8 | 0.131 | 1.31E-01 | 2.76E-01 | 1.31E-01 | 2.76E-01 | 9.95E-02 | 1.63E-03 | 2.00E-06 | 1.63E-03 | 3.54E-05 | 1.87E-05 | 4.03E-05 | 8.33E-04 | 3.61E-06 | -1.85E-02 | -1.86E-02 | -1.39E-02 | -3.69E-01 | 6.14E-03 | 2.48E-01 | 1.20E-02 | 0.00E+00 | 9.79E-07 | 9.65E-08 | 2.13E-08 | 9.03E-07 | 1.00E-05 |
| 9 | 0.15 | 1.49E-01 | 2.76E-01 | 1.49E-01 | 2.76E-01 | 1.13E-01 | 6.14E-04 | 2.00E-06 | 6.19E-04 | 3.27E-05 | 1.87E-05 | 3.82E-05 | 3.26E-04 | 3.61E-06 | -1.81E-02 | -1.84E-02 | -1.36E-02 | -3.62E-01 | 1.63E-02 | 2.62E-01 | 3.07E-02 | 0.00E+00 | 9.50E-07 | 9.65E-08 | 5.01E-08 | 9.03E-07 | 1.00E-05 |
| 10 | 0.168 | 1.68E-01 | 2.76E-01 | 1.67E-01 | 2.76E-01 | 1.27E-01 | 2.61E-04 | 2.00E-06 | 2.66E-04 | 3.02E-05 | 1.87E-05 | 3.60E-05 | 1.48E-04 | 3.61E-06 | -1.74E-02 | -1.80E-02 | -1.33E-02 | -3.48E-01 | 3.83E-02 | 2.78E-01 | 6.74E-02 | 0.00E+00 | 8.98E-07 | 9.65E-08 | 1.02E-07 | 9.03E-07 | 1.00E-05 |
| 11 | 0.187 | 1.86E-01 | 2.76E-01 | 1.85E-01 | 2.76E-01 | 1.40E-01 | 1.12E-04 | 2.00E-06 | 1.17E-04 | 2.80E-05 | 1.87E-05 | 3.40E-05 | 7.26E-05 | 3.61E-06 | -1.60E-02 | -1.70E-02 | -1.30E-02 | -3.21E-01 | 8.96E-02 | 2.94E-01 | 1.38E-01 | 0.00E+00 | 8.08E-07 | 9.65E-08 | 1.92E-07 | 9.03E-07 | 1.00E-05 |
| 12 | 0.206 | 2.03E-01 | 2.76E-01 | 2.01E-01 | 2.76E-01 | 1.53E-01 | 4.84E-05 | 2.00E-06 | 5.33E-05 | 2.61E-05 | 1.87E-05 | 3.21E-05 | 3.97E-05 | 3.61E-06 | -1.38E-02 | -1.47E-02 | -1.27E-02 | -2.76E-01 | 2.06E-01 | 3.12E-01 | 2.52E-01 | 0.00E+00 | 6.72E-07 | 9.65E-08 | 3.28E-07 | 9.03E-07 | 1.00E-05 |
| 13 | 0.224 | 2.17E-01 | 2.76E-01 | 2.15E-01 | 2.76E-01 | 1.66E-01 | 2.35E-05 | 2.00E-06 | 2.70E-05 | 2.45E-05 | 1.87E-05 | 3.03E-05 | 2.58E-05 | 3.61E-06 | -1.12E-02 | -1.05E-02 | -1.23E-02 | -2.24E-01 | 4.26E-01 | 3.30E-01 | 3.88E-01 | 0.00E+00 | 5.24E-07 | 9.65E-08 | 4.76E-07 | 9.03E-07 | 1.00E-05 |
| 14 | 0.243 | 2.28E-01 | 2.76E-01 | 2.26E-01 | 2.76E-01 | 1.78E-01 | 1.40E-05 | 2.00E-06 | 1.56E-05 | 2.33E-05 | 1.87E-05 | 2.87E-05 | 1.95E-05 | 3.61E-06 | -8.75E-03 | -4.91E-03 | -1.20E-02 | -1.75E-01 | 7.12E-01 | 3.48E-01 | 5.14E-01 | 0.00E+00 | 4.00E-07 | 9.65E-08 | 6.00E-07 | 9.03E-07 | 1.00E-05 |
| 15 | 0.262 | 2.33E-01 | 2.76E-01 | 2.34E-01 | 2.76E-01 | 1.90E-01 | 1.10E-05 | 2.00E-06 | 1.01E-05 | 2.25E-05 | 1.87E-05 | 2.73E-05 | 1.63E-05 | 3.61E-06 | -6.82E-03 | -1.14E-03 | -1.16E-02 | -1.36E-01 | 9.07E-01 | 3.67E-01 | 6.13E-01 | 0.00E+00 | 3.11E-07 | 9.65E-08 | 6.89E-07 | 9.03E-07 | 1.00E-05 |
| 16 | 0.281 | 2.34E-01 | 2.76E-01 | 2.41E-01 | 2.76E-01 | 2.02E-01 | 1.04E-05 | 2.00E-06 | 7.77E-06 | 2.18E-05 | 1.87E-05 | 2.59E-05 | 1.48E-05 | 3.61E-06 | -5.61E-03 | -1.27E-04 | -1.12E-02 | -1.12E-01 | 9.59E-01 | 3.86E-01 | 6.76E-01 | 0.00E+00 | 2.63E-07 | 9.65E-08 | 7.37E-07 | 9.03E-07 | 1.00E-05 |
| 17 | 0.299 | 2.34E-01 | 2.76E-01 | 2.47E-01 | 2.76E-01 | 2.13E-01 | 1.04E-05 | 2.00E-06 | 6.25E-06 | 2.13E-05 | 1.87E-05 | 2.47E-05 | 1.38E-05 | 3.61E-06 | -4.63E-03 | -1.06E-05 | -1.09E-02 | -9.26E-02 | 9.65E-01 | 4.05E-01 | 7.27E-01 | 0.00E+00 | 2.27E-07 | 9.65E-08 | 7.73E-07 | 9.03E-07 | 1.00E-05 |
| 18 | 0.318 | 2.34E-01 | 2.76E-01 | 2.52E-01 | 2.76E-01 | 2.24E-01 | 1.04E-05 | 2.00E-06 | 5.22E-06 | 2.08E-05 | 1.87E-05 | 2.35E-05 | 1.30E-05 | 3.61E-06 | -3.84E-03 | -8.46E-07 | -1.05E-02 | -7.69E-02 | 9.66E-01 | 4.25E-01 | 7.67E-01 | 0.00E+00 | 2.00E-07 | 9.65E-08 | 8.00E-07 | 9.03E-07 | 1.00E-05 |
| 19 | 0.337 | 2.34E-01 | 2.76E-01 | 2.55E-01 | 2.76E-01 | 2.34E-01 | 1.04E-05 | 2.00E-06 | 4.49E-06 | 2.05E-05 | 1.87E-05 | 2.25E-05 | 1.25E-05 | 3.61E-06 | -3.20E-03 | -6.75E-08 | -1.01E-02 | -6.41E-02 | 9.66E-01 | 4.45E-01 | 8.00E-01 | 0.00E+00 | 1.80E-07 | 9.65E-08 | 8.20E-07 | 9.03E-07 | 1.00E-05 |
| 20 | 0.355 | 2.34E-01 | 2.76E-01 | 2.59E-01 | 2.76E-01 | 2.45E-01 | 1.04E-05 | 2.00E-06 | 3.97E-06 | 2.02E-05 | 1.87E-05 | 2.15E-05 | 1.21E-05 | 3.61E-06 | -2.68E-03 | -5.38E-09 | -9.69E-03 | -5.37E-02 | 9.66E-01 | 4.65E-01 | 8.27E-01 | 0.00E+00 | 1.64E-07 | 9.65E-08 | 8.36E-07 | 9.03E-07 | 1.00E-05 |
| 21 | 0.374 | 2.34E-01 | 2.76E-01 | 2.61E-01 | 2.76E-01 | 2.54E-01 | 1.04E-05 | 2.00E-06 | 3.57E-06 | 2.00E-05 | 1.87E-05 | 2.06E-05 | 1.18E-05 | 3.61E-06 | -2.25E-03 | -4.29E-10 | -9.30E-03 | -4.51E-02 | 9.66E-01 | 4.85E-01 | 8.49E-01 | 0.00E+00 | 1.52E-07 | 9.65E-08 | 8.48E-07 | 9.03E-07 | 1.00E-05 |
| 22 | 0.393 | 2.34E-01 | 2.76E-01 | 2.64E-01 | 2.76E-01 | 2.64E-01 | 1.04E-05 | 2.00E-06 | 3.27E-06 | 1.98E-05 | 1.87E-05 | 1.98E-05 | 1.15E-05 | 3.61E-06 | -1.90E-03 | -3.42E-11 | -8.91E-03 | -3.80E-02 | 9.66E-01 | 5.06E-01 | 8.68E-01 | 0.00E+00 | 1.42E-07 | 9.65E-08 | 8.58E-07 | 9.03E-07 | 1.00E-05 |
| 23 | 0.411 | 2.34E-01 | 2.76E-01 | 2.65E-01 | 2.76E-01 | 2.72E-01 | 1.04E-05 | 2.00E-06 | 3.04E-06 | 1.96E-05 | 1.87E-05 | 1.90E-05 | 1.13E-05 | 3.61E-06 | -1.61E-03 | -2.73E-12 | -8.52E-03 | -3.21E-02 | 9.66E-01 | 5.26E-01 | 8.83E-01 | 0.00E+00 | 1.34E-07 | 9.65E-08 | 8.66E-07 | 9.03E-07 | 1.00E-05 |
| 24 | 0.43 | 2.34E-01 | 2.76E-01 | 2.67E-01 | 2.76E-01 | 2.81E-01 | 1.04E-05 | 2.00E-06 | 2.85E-06 | 1.95E-05 | 1.87E-05 | 1.83E-05 | 1.12E-05 | 3.61E-06 | -1.36E-03 | -2.18E-13 | -8.13E-03 | -2.72E-02 | 9.66E-01 | 5.46E-01 | 8.96E-01 | 0.00E+00 | 1.28E-07 | 9.65E-08 | 8.72E-07 | 9.03E-07 | 1.00E-05 |
| 25 | 0.449 | 2.34E-01 | 2.76E-01 | 2.68E-01 | 2.76E-01 | 2.89E-01 | 1.04E-05 | 2.00E-06 | 2.71E-06 | 1.94E-05 | 1.87E-05 | 1.77E-05 | 1.10E-05 | 3.61E-06 | -1.15E-03 | -1.74E-14 | -7.74E-03 | -2.30E-02 | 9.66E-01 | 5.66E-01 | 9.06E-01 | 0.00E+00 | 1.23E-07 | 9.65E-08 | 8.77E-07 | 9.03E-07 | 1.00E-05 |
| 26 | 0.468 | 2.34E-01 | 2.76E-01 | 2.70E-01 | 2.76E-01 | 2.97E-01 | 1.04E-05 | 2.00E-06 | 2.59E-06 | 1.93E-05 | 1.87E-05 | 1.71E-05 | 1.09E-05 | 3.61E-06 | -9.78E-04 | -1.37E-15 | -7.36E-03 | -1.96E-02 | 9.66E-01 | 5.86E-01 | 9.15E-01 | 3.75E-24 | 1.18E-07 | 9.65E-08 | 8.82E-07 | 9.03E-07 | 1.00E-05 |
| 27 | 0.486 | 2.34E-01 | 2.76E-01 | 2.71E-01 | 2.76E-01 | 3.04E-01 | 1.04E-05 | 2.00E-06 | 2.49E-06 | 1.92E-05 | 1.87E-05 | 1.65E-05 | 1.08E-05 | 3.61E-06 | -8.32E-04 | -1.42E-16 | -6.99E-03 | -1.66E-02 | 9.66E-01 | 6.05E-01 | 9.23E-01 | 3.75E-24 | 1.15E-07 | 9.65E-08 | 8.85E-07 | 9.03E-07 | 1.00E-05 |
| 28 | 0.505 | 2.34E-01 | 2.76E-01 | 2.71E-01 | 2.76E-01 | 3.11E-01 | 1.04E-05 | 2.00E-06 | 2.41E-06 | 1.91E-05 | 1.87E-05 | 1.60E-05 | 1.08E-05 | 3.61E-06 | -7.08E-04 | -8.60E-18 | -6.62E-03 | -1.42E-02 | 9.66E-01 | 6.24E-01 | 9.29E-01 | 3.75E-24 | 1.12E-07 | 9.65E-08 | 8.88E-07 | 9.03E-07 | 1.00E-05 |
| 29 | 0.524 | 2.34E-01 | 2.76E-01 | 2.72E-01 | 2.76E-01 | 3.18E-01 | 1.04E-05 | 2.00E-06 | 2.35E-06 | 1.90E-05 | 1.87E-05 | 1.56E-05 | 1.07E-05 | 3.61E-06 | -6.03E-04 | -8.60E-18 | -6.26E-03 | -1.21E-02 | 9.66E-01 | 6.43E-01 | 9.35E-01 | 3.75E-24 | 1.10E-07 | 9.65E-08 | 8.90E-07 | 9.03E-07 | 1.00E-05 |
| 30 | 0.542 | 2.34E-01 | 2.76E-01 | 2.73E-01 | 2.76E-01 | 3.24E-01 | 1.04E-05 | 2.00E-06 | 2.29E-06 | 1.90E-05 | 1.87E-05 | 1.51E-05 | 1.06E-05 | 3.61E-06 | -5.14E-04 | -8.60E-18 | -5.91E-03 | -1.03E-02 | 9.66E-01 | 6.61E-01 | 9.39E-01 | 7.50E-24 | 1.08E-07 | 9.65E-08 | 8.92E-07 | 9.03E-07 | 1.00E-05 |
| 81 | 1.496 | 2.34E-01 | 2.76E-01 | 2.76E-01 | 2.76E-01 | 4.09E-01 | 1.04E-05 | 2.00E-06 | 2.00E-06 | 1.87E-05 | 1.87E-05 | 1.04E-05 | 1.04E-05 | 3.61E-06 | -1.76E-07 | -8.60E-18 | -1.08E-04 | -3.52E-06 | 9.66E-01 | 9.60E-01 | 9.66E-01 | 4.29E-14 | 9.65E-08 | 9.65E-08 | 9.03E-07 | 9.03E-07 | 1.00E-05 |
| 82 | 1.515 | 2.34E-01 | 2.76E-01 | 2.76E-01 | 2.76E-01 | 4.09E-01 | 1.04E-05 | 2.00E-06 | 2.00E-06 | 1.87E-05 | 1.87E-05 | 1.04E-05 | 1.04E-05 | 3.61E-06 | -1.50E-07 | -8.60E-18 | -9.88E-05 | -3.01E-06 | 9.66E-01 | 9.61E-01 | 9.66E-01 | 6.59E-14 | 9.65E-08 | 9.65E-08 | 9.03E-07 | 9.03E-07 | 1.00E-05 |
| 83 | 1.533 | 2.34E-01 | 2.76E-01 | 2.76E-01 | 2.76E-01 | 4.09E-01 | 1.04E-05 | 2.00E-06 | 2.00E-06 | 1.87E-05 | 1.87E-05 | 1.04E-05 | 1.04E-05 | 3.61E-06 | -1.29E-07 | -8.60E-18 | -9.06E-05 | -2.58E-06 | 9.66E-01 | 9.61E-01 | 9.66E-01 | 1.01E-13 | 9.65E-08 | 9.65E-08 | 9.03E-07 | 9.03E-07 | 1.00E-05 |
| 84 | 1.552 | 2.34E-01 | 2.76E-01 | 2.76E-01 | 2.76E-01 | 4.09E-01 | 1.04E-05 | 2.00E-06 | 2.00E-06 | 1.87E-05 | 1.87E-05 | 1.04E-05 | 1.04E-05 | 3.61E-06 | -1.10E-07 | -8.60E-18 | -8.32E-05 | -2.20E-06 | 9.66E-01 | 9.62E-01 | 9.66E-01 | 1.56E-13 | 9.65E-08 | 9.65E-08 | 9.03E-07 | 9.03E-07 | 1.00E-05 |
| 85 | 1.571 | 2.34E-01 | 2.76E-01 | 2.76E-01 | 2.76E-01 | 4.09E-01 | 1.04E-05 | 2.00E-06 | 2.00E-06 | 1.87E-05 | 1.87E-05 | 1.04E-05 | 1.04E-05 | 3.61E-06 | -9.42E-08 | -8.60E-18 | -7.64E-05 | -1.88E-06 | 9.66E-01 | 9.62E-01 | 9.66E-01 | 2.40E-13 | 9.65E-08 | 9.65E-08 | 9.03E-07 | 9.03E-07 | 1.00E-05 |
| 86 | 1.59 | 2.34E-01 | 2.76E-01 | 2.76E-01 | 2.76E-01 | 4.09E-01 | 1.04E-05 | 2.00E-06 | 2.00E-06 | 1.87E-05 | 1.87E-05 | 1.04E-05 | 1.04E-05 | 3.61E-06 | -8.06E-08 | -8.60E-18 | -7.01E-05 | -1.61E-06 | 9.66E-01 | 9.62E-01 | 9.66E-01 | 3.69E-13 | 9.65E-08 | 9.65E-08 | 9.03E-07 | 9.03E-07 | 1.00E-05 |
| 87 | 1.608 | 2.34E-01 | 2.76E-01 | 2.76E-01 | 2.76E-01 | 4.09E-01 | 1.04E-05 | 2.00E-06 | 2.00E-06 | 1.87E-05 | 1.87E-05 | 1.04E-05 | 1.04E-05 | 3.61E-06 | -6.90E-08 | -8.60E-18 | -6.43E-05 | -1.38E-06 | 9.66E-01 | 9.63E-01 | 9.66E-01 | 5.68E-13 | 9.65E-08 | 9.65E-08 | 9.03E-07 | 9.03E-07 | 1.00E-05 |
| 88 | 1.627 | 2.34E-01 | 2.76E-01 | 2.76E-01 | 2.76E-01 | 4.09E-01 | 1.04E-05 | 2.00E-06 | 2.00E-06 | 1.87E-05 | 1.87E-05 | 1.04E-05 | 1.04E-05 | 3.61E-06 | -5.90E-08 | -8.60E-18 | -5.90E-05 | -1.18E-06 | 9.66E-01 | 9.63E-01 | 9.66E-01 | 8.74E-13 | 9.65E-08 | 9.66E-08 | 9.03E-07 | 9.03E-07 | 1.00E-05 |
| 89 | 1.646 | 2.34E-01 | 2.76E-01 | 2.76E-01 | 2.76E-01 | 4.09E-01 | 1.04E-05 | 2.00E-06 | 2.00E-06 | 1.87E-05 | 1.87E-05 | 1.04E-05 | 1.04E-05 | 3.61E-06 | -5.05E-08 | -8.60E-18 | -5.41E-05 | -1.01E-06 | 9.66E-01 | 9.63E-01 | 9.66E-01 | 1.35E-12 | 9.65E-08 | 9.66E-08 | 9.03E-07 | 9.03E-07 | 1.00E-05 |
| 90 | 1.664 | 2.34E-01 | 2.76E-01 | 2.76E-01 | 2.76E-01 | 4.09E-01 | 1.04E-05 | 2.00E-06 | 2.00E-06 | 1.87E-05 | 1.87E-05 | 1.04E-05 | 1.04E-05 | 3.61E-06 | -4.32E-08 | -8.60E-18 | -4.97E-05 | -8.64E-07 | 9.66E-01 | 9.63E-01 | 9.66E-01 | 2.07E-12 | 9.65E-08 | 9.66E-08 | 9.03E-07 | 9.03E-07 | 1.00E-05 |
| 91 | 1.683 | 2.34E-01 | 2.76E-01 | 2.76E-01 | 2.76E-01 | 4.10E-01 | 1.04E-05 | 2.00E-06 | 2.00E-06 | 1.87E-05 | 1.87E-05 | 1.04E-05 | 1.04E-05 | 3.61E-06 | -3.70E-08 | -8.60E-18 | -4.56E-05 | -7.39E-07 | -1.72E-16 | -9.12E-04 | 9.66E-01 | 3.19E-12 | 9.65E-08 | 9.66E-08 | 9.03E-07 | 9.03E-07 | 1.00E-05 |
| 92 | 1.702 | 2.34E-01 | 2.76E-01 | 2.76E-01 | 2.76E-01 | 4.10E-01 | 1.04E-05 | 2.00E-06 | 2.00E-06 | 1.87E-05 | 1.87E-05 | 1.04E-05 | 1.04E-05 | 3.61E-06 | -3.16E-08 | -8.60E-18 | -4.18E-05 | -6.32E-07 | -1.72E-16 | -8.37E-04 | 9.66E-01 | 4.91E-12 | 9.65E-08 | 9.66E-08 | 9.03E-07 | 9.03E-07 | 1.00E-05 |
| 93 | 1.72 | 2.34E-01 | 2.76E-01 | 2.76E-01 | 2.76E-01 | 4.10E-01 | 1.04E-05 | 2.00E-06 | 2.00E-06 | 1.87E-05 | 1.87E-05 | 1.04E-05 | 1.04E-05 | 3.62E-06 | -2.70E-08 | -8.60E-18 | -3.84E-05 | -5.41E-07 | -1.72E-16 | -7.68E-04 | 9.66E-01 | 7.56E-12 | 9.65E-08 | 9.67E-08 | 9.03E-07 | 9.03E-07 | 1.00E-05 |
| 94 | 1.739 | 2.34E-01 | 2.76E-01 | 2.76E-01 | 2.76E-01 | 4.10E-01 | 1.04E-05 | 2.00E-06 | 2.00E-06 | 1.87E-05 | 1.87E-05 | 1.04E-05 | 1.04E-05 | 3.62E-06 | -2.31E-08 | -8.60E-18 | -3.52E-05 | -4.63E-07 | -1.72E-16 | -7.04E-04 | 9.66E-01 | 1.16E-11 | 9.65E-08 | 9.68E-08 | 9.03E-07 | 9.03E-07 | 1.00E-05 |
| 95 | 1.758 | 2.34E-01 | 2.76E-01 | 2.76E-01 | 2.76E-01 | 4.10E-01 | 1.04E-05 | 2.01E-06 | 2.00E-06 | 1.87E-05 | 1.87E-05 | 1.04E-05 | 1.04E-05 | 3.62E-06 | -1.98E-08 | -8.60E-18 | -3.23E-05 | -3.96E-07 | -1.72E-16 | -6.46E-04 | 9.66E-01 | 1.79E-11 | 9.65E-08 | 9.69E-08 | 9.03E-07 | 9.03E-07 | 1.00E-05 |
| 96 | 1.777 | 2.34E-01 | 2.76E-01 | 2.76E-01 | 2.76E-01 | 4.10E-01 | 1.04E-05 | 2.01E-06 | 2.00E-06 | 1.87E-05 | 1.87E-05 | 1.04E-05 | 1.04E-05 | 3.63E-06 | -1.69E-08 | -8.60E-18 | -2.97E-05 | -3.39E-07 | -1.72E-16 | -5.93E-04 | 9.66E-01 | 2.77E-11 | 9.65E-08 | 9.70E-08 | 9.03E-07 | 9.03E-07 | 1.00E-05 |
| 97 | 1.795 | 2.34E-01 | 2.76E-01 | 2.76E-01 | 2.76E-01 | 4.10E-01 | 1.04E-05 | 2.02E-06 | 2.00E-06 | 1.87E-05 | 1.87E-05 | 1.04E-05 | 1.04E-05 | 3.64E-06 | -1.45E-08 | -8.60E-18 | -2.72E-05 | -2.90E-07 | -1.72E-16 | -5.44E-04 | 9.66E-01 | 4.29E-11 | 9.65E-08 | 9.73E-08 | 9.03E-07 | 9.03E-07 | 1.00E-05 |
| 98 | 1.814 | 2.34E-01 | 2.76E-01 | 2.76E-01 | 2.77E-01 | 4.10E-01 | 1.04E-05 | 2.02E-06 | 2.00E-06 | 1.87E-05 | 1.87E-05 | 1.04E-05 | 1.04E-05 | 3.65E-06 | -1.24E-08 | -8.60E-18 | -2.50E-05 | -2.48E-07 | -1.72E-16 | -4.99E-04 | 9.66E-01 | 6.66E-11 | 9.65E-08 | 9.78E-08 | 9.03E-07 | 9.02E-07 | 1.00E-05 |
| 99 | 1.833 | 2.34E-01 | 2.75E-01 | 2.76E-01 | 2.77E-01 | 4.10E-01 | 1.04E-05 | 2.04E-06 | 2.00E-06 | 1.87E-05 | 1.87E-05 | 1.04E-05 | 1.04E-05 | 3.67E-06 | -1.06E-08 | -8.60E-18 | -2.29E-05 | -2.12E-07 | -1.72E-16 | -4.58E-04 | 9.66E-01 | 1.04E-10 | 9.65E-08 | 9.84E-08 | 9.03E-07 | 9.02E-07 | 1.00E-05 |
| 100 | 1.851 | 2.34E-01 | 2.75E-01 | 2.76E-01 | 2.77E-01 | 4.10E-01 | 1.04E-05 | 2.06E-06 | 2.00E-06 | 1.87E-05 | 1.86E-05 | 1.04E-05 | 1.04E-05 | 3.71E-06 | -9.07E-09 | -8.60E-18 | -2.10E-05 | -1.81E-07 | -1.72E-16 | -4.20E-04 | 9.66E-01 | 1.64E-10 | 9.65E-08 | 9.95E-08 | 9.03E-07 | 9.01E-07 | 1.00E-05 |
| 101 | 1.87 | 2.34E-01 | 2.74E-01 | 2.76E-01 | 2.78E-01 | 4.10E-01 | 1.04E-05 | 2.09E-06 | 2.00E-06 | 1.87E-05 | 1.86E-05 | 1.04E-05 | 1.04E-05 | 3.76E-06 | -7.76E-09 | -8.60E-18 | -1.93E-05 | -1.55E-07 | -1.72E-16 | -3.86E-04 | 9.66E-01 | 2.64E-10 | 9.65E-08 | 1.01E-07 | 9.03E-07 | 8.99E-07 | 1.00E-05 |
| 102 | 1.889 | 2.34E-01 | 2.73E-01 | 2.76E-01 | 2.79E-01 | 4.10E-01 | 1.04E-05 | 2.15E-06 | 2.00E-06 | 1.87E-05 | 1.86E-05 | 1.04E-05 | 1.04E-05 | 3.85E-06 | -6.64E-09 | -8.60E-18 | -1.77E-05 | -1.33E-07 | -1.72E-16 | -3.54E-04 | 9.66E-01 | 4.34E-10 | 9.65E-08 | 1.04E-07 | 9.03E-07 | 8.96E-07 | 1.00E-05 |
| 103 | 1.907 | 2.34E-01 | 2.72E-01 | 2.76E-01 | 2.81E-01 | 4.10E-01 | 1.04E-05 | 2.24E-06 | 2.00E-06 | 1.87E-05 | 1.85E-05 | 1.04E-05 | 1.04E-05 | 3.99E-06 | -5.68E-09 | -8.60E-18 | -1.62E-05 | -1.14E-07 | -1.72E-16 | -3.25E-04 | 9.66E-01 | 7.46E-10 | 9.65E-08 | 1.08E-07 | 9.03E-07 | 8.92E-07 | 1.00E-05 |
| 104 | 1.926 | 2.34E-01 | 2.69E-01 | 2.76E-01 | 2.85E-01 | 4.10E-01 | 1.04E-05 | 2.39E-06 | 2.00E-06 | 1.87E-05 | 1.83E-05 | 1.04E-05 | 1.04E-05 | 4.23E-06 | -4.86E-09 | -8.60E-18 | -1.49E-05 | -9.72E-08 | -1.72E-16 | -2.98E-04 | 9.66E-01 | 1.39E-09 | 9.65E-08 | 1.16E-07 | 9.03E-07 | 8.84E-07 | 1.00E-05 |
| 105 | 1.945 | 2.34E-01 | 2.63E-01 | 2.76E-01 | 2.93E-01 | 4.10E-01 | 1.04E-05 | 2.68E-06 | 2.00E-06 | 1.87E-05 | 1.80E-05 | 1.04E-05 | 1.04E-05 | 4.67E-06 | -4.16E-09 | -8.60E-18 | -1.37E-05 | -8.32E-08 | -1.72E-16 | -2.73E-04 | 9.66E-01 | 3.08E-09 | 9.65E-08 | 1.29E-07 | 9.03E-07 | 8.71E-07 | 1.00E-05 |
| 106 | 1.964 | 2.34E-01 | 2.41E-01 | 2.76E-01 | 3.62E-01 | 4.10E-01 | 1.04E-05 | 3.32E-06 | 2.00E-06 | 1.87E-05 | 1.74E-05 | 1.04E-05 | 1.04E-05 | 5.57E-06 | -3.56E-09 | -8.60E-18 | -1.25E-05 | -7.12E-08 | -1.72E-16 | -2.51E-04 | 9.66E-01 | 2.21E-08 | 9.65E-08 | 1.60E-07 | 9.03E-07 | 8.40E-07 | 1.00E-05 |
| 107 | 1.982 | 2.34E-01 | 2.34E-01 | 2.76E-01 | 4.10E-01 | 4.10E-01 | 1.04E-05 | 7.89E-06 | 2.00E-06 | 1.87E-05 | 1.28E-05 | 1.04E-05 | 1.04E-05 | 9.77E-06 | -3.04E-09 | -8.60E-18 | -1.15E-05 | -6.09E-08 | -1.72E-16 | -2.30E-04 | 9.66E-01 | 1.19E-08 | 9.65E-08 | 3.81E-07 | 9.03E-07 | 6.19E-07 | 1.00E-05 |
| 108 | 2.001 | 2.34E-01 | 2.34E-01 | 2.76E-01 | 4.10E-01 | 4.10E-01 | 1.04E-05 | 1.04E-05 | 2.00E-06 | 1.87E-05 | 1.04E-05 | 1.04E-05 | 1.04E-05 | 3.61E-06 | -2.60E-09 | -8.60E-18 | -1.05E-05 | -5.21E-08 | 2.50E-01 | 2.67E-02 | 9.66E-01 | 0 | 9.65E-08 | 5.00E-07 | 9.03E-07 | 5.00E-07 | 1.00E-05 |

## Table C3 The FDM Results for the 45°, 2-Meter System using The Modified Kisch Solution

| # | z | hci | hcp | hp | hfp | hfi | kci | kcp | kc | kf | kfp | kfi | kll | kp | dhp | dhpc | dhpf | l | lcx | lfx | l | dq | qci | qcp | qfi | qfp | q-total |
|---|---|---|---|---|---|---|---|---|---|---|---|---|---|---|---|---|---|---|---|---|---|---|---|---|---|---|---|
| 1 | 0 | 0.00E+00 | #NUM! | 1.00E-04 | #NUM! | 0.00E+00 | 1.48E-02 | #NUM! | 1.48E-02 | 4.50E-05 | #NUM! | 4.50E-05 | 7.42E-03 | #NUM! | -1.87E-02 | -1.87E-02 | -1.28E-02 | -3.73E-01 | 6.76E-04 | 2.22E-01 | 1.35E-03 | #NUM! | 9.97E-07 | #NUM! | 3.03E-09 | #NUM! | 1.00E-05 |
| 2 | 0.019 | 1.87E-02 | 1.34E-02 | 1.88E-02 | 2.45E-01 | 1.28E-02 | 1.46E-02 | -5.84E-06 | 1.46E-02 | 4.46E-05 | 3.41E-05 | 4.50E-05 | 7.34E-03 | -1.41E-05 | -1.87E-02 | -1.87E-02 | -1.28E-02 | -3.73E-01 | 6.83E-04 | 2.22E-01 | 1.36E-03 | 4.47E-08 | 9.97E-07 | -2.06E-07 | 3.03E-09 | 1.21E-06 | 1.00E-05 |
| 3 | 0.037 | 3.74E-02 | 2.45E-01 | 3.74E-02 | 2.45E-01 | 2.56E-02 | 1.45E-02 | 6.81E-06 | 1.45E-02 | 4.35E-05 | 2.15E-05 | 4.42E-05 | 7.25E-03 | 1.03E-05 | -1.87E-02 | -1.87E-02 | -1.27E-02 | -3.73E-01 | 6.91E-04 | 2.26E-01 | 1.38E-03 | 5.36E-23 | 9.97E-07 | 2.41E-07 | 3.00E-09 | 7.59E-07 | 1.00E-05 |
| 4 | 0.056 | 5.60E-02 | 2.45E-01 | 5.61E-02 | 2.45E-01 | 3.84E-02 | 1.35E-02 | 6.81E-06 | 1.34E-02 | 4.25E-05 | 2.15E-05 | 4.35E-05 | 6.74E-03 | 1.03E-05 | -1.87E-02 | -1.87E-02 | -1.26E-02 | -3.73E-01 | 7.43E-04 | 2.30E-01 | 1.48E-03 | -4.83E-23 | 9.97E-07 | 2.41E-07 | 3.15E-09 | 7.59E-07 | 1.00E-05 |
| 5 | 0.075 | 7.47E-02 | 2.45E-01 | 7.48E-02 | 2.45E-01 | 5.10E-02 | 1.11E-02 | 6.81E-06 | 1.11E-02 | 4.16E-05 | 2.15E-05 | 4.28E-05 | 5.57E-03 | 1.03E-05 | -1.87E-02 | -1.87E-02 | -1.25E-02 | -3.73E-01 | 9.00E-04 | 2.34E-01 | 1.79E-03 | 5.36E-23 | 9.96E-07 | 2.41E-07 | 3.73E-09 | 7.59E-07 | 1.00E-05 |
| 6 | 0.094 | 9.34E-02 | 2.45E-01 | 9.34E-02 | 2.45E-01 | 6.35E-02 | 7.43E-03 | 6.81E-06 | 7.43E-03 | 4.06E-05 | 2.15E-05 | 4.22E-05 | 3.74E-03 | 1.03E-05 | -1.86E-02 | -1.87E-02 | -1.24E-02 | -3.73E-01 | 1.35E-03 | 2.37E-01 | 2.68E-03 | -4.83E-23 | 9.95E-07 | 2.41E-07 | 5.44E-09 | 7.59E-07 | 1.00E-05 |
| 7 | 0.112 | 1.12E-01 | 2.45E-01 | 1.12E-01 | 2.45E-01 | 7.59E-02 | 3.92E-03 | 6.81E-06 | 3.93E-03 | 3.85E-05 | 2.15E-05 | 4.15E-05 | 1.98E-03 | 1.03E-05 | -1.86E-02 | -1.86E-02 | -1.23E-02 | -3.71E-01 | 2.55E-03 | 2.41E-01 | 5.04E-03 | 5.36E-23 | 9.90E-07 | 2.41E-07 | 9.69E-09 | 7.59E-07 | 1.00E-05 |
| 8 | 0.131 | 1.31E-01 | 2.45E-01 | 1.31E-01 | 2.45E-01 | 8.83E-02 | 1.63E-03 | 6.81E-06 | 1.64E-03 | 3.54E-05 | 2.15E-05 | 4.09E-05 | 8.37E-04 | 1.03E-05 | -1.84E-02 | -1.85E-02 | -1.22E-02 | -3.68E-01 | 6.13E-03 | 2.45E-01 | 1.19E-02 | -4.83E-23 | 9.79E-07 | 2.41E-07 | 2.12E-08 | 7.59E-07 | 1.00E-05 |
| 9 | 0.15 | 1.49E-01 | 2.45E-01 | 1.49E-01 | 2.45E-01 | 1.00E-01 | 6.17E-04 | 6.81E-06 | 6.26E-04 | 3.27E-05 | 2.15E-05 | 4.03E-05 | 3.29E-04 | 1.03E-05 | -1.79E-02 | -1.83E-02 | -1.21E-02 | -3.58E-01 | 1.62E-02 | 2.48E-01 | 3.04E-02 | 5.36E-23 | 9.50E-07 | 2.41E-07 | 4.96E-08 | 7.59E-07 | 1.00E-05 |
| 10 | 0.168 | 1.68E-01 | 2.45E-01 | 1.67E-01 | 2.45E-01 | 1.13E-01 | 2.64E-04 | 6.81E-06 | 2.71E-04 | 3.02E-05 | 2.15E-05 | 3.84E-05 | 1.51E-04 | 1.03E-05 | -1.69E-02 | -1.77E-02 | -1.18E-02 | -3.39E-01 | 3.79E-02 | 2.61E-01 | 6.64E-02 | -4.83E-23 | 9.00E-07 | 2.41E-07 | 1.00E-07 | 7.59E-07 | 1.00E-05 |
| 11 | 0.187 | 1.85E-01 | 2.45E-01 | 1.84E-01 | 2.45E-01 | 1.24E-01 | 1.14E-04 | 6.81E-06 | 1.22E-04 | 2.81E-05 | 2.15E-05 | 3.64E-05 | 7.52E-05 | 1.03E-05 | -1.52E-02 | -1.64E-02 | -1.14E-02 | -3.04E-01 | 8.75E-02 | 2.75E-01 | 1.33E-01 | 5.36E-23 | 8.13E-07 | 2.41E-07 | 1.87E-07 | 7.59E-07 | 1.00E-05 |
| 12 | 0.206 | 2.02E-01 | 2.45E-01 | 1.99E-01 | 2.45E-01 | 1.36E-01 | 5.10E-05 | 6.81E-06 | 5.79E-05 | 2.62E-05 | 2.15E-05 | 3.46E-05 | 4.21E-05 | 1.03E-05 | -1.24E-02 | -1.35E-02 | -1.11E-02 | -2.48E-01 | 1.96E-01 | 2.89E-01 | 2.38E-01 | -4.83E-23 | 6.88E-07 | 2.41E-07 | 3.12E-07 | 7.59E-07 | 1.00E-05 |
| 13 | 0.224 | 2.15E-01 | 2.45E-01 | 2.11E-01 | 2.45E-01 | 1.47E-01 | 2.62E-05 | 6.81E-06 | 3.14E-05 | 2.49E-05 | 2.15E-05 | 3.30E-05 | 2.82E-05 | 1.03E-05 | -9.31E-03 | -8.62E-03 | -1.07E-02 | -1.86E-01 | 3.81E-01 | 3.03E-01 | 3.55E-01 | 5.36E-23 | 5.59E-07 | 2.41E-07 | 4.41E-07 | 7.59E-07 | 1.00E-05 |
| 14 | 0.243 | 2.24E-01 | 2.45E-01 | 2.21E-01 | 2.45E-01 | 1.58E-01 | 1.72E-05 | 6.81E-06 | 1.99E-05 | 2.39E-05 | 2.15E-05 | 3.15E-05 | 2.19E-05 | 1.03E-05 | -6.61E-03 | -3.29E-03 | -1.03E-02 | -1.32E-01 | 5.83E-01 | 3.18E-01 | 4.57E-01 | -4.83E-23 | 4.55E-07 | 2.41E-07 | 5.45E-07 | 7.59E-07 | 1.00E-05 |
| 15 | 0.262 | 2.27E-01 | 2.45E-01 | 2.27E-01 | 2.45E-01 | 1.68E-01 | 1.46E-05 | 6.81E-06 | 1.44E-05 | 2.32E-05 | 2.15E-05 | 3.01E-05 | 1.88E-05 | 1.03E-05 | -4.61E-03 | -5.83E-04 | -9.91E-03 | -9.23E-02 | 6.85E-01 | 3.32E-01 | 5.33E-01 | 5.36E-23 | 3.83E-07 | 2.41E-07 | 6.17E-07 | 7.59E-07 | 1.00E-05 |
| 16 | 0.281 | 2.28E-01 | 2.45E-01 | 2.32E-01 | 2.45E-01 | 1.78E-01 | 1.42E-05 | 6.81E-06 | 1.14E-05 | 2.27E-05 | 2.15E-05 | 2.88E-05 | 1.71E-05 | 1.03E-05 | -3.22E-03 | -5.57E-05 | -9.52E-03 | -6.44E-02 | 7.05E-01 | 3.47E-01 | 5.85E-01 | -4.83E-23 | 3.35E-07 | 2.41E-07 | 6.65E-07 | 7.59E-07 | 1.00E-05 |
| 17 | 0.299 | 2.28E-01 | 2.45E-01 | 2.35E-01 | 2.45E-01 | 1.87E-01 | 1.41E-05 | 6.81E-06 | 9.86E-06 | 2.24E-05 | 2.15E-05 | 2.76E-05 | 1.61E-05 | 1.03E-05 | -2.30E-03 | -4.52E-06 | -9.13E-03 | -4.60E-02 | 7.07E-01 | 3.62E-01 | 6.20E-01 | 5.36E-23 | 3.06E-07 | 2.41E-07 | 6.94E-07 | 7.59E-07 | 1.00E-05 |
| 18 | 0.318 | 2.28E-01 | 2.45E-01 | 2.37E-01 | 2.45E-01 | 1.96E-01 | 1.41E-05 | 6.81E-06 | 9.01E-06 | 2.22E-05 | 2.15E-05 | 2.65E-05 | 1.56E-05 | 1.03E-05 | -1.74E-03 | -3.61E-07 | -8.74E-03 | -3.48E-02 | 7.07E-01 | 3.77E-01 | 6.41E-01 | -4.83E-23 | 2.89E-07 | 2.41E-07 | 7.11E-07 | 7.59E-07 | 1.00E-05 |
| 19 | 0.337 | 2.28E-01 | 2.45E-01 | 2.39E-01 | 2.45E-01 | 2.05E-01 | 1.41E-05 | 6.81E-06 | 8.42E-06 | 2.20E-05 | 2.15E-05 | 2.55E-05 | 1.52E-05 | 1.03E-05 | -1.32E-03 | -2.88E-08 | -8.35E-03 | -2.63E-02 | 7.07E-01 | 3.91E-01 | 6.57E-01 | 5.36E-23 | 2.77E-07 | 2.41E-07 | 7.23E-07 | 7.59E-07 | 1.00E-05 |
| 20 | 0.355 | 2.28E-01 | 2.45E-01 | 2.41E-01 | 2.45E-01 | 2.14E-01 | 1.41E-05 | 6.81E-06 | 8.00E-06 | 2.19E-05 | 2.15E-05 | 2.46E-05 | 1.49E-05 | 1.03E-05 | -9.98E-04 | -2.30E-09 | -7.96E-03 | -2.00E-02 | 7.07E-01 | 4.06E-01 | 6.69E-01 | -4.83E-23 | 2.68E-07 | 2.41E-07 | 7.32E-07 | 7.59E-07 | 1.00E-05 |
| 21 | 0.374 | 2.28E-01 | 2.45E-01 | 2.42E-01 | 2.45E-01 | 2.22E-01 | 1.41E-05 | 6.81E-06 | 7.70E-06 | 2.18E-05 | 2.15E-05 | 2.38E-05 | 1.47E-05 | 1.03E-05 | -7.57E-04 | -1.83E-10 | -7.58E-03 | -1.51E-02 | 7.07E-01 | 4.21E-01 | 6.78E-01 | 5.36E-23 | 2.61E-07 | 2.41E-07 | 7.39E-07 | 7.59E-07 | 1.00E-05 |
| 22 | 0.393 | 2.28E-01 | 2.45E-01 | 2.42E-01 | 2.45E-01 | 2.29E-01 | 1.41E-05 | 6.81E-06 | 7.47E-06 | 2.17E-05 | 2.15E-05 | 2.30E-05 | 1.46E-05 | 1.03E-05 | -5.75E-04 | -1.46E-11 | -7.20E-03 | -1.15E-02 | 7.07E-01 | 4.35E-01 | 6.85E-01 | -4.83E-23 | 2.56E-07 | 2.41E-07 | 7.44E-07 | 7.59E-07 | 1.00E-05 |
| 23 | 0.411 | 2.28E-01 | 2.45E-01 | 2.43E-01 | 2.45E-01 | 2.36E-01 | 1.41E-05 | 6.81E-06 | 7.31E-06 | 2.17E-05 | 2.15E-05 | 2.23E-05 | 1.45E-05 | 1.03E-05 | -4.37E-04 | -1.17E-12 | -6.83E-03 | -8.75E-03 | 7.07E-01 | 4.49E-01 | 6.91E-01 | 5.36E-23 | 2.52E-07 | 2.41E-07 | 7.48E-07 | 7.59E-07 | 1.00E-05 |
| 24 | 0.43 | 2.28E-01 | 2.45E-01 | 2.43E-01 | 2.45E-01 | 2.43E-01 | 1.41E-05 | 6.81E-06 | 7.19E-06 | 2.16E-05 | 2.15E-05 | 2.16E-05 | 1.44E-05 | 1.03E-05 | -3.33E-04 | -9.30E-14 | -6.47E-03 | -6.65E-03 | 7.07E-01 | 4.62E-01 | 6.95E-01 | -4.83E-23 | 2.50E-07 | 2.41E-07 | 7.50E-07 | 7.59E-07 | 1.00E-05 |
| 25 | 0.449 | 2.28E-01 | 2.45E-01 | 2.44E-01 | 2.45E-01 | 2.50E-01 | 1.41E-05 | 6.81E-06 | 7.09E-06 | 2.16E-05 | 2.15E-05 | 2.10E-05 | 1.43E-05 | 1.03E-05 | -2.53E-04 | -7.38E-15 | -6.12E-03 | -5.07E-03 | 7.07E-01 | 4.76E-01 | 6.98E-01 | 5.36E-23 | 2.47E-07 | 2.41E-07 | 7.53E-07 | 7.59E-07 | 1.00E-05 |
| 26 | 0.468 | 2.28E-01 | 2.45E-01 | 2.44E-01 | 2.45E-01 | 2.56E-01 | 1.41E-05 | 6.81E-06 | 7.02E-06 | 2.16E-05 | 2.15E-05 | 2.05E-05 | 1.43E-05 | 1.03E-05 | -1.93E-04 | -6.40E-16 | -5.78E-03 | -3.86E-03 | 7.07E-01 | 4.89E-01 | 7.00E-01 | -4.83E-23 | 2.46E-07 | 2.41E-07 | 7.54E-07 | 7.59E-07 | 1.00E-05 |
| 27 | 0.486 | 2.28E-01 | 2.45E-01 | 2.44E-01 | 2.45E-01 | 2.62E-01 | 1.41E-05 | 6.81E-06 | 6.97E-06 | 2.15E-05 | 2.15E-05 | 2.00E-05 | 1.43E-05 | 1.03E-05 | -1.47E-04 | -1.17E-17 | -5.44E-03 | -2.94E-03 | 7.07E-01 | 5.01E-01 | 7.02E-01 | 5.36E-23 | 2.45E-07 | 2.41E-07 | 7.55E-07 | 7.59E-07 | 1.00E-05 |
| 28 | 0.505 | 2.28E-01 | 2.45E-01 | 2.44E-01 | 2.45E-01 | 2.67E-01 | 1.41E-05 | 6.81E-06 | 6.93E-06 | 2.15E-05 | 2.15E-05 | 1.95E-05 | 1.42E-05 | 1.03E-05 | -1.12E-04 | -1.17E-17 | -5.12E-03 | -2.24E-03 | 7.07E-01 | 5.13E-01 | 7.03E-01 | -4.83E-23 | 2.44E-07 | 2.41E-07 | 7.56E-07 | 7.59E-07 | 1.00E-05 |
| 29 | 0.524 | 2.28E-01 | 2.45E-01 | 2.44E-01 | 2.45E-01 | 2.72E-01 | 1.41E-05 | 6.81E-06 | 6.90E-06 | 2.15E-05 | 2.15E-05 | 1.90E-05 | 1.42E-05 | 1.03E-05 | -8.53E-05 | -1.17E-17 | -4.82E-03 | -1.71E-03 | 7.07E-01 | 5.25E-01 | 7.04E-01 | 5.36E-23 | 2.43E-07 | 2.41E-07 | 7.57E-07 | 7.59E-07 | 1.00E-05 |
| 30 | 0.542 | 2.28E-01 | 2.45E-01 | 2.44E-01 | 2.45E-01 | 2.77E-01 | 1.41E-05 | 6.81E-06 | 6.88E-06 | 2.15E-05 | 2.15E-05 | 1.86E-05 | 1.42E-05 | 1.03E-05 | -6.50E-05 | -1.17E-17 | -4.52E-03 | -1.30E-03 | 7.07E-01 | 5.36E-01 | 7.05E-01 | -4.83E-23 | 2.42E-07 | 2.41E-07 | 7.58E-07 | 7.59E-07 | 1.00E-05 |
| 81 | 1.496 | 2.28E-01 | 2.45E-01 | 2.45E-01 | 2.45E-01 | 3.39E-01 | 1.41E-05 | 6.81E-06 | 6.81E-06 | 2.15E-05 | 2.15E-05 | 1.42E-05 | 1.41E-05 | 1.03E-05 | -6.39E-11 | -1.17E-17 | -7.39E-05 | -1.28E-09 | 7.07E-01 | 7.04E-01 | 7.07E-01 | 5.36E-23 | 2.41E-07 | 2.41E-07 | 7.59E-07 | 7.59E-07 | 1.00E-05 |
| 82 | 1.515 | 2.28E-01 | 2.45E-01 | 2.45E-01 | 2.45E-01 | 3.39E-01 | 1.41E-05 | 6.81E-06 | 6.81E-06 | 2.15E-05 | 2.15E-05 | 1.42E-05 | 1.41E-05 | 1.03E-05 | -4.87E-11 | -1.17E-17 | -6.79E-05 | -9.75E-10 | 7.07E-01 | 7.05E-01 | 7.07E-01 | -4.83E-23 | 2.41E-07 | 2.41E-07 | 7.59E-07 | 7.59E-07 | 1.00E-05 |
| 83 | 1.533 | 2.28E-01 | 2.45E-01 | 2.45E-01 | 2.45E-01 | 3.39E-01 | 1.41E-05 | 6.81E-06 | 6.81E-06 | 2.15E-05 | 2.15E-05 | 1.42E-05 | 1.41E-05 | 1.03E-05 | -3.72E-11 | -1.17E-17 | -6.23E-05 | -7.43E-10 | 7.07E-01 | 7.05E-01 | 7.07E-01 | 5.36E-23 | 2.41E-07 | 2.41E-07 | 7.59E-07 | 7.59E-07 | 1.00E-05 |
| 84 | 1.552 | 2.28E-01 | 2.45E-01 | 2.45E-01 | 2.45E-01 | 3.39E-01 | 1.41E-05 | 6.81E-06 | 6.81E-06 | 2.15E-05 | 2.15E-05 | 1.42E-05 | 1.41E-05 | 1.03E-05 | -2.83E-11 | -1.17E-17 | -5.71E-05 | -5.67E-10 | 7.07E-01 | 7.05E-01 | 7.07E-01 | -4.83E-23 | 2.41E-07 | 2.41E-07 | 7.59E-07 | 7.59E-07 | 1.00E-05 |
| 85 | 1.571 | 2.28E-01 | 2.45E-01 | 2.45E-01 | 2.45E-01 | 3.39E-01 | 1.41E-05 | 6.81E-06 | 6.81E-06 | 2.15E-05 | 2.15E-05 | 1.42E-05 | 1.41E-05 | 1.03E-05 | -2.16E-11 | -1.17E-17 | -5.24E-05 | -4.32E-10 | 7.07E-01 | 7.05E-01 | 7.07E-01 | 6.44E-23 | 2.41E-07 | 2.41E-07 | 7.59E-07 | 7.59E-07 | 1.00E-05 |
| 86 | 1.59 | 2.28E-01 | 2.45E-01 | 2.45E-01 | 2.45E-01 | 3.39E-01 | 1.41E-05 | 6.81E-06 | 6.81E-06 | 2.15E-05 | 2.15E-05 | 1.42E-05 | 1.41E-05 | 1.03E-05 | -1.65E-11 | -1.17E-17 | -4.81E-05 | -3.29E-10 | 7.07E-01 | 7.05E-01 | 7.07E-01 | 6.97E-23 | 2.41E-07 | 2.41E-07 | 7.59E-07 | 7.59E-07 | 1.00E-05 |
| 87 | 1.608 | 2.28E-01 | 2.45E-01 | 2.45E-01 | 2.45E-01 | 3.39E-01 | 1.41E-05 | 6.81E-06 | 6.81E-06 | 2.15E-05 | 2.15E-05 | 1.42E-05 | 1.41E-05 | 1.03E-05 | -1.26E-11 | -1.17E-17 | -4.42E-05 | -2.51E-10 | 7.07E-01 | 7.05E-01 | 7.07E-01 | 3.06E-22 | 2.41E-07 | 2.41E-07 | 7.59E-07 | 7.59E-07 | 1.00E-05 |
| 88 | 1.627 | 2.28E-01 | 2.45E-01 | 2.45E-01 | 2.45E-01 | 3.39E-01 | 1.41E-05 | 6.81E-06 | 6.81E-06 | 2.15E-05 | 2.15E-05 | 1.42E-05 | 1.41E-05 | 1.03E-05 | -9.58E-12 | -1.17E-17 | -4.05E-05 | -1.92E-10 | 7.07E-01 | 7.06E-01 | 7.07E-01 | 1.64E-21 | 2.41E-07 | 2.41E-07 | 7.59E-07 | 7.59E-07 | 1.00E-05 |
| 89 | 1.646 | 2.28E-01 | 2.45E-01 | 2.45E-01 | 2.45E-01 | 3.39E-01 | 1.41E-05 | 6.81E-06 | 6.81E-06 | 2.15E-05 | 2.15E-05 | 1.42E-05 | 1.41E-05 | 1.03E-05 | -7.30E-12 | -1.17E-17 | -3.72E-05 | -1.46E-10 | 7.07E-01 | 7.06E-01 | 7.07E-01 | 7.63E-21 | 2.41E-07 | 2.41E-07 | 7.59E-07 | 7.59E-07 | 1.00E-05 |
| 90 | 1.664 | 2.28E-01 | 2.45E-01 | 2.45E-01 | 2.45E-01 | 3.39E-01 | 1.41E-05 | 6.81E-06 | 6.81E-06 | 2.15E-05 | 2.15E-05 | 1.42E-05 | 1.41E-05 | 1.03E-05 | -5.57E-12 | -1.17E-17 | -3.41E-05 | -1.11E-10 | 7.07E-01 | 7.06E-01 | 7.07E-01 | 3.57E-20 | 2.41E-07 | 2.41E-07 | 7.59E-07 | 7.59E-07 | 1.00E-05 |
| 91 | 1.683 | 2.28E-01 | 2.45E-01 | 2.45E-01 | 2.45E-01 | 3.39E-01 | 1.41E-05 | 6.81E-06 | 6.81E-06 | 2.15E-05 | 2.15E-05 | 1.42E-05 | 1.41E-05 | 1.03E-05 | -4.25E-12 | -1.17E-17 | -3.13E-05 | -8.49E-11 | -2.35E-16 | -6.26E-04 | 7.07E-01 | 1.67E-19 | 2.41E-07 | 2.41E-07 | 7.59E-07 | 7.59E-07 | 1.00E-05 |
| 92 | 1.702 | 2.28E-01 | 2.45E-01 | 2.45E-01 | 2.45E-01 | 3.39E-01 | 1.41E-05 | 6.81E-06 | 6.81E-06 | 2.15E-05 | 2.15E-05 | 1.42E-05 | 1.41E-05 | 1.03E-05 | -3.24E-12 | -1.17E-17 | -2.87E-05 | -6.47E-11 | -2.35E-16 | -5.74E-04 | 7.07E-01 | 7.80E-19 | 2.41E-07 | 2.41E-07 | 7.59E-07 | 7.59E-07 | 1.00E-05 |
| 93 | 1.72 | 2.28E-01 | 2.45E-01 | 2.45E-01 | 2.45E-01 | 3.39E-01 | 1.41E-05 | 6.81E-06 | 6.81E-06 | 2.15E-05 | 2.15E-05 | 1.42E-05 | 1.41E-05 | 1.03E-05 | -2.47E-12 | -1.17E-17 | -2.63E-05 | -4.94E-11 | -2.35E-16 | -5.27E-04 | 7.07E-01 | 3.64E-18 | 2.41E-07 | 2.41E-07 | 7.59E-07 | 7.59E-07 | 1.00E-05 |
| 94 | 1.739 | 2.28E-01 | 2.45E-01 | 2.45E-01 | 2.45E-01 | 3.39E-01 | 1.41E-05 | 6.81E-06 | 6.81E-06 | 2.15E-05 | 2.15E-05 | 1.42E-05 | 1.41E-05 | 1.03E-05 | -1.88E-12 | -1.17E-17 | -2.42E-05 | -3.76E-11 | -2.35E-16 | -4.83E-04 | 7.07E-01 | 1.70E-17 | 2.41E-07 | 2.41E-07 | 7.59E-07 | 7.59E-07 | 1.00E-05 |
| 95 | 1.758 | 2.28E-01 | 2.45E-01 | 2.45E-01 | 2.45E-01 | 3.39E-01 | 1.41E-05 | 6.81E-06 | 6.81E-06 | 2.15E-05 | 2.15E-05 | 1.42E-05 | 1.41E-05 | 1.03E-05 | -1.43E-12 | -1.17E-17 | -2.22E-05 | -2.87E-11 | -2.35E-16 | -4.44E-04 | 7.07E-01 | 7.96E-17 | 2.41E-07 | 2.41E-07 | 7.59E-07 | 7.59E-07 | 1.00E-05 |
| 96 | 1.777 | 2.28E-01 | 2.45E-01 | 2.45E-01 | 2.45E-01 | 3.39E-01 | 1.41E-05 | 6.81E-06 | 6.81E-06 | 2.15E-05 | 2.15E-05 | 1.42E-05 | 1.41E-05 | 1.03E-05 | -1.09E-12 | -1.17E-17 | -2.03E-05 | -2.19E-11 | -2.35E-16 | -4.07E-04 | 7.07E-01 | 3.72E-16 | 2.41E-07 | 2.41E-07 | 7.59E-07 | 7.59E-07 | 1.00E-05 |
| 97 | 1.795 | 2.28E-01 | 2.45E-01 | 2.45E-01 | 2.45E-01 | 3.39E-01 | 1.41E-05 | 6.81E-06 | 6.81E-06 | 2.15E-05 | 2.15E-05 | 1.42E-05 | 1.41E-05 | 1.03E-05 | -8.34E-13 | -1.17E-17 | -1.87E-05 | -1.67E-11 | -2.35E-16 | -3.73E-04 | 7.07E-01 | 1.74E-15 | 2.41E-07 | 2.41E-07 | 7.59E-07 | 7.59E-07 | 1.00E-05 |
| 98 | 1.814 | 2.28E-01 | 2.45E-01 | 2.45E-01 | 2.45E-01 | 3.39E-01 | 1.41E-05 | 6.81E-06 | 6.81E-06 | 2.15E-05 | 2.15E-05 | 1.42E-05 | 1.41E-05 | 1.03E-05 | -6.36E-13 | -1.17E-17 | -1.71E-05 | -1.27E-11 | -2.35E-16 | -3.43E-04 | 7.07E-01 | 8.13E-15 | 2.41E-07 | 2.41E-07 | 7.59E-07 | 7.59E-07 | 1.00E-05 |
| 99 | 1.833 | 2.28E-01 | 2.45E-01 | 2.45E-01 | 2.45E-01 | 3.39E-01 | 1.41E-05 | 6.81E-06 | 6.81E-06 | 2.15E-05 | 2.15E-05 | 1.42E-05 | 1.41E-05 | 1.03E-05 | -4.85E-13 | -1.17E-17 | -1.57E-05 | -9.70E-12 | -2.35E-16 | -3.14E-04 | 7.07E-01 | 3.80E-14 | 2.41E-07 | 2.41E-07 | 7.59E-07 | 7.59E-07 | 1.00E-05 |
| 100 | 1.851 | 2.28E-01 | 2.45E-01 | 2.45E-01 | 2.45E-01 | 3.39E-01 | 1.41E-05 | 6.81E-06 | 6.81E-06 | 2.15E-05 | 2.15E-05 | 1.42E-05 | 1.41E-05 | 1.03E-05 | -3.70E-13 | -1.17E-17 | -1.44E-05 | -7.39E-12 | -2.35E-16 | -2.88E-04 | 7.07E-01 | 1.78E-13 | 2.41E-07 | 2.41E-07 | 7.59E-07 | 7.59E-07 | 1.00E-05 |
| 101 | 1.87 | 2.28E-01 | 2.45E-01 | 2.45E-01 | 2.45E-01 | 3.39E-01 | 1.41E-05 | 6.81E-06 | 6.81E-06 | 2.15E-05 | 2.15E-05 | 1.42E-05 | 1.41E-05 | 1.03E-05 | -2.82E-13 | -1.17E-17 | -1.32E-05 | -5.64E-12 | -2.35E-16 | -2.65E-04 | 7.07E-01 | 8.30E-13 | 2.41E-07 | 2.41E-07 | 7.59E-07 | 7.59E-07 | 1.00E-05 |
| 102 | 1.889 | 2.28E-01 | 2.45E-01 | 2.45E-01 | 2.45E-01 | 3.39E-01 | 1.41E-05 | 6.81E-06 | 6.81E-06 | 2.15E-05 | 2.15E-05 | 1.42E-05 | 1.41E-05 | 1.03E-05 | -2.15E-13 | -1.17E-17 | -1.21E-05 | -4.30E-12 | -2.35E-16 | -2.43E-04 | 7.07E-01 | 3.88E-12 | 2.41E-07 | 2.41E-07 | 7.59E-07 | 7.59E-07 | 1.00E-05 |
| 103 | 1.907 | 2.28E-01 | 2.45E-01 | 2.45E-01 | 2.45E-01 | 3.39E-01 | 1.41E-05 | 6.81E-06 | 6.81E-06 | 2.15E-05 | 2.15E-05 | 1.42E-05 | 1.41E-05 | 1.03E-05 | -1.64E-13 | -1.17E-17 | -1.11E-05 | -3.28E-12 | -2.35E-16 | -2.23E-04 | 7.07E-01 | 1.82E-11 | 2.41E-07 | 2.41E-07 | 7.59E-07 | 7.59E-07 | 1.00E-05 |
| 104 | 1.926 | 2.28E-01 | 2.45E-01 | 2.45E-01 | 2.45E-01 | 3.39E-01 | 1.41E-05 | 6.81E-06 | 6.81E-06 | 2.15E-05 | 2.15E-05 | 1.41E-05 | 1.41E-05 | 1.03E-05 | -1.25E-13 | -1.17E-17 | -1.02E-05 | -2.50E-12 | -2.35E-16 | -2.04E-04 | 7.07E-01 | 8.62E-11 | 2.41E-07 | 2.41E-07 | 7.59E-07 | 7.59E-07 | 1.00E-05 |
| 105 | 1.945 | 2.28E-01 | 2.44E-01 | 2.45E-01 | 2.46E-01 | 3.39E-01 | 1.41E-05 | 6.84E-06 | 6.81E-06 | 2.15E-05 | 2.14E-05 | 1.41E-05 | 1.41E-05 | 1.04E-05 | -9.53E-14 | -1.17E-17 | -9.37E-06 | -1.91E-12 | -2.35E-16 | -1.87E-04 | 7.07E-01 | 4.31E-10 | 2.41E-07 | 2.42E-07 | 7.59E-07 | 7.58E-07 | 1.00E-05 |
| 106 | 1.964 | 2.28E-01 | 2.40E-01 | 2.45E-01 | 2.58E-01 | 3.39E-01 | 1.41E-05 | 6.96E-06 | 6.81E-06 | 2.15E-05 | 2.13E-05 | 1.41E-05 | 1.41E-05 | 1.05E-05 | -7.27E-14 | -1.17E-17 | -8.60E-06 | -1.45E-12 | -2.35E-16 | -1.72E-04 | 7.07E-01 | 3.80E-09 | 2.41E-07 | 2.46E-07 | 7.59E-07 | 7.54E-07 | 1.00E-05 |
| 107 | 1.982 | 2.28E-01 | 2.28E-01 | 2.45E-01 | 3.39E-01 | 3.39E-01 | 1.41E-05 | 8.03E-06 | 6.81E-06 | 2.15E-05 | 2.03E-05 | 1.41E-05 | 1.41E-05 | 1.15E-05 | -5.54E-14 | -1.17E-17 | -7.89E-06 | -1.11E-12 | -2.35E-16 | -1.58E-04 | 7.07E-01 | 2.16E-08 | 2.41E-07 | 2.84E-07 | 7.59E-07 | 7.16E-07 | 1.00E-05 |
| 108 | 2.001 | 2.28E-01 | 2.28E-01 | 2.45E-01 | 3.39E-01 | 3.39E-01 | 1.41E-05 | 1.41E-05 | 6.81E-06 | 2.15E-05 | 1.41E-05 | 1.41E-05 | 1.41E-05 | 1.03E-05 | -4.22E-14 | -1.17E-17 | -7.24E-06 | -8.44E-13 | 7.35E-02 | 2.33E-02 | 7.07E-01 | 0 | 2.41E-07 | 5.00E-07 | 7.59E-07 | 5.00E-07 | 1.00E-05 |

## Table C4 The FDM Results for the 90°, 1.14-Meter System using The Modified Kisch Solution

| # | z | hci | hcp | hp | hfp | hfi | kci | kcp | kc | kf | kfp | kfi | kll | kp | dhp | dhpc | dhpf | l | dq | qci | qcp | qfi | qfp | q-total |
|---|---|---|---|---|---|---|---|---|---|---|---|---|---|---|---|---|---|---|---|---|---|---|---|---|
| 1 | 0 | 0.00E+00 | | 1.00E-04 | | 0.00E+00 | 1.48E-02 | #N/A | 1.49E-02 | 3.00E-05 | #N/A | 4.50E-05 | 7.47E-03 | #N/A | -1.06E-02 | -1.06E-02 | -8.28E-03 | 1.34E-03 | #N/A | 9.98E-07 | #N/A | 2.01E-09 | #N/A | 1.00E-05 |
| 2 | 0.011 | 1.06E-02 | | 1.07E-02 | | 8.28E-03 | 1.48E-02 | #N/A | 1.48E-02 | 3.00E-05 | #N/A | 3.00E-05 | 7.40E-03 | #N/A | -1.06E-02 | -1.06E-02 | -7.10E-03 | 1.35E-03 | #N/A | 9.98E-07 | #N/A | 2.03E-09 | #N/A | 1.00E-05 |
| 3 | 0.021 | 2.13E-02 | | 2.14E-02 | | 1.54E-02 | 1.47E-02 | #N/A | 1.47E-02 | 3.00E-05 | #N/A | 3.00E-05 | 7.34E-03 | #N/A | -1.06E-02 | -1.06E-02 | -7.10E-03 | 1.36E-03 | #N/A | 9.98E-07 | #N/A | 2.04E-09 | #N/A | 1.00E-05 |
| 4 | 0.032 | 3.19E-02 | #N/A | 3.20E-02 | #N/A | 2.25E-02 | 1.46E-02 | #N/A | 1.46E-02 | 3.00E-05 | #N/A | 3.00E-05 | 7.31E-03 | #N/A | -1.06E-02 | -1.06E-02 | -7.10E-03 | 1.37E-03 | #N/A | 9.98E-07 | #N/A | 2.05E-09 | #N/A | 1.00E-05 |
| 5 | 0.043 | 4.26E-02 | #N/A | 4.26E-02 | #N/A | 2.96E-02 | 1.43E-02 | #N/A | 1.43E-02 | 2.99E-05 | #N/A | 3.00E-05 | 7.18E-03 | #N/A | -1.06E-02 | -1.06E-02 | -7.10E-03 | 1.39E-03 | #N/A | 9.98E-07 | #N/A | 2.09E-09 | #N/A | 1.00E-05 |
| 6 | 0.053 | 5.32E-02 | #N/A | 5.33E-02 | #N/A | 3.67E-02 | 1.37E-02 | #N/A | 1.37E-02 | 2.99E-05 | #N/A | 2.99E-05 | 6.86E-03 | #N/A | -1.06E-02 | -1.06E-02 | -7.09E-03 | 1.46E-03 | #N/A | 9.98E-07 | #N/A | 2.18E-09 | #N/A | 1.00E-05 |
| 7 | 0.064 | 6.39E-02 | #N/A | 6.39E-02 | #N/A | 4.38E-02 | 1.25E-02 | #N/A | 1.25E-02 | 2.99E-05 | #N/A | 2.99E-05 | 6.29E-03 | #N/A | -1.06E-02 | -1.06E-02 | -7.09E-03 | 1.59E-03 | #N/A | 9.98E-07 | #N/A | 2.38E-09 | #N/A | 1.00E-05 |
| 8 | 0.075 | 7.45E-02 | #N/A | 7.45E-02 | #N/A | 5.09E-02 | 1.11E-02 | #N/A | 1.11E-02 | 2.98E-05 | #N/A | 2.99E-05 | 5.58E-03 | #N/A | -1.06E-02 | -1.06E-02 | -7.09E-03 | 1.79E-03 | #N/A | 9.97E-07 | #N/A | 2.67E-09 | #N/A | 1.00E-05 |
| 9 | 0.085 | 8.51E-02 | #N/A | 8.52E-02 | #N/A | 5.80E-02 | 8.96E-03 | #N/A | 8.95E-03 | 2.98E-05 | #N/A | 2.99E-05 | 4.49E-03 | #N/A | -1.06E-02 | -1.06E-02 | -7.09E-03 | 2.23E-03 | #N/A | 9.97E-07 | #N/A | 3.32E-09 | #N/A | 1.00E-05 |
| 10 | 0.096 | 9.58E-02 | #N/A | 9.58E-02 | #N/A | 6.50E-02 | 7.05E-03 | #N/A | 7.04E-03 | 2.98E-05 | #N/A | 2.99E-05 | 3.54E-03 | #N/A | -1.06E-02 | -1.06E-02 | -7.08E-03 | 2.83E-03 | #N/A | 9.96E-07 | #N/A | 4.21E-09 | #N/A | 1.00E-05 |
| 11 | 0.107 | 1.06E-01 | #N/A | 1.06E-01 | #N/A | 7.21E-02 | 4.85E-03 | #N/A | 4.85E-03 | 2.98E-05 | #N/A | 2.99E-05 | 2.44E-03 | #N/A | -1.06E-02 | -1.06E-02 | -7.08E-03 | 4.10E-03 | #N/A | 9.94E-07 | #N/A | 6.10E-09 | #N/A | 1.00E-05 |
| 12 | 0.117 | 1.17E-01 | #N/A | 1.17E-01 | #N/A | 7.92E-02 | 3.14E-03 | #N/A | 3.14E-03 | 2.97E-05 | #N/A | 2.98E-05 | 1.59E-03 | #N/A | -1.06E-02 | -1.06E-02 | -7.08E-03 | 6.31E-03 | #N/A | 9.91E-07 | #N/A | 9.37E-09 | #N/A | 1.00E-05 |
| 13 | 0.128 | 1.28E-01 | #N/A | 1.28E-01 | #N/A | 8.63E-02 | 1.78E-03 | #N/A | 1.78E-03 | 2.97E-05 | #N/A | 2.98E-05 | 9.05E-04 | #N/A | -1.05E-02 | -1.06E-02 | -7.08E-03 | 1.11E-02 | #N/A | 9.84E-07 | #N/A | 1.64E-08 | #N/A | 1.00E-05 |
| 14 | 0.138 | 1.38E-01 | #N/A | 1.38E-01 | #N/A | 9.34E-02 | 8.34E-04 | #N/A | 8.42E-04 | 2.97E-05 | #N/A | 2.98E-05 | 4.36E-04 | #N/A | -1.04E-02 | -1.05E-02 | -7.08E-03 | 2.29E-02 | #N/A | 9.66E-07 | #N/A | 3.40E-08 | #N/A | 1.00E-05 |
| 15 | 0.149 | 1.49E-01 | #N/A | 1.49E-01 | #N/A | 1.00E-01 | 3.10E-04 | #N/A | 3.16E-04 | 2.96E-05 | #N/A | 2.98E-05 | 1.73E-04 | #N/A | -1.00E-02 | -1.03E-02 | -7.07E-03 | 5.79E-02 | #N/A | 9.14E-07 | #N/A | 8.58E-08 | #N/A | 1.00E-05 |
| 16 | 0.16 | 1.59E-01 | #N/A | 1.59E-01 | #N/A | 1.08E-01 | 1.17E-04 | #N/A | 1.23E-04 | 2.96E-05 | #N/A | 2.98E-05 | 7.62E-05 | #N/A | -9.25E-03 | -9.74E-03 | -7.07E-03 | 1.31E-01 | #N/A | 8.06E-07 | #N/A | 1.94E-07 | #N/A | 1.00E-05 |
| 17 | 0.17 | 1.69E-01 | #N/A | 1.68E-01 | #N/A | 1.15E-01 | 4.68E-05 | #N/A | 5.14E-05 | 2.96E-05 | #N/A | 2.97E-05 | 4.05E-05 | #N/A | -8.02E-03 | -8.38E-03 | -7.07E-03 | 2.47E-01 | #N/A | 6.35E-07 | #N/A | 3.65E-07 | #N/A | 1.00E-05 |
| 18 | 0.181 | 1.77E-01 | #N/A | 1.76E-01 | #N/A | 1.22E-01 | 2.13E-05 | #N/A | 2.41E-05 | 2.96E-05 | #N/A | 2.97E-05 | 2.69E-05 | #N/A | -6.68E-03 | -5.65E-03 | -7.07E-03 | 3.72E-01 | #N/A | 4.49E-07 | #N/A | 5.51E-07 | #N/A | 1.00E-05 |
| 19 | 0.192 | 1.83E-01 | #N/A | 1.83E-01 | #N/A | 1.29E-01 | 1.25E-05 | #N/A | 1.29E-05 | 2.95E-05 | #N/A | 2.97E-05 | 2.12E-05 | #N/A | -5.63E-03 | -2.13E-03 | -7.06E-03 | 4.72E-01 | #N/A | 3.03E-07 | #N/A | 6.97E-07 | #N/A | 1.00E-05 |
| 20 | 0.202 | 1.85E-01 | #N/A | 1.88E-01 | #N/A | 1.36E-01 | 1.02E-05 | #N/A | 6.25E-06 | 2.95E-05 | #N/A | 2.97E-05 | 1.79E-05 | #N/A | -4.70E-03 | -2.38E-04 | -7.06E-03 | 5.59E-01 | #N/A | 1.75E-07 | #N/A | 8.25E-07 | #N/A | 1.00E-05 |
| 21 | 0.213 | 1.85E-01 | #N/A | 1.93E-01 | #N/A | 1.43E-01 | 9.88E-06 | #N/A | 3.02E-06 | 2.95E-05 | #N/A | 2.97E-05 | 1.63E-05 | #N/A | -4.10E-03 | 0.00E+00 | -7.06E-03 | 6.15E-01 | #N/A | 9.28E-08 | #N/A | 9.07E-07 | #N/A | 1.00E-05 |
| 22 | 0.224 | 1.85E-01 | #N/A | 1.97E-01 | #N/A | 1.50E-01 | 9.88E-06 | #N/A | 1.60E-06 | 2.95E-05 | #N/A | 2.96E-05 | 1.56E-05 | #N/A | -3.80E-03 | 0.00E+00 | -7.06E-03 | 6.43E-01 | #N/A | 5.14E-08 | #N/A | 9.49E-07 | #N/A | 1.00E-05 |
| 23 | 0.234 | 1.85E-01 | #N/A | 2.01E-01 | #N/A | 1.57E-01 | 9.88E-06 | #N/A | 9.14E-07 | 2.95E-05 | #N/A | 2.96E-05 | 1.52E-05 | #N/A | -3.65E-03 | 0.00E+00 | -7.05E-03 | 6.58E-01 | #N/A | 3.01E-08 | #N/A | 9.70E-07 | #N/A | 1.00E-05 |
| 24 | 0.245 | 1.85E-01 | #N/A | 2.04E-01 | #N/A | 1.64E-01 | 9.88E-06 | #N/A | 5.97E-07 | 2.95E-05 | #N/A | 2.96E-05 | 1.50E-05 | #N/A | -3.57E-03 | 0.00E+00 | -7.05E-03 | 6.65E-01 | #N/A | 1.99E-08 | #N/A | 9.80E-07 | #N/A | 1.00E-05 |
| 25 | 0.256 | 1.85E-01 | #N/A | 2.08E-01 | #N/A | 1.71E-01 | 9.88E-06 | #N/A | 3.94E-07 | 2.95E-05 | #N/A | 2.96E-05 | 1.49E-05 | #N/A | -3.52E-03 | 0.00E+00 | -7.05E-03 | 6.69E-01 | #N/A | 1.32E-08 | #N/A | 9.87E-07 | #N/A | 1.00E-05 |
| 26 | 0.266 | 1.85E-01 | #N/A | 2.12E-01 | #N/A | 1.78E-01 | 9.88E-06 | #N/A | 2.61E-07 | 2.95E-05 | #N/A | 2.96E-05 | 1.49E-05 | #N/A | -3.49E-03 | 0.00E+00 | -7.05E-03 | 6.73E-01 | #N/A | 8.78E-09 | #N/A | 9.91E-07 | #N/A | 1.00E-05 |
| 27 | 0.277 | 1.85E-01 | #N/A | 2.15E-01 | #N/A | 1.85E-01 | 9.88E-06 | #N/A | 1.74E-07 | 2.95E-05 | #N/A | 2.95E-05 | 1.48E-05 | #N/A | -3.46E-03 | 0.00E+00 | -7.05E-03 | 6.75E-01 | #N/A | 5.87E-09 | #N/A | 9.94E-07 | #N/A | 1.00E-05 |
| 28 | 0.288 | 1.85E-01 | #N/A | 2.18E-01 | #N/A | 1.92E-01 | 9.88E-06 | #N/A | 1.16E-07 | 2.95E-05 | #N/A | 2.95E-05 | 1.48E-05 | #N/A | -3.45E-03 | 0.00E+00 | -7.04E-03 | 6.76E-01 | #N/A | 3.93E-09 | #N/A | 9.96E-07 | #N/A | 1.00E-05 |
| 29 | 0.298 | 1.85E-01 | #N/A | 2.22E-01 | #N/A | 1.99E-01 | 9.88E-06 | #N/A | 7.77E-08 | 2.94E-05 | #N/A | 2.95E-05 | 1.48E-05 | #N/A | -3.43E-03 | 0.00E+00 | -7.04E-03 | 6.77E-01 | #N/A | 2.63E-09 | #N/A | 9.97E-07 | #N/A | 1.00E-05 |
| 30 | 0.309 | 1.85E-01 | #N/A | 2.25E-01 | #N/A | 2.06E-01 | 9.88E-06 | #N/A | 5.20E-08 | 2.94E-05 | #N/A | 2.95E-05 | 1.47E-05 | #N/A | -3.43E-03 | 0.00E+00 | -7.04E-03 | 6.78E-01 | #N/A | 1.76E-09 | #N/A | 9.98E-07 | #N/A | 1.00E-05 |
| 81 | 0.852 | 1.85E-01 | #N/A | 3.95E-01 | #N/A | 4.30E-01 | 9.88E-06 | #N/A | 3.73E-11 | 2.38E-05 | #N/A | 1.00E-05 | 1.19E-05 | #N/A | -1.69E-03 | 0.00E+00 | -1.27E-05 | 8.41E-01 | #N/A | 1.57E-12 | #N/A | 1.00E-06 | #N/A | 1.00E-05 |
| 82 | 0.863 | 1.85E-01 | #N/A | 3.97E-01 | #N/A | 4.30E-01 | 9.88E-06 | #N/A | 3.58E-11 | 2.27E-05 | #N/A | 1.00E-05 | 1.14E-05 | #N/A | -1.29E-03 | 0.00E+00 | -9.47E-06 | 8.79E-01 | #N/A | 1.57E-12 | #N/A | 1.00E-06 | #N/A | 1.00E-05 |
| 83 | 0.873 | 1.85E-01 | #N/A | 3.98E-01 | #N/A | 4.30E-01 | 9.88E-06 | #N/A | 3.47E-11 | 2.20E-05 | #N/A | 1.00E-05 | 1.10E-05 | #N/A | -9.66E-04 | 0.00E+00 | -7.04E-06 | 9.09E-01 | #N/A | 1.58E-12 | #N/A | 1.00E-06 | #N/A | 1.00E-05 |
| 84 | 0.884 | 1.85E-01 | #N/A | 3.99E-01 | #N/A | 4.30E-01 | 9.88E-06 | #N/A | 3.39E-11 | 2.14E-05 | #N/A | 1.00E-05 | 1.07E-05 | #N/A | -7.19E-04 | 0.00E+00 | -5.24E-06 | 9.33E-01 | #N/A | 1.58E-12 | #N/A | 1.00E-06 | #N/A | 1.00E-05 |
| 85 | 0.895 | 1.85E-01 | #N/A | 4.00E-01 | #N/A | 4.30E-01 | 9.88E-06 | #N/A | 3.33E-11 | 2.10E-05 | #N/A | 1.00E-05 | 1.05E-05 | #N/A | -5.31E-04 | 0.00E+00 | -3.89E-06 | 9.50E-01 | #N/A | 1.58E-12 | #N/A | 1.00E-06 | #N/A | 1.00E-05 |
| 86 | 0.905 | 1.85E-01 | #N/A | 4.00E-01 | #N/A | 4.30E-01 | 9.88E-06 | #N/A | 3.29E-11 | 2.08E-05 | #N/A | 1.00E-05 | 1.04E-05 | #N/A | -3.89E-04 | 0.00E+00 | -2.90E-06 | 9.63E-01 | #N/A | 1.58E-12 | #N/A | 1.00E-06 | #N/A | 1.00E-05 |
| 87 | 0.916 | 1.85E-01 | #N/A | 4.01E-01 | #N/A | 4.30E-01 | 9.88E-06 | #N/A | 3.26E-11 | 2.05E-05 | #N/A | 1.00E-05 | 1.03E-05 | #N/A | -2.84E-04 | 0.00E+00 | -2.15E-06 | 9.73E-01 | #N/A | 1.58E-12 | #N/A | 1.00E-06 | #N/A | 1.00E-05 |
| 88 | 0.927 | 1.85E-01 | #N/A | 4.01E-01 | 4.02E-01 | 4.30E-01 | 9.88E-06 | #N/A | 3.23E-11 | 2.04E-05 | #N/A | 1.00E-05 | 1.02E-05 | #N/A | -2.07E-04 | 0.00E+00 | -1.60E-06 | 9.81E-01 | #N/A | 1.59E-12 | #N/A | 1.00E-06 | #N/A | 1.00E-05 |
| 89 | 0.937 | 1.85E-01 | 1.34E-01 | 4.01E-01 | 4.02E-01 | 4.30E-01 | 9.88E-06 | -3.27E-15 | 3.22E-11 | 2.03E-05 | 2.00E-05 | 1.00E-05 | 1.01E-05 | -6.54E-15 | -1.51E-04 | 0.00E+00 | -1.19E-06 | 9.86E-01 | 1.32E-16 | 1.59E-12 | -1.64E-16 | 1.00E-06 | 1.00E-06 | 1.00E-05 |
| 90 | 0.948 | 1.85E-01 | 1.82E-01 | 4.01E-01 | 4.02E-01 | 4.30E-01 | 9.88E-06 | 2.32E-14 | 3.21E-11 | 2.02E-05 | 2.00E-05 | 1.00E-05 | 1.01E-05 | 4.65E-14 | -1.09E-04 | 0.00E+00 | -8.85E-07 | 9.90E-01 | 1.76E-15 | 1.59E-12 | 1.16E-15 | 1.00E-06 | 1.00E-06 | 1.00E-05 |
| 91 | 0.959 | 1.85E-01 | 2.11E-01 | 4.01E-01 | 4.02E-01 | 4.30E-01 | 9.88E-06 | 3.75E-13 | 3.20E-11 | 2.01E-05 | 2.00E-05 | 1.00E-05 | 1.01E-05 | 7.51E-13 | -7.91E-05 | 0.00E+00 | -6.58E-07 | 9.93E-01 | 8.28E-15 | 1.59E-12 | 1.88E-14 | 1.00E-06 | 1.00E-06 | 1.00E-05 |
| 92 | 0.969 | 1.85E-01 | 2.32E-01 | 4.01E-01 | 4.02E-01 | 4.30E-01 | 9.88E-06 | 2.03E-12 | 3.19E-11 | 2.01E-05 | 2.00E-05 | 1.00E-05 | 1.01E-05 | 4.06E-12 | -5.72E-05 | 0.00E+00 | -4.89E-07 | 9.95E-01 | 2.64E-14 | 1.59E-12 | 1.02E-13 | 1.00E-06 | 1.00E-06 | 1.00E-05 |
| 93 | 0.98 | 1.85E-01 | 2.50E-01 | 4.01E-01 | 4.02E-01 | 4.30E-01 | 9.88E-06 | 7.30E-12 | 3.19E-11 | 2.01E-05 | 2.00E-05 | 1.00E-05 | 1.00E-05 | 1.46E-11 | -4.14E-05 | 0.00E+00 | -3.64E-07 | 9.96E-01 | 6.67E-14 | 1.59E-12 | 3.65E-13 | 1.00E-06 | 1.00E-06 | 1.00E-05 |
| 94 | 0.99 | 1.85E-01 | 2.65E-01 | 4.01E-01 | 4.02E-01 | 4.30E-01 | 9.88E-06 | 2.06E-11 | 3.18E-11 | 2.01E-05 | 2.00E-05 | 1.00E-05 | 1.00E-05 | 4.13E-11 | -2.99E-05 | 0.00E+00 | -2.71E-07 | 9.97E-01 | 1.44E-13 | 1.59E-12 | 1.03E-12 | 1.00E-06 | 1.00E-06 | 1.00E-05 |
| 95 | 1.001 | 1.85E-01 | 2.78E-01 | 4.02E-01 | 4.02E-01 | 4.30E-01 | 9.88E-06 | 4.94E-11 | 3.18E-11 | 2.00E-05 | 2.00E-05 | 1.00E-05 | 1.00E-05 | 9.89E-11 | -2.16E-05 | 0.00E+00 | -2.01E-07 | 9.98E-01 | 2.76E-13 | 1.59E-12 | 2.47E-12 | 1.00E-06 | 1.00E-06 | 1.00E-05 |
| 96 | 1.012 | 1.85E-01 | 2.89E-01 | 4.02E-01 | 4.02E-01 | 4.30E-01 | 9.88E-06 | 1.05E-10 | 3.18E-11 | 2.00E-05 | 2.00E-05 | 1.00E-05 | 1.00E-05 | 2.09E-10 | -1.56E-05 | 0.00E+00 | -1.50E-07 | 9.99E-01 | 4.84E-13 | 1.59E-12 | 5.24E-12 | 1.00E-06 | 1.00E-06 | 1.00E-05 |
| 97 | 1.022 | 1.85E-01 | 2.99E-01 | 4.02E-01 | 4.02E-01 | 4.30E-01 | 9.88E-06 | 2.01E-10 | 3.18E-11 | 2.00E-05 | 2.00E-05 | 1.00E-05 | 1.00E-05 | 4.03E-10 | -1.13E-05 | 0.00E+00 | -1.11E-07 | 9.99E-01 | 7.86E-13 | 1.59E-12 | 1.01E-11 | 1.00E-06 | 1.00E-06 | 1.00E-05 |
| 98 | 1.033 | 1.85E-01 | 2.90E-01 | 4.02E-01 | 4.02E-01 | 4.30E-01 | 9.88E-06 | 3.59E-10 | 3.18E-11 | 2.00E-05 | 2.00E-05 | 1.00E-05 | 1.00E-05 | 7.17E-10 | -8.14E-06 | 0.00E+00 | -8.27E-08 | 9.99E-01 | 1.65E-12 | 1.59E-12 | 1.79E-11 | 1.00E-06 | 1.00E-06 | 1.00E-05 |
| 99 | 1.044 | 1.85E-01 | 2.76E-01 | 4.02E-01 | 4.02E-01 | 4.30E-01 | 9.88E-06 | 6.88E-10 | 3.18E-11 | 2.00E-05 | 2.00E-05 | 1.00E-05 | 1.00E-05 | 1.38E-09 | -5.88E-06 | 0.00E+00 | -6.15E-08 | 9.99E-01 | 3.96E-12 | 1.59E-12 | 3.44E-11 | 1.00E-06 | 1.00E-06 | 1.00E-05 |
| 100 | 1.054 | 1.85E-01 | 2.60E-01 | 4.02E-01 | 4.02E-01 | 4.30E-01 | 9.88E-06 | 1.48E-09 | 3.18E-11 | 2.00E-05 | 2.00E-05 | 1.00E-05 | 1.00E-05 | 2.96E-09 | -4.24E-06 | 0.00E+00 | -4.57E-08 | 1.00E+00 | 1.13E-11 | 1.59E-12 | 7.40E-11 | 1.00E-06 | 1.00E-06 | 1.00E-05 |
| 101 | 1.065 | 1.85E-01 | 2.40E-01 | 4.02E-01 | 4.02E-01 | 4.30E-01 | 9.88E-06 | 3.74E-09 | 3.18E-11 | 2.00E-05 | 2.00E-05 | 1.00E-05 | 1.00E-05 | 7.47E-09 | -3.06E-06 | 0.00E+00 | -3.40E-08 | 1.00E+00 | 4.17E-11 | 1.59E-12 | 1.87E-10 | 1.00E-06 | 1.00E-06 | 1.00E-05 |
| 102 | 1.076 | 1.85E-01 | 2.26E-01 | 4.02E-01 | 4.02E-01 | 4.30E-01 | 9.88E-06 | 1.21E-08 | 3.18E-11 | 2.00E-05 | 2.00E-05 | 1.00E-05 | 1.00E-05 | 2.41E-08 | -2.21E-06 | 0.00E+00 | -2.53E-08 | 1.00E+00 | 1.79E-10 | 1.59E-12 | 6.04E-10 | 1.00E-06 | 9.99E-07 | 1.00E-05 |
| 103 | 1.086 | 1.85E-01 | 2.12E-01 | 4.02E-01 | 4.02E-01 | 4.30E-01 | 9.88E-06 | 4.79E-08 | 3.18E-11 | 2.00E-05 | 2.00E-05 | 1.00E-05 | 1.00E-05 | 9.56E-08 | -1.60E-06 | 0.00E+00 | -1.88E-08 | 1.00E+00 | 9.61E-10 | 1.59E-12 | 2.40E-09 | 1.00E-06 | 9.98E-07 | 1.00E-05 |
| 104 | 1.097 | 1.85E-01 | 1.98E-01 | 4.02E-01 | 4.04E-01 | 4.30E-01 | 9.88E-06 | 2.40E-07 | 3.18E-11 | 2.00E-05 | 1.98E-05 | 1.00E-05 | 1.00E-05 | 4.74E-07 | -1.15E-06 | 0.00E+00 | -1.40E-08 | 1.00E+00 | 5.48E-09 | 1.59E-12 | 1.20E-08 | 1.00E-06 | 9.88E-07 | 1.00E-05 |
| 105 | 1.108 | 1.85E-01 | 1.90E-01 | 4.02E-01 | 4.12E-01 | 4.30E-01 | 9.88E-06 | 1.34E-06 | 3.18E-11 | 2.00E-05 | 1.87E-05 | 1.00E-05 | 1.00E-05 | 2.49E-06 | -8.32E-07 | 0.00E+00 | -1.04E-08 | 1.00E+00 | 1.73E-08 | 1.59E-12 | 6.68E-08 | 1.00E-06 | 9.33E-07 | 1.00E-05 |
| 106 | 1.118 | 1.85E-01 | 1.85E-01 | 4.02E-01 | 4.30E-01 | 4.30E-01 | 9.88E-06 | 4.79E-06 | 3.18E-11 | 2.00E-05 | 1.52E-05 | 1.00E-05 | 1.00E-05 | 7.28E-06 | -6.00E-07 | 0.00E+00 | -7.73E-09 | 1.00E+00 | 2.61E-08 | 1.59E-12 | 2.39E-07 | 1.00E-06 | 7.61E-07 | 1.00E-05 |
| 107 | 1.129 | 1.85E-01 | 1.85E-01 | 4.02E-01 | 4.30E-01 | 4.30E-01 | 9.88E-06 | 1.00E-05 | 3.18E-11 | 2.00E-05 | 1.00E-05 | 1.00E-05 | 1.00E-05 | 1.00E-05 | -4.33E-07 | 0.00E+00 | -5.75E-09 | 1.00E+00 | 1.66E-13 | 1.59E-12 | 5.00E-07 | 1.00E-06 | 5.00E-07 | 1.00E-05 |
| 108 | 1.14 | 1.85E-01 | 1.85E-01 | 4.02E-01 | 4.30E-01 | 4.30E-01 | 9.88E-06 | 1.00E-05 | 3.18E-11 | 2.00E-05 | 1.00E-05 | 1.00E-05 | 1.00E-05 | 6.35E-11 | -3.13E-07 | 0.00E+00 | -4.27E-09 | 1.00E+00 | 0 | 1.59E-12 | 5.00E-07 | 1.00E-06 | 5.00E-07 | 1.00E-05 |

## Table C5 The FDM Results for the 75°, 2-Meter System using The Modified Kisch Solution

| # | z | hci | hcp | hp | hfp | hfi | kci | kcp | kc | kf | kfp | kfi | kll | kp | dhp | dhpc | dhpf | l | dq | qci | qcp | qfi | qfp | q-total |
|---|---|---|---|---|---|---|---|---|---|---|---|---|---|---|---|---|---|---|---|---|---|---|---|---|
| 1 | 0 | 0.00E+00 | | 1.00E-04 | | 0.00E+00 | 1.48E-02 | #N/A | 1.49E-02 | 3.00E-05 | #N/A | 4.50E-05 | 7.47E-03 | #N/A | -1.86E-02 | -1.86E-02 | -1.44E-02 | 1.34E-03 | #N/A | 9.98E-07 | #N/A | 2.01E-09 | #N/A | 1.00E-05 |
| 2 | 0.019 | 1.86E-02 | | 1.87E-02 | | 1.44E-02 | 1.46E-02 | #N/A | 1.46E-02 | 3.00E-05 | #N/A | 3.00E-05 | 7.33E-03 | #N/A | -1.86E-02 | -1.86E-02 | -1.22E-02 | 1.36E-03 | #N/A | 9.98E-07 | #N/A | 2.05E-09 | #N/A | 1.00E-05 |
| 3 | 0.037 | 3.73E-02 | | 3.73E-02 | | 2.66E-02 | 1.45E-02 | #N/A | 1.45E-02 | 2.99E-05 | #N/A | 3.00E-05 | 7.25E-03 | #N/A | -1.86E-02 | -1.86E-02 | -1.22E-02 | 1.38E-03 | #N/A | 9.98E-07 | #N/A | 2.07E-09 | #N/A | 1.00E-05 |
| 4 | 0.056 | 5.59E-02 | #N/A | 5.60E-02 | #N/A | 3.88E-02 | 1.35E-02 | #N/A | 1.35E-02 | 2.99E-05 | #N/A | 2.99E-05 | 6.74E-03 | #N/A | -1.86E-02 | -1.86E-02 | -1.22E-02 | 1.48E-03 | #N/A | 9.98E-07 | #N/A | 2.22E-09 | #N/A | 1.00E-05 |
| 5 | 0.075 | 7.45E-02 | #N/A | 7.46E-02 | #N/A | 5.10E-02 | 1.11E-02 | #N/A | 1.11E-02 | 2.98E-05 | #N/A | 2.99E-05 | 5.58E-03 | #N/A | -1.86E-02 | -1.86E-02 | -1.22E-02 | 1.79E-03 | #N/A | 9.97E-07 | #N/A | 2.67E-09 | #N/A | 1.00E-05 |
| 6 | 0.093 | 9.32E-02 | #N/A | 9.32E-02 | #N/A | 6.32E-02 | 7.47E-03 | #N/A | 7.47E-03 | 2.98E-05 | #N/A | 2.99E-05 | 3.75E-03 | #N/A | -1.86E-02 | -1.86E-02 | -1.22E-02 | 2.67E-03 | #N/A | 9.96E-07 | #N/A | 3.97E-09 | #N/A | 1.00E-05 |
| 7 | 0.112 | 1.12E-01 | #N/A | 1.12E-01 | #N/A | 7.54E-02 | 3.96E-03 | #N/A | 3.96E-03 | 2.97E-05 | #N/A | 2.98E-05 | 2.00E-03 | #N/A | -1.86E-02 | -1.86E-02 | -1.22E-02 | 5.01E-03 | #N/A | 9.93E-07 | #N/A | 7.45E-09 | #N/A | 1.00E-05 |
| 8 | 0.131 | 1.30E-01 | #N/A | 1.30E-01 | #N/A | 8.75E-02 | 1.51E-03 | #N/A | 1.52E-03 | 2.97E-05 | #N/A | 2.98E-05 | 7.73E-04 | #N/A | -1.84E-02 | -1.85E-02 | -1.22E-02 | 1.29E-02 | #N/A | 9.81E-07 | #N/A | 1.92E-08 | #N/A | 1.00E-05 |
| 9 | 0.149 | 1.49E-01 | #N/A | 1.49E-01 | #N/A | 9.97E-02 | 3.05E-04 | #N/A | 3.10E-04 | 2.96E-05 | #N/A | 2.98E-05 | 1.70E-04 | #N/A | -1.75E-02 | -1.80E-02 | -1.22E-02 | 5.89E-02 | #N/A | 9.13E-07 | #N/A | 8.73E-08 | #N/A | 1.00E-05 |
| 10 | 0.168 | 1.67E-01 | #N/A | 1.66E-01 | #N/A | 1.12E-01 | 5.59E-05 | #N/A | 5.95E-05 | 2.96E-05 | #N/A | 2.97E-05 | 4.46E-05 | #N/A | -1.43E-02 | -1.52E-02 | -1.22E-02 | 2.24E-01 | #N/A | 6.68E-07 | #N/A | 3.32E-07 | #N/A | 1.00E-05 |
| 11 | 0.187 | 1.82E-01 | #N/A | 1.81E-01 | #N/A | 1.24E-01 | 1.34E-05 | #N/A | 1.55E-05 | 2.96E-05 | #N/A | 2.97E-05 | 2.25E-05 | #N/A | -1.01E-02 | -4.19E-03 | -1.22E-02 | 4.44E-01 | #N/A | 3.43E-07 | #N/A | 6.57E-07 | #N/A | 1.00E-05 |
| 12 | 0.205 | 1.86E-01 | #N/A | 1.91E-01 | #N/A | 1.36E-01 | 8.30E-06 | #N/A | 4.25E-06 | 2.95E-05 | #N/A | 2.97E-05 | 1.69E-05 | #N/A | -7.22E-03 | 0.00E+00 | -1.21E-02 | 5.92E-01 | #N/A | 1.26E-07 | #N/A | 8.74E-07 | #N/A | 1.00E-05 |
| 13 | 0.224 | 1.86E-01 | #N/A | 1.98E-01 | #N/A | 1.48E-01 | 8.30E-06 | #N/A | 1.39E-06 | 2.95E-05 | #N/A | 2.96E-05 | 1.54E-05 | #N/A | -6.15E-03 | 0.00E+00 | -1.21E-02 | 6.47E-01 | #N/A | 4.50E-08 | #N/A | 9.55E-07 | #N/A | 1.00E-05 |
| 14 | 0.242 | 1.86E-01 | #N/A | 2.04E-01 | #N/A | 1.60E-01 | 8.30E-06 | #N/A | 6.25E-07 | 2.95E-05 | #N/A | 2.96E-05 | 1.51E-05 | #N/A | -5.83E-03 | 0.00E+00 | -1.21E-02 | 6.64E-01 | #N/A | 2.08E-08 | #N/A | 9.79E-07 | #N/A | 1.00E-05 |
| 15 | 0.261 | 1.86E-01 | #N/A | 2.10E-01 | #N/A | 1.73E-01 | 8.30E-06 | #N/A | 3.17E-07 | 2.95E-05 | #N/A | 2.96E-05 | 1.49E-05 | #N/A | -5.69E-03 | 0.00E+00 | -1.21E-02 | 6.71E-01 | #N/A | 1.06E-08 | #N/A | 9.89E-07 | #N/A | 1.00E-05 |
| 16 | 0.28 | 1.86E-01 | #N/A | 2.16E-01 | #N/A | 1.85E-01 | 8.30E-06 | #N/A | 1.63E-07 | 2.95E-05 | #N/A | 2.95E-05 | 1.48E-05 | #N/A | -5.61E-03 | 0.00E+00 | -1.21E-02 | 6.75E-01 | #N/A | 5.51E-09 | #N/A | 9.94E-07 | #N/A | 1.00E-05 |
| 17 | 0.298 | 1.86E-01 | #N/A | 2.21E-01 | #N/A | 1.97E-01 | 8.30E-06 | #N/A | 8.47E-08 | 2.94E-05 | #N/A | 2.95E-05 | 1.48E-05 | #N/A | -5.57E-03 | 0.00E+00 | -1.21E-02 | 6.77E-01 | #N/A | 2.87E-09 | #N/A | 9.97E-07 | #N/A | 1.00E-05 |
| 18 | 0.317 | 1.86E-01 | #N/A | 2.27E-01 | #N/A | 2.09E-01 | 8.30E-06 | #N/A | 4.42E-08 | 2.94E-05 | #N/A | 2.95E-05 | 1.47E-05 | #N/A | -5.55E-03 | 0.00E+00 | -1.21E-02 | 6.79E-01 | #N/A | 1.50E-09 | #N/A | 9.98E-07 | #N/A | 1.00E-05 |
| 19 | 0.336 | 1.86E-01 | #N/A | 2.32E-01 | #N/A | 2.21E-01 | 8.30E-06 | #N/A | 2.31E-08 | 2.94E-05 | #N/A | 2.94E-05 | 1.47E-05 | #N/A | -5.53E-03 | 0.00E+00 | -1.21E-02 | 6.79E-01 | #N/A | 7.86E-10 | #N/A | 9.99E-07 | #N/A | 1.00E-05 |
| 20 | 0.354 | 1.86E-01 | #N/A | 2.38E-01 | #N/A | 2.33E-01 | 8.30E-06 | #N/A | 1.35E-08 | 2.94E-05 | #N/A | 2.94E-05 | 1.47E-05 | #N/A | -5.52E-03 | 0.00E+00 | -1.21E-02 | 6.80E-01 | #N/A | 4.59E-10 | #N/A | 1.00E-06 | #N/A | 1.00E-05 |
| 21 | 0.373 | 1.86E-01 | #N/A | 2.43E-01 | #N/A | 2.45E-01 | 8.30E-06 | #N/A | 9.84E-09 | 2.94E-05 | #N/A | 2.94E-05 | 1.47E-05 | #N/A | -5.51E-03 | 0.00E+00 | -1.21E-02 | 6.80E-01 | #N/A | 3.35E-10 | #N/A | 1.00E-06 | #N/A | 1.00E-05 |
| 22 | 0.392 | 1.86E-01 | #N/A | 2.49E-01 | #N/A | 2.57E-01 | 8.30E-06 | #N/A | 7.16E-09 | 2.94E-05 | #N/A | 2.93E-05 | 1.47E-05 | #N/A | -5.51E-03 | 0.00E+00 | -1.21E-02 | 6.81E-01 | #N/A | 2.44E-10 | #N/A | 1.00E-06 | #N/A | 1.00E-05 |
| 23 | 0.41 | 1.86E-01 | #N/A | 2.54E-01 | #N/A | 2.69E-01 | 8.30E-06 | #N/A | 5.22E-09 | 2.94E-05 | #N/A | 2.93E-05 | 1.47E-05 | #N/A | -5.50E-03 | 0.00E+00 | -1.21E-02 | 6.81E-01 | #N/A | 1.78E-10 | #N/A | 1.00E-06 | #N/A | 1.00E-05 |
| 24 | 0.429 | 1.86E-01 | #N/A | 2.60E-01 | #N/A | 2.81E-01 | 8.30E-06 | #N/A | 3.80E-09 | 2.93E-05 | #N/A | 2.93E-05 | 1.47E-05 | #N/A | -5.49E-03 | 0.00E+00 | -1.21E-02 | 6.82E-01 | #N/A | 1.30E-10 | #N/A | 1.00E-06 | #N/A | 1.00E-05 |
| 25 | 0.448 | 1.86E-01 | #N/A | 2.65E-01 | #N/A | 2.93E-01 | 8.30E-06 | #N/A | 2.77E-09 | 2.93E-05 | #N/A | 2.93E-05 | 1.47E-05 | #N/A | -5.48E-03 | 0.00E+00 | -1.20E-02 | 6.82E-01 | #N/A | 9.46E-11 | #N/A | 1.00E-06 | #N/A | 1.00E-05 |
| 26 | 0.466 | 1.86E-01 | #N/A | 2.71E-01 | #N/A | 3.06E-01 | 8.30E-06 | #N/A | 2.02E-09 | 2.93E-05 | #N/A | 2.92E-05 | 1.47E-05 | #N/A | -5.48E-03 | 0.00E+00 | -1.20E-02 | 6.82E-01 | #N/A | 6.90E-11 | #N/A | 1.00E-06 | #N/A | 1.00E-05 |
| 27 | 0.485 | 1.86E-01 | #N/A | 2.76E-01 | #N/A | 3.18E-01 | 8.30E-06 | #N/A | 1.48E-09 | 2.93E-05 | #N/A | 2.92E-05 | 1.46E-05 | #N/A | -5.47E-03 | 0.00E+00 | -1.20E-02 | 6.83E-01 | #N/A | 5.04E-11 | #N/A | 1.00E-06 | #N/A | 1.00E-05 |
| 28 | 0.504 | 1.86E-01 | #N/A | 2.82E-01 | #N/A | 3.30E-01 | 8.30E-06 | #N/A | 1.08E-09 | 2.93E-05 | #N/A | 2.92E-05 | 1.46E-05 | #N/A | -5.46E-03 | 0.00E+00 | -1.20E-02 | 6.83E-01 | #N/A | 3.68E-11 | #N/A | 1.00E-06 | #N/A | 1.00E-05 |
| 29 | 0.522 | 1.86E-01 | #N/A | 2.87E-01 | #N/A | 3.42E-01 | 8.30E-06 | #N/A | 7.88E-10 | 2.93E-05 | #N/A | 2.91E-05 | 1.46E-05 | #N/A | -5.46E-03 | 0.00E+00 | -1.20E-02 | 6.83E-01 | #N/A | 2.69E-11 | #N/A | 1.00E-06 | #N/A | 1.00E-05 |
| 30 | 0.541 | 1.86E-01 | #N/A | 2.93E-01 | #N/A | 3.54E-01 | 8.30E-06 | #N/A | 5.76E-10 | 2.93E-05 | #N/A | 2.91E-05 | 1.46E-05 | #N/A | -5.45E-03 | 0.00E+00 | -1.20E-02 | 6.84E-01 | #N/A | 1.97E-11 | #N/A | 1.00E-06 | #N/A | 1.00E-05 |
| 81 | 1.492 | 1.86E-01 | #N/A | 4.00E-01 | #N/A | 4.28E-01 | 8.30E-06 | #N/A | 3.28E-11 | 2.07E-05 | #N/A | 1.04E-05 | 1.04E-05 | #N/A | -1.79E-12 | 0.00E+00 | -1.47E-14 | 9.66E-01 | #N/A | 1.58E-12 | #N/A | 1.00E-06 | #N/A | 1.00E-05 |
| 82 | 1.511 | 1.86E-01 | #N/A | 4.00E-01 | #N/A | 4.28E-01 | 8.30E-06 | #N/A | 3.28E-11 | 2.07E-05 | #N/A | 1.04E-05 | 1.04E-05 | #N/A | -9.20E-13 | 0.00E+00 | -8.12E-15 | 9.66E-01 | #N/A | 1.58E-12 | #N/A | 1.00E-06 | #N/A | 1.00E-05 |
| 83 | 1.529 | 1.86E-01 | #N/A | 4.00E-01 | #N/A | 4.28E-01 | 8.30E-06 | #N/A | 3.28E-11 | 2.07E-05 | #N/A | 1.04E-05 | 1.04E-05 | #N/A | -4.72E-13 | 0.00E+00 | -4.48E-15 | 9.66E-01 | #N/A | 1.58E-12 | #N/A | 1.00E-06 | #N/A | 1.00E-05 |
| 84 | 1.548 | 1.86E-01 | #N/A | 4.00E-01 | #N/A | 4.28E-01 | 8.30E-06 | #N/A | 3.28E-11 | 2.07E-05 | #N/A | 1.04E-05 | 1.04E-05 | #N/A | -2.42E-13 | 0.00E+00 | -2.46E-15 | 9.66E-01 | #N/A | 1.58E-12 | #N/A | 1.00E-06 | #N/A | 1.00E-05 |
| 85 | 1.567 | 1.86E-01 | #N/A | 4.00E-01 | #N/A | 4.28E-01 | 8.30E-06 | #N/A | 3.28E-11 | 2.07E-05 | #N/A | 1.04E-05 | 1.04E-05 | #N/A | -1.24E-13 | 0.00E+00 | -1.37E-15 | 9.66E-01 | #N/A | 1.58E-12 | #N/A | 1.00E-06 | #N/A | 1.00E-05 |
| 86 | 1.585 | 1.86E-01 | #N/A | 4.00E-01 | #N/A | 4.28E-01 | 8.30E-06 | #N/A | 3.28E-11 | 2.07E-05 | #N/A | 1.04E-05 | 1.04E-05 | #N/A | -6.36E-14 | 0.00E+00 | -7.67E-16 | 9.66E-01 | #N/A | 1.58E-12 | #N/A | 1.00E-06 | #N/A | 1.00E-05 |
| 87 | 1.604 | 1.86E-01 | #N/A | 4.00E-01 | #N/A | 4.28E-01 | 8.30E-06 | #N/A | 3.28E-11 | 2.07E-05 | #N/A | 1.04E-05 | 1.04E-05 | #N/A | -3.26E-14 | 0.00E+00 | -4.05E-16 | 9.66E-01 | #N/A | 1.58E-12 | #N/A | 1.00E-06 | #N/A | 1.00E-05 |
| 88 | 1.623 | 1.86E-01 | #N/A | 4.00E-01 | #N/A | 4.28E-01 | 8.30E-06 | #N/A | 3.28E-11 | 2.07E-05 | #N/A | 1.04E-05 | 1.04E-05 | #N/A | -1.68E-14 | 0.00E+00 | -2.06E-16 | 9.66E-01 | #N/A | 1.58E-12 | #N/A | 1.00E-06 | #N/A | 1.00E-05 |
| 89 | 1.641 | 1.86E-01 | #N/A | 4.00E-01 | #N/A | 4.28E-01 | 8.30E-06 | #N/A | 3.28E-11 | 2.07E-05 | #N/A | 1.04E-05 | 1.04E-05 | #N/A | -8.58E-15 | 0.00E+00 | -1.07E-16 | 9.66E-01 | #N/A | 1.58E-12 | #N/A | 1.00E-06 | #N/A | 1.00E-05 |
| 90 | 1.66 | 1.86E-01 | #N/A | 4.00E-01 | #N/A | 4.28E-01 | 8.30E-06 | #N/A | 3.28E-11 | 2.07E-05 | #N/A | 1.04E-05 | 1.04E-05 | #N/A | -4.41E-15 | 0.00E+00 | -7.50E-17 | 9.66E-01 | #N/A | 1.58E-12 | #N/A | 1.00E-06 | #N/A | 1.00E-05 |
| 91 | 1.679 | 1.86E-01 | #N/A | 4.00E-01 | #N/A | 4.28E-01 | 8.30E-06 | #N/A | 3.28E-11 | 2.07E-05 | #N/A | 1.04E-05 | 1.04E-05 | #N/A | -2.25E-15 | 0.00E+00 | -4.07E-17 | 9.66E-01 | #N/A | 1.58E-12 | #N/A | 1.00E-06 | #N/A | 1.00E-05 |
| 92 | 1.697 | 1.86E-01 | #N/A | 4.00E-01 | #N/A | 4.28E-01 | 8.30E-06 | #N/A | 3.28E-11 | 2.07E-05 | #N/A | 1.04E-05 | 1.04E-05 | #N/A | -1.16E-15 | 0.00E+00 | -4.07E-17 | 9.66E-01 | #N/A | 1.58E-12 | #N/A | 1.00E-06 | #N/A | 1.00E-05 |
| 93 | 1.716 | 1.86E-01 | #N/A | 4.00E-01 | #N/A | 4.28E-01 | 8.30E-06 | #N/A | 3.28E-11 | 2.07E-05 | #N/A | 1.04E-05 | 1.04E-05 | #N/A | -5.66E-16 | 0.00E+00 | -6.43E-18 | 9.66E-01 | #N/A | 1.58E-12 | #N/A | 1.00E-06 | #N/A | 1.00E-05 |
| 94 | 1.734 | 1.86E-01 | #N/A | 4.00E-01 | #N/A | 4.28E-01 | 8.30E-06 | #N/A | 3.28E-11 | 2.07E-05 | #N/A | 1.04E-05 | 1.04E-05 | #N/A | -2.98E-16 | 0.00E+00 | -6.43E-18 | 9.66E-01 | #N/A | 1.58E-12 | #N/A | 1.00E-06 | #N/A | 1.00E-05 |
| 95 | 1.753 | 1.86E-01 | #N/A | 4.00E-01 | #N/A | 4.28E-01 | 8.30E-06 | #N/A | 3.28E-11 | 2.07E-05 | #N/A | 1.04E-05 | 1.04E-05 | #N/A | -1.65E-16 | 0.00E+00 | -6.43E-18 | 9.66E-01 | #N/A | 1.58E-12 | #N/A | 1.00E-06 | #N/A | 1.00E-05 |
| 96 | 1.772 | 1.86E-01 | #N/A | 4.00E-01 | #N/A | 4.28E-01 | 8.30E-06 | #N/A | 3.28E-11 | 2.07E-05 | #N/A | 1.04E-05 | 1.04E-05 | #N/A | -6.65E-17 | 0.00E+00 | -6.43E-18 | 9.66E-01 | #N/A | 1.58E-12 | #N/A | 1.00E-06 | #N/A | 1.00E-05 |
| 97 | 1.79 | 1.86E-01 | #N/A | 4.00E-01 | #N/A | 4.28E-01 | 8.30E-06 | #N/A | 3.28E-11 | 2.07E-05 | #N/A | 1.04E-05 | 1.04E-05 | #N/A | -6.65E-17 | 0.00E+00 | -6.43E-18 | 9.66E-01 | #N/A | 1.58E-12 | #N/A | 1.00E-06 | #N/A | 1.00E-05 |
| 98 | 1.809 | 1.86E-01 | #N/A | 4.00E-01 | #N/A | 4.28E-01 | 8.30E-06 | #N/A | 3.28E-11 | 2.07E-05 | #N/A | 1.04E-05 | 1.04E-05 | #N/A | -3.22E-17 | 0.00E+00 | -6.43E-18 | 9.66E-01 | #N/A | 1.58E-12 | #N/A | 1.00E-06 | #N/A | 1.00E-05 |
| 99 | 1.828 | 1.86E-01 | #N/A | 4.00E-01 | #N/A | 4.28E-01 | 8.30E-06 | #N/A | 3.28E-11 | 2.07E-05 | #N/A | 1.04E-05 | 1.04E-05 | #N/A | -2.14E-18 | 0.00E+00 | -6.43E-18 | 9.66E-01 | #N/A | 1.58E-12 | #N/A | 1.00E-06 | #N/A | 1.00E-05 |
| 100 | 1.846 | 1.86E-01 | #N/A | 4.00E-01 | #N/A | 4.28E-01 | 8.30E-06 | #N/A | 3.28E-11 | 2.07E-05 | #N/A | 1.04E-05 | 1.04E-05 | #N/A | -2.14E-18 | 0.00E+00 | -6.43E-18 | 9.66E-01 | #N/A | 1.58E-12 | #N/A | 1.00E-06 | #N/A | 1.00E-05 |
| 101 | 1.865 | 1.86E-01 | #N/A | 4.00E-01 | #N/A | 4.28E-01 | 8.30E-06 | #N/A | 3.28E-11 | 2.07E-05 | #N/A | 1.04E-05 | 1.04E-05 | #N/A | -2.14E-18 | 0.00E+00 | -6.43E-18 | 9.66E-01 | #N/A | 1.58E-12 | #N/A | 1.00E-06 | #N/A | 1.00E-05 |
| 102 | 1.884 | 1.86E-01 | #N/A | 4.00E-01 | #N/A | 4.28E-01 | 8.30E-06 | #N/A | 3.28E-11 | 2.07E-05 | #N/A | 1.04E-05 | 1.04E-05 | #N/A | -2.14E-18 | 0.00E+00 | -6.43E-18 | 9.66E-01 | #N/A | 1.58E-12 | #N/A | 1.00E-06 | #N/A | 1.00E-05 |
| 103 | 1.902 | 1.86E-01 | #N/A | 4.00E-01 | #N/A | 4.28E-01 | 8.30E-06 | #N/A | 3.28E-11 | 2.07E-05 | #N/A | 1.04E-05 | 1.04E-05 | #N/A | -2.14E-18 | 0.00E+00 | -6.43E-18 | 9.66E-01 | #N/A | 1.58E-12 | #N/A | 1.00E-06 | #N/A | 1.00E-05 |
| 104 | 1.921 | 1.86E-01 | #N/A | 4.00E-01 | 4.00E-01 | 4.28E-01 | 8.30E-06 | #N/A | 3.28E-11 | 2.07E-05 | #N/A | 1.04E-05 | 1.04E-05 | #N/A | -2.14E-18 | 0.00E+00 | -6.43E-18 | 9.66E-01 | #N/A | 1.58E-12 | #N/A | 1.00E-06 | #N/A | 1.00E-05 |
| 105 | 1.94 | 1.86E-01 | 2.04E-01 | 4.00E-01 | 4.02E-01 | 4.28E-01 | 8.30E-06 | -2.96E-07 | 3.28E-11 | 2.07E-05 | 2.10E-05 | 1.04E-05 | 1.04E-05 | -6.00E-07 | -2.14E-18 | 0.00E+00 | -6.43E-18 | 9.66E-01 | 4.40E-09 | 1.58E-12 | -1.43E-08 | 1.00E-06 | 1.01E-06 | 1.00E-05 |
| 106 | 1.958 | 1.86E-01 | 1.85E-01 | 4.00E-01 | 4.28E-01 | 4.28E-01 | 8.30E-06 | 6.15E-07 | 3.28E-11 | 2.07E-05 | 2.01E-05 | 1.04E-05 | 1.04E-05 | 1.19E-06 | -2.14E-18 | 0.00E+00 | -6.43E-18 | 9.66E-01 | 4.70E-08 | 1.58E-12 | 2.97E-08 | 1.00E-06 | 9.70E-07 | 1.00E-05 |
| 107 | 1.977 | 1.86E-01 | 1.85E-01 | 4.00E-01 | 4.30E-01 | 4.28E-01 | 8.30E-06 | 1.04E-05 | 3.28E-11 | 2.07E-05 | 1.04E-05 | 1.04E-05 | 1.04E-05 | 1.04E-05 | -2.14E-18 | 0.00E+00 | -6.43E-18 | 9.66E-01 | 2.99E-13 | 1.58E-12 | 5.00E-07 | 1.00E-06 | 5.00E-07 | 1.00E-05 |
| 108 | 1.996 | 1.86E-01 | 1.86E-01 | 4.00E-01 | 4.28E-01 | 4.28E-01 | 8.30E-06 | 1.00E-05 | 3.28E-11 | 2.07E-05 | 1.00E-05 | 1.04E-05 | 1.04E-05 | 6.56E-11 | -2.14E-18 | 0.00E+00 | -6.43E-18 | 9.66E-01 | 0 | 1.58E-12 | 5.00E-07 | 1.00E-06 | 5.00E-07 | 1.00E-05 |

**Table C6 The FDM Results for the 45°, 2-Meter System using The Modified Kisch Solution**

| # | z | hci | hcp | hp | hfp | hfi | kci | kcp | kc | kf | kfp | kfi | kll | kp | dhp | dhpc | dhpf | l | dq | qci | qcp | qfi | qfp | q-total |
|---|---|---|---|---|---|---|---|---|---|---|---|---|---|---|---|---|---|---|---|---|---|---|---|---|
| 1 | 0 | 0.00E+00 | | 1.00E-04 | | 0.00E+00 | 1.48E-02 | #N/A | 1.49E-02 | 3.00E-05 | #N/A | 4.50E-05 | 7.47E-03 | #N/A | -1.86E-02 | -1.86E-02 | -1.28E-02 | 1.34E-03 | #N/A | 9.98E-07 | #N/A | 2.01E-09 | #N/A | 1.00E-05 |
| 2 | 0.019 | 1.86E-02 | | 1.87E-02 | | 1.28E-02 | 1.46E-02 | #N/A | 1.46E-02 | 3.00E-05 | #N/A | 3.00E-05 | 7.33E-03 | #N/A | -1.86E-02 | -1.86E-02 | -9.86E-03 | 1.36E-03 | #N/A | 9.98E-07 | #N/A | 2.05E-09 | #N/A | 1.00E-05 |
| 3 | 0.037 | 3.73E-02 | | 3.73E-02 | | 2.27E-02 | 1.45E-02 | #N/A | 1.45E-02 | 2.99E-05 | #N/A | 3.00E-05 | 7.25E-03 | #N/A | -1.86E-02 | -1.86E-02 | -9.85E-03 | 1.38E-03 | #N/A | 9.98E-07 | #N/A | 2.07E-09 | #N/A | 1.00E-05 |
| 4 | 0.056 | 5.59E-02 | #N/A | 5.59E-02 | #N/A | 3.25E-02 | 1.35E-02 | #N/A | 1.35E-02 | 2.99E-05 | #N/A | 3.00E-05 | 6.74E-03 | #N/A | -1.86E-02 | -1.86E-02 | -9.85E-03 | 1.48E-03 | #N/A | 9.98E-07 | #N/A | 2.22E-09 | #N/A | 1.00E-05 |
| 5 | 0.075 | 7.45E-02 | #N/A | 7.46E-02 | #N/A | 4.24E-02 | 1.11E-02 | #N/A | 1.11E-02 | 2.98E-05 | #N/A | 2.99E-05 | 5.58E-03 | #N/A | -1.86E-02 | -1.86E-02 | -9.84E-03 | 1.79E-03 | #N/A | 9.97E-07 | #N/A | 2.67E-09 | #N/A | 1.00E-05 |
| 6 | 0.093 | 9.32E-02 | #N/A | 9.32E-02 | #N/A | 5.22E-02 | 7.48E-03 | #N/A | 7.48E-03 | 2.98E-05 | #N/A | 2.99E-05 | 3.75E-03 | #N/A | -1.86E-02 | -1.86E-02 | -9.83E-03 | 2.66E-03 | #N/A | 9.96E-07 | #N/A | 3.97E-09 | #N/A | 1.00E-05 |
| 7 | 0.112 | 1.12E-01 | #N/A | 1.12E-01 | #N/A | 6.20E-02 | 3.97E-03 | #N/A | 3.97E-03 | 2.97E-05 | #N/A | 2.99E-05 | 2.00E-03 | #N/A | -1.85E-02 | -1.86E-02 | -9.82E-03 | 5.00E-03 | #N/A | 9.93E-07 | #N/A | 7.43E-09 | #N/A | 1.00E-05 |
| 8 | 0.131 | 1.30E-01 | #N/A | 1.30E-01 | #N/A | 7.18E-02 | 1.52E-03 | #N/A | 1.53E-03 | 2.97E-05 | #N/A | 2.99E-05 | 7.78E-04 | #N/A | -1.83E-02 | -1.85E-02 | -9.81E-03 | 1.29E-02 | #N/A | 9.81E-07 | #N/A | 1.91E-08 | #N/A | 1.00E-05 |
| 9 | 0.149 | 1.49E-01 | #N/A | 1.49E-01 | #N/A | 8.17E-02 | 3.08E-04 | #N/A | 3.16E-04 | 2.96E-05 | #N/A | 2.98E-05 | 1.73E-04 | #N/A | -1.71E-02 | -1.78E-02 | -9.81E-03 | 5.79E-02 | #N/A | 9.14E-07 | #N/A | 8.59E-08 | #N/A | 1.00E-05 |
| 10 | 0.168 | 1.67E-01 | #N/A | 1.66E-01 | #N/A | 9.15E-02 | 5.76E-05 | #N/A | 6.29E-05 | 2.96E-05 | #N/A | 2.98E-05 | 4.62E-05 | #N/A | -1.29E-02 | -1.41E-02 | -9.80E-03 | 2.16E-01 | #N/A | 6.80E-07 | #N/A | 3.20E-07 | #N/A | 1.00E-05 |
| 11 | 0.187 | 1.81E-01 | #N/A | 1.79E-01 | #N/A | 1.01E-01 | 1.53E-05 | #N/A | 1.86E-05 | 2.96E-05 | #N/A | 2.98E-05 | 2.41E-05 | #N/A | -7.69E-03 | -1.42E-03 | -9.79E-03 | 4.15E-01 | #N/A | 3.86E-07 | #N/A | 6.14E-07 | #N/A | 1.00E-05 |
| 12 | 0.205 | 1.82E-01 | #N/A | 1.86E-01 | #N/A | 1.11E-01 | 1.34E-05 | #N/A | 8.31E-06 | 2.95E-05 | #N/A | 2.97E-05 | 1.89E-05 | #N/A | -4.71E-03 | 0.00E+00 | -9.78E-03 | 5.28E-01 | #N/A | 2.19E-07 | #N/A | 7.81E-07 | #N/A | 1.00E-05 |
| 13 | 0.224 | 1.82E-01 | #N/A | 1.91E-01 | #N/A | 1.21E-01 | 1.34E-05 | #N/A | 4.01E-06 | 2.95E-05 | #N/A | 2.97E-05 | 1.68E-05 | #N/A | -2.92E-03 | 0.00E+00 | -9.77E-03 | 5.96E-01 | #N/A | 1.19E-07 | #N/A | 8.81E-07 | #N/A | 1.00E-05 |
| 14 | 0.242 | 1.82E-01 | #N/A | 1.94E-01 | #N/A | 1.31E-01 | 1.34E-05 | #N/A | 2.55E-06 | 2.95E-05 | #N/A | 2.97E-05 | 1.60E-05 | #N/A | -2.20E-03 | 0.00E+00 | -9.77E-03 | 6.24E-01 | #N/A | 7.95E-08 | #N/A | 9.21E-07 | #N/A | 1.00E-05 |
| 15 | 0.261 | 1.82E-01 | #N/A | 1.96E-01 | #N/A | 1.40E-01 | 1.34E-05 | #N/A | 1.81E-06 | 2.95E-05 | #N/A | 2.97E-05 | 1.57E-05 | #N/A | -1.81E-03 | 0.00E+00 | -9.76E-03 | 6.38E-01 | #N/A | 5.79E-08 | #N/A | 9.42E-07 | #N/A | 1.00E-05 |
| 16 | 0.28 | 1.82E-01 | #N/A | 1.98E-01 | #N/A | 1.50E-01 | 1.34E-05 | #N/A | 1.37E-06 | 2.95E-05 | #N/A | 2.96E-05 | 1.54E-05 | #N/A | -1.57E-03 | 0.00E+00 | -9.75E-03 | 6.48E-01 | #N/A | 4.44E-08 | #N/A | 9.56E-07 | #N/A | 1.00E-05 |
| 17 | 0.298 | 1.82E-01 | #N/A | 2.00E-01 | #N/A | 1.60E-01 | 1.34E-05 | #N/A | 1.07E-06 | 2.95E-05 | #N/A | 2.96E-05 | 1.53E-05 | #N/A | -1.40E-03 | 0.00E+00 | -9.74E-03 | 6.54E-01 | #N/A | 3.51E-08 | #N/A | 9.65E-07 | #N/A | 1.00E-05 |
| 18 | 0.317 | 1.82E-01 | #N/A | 2.01E-01 | #N/A | 1.70E-01 | 1.34E-05 | #N/A | 8.97E-07 | 2.95E-05 | #N/A | 2.96E-05 | 1.52E-05 | #N/A | -1.30E-03 | 0.00E+00 | -9.73E-03 | 6.58E-01 | #N/A | 2.95E-08 | #N/A | 9.70E-07 | #N/A | 1.00E-05 |
| 19 | 0.336 | 1.82E-01 | #N/A | 2.02E-01 | #N/A | 1.79E-01 | 1.34E-05 | #N/A | 7.71E-07 | 2.95E-05 | #N/A | 2.96E-05 | 1.51E-05 | #N/A | -1.22E-03 | 0.00E+00 | -9.73E-03 | 6.61E-01 | #N/A | 2.55E-08 | #N/A | 9.75E-07 | #N/A | 1.00E-05 |
| 20 | 0.354 | 1.82E-01 | #N/A | 2.03E-01 | #N/A | 1.89E-01 | 1.34E-05 | #N/A | 6.69E-07 | 2.95E-05 | #N/A | 2.95E-05 | 1.51E-05 | #N/A | -1.16E-03 | 0.00E+00 | -9.72E-03 | 6.63E-01 | #N/A | 2.22E-08 | #N/A | 9.78E-07 | #N/A | 1.00E-05 |
| 21 | 0.373 | 1.82E-01 | #N/A | 2.05E-01 | #N/A | 1.99E-01 | 1.34E-05 | #N/A | 5.84E-07 | 2.95E-05 | #N/A | 2.95E-05 | 1.50E-05 | #N/A | -1.11E-03 | 0.00E+00 | -9.71E-03 | 6.65E-01 | #N/A | 1.94E-08 | #N/A | 9.81E-07 | #N/A | 1.00E-05 |
| 22 | 0.392 | 1.82E-01 | #N/A | 2.06E-01 | #N/A | 2.09E-01 | 1.34E-05 | #N/A | 5.13E-07 | 2.95E-05 | #N/A | 2.95E-05 | 1.50E-05 | #N/A | -1.07E-03 | 0.00E+00 | -9.70E-03 | 6.67E-01 | #N/A | 1.71E-08 | #N/A | 9.83E-07 | #N/A | 1.00E-05 |
| 23 | 0.41 | 1.82E-01 | #N/A | 2.07E-01 | #N/A | 2.18E-01 | 1.34E-05 | #N/A | 4.53E-07 | 2.95E-05 | #N/A | 2.95E-05 | 1.50E-05 | #N/A | -1.03E-03 | 0.00E+00 | -9.70E-03 | 6.68E-01 | #N/A | 1.51E-08 | #N/A | 9.85E-07 | #N/A | 1.00E-05 |
| 24 | 0.429 | 1.82E-01 | #N/A | 2.08E-01 | #N/A | 2.28E-01 | 1.34E-05 | #N/A | 4.02E-07 | 2.95E-05 | #N/A | 2.94E-05 | 1.49E-05 | #N/A | -9.98E-04 | 0.00E+00 | -9.69E-03 | 6.69E-01 | #N/A | 1.34E-08 | #N/A | 9.87E-07 | #N/A | 1.00E-05 |
| 25 | 0.448 | 1.82E-01 | #N/A | 2.09E-01 | #N/A | 2.38E-01 | 1.34E-05 | #N/A | 3.58E-07 | 2.95E-05 | #N/A | 2.94E-05 | 1.49E-05 | #N/A | -9.70E-04 | 0.00E+00 | -9.68E-03 | 6.70E-01 | #N/A | 1.20E-08 | #N/A | 9.88E-07 | #N/A | 1.00E-05 |
| 26 | 0.466 | 1.82E-01 | #N/A | 2.10E-01 | #N/A | 2.47E-01 | 1.34E-05 | #N/A | 3.19E-07 | 2.95E-05 | #N/A | 2.94E-05 | 1.49E-05 | #N/A | -9.46E-04 | 0.00E+00 | -9.67E-03 | 6.71E-01 | #N/A | 1.07E-08 | #N/A | 9.89E-07 | #N/A | 1.00E-05 |
| 27 | 0.485 | 1.82E-01 | #N/A | 2.11E-01 | #N/A | 2.57E-01 | 1.34E-05 | #N/A | 2.86E-07 | 2.95E-05 | #N/A | 2.93E-05 | 1.49E-05 | #N/A | -9.24E-04 | 0.00E+00 | -9.66E-03 | 6.72E-01 | #N/A | 9.61E-09 | #N/A | 9.90E-07 | #N/A | 1.00E-05 |
| 28 | 0.504 | 1.82E-01 | #N/A | 2.12E-01 | #N/A | 2.67E-01 | 1.34E-05 | #N/A | 2.57E-07 | 2.95E-05 | #N/A | 2.93E-05 | 1.49E-05 | #N/A | -9.05E-04 | 0.00E+00 | -9.66E-03 | 6.73E-01 | #N/A | 8.64E-09 | #N/A | 9.91E-07 | #N/A | 1.00E-05 |
| 29 | 0.522 | 1.82E-01 | #N/A | 2.13E-01 | #N/A | 2.76E-01 | 1.34E-05 | #N/A | 2.31E-07 | 2.95E-05 | #N/A | 2.93E-05 | 1.48E-05 | #N/A | -8.89E-04 | 0.00E+00 | -9.65E-03 | 6.73E-01 | #N/A | 7.78E-09 | #N/A | 9.92E-07 | #N/A | 1.00E-05 |
| 30 | 0.541 | 1.82E-01 | #N/A | 2.13E-01 | #N/A | 2.86E-01 | 1.34E-05 | #N/A | 2.08E-07 | 2.95E-05 | #N/A | 2.93E-05 | 1.48E-05 | #N/A | -8.74E-04 | 0.00E+00 | -9.64E-03 | 6.74E-01 | #N/A | 7.02E-09 | #N/A | 9.93E-07 | #N/A | 1.00E-05 |
| 81 | 1.492 | 1.82E-01 | #N/A | 2.51E-01 | #N/A | 4.15E-01 | 1.34E-05 | #N/A | 6.18E-09 | 2.94E-05 | #N/A | 1.41E-05 | 1.47E-05 | #N/A | -6.89E-04 | 0.00E+00 | -7.46E-13 | 6.81E-01 | #N/A | 2.10E-10 | #N/A | 1.00E-06 | #N/A | 1.00E-05 |
| 82 | 1.511 | 1.82E-01 | #N/A | 2.52E-01 | #N/A | 4.15E-01 | 1.34E-05 | #N/A | 5.94E-09 | 2.94E-05 | #N/A | 1.41E-05 | 1.47E-05 | #N/A | -6.88E-04 | 0.00E+00 | -4.11E-13 | 6.81E-01 | #N/A | 2.02E-10 | #N/A | 1.00E-06 | #N/A | 1.00E-05 |
| 83 | 1.529 | 1.82E-01 | #N/A | 2.53E-01 | #N/A | 4.15E-01 | 1.34E-05 | #N/A | 5.71E-09 | 2.94E-05 | #N/A | 1.41E-05 | 1.47E-05 | #N/A | -6.87E-04 | 0.00E+00 | -2.26E-13 | 6.81E-01 | #N/A | 1.94E-10 | #N/A | 1.00E-06 | #N/A | 1.00E-05 |
| 84 | 1.548 | 1.82E-01 | #N/A | 2.53E-01 | #N/A | 4.15E-01 | 1.34E-05 | #N/A | 5.49E-09 | 2.94E-05 | #N/A | 1.41E-05 | 1.47E-05 | #N/A | -6.86E-04 | 0.00E+00 | -1.25E-13 | 6.81E-01 | #N/A | 1.87E-10 | #N/A | 1.00E-06 | #N/A | 1.00E-05 |
| 85 | 1.567 | 1.82E-01 | #N/A | 2.54E-01 | #N/A | 4.15E-01 | 1.34E-05 | #N/A | 5.27E-09 | 2.94E-05 | #N/A | 1.41E-05 | 1.47E-05 | #N/A | -6.84E-04 | 0.00E+00 | -6.87E-14 | 6.81E-01 | #N/A | 1.80E-10 | #N/A | 1.00E-06 | #N/A | 1.00E-05 |
| 86 | 1.585 | 1.82E-01 | #N/A | 2.55E-01 | #N/A | 4.15E-01 | 1.34E-05 | #N/A | 5.07E-09 | 2.94E-05 | #N/A | 1.41E-05 | 1.47E-05 | #N/A | -6.83E-04 | 0.00E+00 | -3.78E-14 | 6.81E-01 | #N/A | 1.73E-10 | #N/A | 1.00E-06 | #N/A | 1.00E-05 |
| 87 | 1.604 | 1.82E-01 | #N/A | 2.56E-01 | #N/A | 4.15E-01 | 1.34E-05 | #N/A | 4.88E-09 | 2.94E-05 | #N/A | 1.41E-05 | 1.47E-05 | #N/A | -6.82E-04 | 0.00E+00 | -2.08E-14 | 6.81E-01 | #N/A | 1.66E-10 | #N/A | 1.00E-06 | #N/A | 1.00E-05 |
| 88 | 1.623 | 1.82E-01 | #N/A | 2.56E-01 | #N/A | 4.15E-01 | 1.34E-05 | #N/A | 4.69E-09 | 2.94E-05 | #N/A | 1.41E-05 | 1.47E-05 | #N/A | -6.81E-04 | 0.00E+00 | -1.15E-14 | 6.81E-01 | #N/A | 1.60E-10 | #N/A | 1.00E-06 | #N/A | 1.00E-05 |
| 89 | 1.641 | 1.82E-01 | #N/A | 2.57E-01 | #N/A | 4.15E-01 | 1.34E-05 | #N/A | 4.51E-09 | 2.93E-05 | #N/A | 1.41E-05 | 1.47E-05 | #N/A | -6.79E-04 | 0.00E+00 | -6.30E-15 | 6.81E-01 | #N/A | 1.54E-10 | #N/A | 1.00E-06 | #N/A | 1.00E-05 |
| 90 | 1.66 | 1.82E-01 | #N/A | 2.58E-01 | #N/A | 4.15E-01 | 1.34E-05 | #N/A | 4.34E-09 | 2.93E-05 | #N/A | 1.41E-05 | 1.47E-05 | #N/A | -6.78E-04 | 0.00E+00 | -3.49E-15 | 6.81E-01 | #N/A | 1.48E-10 | #N/A | 1.00E-06 | #N/A | 1.00E-05 |
| 91 | 1.679 | 1.82E-01 | #N/A | 2.58E-01 | #N/A | 4.15E-01 | 1.34E-05 | #N/A | 4.17E-09 | 2.93E-05 | #N/A | 1.41E-05 | 1.47E-05 | #N/A | -6.77E-04 | 0.00E+00 | -1.93E-15 | 6.81E-01 | #N/A | 1.42E-10 | #N/A | 1.00E-06 | #N/A | 1.00E-05 |
| 92 | 1.697 | 1.82E-01 | #N/A | 2.59E-01 | #N/A | 4.15E-01 | 1.34E-05 | #N/A | 4.01E-09 | 2.93E-05 | #N/A | 1.41E-05 | 1.47E-05 | #N/A | -6.76E-04 | 0.00E+00 | -1.04E-15 | 6.81E-01 | #N/A | 1.37E-10 | #N/A | 1.00E-06 | #N/A | 1.00E-05 |
| 93 | 1.716 | 1.82E-01 | #N/A | 2.60E-01 | #N/A | 4.15E-01 | 1.34E-05 | #N/A | 3.86E-09 | 2.93E-05 | #N/A | 1.41E-05 | 1.47E-05 | #N/A | -6.74E-04 | 0.00E+00 | -5.42E-16 | 6.82E-01 | #N/A | 1.31E-10 | #N/A | 1.00E-06 | #N/A | 1.00E-05 |
| 94 | 1.734 | 1.82E-01 | #N/A | 2.60E-01 | #N/A | 4.15E-01 | 1.34E-05 | #N/A | 3.71E-09 | 2.93E-05 | #N/A | 1.41E-05 | 1.47E-05 | #N/A | -6.73E-04 | 0.00E+00 | -3.10E-16 | 6.82E-01 | #N/A | 1.26E-10 | #N/A | 1.00E-06 | #N/A | 1.00E-05 |
| 95 | 1.753 | 1.82E-01 | #N/A | 2.61E-01 | #N/A | 4.15E-01 | 1.34E-05 | #N/A | 3.57E-09 | 2.93E-05 | #N/A | 1.41E-05 | 1.47E-05 | #N/A | -6.72E-04 | 0.00E+00 | -1.76E-16 | 6.82E-01 | #N/A | 1.22E-10 | #N/A | 1.00E-06 | #N/A | 1.00E-05 |
| 96 | 1.772 | 1.82E-01 | #N/A | 2.62E-01 | #N/A | 4.15E-01 | 1.34E-05 | #N/A | 3.43E-09 | 2.93E-05 | #N/A | 1.41E-05 | 1.47E-05 | #N/A | -6.71E-04 | 0.00E+00 | -7.61E-17 | 6.82E-01 | #N/A | 1.17E-10 | #N/A | 1.00E-06 | #N/A | 1.00E-05 |
| 97 | 1.79 | 1.82E-01 | #N/A | 2.62E-01 | #N/A | 4.15E-01 | 1.34E-05 | #N/A | 3.30E-09 | 2.93E-05 | #N/A | 1.41E-05 | 1.47E-05 | #N/A | -6.70E-04 | 0.00E+00 | -4.39E-17 | 6.82E-01 | #N/A | 1.13E-10 | #N/A | 1.00E-06 | #N/A | 1.00E-05 |
| 98 | 1.809 | 1.82E-01 | #N/A | 2.63E-01 | #N/A | 4.15E-01 | 1.34E-05 | #N/A | 3.18E-09 | 2.93E-05 | #N/A | 1.41E-05 | 1.47E-05 | #N/A | -6.68E-04 | 0.00E+00 | -4.39E-17 | 6.82E-01 | #N/A | 1.08E-10 | #N/A | 1.00E-06 | #N/A | 1.00E-05 |
| 99 | 1.828 | 1.82E-01 | #N/A | 2.64E-01 | #N/A | 4.15E-01 | 1.34E-05 | #N/A | 3.06E-09 | 2.93E-05 | #N/A | 1.41E-05 | 1.47E-05 | #N/A | -6.67E-04 | 0.00E+00 | -1.17E-17 | 6.82E-01 | #N/A | 1.04E-10 | #N/A | 1.00E-06 | #N/A | 1.00E-05 |
| 100 | 1.846 | 1.82E-01 | #N/A | 2.64E-01 | #N/A | 4.15E-01 | 1.34E-05 | #N/A | 2.94E-09 | 2.93E-05 | #N/A | 1.41E-05 | 1.47E-05 | #N/A | -6.66E-04 | 0.00E+00 | -1.17E-17 | 6.82E-01 | #N/A | 1.00E-10 | #N/A | 1.00E-06 | #N/A | 1.00E-05 |
| 101 | 1.865 | 1.82E-01 | #N/A | 2.65E-01 | #N/A | 4.15E-01 | 1.34E-05 | #N/A | 2.83E-09 | 2.93E-05 | #N/A | 1.41E-05 | 1.47E-05 | #N/A | -6.65E-04 | 0.00E+00 | -1.17E-17 | 6.82E-01 | #N/A | 9.66E-11 | #N/A | 1.00E-06 | #N/A | 1.00E-05 |
| 102 | 1.884 | 1.82E-01 | #N/A | 2.66E-01 | #N/A | 4.15E-01 | 1.34E-05 | #N/A | 2.73E-09 | 2.93E-05 | #N/A | 1.41E-05 | 1.47E-05 | #N/A | -6.64E-04 | 0.00E+00 | -1.17E-17 | 6.82E-01 | #N/A | 9.30E-11 | #N/A | 1.00E-06 | #N/A | 1.00E-05 |
| 103 | 1.902 | 1.82E-01 | #N/A | 2.66E-01 | #N/A | 4.15E-01 | 1.34E-05 | #N/A | 2.63E-09 | 2.93E-05 | #N/A | 1.41E-05 | 1.47E-05 | #N/A | -6.63E-04 | 0.00E+00 | -1.17E-17 | 6.82E-01 | #N/A | 8.95E-11 | #N/A | 1.00E-06 | #N/A | 1.00E-05 |
| 104 | 1.921 | 1.82E-01 | #N/A | 2.67E-01 | #N/A | 4.15E-01 | 1.34E-05 | #N/A | 2.53E-09 | 2.93E-05 | #N/A | 1.41E-05 | 1.47E-05 | #N/A | -6.61E-04 | 0.00E+00 | -1.17E-17 | 6.82E-01 | #N/A | 8.62E-11 | #N/A | 1.00E-06 | #N/A | 1.00E-05 |
| 105 | 1.94 | 1.82E-01 | #N/A | 2.68E-01 | #N/A | 4.15E-01 | 1.34E-05 | #N/A | 2.43E-09 | 2.93E-05 | #N/A | 1.41E-05 | 1.47E-05 | #N/A | -6.60E-04 | 0.00E+00 | -1.17E-17 | 6.82E-01 | #N/A | 8.30E-11 | #N/A | 1.00E-06 | #N/A | 1.00E-05 |
| 106 | 1.958 | 1.82E-01 | 1.82E-01 | 2.68E-01 | 4.15E-01 | 4.15E-01 | 1.34E-05 | -3.31E-06 | 2.34E-09 | 2.93E-05 | 3.16E-05 | 1.41E-05 | 1.47E-05 | -7.40E-06 | -6.59E-04 | 0.00E+00 | -1.17E-17 | 6.82E-01 | 6.17E-08 | 7.99E-11 | -1.17E-07 | 1.00E-06 | 1.12E-06 | 1.00E-05 |
| 107 | 1.977 | 1.82E-01 | 1.85E-01 | 2.69E-01 | 4.30E-01 | 4.15E-01 | 1.34E-05 | 1.41E-05 | 2.26E-09 | 2.93E-05 | 1.41E-05 | 1.41E-05 | 1.47E-05 | 1.41E-05 | -6.58E-04 | 0.00E+00 | -1.17E-17 | 6.82E-01 | 1.98E-11 | 7.69E-11 | 5.00E-07 | 1.00E-06 | 5.00E-07 | 1.00E-05 |
| 108 | 1.996 | 1.82E-01 | 1.82E-01 | 2.70E-01 | 4.15E-01 | 4.15E-01 | 1.34E-05 | 1.00E-05 | 2.17E-09 | 2.93E-05 | 1.00E-05 | 1.41E-05 | 1.47E-05 | 4.34E-09 | -6.57E-04 | 0.00E+00 | -1.17E-17 | 6.82E-01 | 0 | 7.41E-11 | 5.00E-07 | 1.00E-06 | 5.00E-07 | 1.00E-05 |